

AD-A255 548

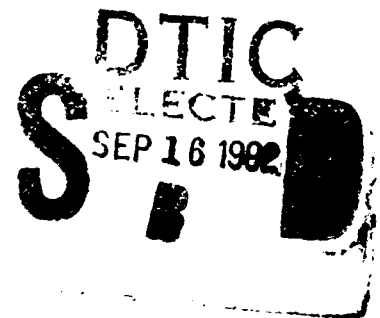


WL-TR-92-3025

DETERMINATION OF STRESSES ON LAMINATED AIRCRAFT  
TRANSPARENCIES BY THE STRAIN GAGE-HOLE DRILLING  
AND SECTIONING METHOD



Thomas J. Whitney  
Gregory J. Stenger  
University of Dayton Research Institute  
300 College Park  
Dayton, Ohio 45469-0110



APRIL 1992

Final Report for Period January 1989 - September 1990

Approved for public release; distribution is unlimited

92 9 15 040

105402  
92-25262  
205 p4

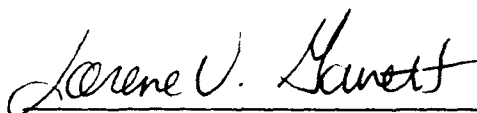
FLIGHT DYNAMICS DIRECTORATE  
WRIGHT LABORATORY  
AIR FORCE SYSTEM COMMAND  
WRIGHT-PATTERSON AIR FORCE BASE, OHIO 45433-6553

## NOTICE

When Government drawings, specifications, or other data are used for any purpose other than in connection with a definitely Government-related procurement, the United States Government incurs no responsibility or any obligation whatsoever. The fact that the government may have formulated or in any way supplied the said drawings, specifications, or other data, is not to be regarded by implication, or otherwise in any manner construed, as licensing the holder, or any other person or corporation; or as conveying any rights or permission to manufacture, use, or sell any patented invention that may in any way be related thereto.

This report is releasable to the National Technical Information Service (NTIS). At NTIS, it will be available to the general public, including foreign nations.

This technical report has been reviewed and is approved for publication.

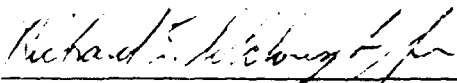


LORENE V. GARRETT  
Aerospace Engineer



RALPH J. SPEELMAN III, Chief  
Aircrew Protection Branch

FOR THE COMMANDER



RICHARD E. COLCLOUGH JR., Chief  
Vehicle Subsystems Division

If your address has changed, if you wish to be removed from our mailing list, or if the addressee is no longer employed by your organization please notify WL/FIVR, WPAFB OH 45433-6553 to help us maintain a current mailing list.

Copies of this report should not be returned unless return is required by security considerations, contractual obligations, or notice on a specific document.

UNCLASSIFIED

SECURITY CLASSIFICATION OF THIS PAGE

REPORT DOCUMENTATION PAGE				Form Approved OMB No. 0704-0188	
1a. REPORT SECURITY CLASSIFICATION UNCLASSIFIED			1b. RESTRICTIVE MARKINGS		
2a. SECURITY CLASSIFICATION AUTHORITY			3. DISTRIBUTION/AVAILABILITY OF REPORT Approved for public release; distribution is unlimited.		
2b. DECLASSIFICATION/DOWNGRADING SCHEDULE					
4. PERFORMING ORGANIZATION REPORT NUMBER(S) UDR-TR-90-106			5. MONITORING ORGANIZATION REPORT NUMBER(S) WL-TR-92-3025		
6a. NAME OF PERFORMING ORGANIZATION University of Dayton Research Institute		6b. OFFICE SYMBOL (If applicable)		7a. NAME OF MONITORING ORGANIZATION Flight Dynamics Directorate Wright Laboratory	
6c. ADDRESS (City, State, and ZIP Code) 300 College Park Dayton OH 45469-0110			7b. ADDRESS (City, State, and ZIP Code) WL/FIVR Wright-Patterson AFB, OH 45433-6553		
8a. NAME OF FUNDING/SPONSORING ORGANIZATION		8b. OFFICE SYMBOL (If applicable)		9. PROCUREMENT INSTRUMENT IDENTIFICATION NUMBER F33615-84-C-3404	
8c. ADDRESS (City, State, and ZIP Code)			10. SOURCE OF FUNDING NUMBERS		
			PROGRAM ELEMENT NO. 64212F	PROJECT NO. 1926	TASK NO. 01
			WORK UNIT ACCESSION NO. 12		
11. TITLE (Include Security Classification) DETERMINATION OF STRESSES ON LAMINATED AIRCRAFT TRANSPARENCIES BY THE STRAIN GAGE-HOLE DRILLING AND SECTIONING METHOD					
12. PERSONAL AUTHOR(S) Thomas J. Whitney and Gregory J. Stenger					
13a. TYPE OF REPORT Final		13b. TIME COVERED FROM JAN89 TO SEP90		14. DATE OF REPORT (Year, Month, Day) 1992 April	
15. PAGE COUNT 206					
16. SUPPLEMENTARY NOTATION					
17. COSATI CODES			18. SUBJECT TERMS (Continue on reverse if necessary and identify by block number)		
FIELD	GROUP	SUB-GROUP			
19. ABSTRACT (Continue on reverse if necessary and identify by block number) Reducing the incidence of transparency changeouts due to craze of the outer acrylic ply requires knowledge of stress levels in in-service aircraft transparencies. Laboratory and field craze data may then be correlated to predict craze onset. Experiments conducted during the first phase of this study verified that the strain gage-hole drilling method, with calibration modification, can measure biaxial stress states in laminated transparencies with an error of less than 10% for stresses over 500 psi. A device to apply this method to full-scale transparencies was then designed and fabricated. In the second phase, stresses due to three mechanisms (residual stress, installation, and cabin pressurizing) in full-scale transparencies were measured. For comparison purposes and to identify the contribution of particular mechanisms to the total stress state, the sectioning method was also used. The measurements made on full-scale transparencies removed from service due to craze indicate residual stresses are too low to cause crazing in a "uniform" environment (one free from wide temperature variation and extended contact with crazing agents). Stresses due to transparency (continued)					
20. DISTRIBUTION/AVAILABILITY OF ABSTRACT <input checked="" type="checkbox"/> UNCLASSIFIED/UNLIMITED <input type="checkbox"/> SAME AS RPT <input type="checkbox"/> DTIC USERS			21. ABSTRACT SECURITY CLASSIFICATION UNCLASSIFIED		
22a. NAME OF RESPONSIBLE INDIVIDUAL L. V. Garrett			22b. TELEPHONE (Include Area Code) 513-255-2516		22c. OFFICE SYMBOL WL/FIVR

CONTINUATION OF BLOCK 19:

installation and cabin pressurizing were also low relative to the maximum principal stress criteria used in this study. Recommendations include examination of other craze criteria, examination of other stress inducing mechanisms such as moisture desorption from the surface, and examination of cyclic loading and chemical exposure on craze.

## PREFACE

The efforts reported herein were performed by the Aerospace Mechanics Division of the University of Dayton Research Institute (UDRI), Dayton, Ohio, under Air Force Contract F33615-84-C-3404. The program was sponsored by the Flight Dynamics Directorate, Wright Laboratory, Wright-Patterson Air Force Base, Ohio. Air Force administrative direction was provided by Capt. Paul J. Kolodziejski, WL/FIVR, Air Force Project Engineer. Air Force Technical support was provided by Mr. Michael G. Gran and Ms. Lorene V. Garrett, WL/FIVR.

The work was conducted during the period 2 January 1989 to September 1990. University of Dayton project supervision was provided by Mr. Dale H. Whitford, Supervisor, Aerospace Mechanics Division, and Mr. Blaine S. West, Head, Structures Group. Technical effort was accomplished under Messrs. G. J. Stenger and T. J. Whitney as Principal Investigators, with Mr. Whitney being responsible for overall coordination of testing, analysis, and hardware development. The authors wish to acknowledge the contributions of Mr. James Higgins, experimental fabrications; Mr. Phil Graf and Mr. Fred Davis, test method consultation and strain gage installation; and Mr. John Murphy, optical systems consultation.

DTIC QUALITY INSPECTED 3

Accession For	
NTIS GFA&I	<input checked="checked" type="checkbox"/>
DTIC TAB	<input type="checkbox"/>
Unannounced	<input type="checkbox"/>
Justification	
By	
Distribution/	
Availability Codes	
Dist	Avail and/or Special
A-1	

## TABLE OF CONTENTS

	PAGE
1. Introduction	1
1.1 Background	1
1.2 Objective	2
2. Strain Gage Center Hole Drilling Method	3
2.1 Principals of Technique	3
2.2 Preliminary Investigations	6
2.2.1 Gage Type	7
2.2.2 Encapsulation/Installation Techniques	7
2.2.3 Adhesives	11
2.2.4 Instrumentation	14
2.3 Calibration of Strain Gage Method	14
2.3.1 Loading Fixture	14
2.3.2 Calibration Loading Path and Data Reduction	16
2.4 Verification Tests	22
2.4.1 Uniaxial Tension and Compression	22
2.4.2 Uniaxial Tension - Transversely Curved Surface	26
2.4.3 Biaxial Stress - Curved Surface	26
2.4.4 Uniaxial Tension on Laminated Transparency Material	29
2.5 Summary	32
3. Design of a Portable Drilling Unit for Use on Compound Curved Surfaces	33
3.1 System Requirements	33
3.2 Drilling Device, Design Drivers, and Features	39
3.3 Stress Free Drilling Verification and Performance	48
4. Sectioning Method	51
4.1 Introduction	51
4.2 Calibration	51
5. Preliminary Determination of Stresses in Laminated F-16 Canopies	55
5.1 Test Specimens	55
5.2 Alignment Facility/Gage Layout	55

## TABLE OF CONTENTS (continued)

5.3	Testing Procedure	64
5.3.1	Initial State	64
5.3.2	Installation	64
5.3.3	Pressurization	68
5.3.4	Residual Stresses	68
5.3.5	Sierracin Canopy Procedure Alterations	70
5.4	Test Results	71
5.4.1	Sectioning Method	71
5.4.1.1	Installed State	71
5.4.1.2	Pressurized State	71
5.4.1.3	Residual Stresses	84
5.4.2	Hole Drilling and Superimposed Regular Rosette Results	91
5.4.2.1	Hole Drilling on Installed Canopies	91
5.4.2.2	Hole Drilling on Pressurized Canopies	91
6.	Determination of Residual Stresses by the Hole Drilling Method	101
6.1	Test Specimens	101
6.2	Strain Gages/Alignment Facility	101
6.3	Test Procedure	103
6.4	Results	103
7.	Discussion and Recommendations	108
	References	111
Appendix A	Procedures for use of VALAPODD	113
Appendix B	Detail Drawings of Hole Drilling Device	117
Appendix C	Hole Drilling Locations for In-Serviced Canopies	174

## LIST OF ILLUSTRATIONS

FIGURE	PAGE
2.1 Theoretical Basis for Hole Drilling Method	4
2.2 Hole Drilling Gages Available from Measurements Group	8
2.3 Heat Affected Zone in Strain Gages	10
2.4 Acrylic Calibration Fixture	15
2.5 Acrylic Calibration Specimens	17
2.6 Calibration Loading Path for Elastic Materials	18
2.7 Calibration Loading Path for Viscoelastic Materials	19
2.8 Strain Data from Acrylic Calibration	21
2.9 Uniaxial Verification Results	24
2.10 Compression Verification Tests	25
2.11 Curved Surface Uniaxial Verification Results	27
2.12 Curved Surface Biaxial Verification Test	28
2.13 Trimming to Locate the Normal in Biaxial Verification Tests	28
3.1 Theoretical Residual Stress Error	35
3.2 Optimal Machining Methods for Acrylic	36
3.3 High Speed Air Turbine Machining Induced Stress	37
3.4 Optimal Drilling Parameters	38
3.5 Vacuum Attached Laser Aligned Portable Drilling Device	40
3.6 Front View of VALAPODD Base	41
3.7 VALAPODD Alignment Configuration	43
3.8 Optical Paths in Alignment Components	44
3.9 VALAPODD Drilling Configuration	45
3.10 Vacuum, Air Feed Lines, and Control Box	46
3.11 External Drill Motor and Flexible Shaft	47
3.12 Hole Drilling on Installed and Pressurized Canopy	50
4.1 Strain Data from Regular Rosette Calibration	54
5.1 Gage Type Used for Sectioning [16]	56
5.2 Typical Sectioned Sample with Bullet Connectors	57
5.3 Rosette Alignment and Layout Facility	58



## LIST OF ILLUSTRATIONS (continued)

FIGURE	PAGE
5.4 Fuselage Station Indicator	60
5.5 Use of Laser to Produce Rosette Layout Lines	61
5.6 Forward Bolts on Canopy T-Frame	65
5.7 Aft Restraining Collars on Canopy T-Frame	66
5.8 Full-Scale F-16 Tabletop Pressure Fixture	67
5.9 4- x 4-inch Sectioning Specimens	69
5.10 Maximum Installation Stresses - Canopy T1	72
5.11 Maximum Installation Stresses - Canopy S1: Forward	73
5.12 Maximum Installation Stresses - Canopy S1: Aft	74
5.13 Minimum Installation Stresses - Canopy T1	75
5.14 Minimum Installation Stresses - Canopy S1: Forward	76
5.15 Minimum Installation Stresses - Canopy S1: Aft	77
5.16 Maximum Pressure Stress - Canopy T1	78
5.17 Maximum Pressurization Stress - Canopy S1: Forward	79
5.18 Maximum Pressurization Stress - Canopy S1: Aft	80
5.19 Minimum Pressure Stress - Canopy T1	81
5.20 Minimum Pressurization Stress - Canopy S1: Forward	82
5.21 Minimum Pressurization Stress - Canopy S1: Aft	83
5.22 Maximum Residual Stress - Canopy T1	85
5.23 Residual Stress Using Initial Strain Baseline - Canopy S1: Forward	86
5.24 Residual Stress Using Initial Strain Baseline - Canopy S1: Aft	87
5.25 Minimum Residual Stress - Canopy T1	88
5.26 Minimum Residual Stress - Initial Strain Baseline - Canopy S1: Forward	89
5.27 Minimum Residual Stress - Initial Strain Baseline - Canopy S1: Aft	90
5.28 Maximum Stress (Installed Plus Residual) Canopy T1	93
5.29 Maximum Stress (Installed Plus Residual) Canopy S1: Forward	94
5.30 Maximum Stress (Installed Plus Residual) Canopy S1: Aft	95
5.31 Maximum Superimposed Stress Canopy T1	97

## LIST OF ILLUSTRATIONS (continued)

FIGURE		PAGE
5.32	Maximum Superimposed Stress Canopy S1: Forward	98
5.33	Maximum Superimposed Stress Canopy S1: Aft	99
6.1	Stress Resulting from Deflection by the Spreader Bar	105

## LIST OF TABLES

TABLE	PAGE
2.1 Effect of Abrading and Encapsulation on Strain Readings	9
2.2 Follow-Up Test of "Heat-Affected Zone" Reinforcing Effects	12
2.3 Adhesive Craze Tests	13
2.4 Verification of Hole Drilling Constants for Type TEA-XX-062RK-120	
Rosettes	23
2.5 Biaxial/Curved Surface Hole Drilling Summary	30
2.6 Laminated Beam Hole Drilling Summary	31
3.1 VALAPODD Verification Results	49
5.1 Sectioning Rosette Locations	62
5.2 Locations of Residual Stress Hole-Drilling Tests	63
5.3 Hole Drilling Results: Installed Canopies, Canopy T1	92
5.4 Hole Drilling Results: Pressurized Canopies	96
6.1 Full-Scale Test Specimen Profile	102
6.2 Full-Scale F-16 Hole Drilling Results	106

## SECTION 1

### INTRODUCTION

#### 1.1 BACKGROUND

Significant cost savings can be realized by increasing the service life of transparency systems. Many factors influence the durability of such systems. Among laminated polycarbonate/acrylic transparencies, craze of the acrylic surface layer is a significant cause for removal. By understanding the craze phenomena, methods of improved craze resistance may be developed, and the cost of transparency ownership lowered.

The approach to reducing the occurrence of craze involves correlating laboratory craze data (such as time to craze vs. stress information for various chemicals) with field craze data (e.g., material and fabrication technique information, environment and service history). The correlation would evolve into an analytical or statistical expression for the predicted craze durability of a transparency system based on stress in the part, the fabrication method, and the planned service environment. The procurement process would implement this approach by measuring stress levels on finished parts (or samples from batches of finished parts). The process would accept only those transparencies which contained low stress levels compatible with craze resistance in the intended service environment of the transparency system. This craze level would be obtained from the durability expression.

To implement this approach requires a nondestructive inspection technique to measure the stress in the transparencies. Previous work [1] has shown the technology associated with two of the most well known techniques: scattered light photoelasticity and surface wave ultrasonics, to be insufficiently developed to be used on the acrylic face plies of laminated transparencies. Until this technology sufficiently advances, timely advancement of the effort to enhance transparency craze resistance requires some kind of stress measurement technique, be it destructive or semidestructive.

The strain gage hole drilling method was selected for this purpose because of its past success in other (primarily metals) applications. Since only a small hole is drilled into the material, it also possesses the long term possibility of becoming semidestructive in acrylic applications, should the technology be developed to refill the hole in a manner which satisfies

optical requirements. However, the method is not used regularly on thermoplastic materials, and hence requires validation that it can successfully and accurately measure surface stress.

## 1.2 OBJECTIVE

In order to verify that the hole drilling strain gage method of residual stress determination was valid for use on transparency acrylic face plies, the following primary objectives were defined:

- Experimentally verify the accuracy of the strain gage hole drilling method for use on laminated aircraft transparencies by comparing test results to known stress levels in samples of various geometries under various loading conditions.
- Specify gage type, adhesive, installation technique and instrumentation necessary for the test method.
- Design, fabricate, test and establish a procedure for a portable unit for executing the hole drilling operation.

Once a method is verified, lab and field data must be correlated by relating stress measurements in transparencies and their related craze data to laboratory data involving the time to craze for a given stress level. To make preliminary evaluations of the stress levels in F-16 canopies and their sources, the following secondary objectives were established:

- Determine the stresses due to installation, cabin pressure, and residual manufacturing stresses in two full-scale F-16 forward canopies by the hole drilling method and by the sectioning method.
- Determine residual stresses, by the hole drilling method, in 20 canopies (10 each from Texstar and Sierracin) removed from service for craze.

## SECTION 2

### STRAIN GAGE CENTER HOLE DRILLING METHOD

#### 2.1 PRINCIPALS OF TECHNIQUE

The strain gage hole drilling method (ASTM E837-81) for determining residual stress consists of drilling a small, blind or through hole in the center of a rosette of strain gages, measuring the strains relieved due to the removal of the material, and back-calculating the magnitude and directions of the principal biaxial stresses responsible for the strain relief. The equations for calculating the stresses are based on the elasticity solution [2,3] for the stress field around a hole in an infinite plate under a uniform far-field stress, Figure 2.1, and are as follows:

$$\tan 2\alpha = \frac{-e_1 + 2e_2 - e_3}{-e_1 + e_3} \quad (1)$$

$$\sigma_{\max} = \frac{e_1(A + B\sin\gamma) - e_2(A - B\cos\gamma)}{2AB(\sin\gamma + \cos\gamma)} \quad (2)$$

$$\sigma_{\min} = \frac{e_2(A + B\cos\gamma) - e_1(A - B\sin\gamma)}{2AB(\sin\gamma + \cos\gamma)} \quad (3)$$

in which:

$\alpha$  = Counter-clockwise angle from gage 1 to direction of maximum algebraic stress

$e_i$  = strain measured at gage i (i=1,2,3)

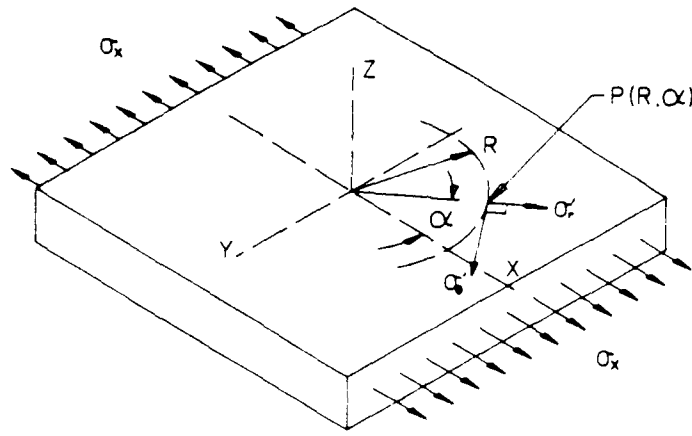
$$\gamma = 2\alpha$$

$$A = -\frac{1+\nu}{2E} \left( \frac{1}{r^2} \right)$$

$$B = -\frac{1+\nu}{2E} \left[ \left( \frac{4}{1+\nu} \right) \frac{1}{r^2} - \frac{3}{r^4} \right]$$

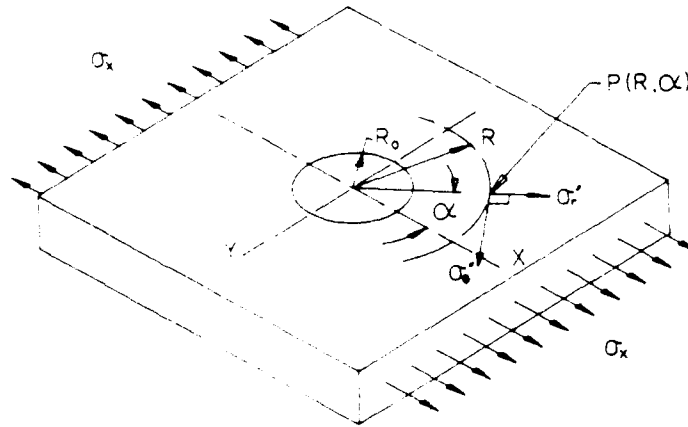
$$r = \left( \frac{R}{R_0} \right) = \text{Ratio of distance from center of hole to an arbitrary point P to the radius of the hole}$$

and E and  $\nu$  are Young's modulus and Poisson's ratio, respectively, for an isotropic material.



$$\sigma'_r = \frac{\sigma_x}{2} (1 + \cos 2\alpha)$$

$$\sigma''_\theta = \frac{\sigma_x}{2} (1 - \cos 2\alpha)$$



$$\sigma'_r = \frac{\sigma_x}{2} \left( 1 - \left( \frac{R_o}{R} \right)^2 \right) + \frac{\sigma_x}{2} \left( 1 + 3 \left( \frac{R_o}{R} \right)^4 - 4 \left( \frac{R_o}{R} \right)^2 \right) \cos 2\alpha$$

$$\sigma''_\theta = \frac{\sigma_x}{2} \left( 1 + \left( \frac{R_o}{R} \right)^2 \right) - \frac{\sigma_x}{2} \left( 1 + 3 \left( \frac{R_o}{R} \right)^4 \right) \cos 2\alpha$$

Stress measured by drilling hole:  $\Delta\sigma_r = \sigma'_r - \sigma''_\theta$  ;  $\Delta\sigma_\theta = \sigma''_\theta - \sigma'_r$

Strain relieved by drilling hole:  $\epsilon_r = \frac{1}{E} \Delta\sigma_r - \frac{\nu}{E} \Delta\sigma_\theta$

$$= - \frac{\sigma_x(1+\nu)}{2E} \left[ \left( \frac{R_o}{R} \right)^3 - 3 \left( \frac{R_o}{R} \right)^4 \cos 2\alpha + \frac{4}{(1+\nu)} \left( \frac{R_o}{R} \right)^2 \cos 2\alpha \right]$$

Figure 2.1. Theoretical Basis for Hole Drilling Method.

Because an inverse tangent function is involved in the calculation, the data reduction algorithm used must correct the angle calculated by (1) to ensure that the result occurs in the correct quadrant [4]. This correction is based on the signs of the numerator and denominator of equation (1) and takes the following form:

<u>Sign of Numerator</u>	<u>Sign of Denominator</u>	<u>Correction</u>
+	+	0
+	-	$+\pi$
-	+	0
-	-	$+\pi$

The above equations are valid for the precise stresses around a small through hole in a thin flat plate at an infinitesimal point. Further analysis is necessary to account for the integrating effects of the strain gages, the effect of nonflat surfaces, and the effects of viscoelastic and laminated materials (such as those of aircraft transparencies).

Researchers such as Schajer [5], Kabiri [6] and Flaman, Mills and Boag [7] have done numerical studies relating the constants A and B to hole size and configuration of various gage rosettes, depth of hole (for blind hole drilling), and material properties. Schajer's results show the above constants can be computed as follows:

$$A = -\left(\frac{1+\nu}{2E}\right)a \quad (4)$$

$$B = -\left(\frac{1}{2E}\right)b \quad (5)$$

in which a and b are determined from charts of numerical results based on hole diameter and gage circle diameter for a specific hole depth (e.g., [3]). Coefficient b, however, has some dependence on material properties. Flaman's finite element results indicate that stresses on the surface of the material are responsible for the majority of strain relief measured, and therefore performance of hole drilling test to determine stress below the surface is often significantly in error. More importantly, a literature survey conducted prior to the beginning of this study indicated a general lack of experience in carrying out this procedure on viscoelastic materials.

Due to a lack of information on hole drilling in viscoelastic materials, calibration tests were initiated as suggested by ASTM E837-81. Uniform known stresses were induced



in a flat sample, the hole was drilled and strains recorded, and the constants A and B back calculated. With the constants determined, a series of verification tests for various loadings and sample geometries was undertaken. With successful verification, the coefficients can be used with confidence on hole-drilling strains from the transparencies.

Prior to and in conjunction with the calibration tests, a series of tests was conducted to evaluate specific gage types, adhesives, installation techniques, methods of drilling the hole, and instrumentation. This was again due to a general lack of experience and references in the literature concerning strain gaging of acrylic. Each of these topics, including the calibration/verification studies, will be discussed in detail in the next section.

## 2.2 PRELIMINARY INVESTIGATIONS

The body of literature concerning strain gage technology contains little information on plastics. Gage manufacturer installation manuals generally specify procedures with minimal regard to the material actually instrumented. In plastics, the following factors may influence strain gage accuracy and in particular the hole drilling technique:

- Adhesive
- Gage type
- Reinforcing effects
- Installation techniques

Adhesives normally present little difficulty even in gaging of polymers. However, in the hole drilling application the test article contains residual stresses which may induce craze when the adhesive contacts the material. Reinforcing effects may cause significant problems in strain gaging of polymers, because the gage backing material may be stiffer than the polymer itself, producing artificially low strain readings. Since the hole drilling technique involves strains of low magnitude, installation techniques must avoid procedures which would influence the state of stress in the material or degrade the accuracy of the measurement. Surface abrasion and lead wire soldering (and subsequent degradation of the cement layer and acrylic due to their low thermal transfer abilities) are two steps normally implemented in strain gage installation which may negatively influence hole drilling accuracy.

The following summarizes preliminary tests and their results which provided specification of gage type, adhesive, installation technique, and proper instrumentation.

### 2.2.1 Gage Type

Several manufacturers, including Measurement Group, Inc., Hottinger Baldwin Messtechnik, and Precision Foil Technology, Inc., produce strain gage rosettes suited for hole drilling. A review of literature from these companies indicated that the line of rosettes manufactured by Measurements Group would best serve the needs of this study, based on their successful use in previous work, availability, range of rosette geometries, and the detailed technical information available from the manufacturer.

Figure 2.2 displays the available hole drilling rosettes from Measurements Group, Inc. Larger geometries reduce errors due to alignment and produce more stable output, but present installation problems (such as uneven glue lines) due to their size, require larger calibration specimens, and must be located further from the edge of test parts. Rosette types EA-XX-062RE-120 and TEA-XX-062RK-120 provided the best compromise between the two extremes and were chosen for use throughout this study.

### 2.2.2 Encapsulation/Installation Techniques

Table 2.1 shows results of a preliminary study which determined the affects of surface abrading and rosette encapsulation on strain readings. Two acrylic specimens each contained six uniaxial gages. Specimen loadings and accompanying strain readings provided data for Young's modulus calculations, which when compared to the published value of 450 ksi, gave an indication of the effect of each of the parameters. Nonencapsulated gages had an average calculated modulus of 452 ksi, while encapsulated gages averaged 4% higher. However, the difference was within two standard deviations and was not considered significant. Abrading had a negligible effect on the results.

Because acrylic is such a poor heat conductor, soldering of lead wires to the strain gages presented problems not normally encountered when instrumenting metals. Figure 2.3 displays a "heat affected" zone which accompanies lead wire attachment. High temperatures apparently produce changes in the acrylic and possibly in the adhesive layer. In order to study the effect of this, installation of two of the gages in Table 2.1 included pre-attachment of lead wires to the gages before bonding of the gages to the acrylic. These two






PATTERN INFORMATION	RES. LINE DIM.	DIMENSION					
		GAGE LENGTH	GRID CTR'LINE DIA.	TYPICAL HOLE DIA.		MATRIX	
				Min.	Max.	Length	Width
EA-XX-031RE-120 EA-XX-031RE-120/Option SE 	120 $\pm$ 0.2% 120 $\pm$ 0.4%	0.011	0.101	0.01	0.04	0.29	0.29
		0.79	2.56	0.8	1.0	7.4	7.4
		Due to small pattern size, measurement error can be magnified by slight mislocation of drill hole. Pattern not recommended for general-purpose applications.					
EA-XX-062RE-120 EA-XX-062RE-120/Option SE 	120 $\pm$ 0.2% 120 $\pm$ 0.4%	0.062	0.202	0.06	0.08	0.42	0.42
		1.57	5.13	1.5	2.0	10.7	10.7
		Most widely used RE pattern for general-purpose residual stress measurement applications.					
EA-XX-125RE-120 EA-XX-125RE-120/Option SE 	120 $\pm$ 0.2% 120 $\pm$ 0.4%	0.125	0.404	0.12	0.16	0.78	0.78
		3.18	10.26	3.0	4.1	19.8	19.8
		Larger version of the 062RE pattern.					
TEA-XX-062RK-120 	120 $\pm$ 0.4%	0.062	0.202	0.06	0.08	0.60	0.60
		1.57	5.13	1.5	2.0	15.2	15.2
		Fully encapsulated, with copper terminals for ease of soldering. Same pattern geometry as 062RE pattern.					
CEA-XX-062UM-120 	120 $\pm$ 0.4%	0.062	0.202	0.06	0.08	0.38	0.48
		1.57	5.13	1.5	2.0	9.6	12.2
		Fully encapsulated with large copper-coated soldering tabs and special trim alignment marks. Trim line spaced 0.068 in (1.73 mm) from hole center.					

Figure 2.2. Hole Drilling Gages Available from Measurements Group.

TABLE 2.1  
EFFECT OF ABRADING AND  
ENCAPSULATION ON STRAIN READINGS

Specimen	Installation	Calculated Modulus for a Uniaxial Stress Level of:			Average Modulus (E) Standard Deviation (s)
		$\sigma = 500$	$\sigma = 1000$	$\sigma = 1500$	
1A/1	Abrading	485,700	481,900	465,800	$\bar{E} = 452,500$
1A/2	No Encapsulation	474,800	452,900	446,300	$s = 26,426$
1A/3		425,900	422,300	416,800	
<hr/>					
1A/4	No Abrading	492,600	474,200	463,500	$\bar{E} = 450,700$
1A/5	No Encapsulation	451,700	449,000	441,600	$s = 22,896$
1A/6*		433,300	429,200	421,200	
<hr/>					
2A/1	Abrading	467,300	465,600	465,700	$\bar{E} = 477,100$
2A/2	Encapsulation	503,500	484,000	476,000	$s = 12,209$
2A/3		484,500	476,000	471,400	
<hr/>					
2A/4	No Abrading	480,800	474,200	468,900	$\bar{E} = 465,200$
2A/5	Encapsulation	466,850	457,500	460,690	$s = 8,714$
2A/6*		459,900	465,600	452,600	

SUMMARY:

- Encapsulated gages have generally higher values of E.
- Surface abrading yields slightly higher values of E.

\*Preattached lead wires

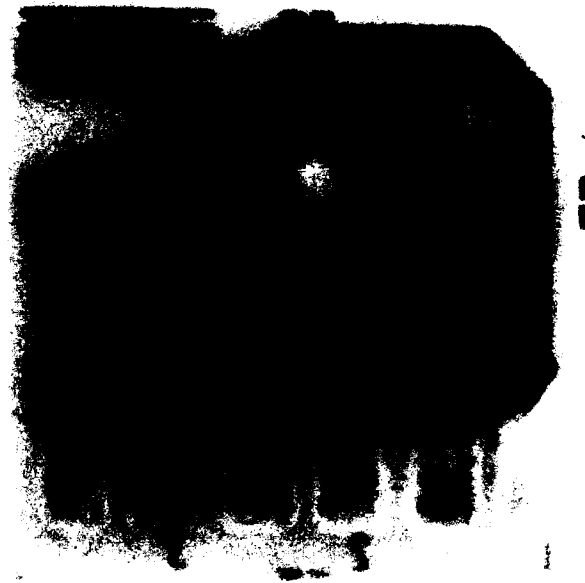


Figure 2.3. Heat Affected Zone in Strain Gages.

gages produced moduli almost 10% lower than average. In addition, the raised solder dots create an uneven top surface, resulting in uneven glue lines during bonding. This apparent softening when wires are preattached suggests that soldering after bonding may produce "heat-affected" zones near the gage which are softer than the normal material, producing higher strain readings for a given stress.

Table 2.2 shows the results of a follow-up study of this effect. The same specimens loaded to three different stress levels, generated strain data for a "baseline" installation state. Terminal strips and solder then installed in the vicinity of the gages created "heat affected" zones. Reloading of the specimens produced strain data only 3.5% higher than the baseline data, and some cases produced lower strains. These data indicate only a small attenuation of strain from the "heat affected" zone for attachment points sufficiently far from the gages themselves and demonstrate the preattachment of lead wires was not necessary for accurate data.

### 2.2.3 Adhesives

Adhesive types generally present problems on strain gaging only if the temperature of the test deviates substantially from room temperature, or if the test article undergoes large strains. In the hole drilling application, however, the test part may already contain sizeable residual stresses, which in the case of polymers, may contribute to craze during adhesive application. Such phenomena undoubtedly alter the stress field in the test part and must be avoided.

Table 2.3 presents results of a short study to specify appropriate adhesive type. Measurements Groups, Inc., manufactures three of the adhesives tested (MBOND 200, AE-10, GA-2). Their widespread use in other strain gage applications formed the basis for their selection. UDRI Materials Division personnel suggested the use of Versilok adhesives, manufactured by the Lord Corporation. All the adhesives, except for MBOND 200 (cyanoacrylate) are epoxy based.

The craze data indicate that MBOND 200, the quick curing adhesive, was not suitable for use for stresses over 1200 psi. This craze level and the expected canopy stress level of 1000-2000 psi resulted in MBOND 200 rejection. For similar reasons, the Versilok

TABLE 2.2  
FOLLOW-UP TEST OF  
"HEAT-AFFECTED ZONE" REINFORCING EFFECTS

Spec/Gage	$\sigma = 500$			$\sigma = 1000$			$\sigma = 1500$		
	$\epsilon_{\text{Baseline}}$	$\epsilon_{\text{heat affected}}$	% $\Delta$	$\epsilon_{\text{Baseline}}$	$\epsilon_{\text{heat affected}}$	% $\Delta$	$\epsilon_{\text{Baseline}}$	$\epsilon_{\text{heat affected}}$	% $\Delta$
1A/1*	1197	1182	-1.2	2275	2275	0	3549	3329	-6.2
1A/2*	1204	1260	4.6	2349	2484	5.75	3451	3546	2.75
1A/3*	1240	1261	1.69	2463	2473	0.41	3672	3636	-0.98
1A/4*	1196	1241	3.76	2301	2391	3.9	3378	3472	2.8
1A/5*	1256	1255	-0.64	2402	2461	2.4	3546	3620	2.1
1A/6*	1305	1347	3.2	2531	2564	1.3	3724	3723	-0.03

\*No terminal strips installed. Specimen merely reloaded for an indication of spread on baseline data.

+Terminal strips installed prior to baseline test to give an indication of spread in "heat affected" data.

TABLE 2.3  
ADHESIVE CRAZE TESTS

ADHESIVE	STRESS (psi)	TIME TO CRAZE (min)	COMMENTS
MBOND 200 (cyanoacrylate)	1000	10	No catalyst
	1000	No craze	Catalyst used
	1200	3.5	Catalyst used
AE-10 (two-part epoxy)	1333	No craze	Curing agent only
	1200	No craze	Epoxy only
	1866	No craze	Both parts
GA-2 (two-part epoxy)	1866	No craze	Both parts
AE-10/9252TR	1700	10	
Versilok 521/4	1866	< 2.0	Craze to failure ~ 20 min.
Versilok 521/17	1866	< 2.0	Craze to failure ~ 2 min.



adhesives proved unusable. Only the AE-10 and GA-2 systems did not cause crazing in acrylic to about 2000 psi.

Both of these systems possessed drawbacks, however. Both required elevated temperature cure for extended time periods under pressures greater than atmospheric. In addition, adequate rosette-to-surface bond strength occurred only when slight surface abrasion precedes bonding, which may induce low magnitude residual stresses. Samples of Bostic 9252TR, an epoxy primer successfully used by the SAAB-Scania company to reduce the occurrence of failure in acrylic tensile samples at strain gage sites, provided a possible alternative to abrasion during installation. However, as Table 2.3 demonstrates, application of the primer to prestressed acrylic samples resulted in unacceptable craze formation.

The test results indicated that an acceptable method for bonding gages is to use AE-10 adhesive with slight abrasion prior to installation. Although the process likely induced some surface stress, the level of this stress was considered negligible in comparison to the magnitude of the stresses measured in the canopy. MBOND 200 remained suitable for use in test specimens, since gage installation occurred prior to loading in these parts.

#### 2.2.4 Instrumentation

Because acrylic is an extremely poor heat conductor, electric current passing through a strain gage bonded to acrylic creates a local temperature increase sufficient to produce significant error in strain readings. The fact that all hole drilling rosettes use low resistance gage grids and the gage is thermally mismatched with the acrylic increase the severity of the effect. To compensate, an identical rosette, mechanically unstrained and at the same temperature as the active gage, must be located in the adjacent arm of the Wheatstone bridge. As identical current runs through both arms, both rosettes will see the same temperature increase and the configuration will cause the two increases to cancel out. All tests in this program utilized this temperature compensating bridge configuration.

### 2.3 CALIBRATION OF STRAIN GAGE METHOD

#### 2.3.1 Loading Fixture

A fixture to apply tensile and compressive loads to calibration samples was constructed and is shown in Figure 2.4. Consisting of a base plate, block uprights, loading bolts and pin type clevis grips, the device was designed to apply constant displacement loads

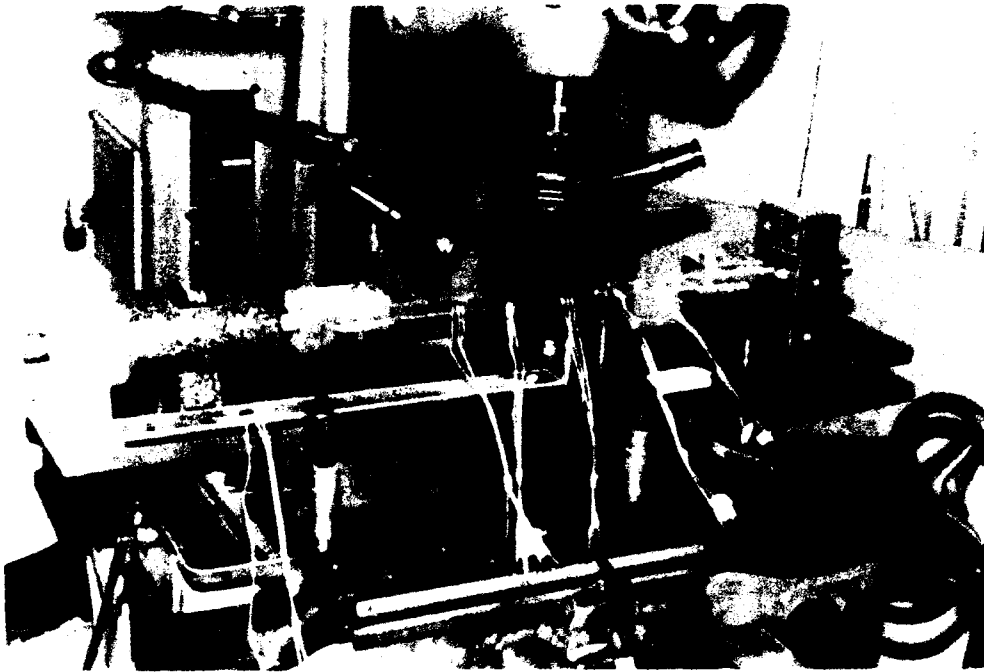


Figure 2.4. Acrylic Calibration Fixture.

to test samples. The device uses this end condition (as opposed to constant load) because it is most like the boundary conditions seen by a canopy in the installed state. A 2-Kip load cell connected to a portable multimeter through a Honeywell signal conditioner provided load readouts.

Figure 2.5 shows the specimen configuration. Five rosettes positioned evenly along the length of the specimen allowed convenient drilling of multiple holes in a short time period. The use of through holes in 1/8-inch-thick specimens duplicates the conditions in the canopy outer acrylic ply, as the soft inner layer locally "decouples" the acrylic from the polycarbonate ply. Measurement Group, Inc., residual stress rosette type EA-06-062RE-120 gages were selected for these tests due to their wide use in other residual stress applications [8-11]. Strain indicator type P3500 with an SB-10 Switch and Balance unit (also from Measurements Groups, Inc.) provided direct readout of microstrain.

A Moore jig borer was used to introduce the hole into the acrylic. This device allowed adjustable drill feed and speed as well as highly accurate positioning of the drill. A 1/16-inch-diameter high speed steel drill was utilized during the testing. Drilling proceeded at 1200 rpm and at a feed of 0.001 inch/revolution. A Fowler 40x centering microscope allowed precision ( $\pm 0.0005$  inch) centering of the drill.

### 2.3.2 Calibration Loading Path and Data Reduction

Due to the viscoelastic nature of the acrylic, the loading path taken by a given gage on the material during the test is time dependent and therefore more complex than in ordinary hole drilling calibration tests. For clarity, Figure 2.6 shows the loading path for an arbitrary gage on an elastic material. The sample is loaded to point A. Drilling relieves strain to point B. In addition, any stresses due to the drilling, or residual stresses on the test part, are also relieved during drilling. Releasing the load from the specimen, point C, indicates the portion of the relieved strain attributable to this stress. Subtracting the strain at C from the difference in strains between points B and A yields the actual strain relieved due to the mechanical load. Alternatively, zeroing out the strain at C and reloading to D also gives the level of relieved strain due to the load  $(\epsilon_D - \epsilon_A)$ .

The presence of viscoelastic properties in the acrylic introduces time into the load path for a given gage. Point A, Figure 2.7, represents the point of initial loading.



Figure 2.5. Acrylic Calibration Specimens.

# Summary of Calibration Test Methodology

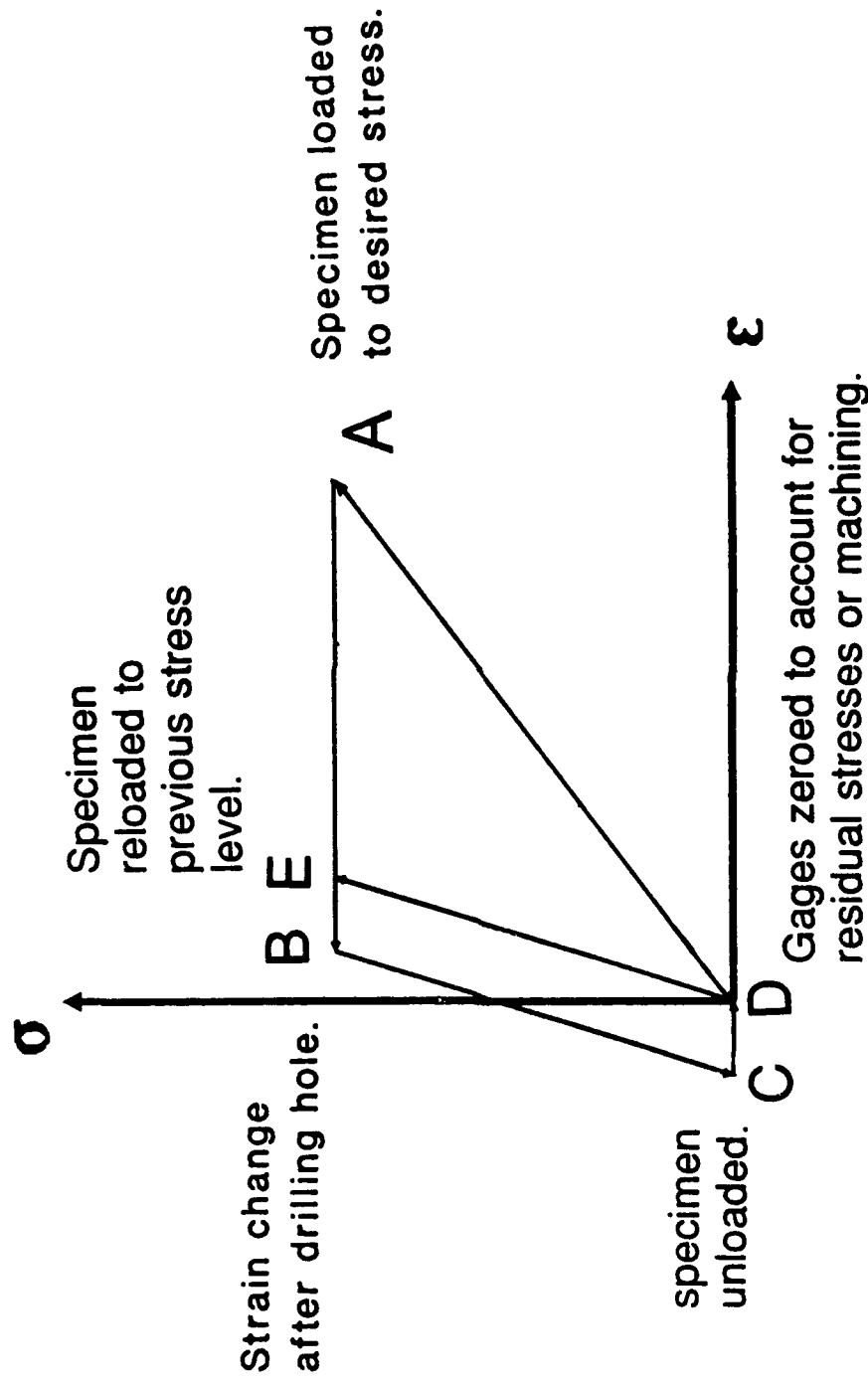


Figure 2.6. Calibration Loading Path for Elastic Materials.

# Calibration Test Load Path

Typical  $\epsilon - \sigma - t$  Curve for a Hole Drilling Strain Gage

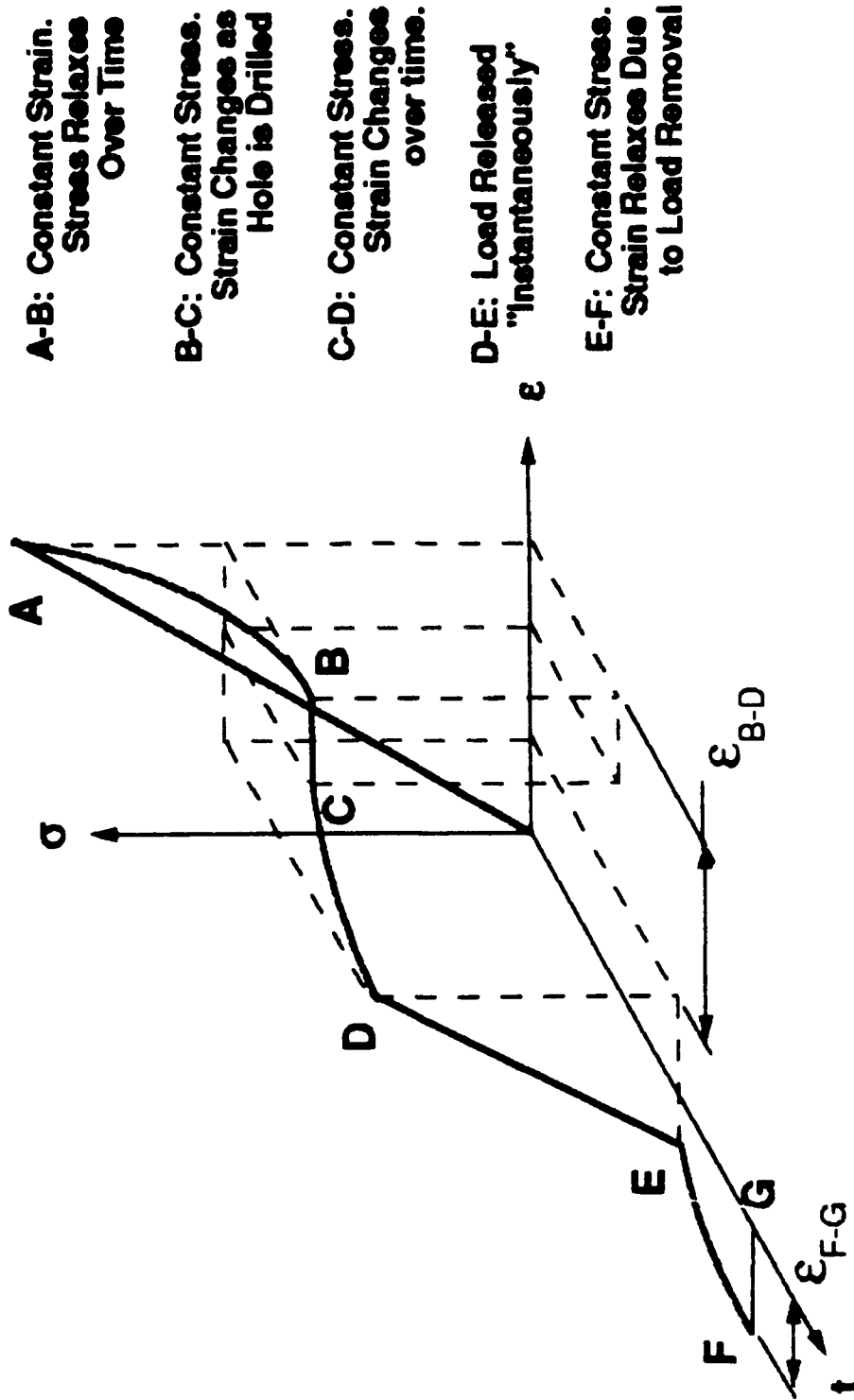


Figure 2.7. Calibration Loading Path for Viscoelastic Materials.

Since the fixture prescribes a constant fixed displacement on the specimen, the stress in the sample relaxes. This relaxation occurred over an 8-minute period, during which the drill was centered. Allowing the specimens to relax for 8 minutes permitted the existence of a nearly "constant" stress state for drilling, as would exist in a canopy outer layer (by assumption, the installation of a canopy is a fixed displacement condition, which results in stress relaxation of initial installation stresses to a constant level over time). The stress in the specimen is "constant" in the sense that the stress does not change significantly in the time it takes to drill the hole. Drilling relieves strain from point B to C. However, as the new stress state is constant, the strain continues to change over time (creep) from C to D. After an 8-minute period, release of the load (point E) as in the elastic case, indicates drilling induced stresses (other stresses) not associated with the mechanical loading. As this is a fixed change in load (load at drill to zero load), creep again occurs (E to F). After an 8-10 minute period, during which the strain approaches a "constant" value, the strain at F is taken as the nonmechanical strain. Subtraction of the strain at F from the strain difference (D-B) is taken as the strain relieved due to a constant stress at B. Using this calibration technique allows the hole drilling method to be calibrated to the relaxed strain state (strain after creep) achieved by drilling the hole. The advantage is that the relaxed strain state is much easier to identify than any other transient strain state.

The above procedure was implemented on 12 rosettes at various load levels. The resulting relieved strain data, plotted in Figure 2.8 show good agreement with a weighted linear least squares fit. This demonstrates the validity of the "relaxed strain state" calibration technique. Noting that equations (2) and (3) simplify for the calibration tests ( $\sigma_{\max} = \sigma$ ,  $\sigma_{\min} = 0$ ,  $\theta = 90^\circ$ ), the equations

$$A = \frac{\epsilon_3 + \epsilon_1}{2\sigma_o} \quad (6)$$

$$B = \frac{\epsilon_3 - \epsilon_1}{2\sigma_o} \quad (7)$$

yield the required calibration coefficients. For acrylic, equations (6) and (7) give the values

# Determination of Calibration Constants for Acrylic

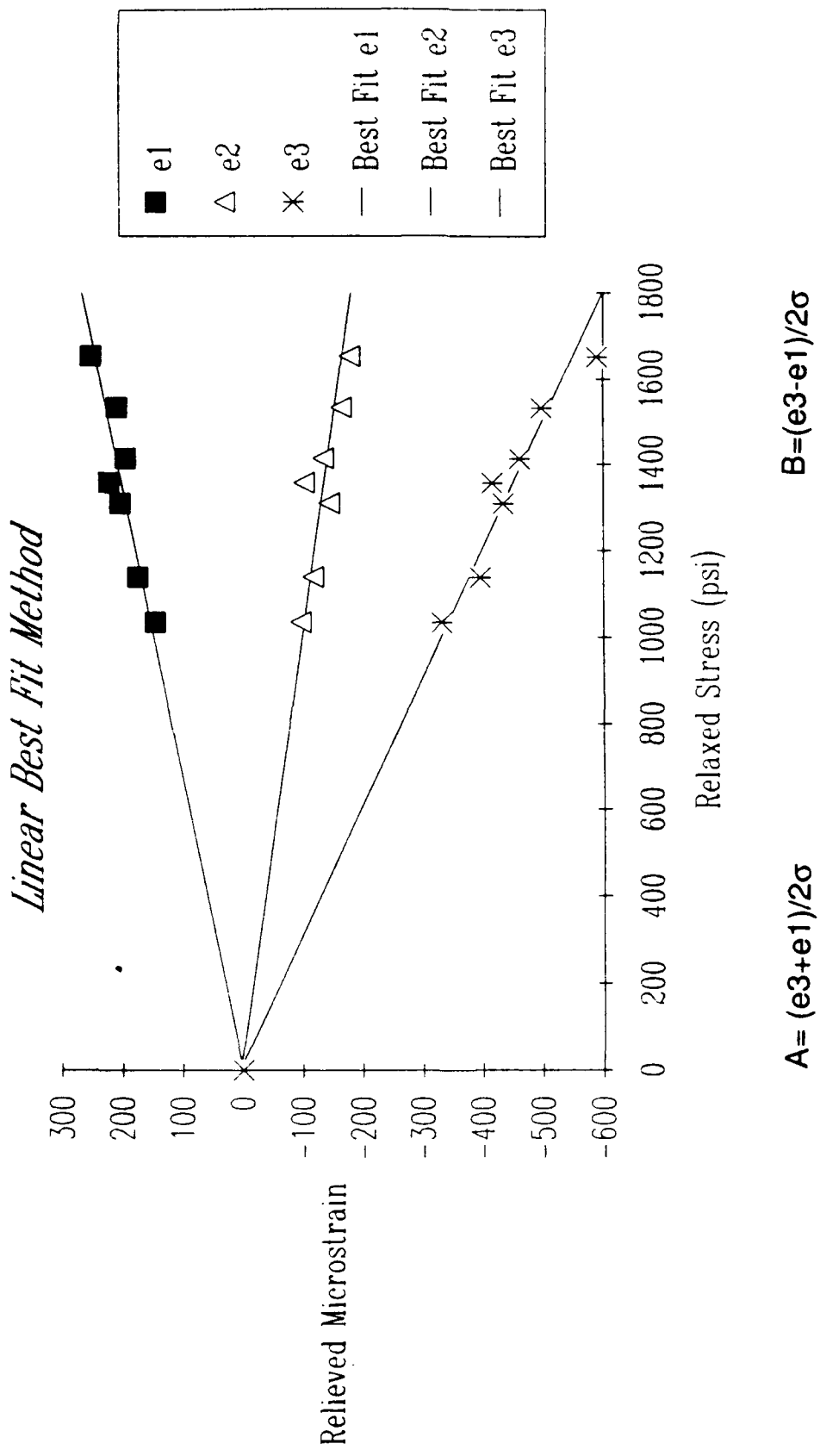


Figure 2.8. Strain Data from Acrylic Calibration.



$$A = -1.4712 \times 10^{-7} \text{in}^2/\text{lb} \quad (8)$$

$$B = -3.5215 \times 10^{-7} \text{in}^2/\text{lb} \quad (9)$$

These were the values used in all verification tests and subsequent canopy tests.

## 2.4 VERIFICATION TESTS

The use of the hole drilling technique strictly applies only to elastic materials. The use of the above "strain relaxed" calibration technique required a series of tests to verify the validity of the calibration constants for use in various load configurations. The test matrix included the following factors and specimen geometries:

- (a) Rosette orientation to principal stress direction
- (b) Uniaxial tension and compression
- (c) Uniaxial tension on curved surfaces
- (d) Biaxial stress on curved surfaces
- (e) Uniaxial tension in laminated transparency material.

The order and use of these tests permitted the identification of factors (such as surface curvature) which might adversely affect the accuracy of the method. Given the simplified extension of this technique to viscoelastic materials, an accuracy of  $\pm 10\%$  (measured vs. actual) for any particular tests was considered acceptable. All tests utilized the calibration technique of subtracting out strains after unloading to account for drill induced or locked in stresses. In addition, these experiments employed a different rosette type (TEA-06-062RE-120) which increased ease of installation because terminal strips and jumper wires were not required. The actual gage layout was identical to that of the rosettes used in calibration, and as shown in Table 2.4, the calibration coefficients are valid for this rosette type.

### 2.4.1 Uniaxial Tension and Compression

Figure 2.9 displays accuracy results for verification tests run in uniaxial tension and compression. Test samples retained the exact configuration as the calibration specimens. Antibuckling rails prevented buckling of the compression samples as seen on Figure 2.10. Previous work [12] indicated residual stresses in the range 300-2000 psi may exist in the acrylic layer. This work dictated the range of uniaxial verification loads used in this study.

TABLE 2.4

VERIFICATION OF HOLE DRILLING CONSTANTS  
FOR TYPE TEA-XX-062RK-120 ROSETTES

ROSETTE	STRESS (psi)			MAXIMUM PRINCIPAL STRESS ANGLE (degrees)	
	$\sigma_{\text{actual}}$	$\sigma_{\text{measured}}$	$\Delta\%$	$\beta_{\text{actual}}$	$\beta_{\text{measured}}$
A	1647	1694	2.85	90	89.8
B	1392	1375	-1.22	90	90.7
C	1627	1667	2.46	60	59.2
D	1389	1342	-3.38	45	45.2
E	1652	1602	-3.03	45	43.8

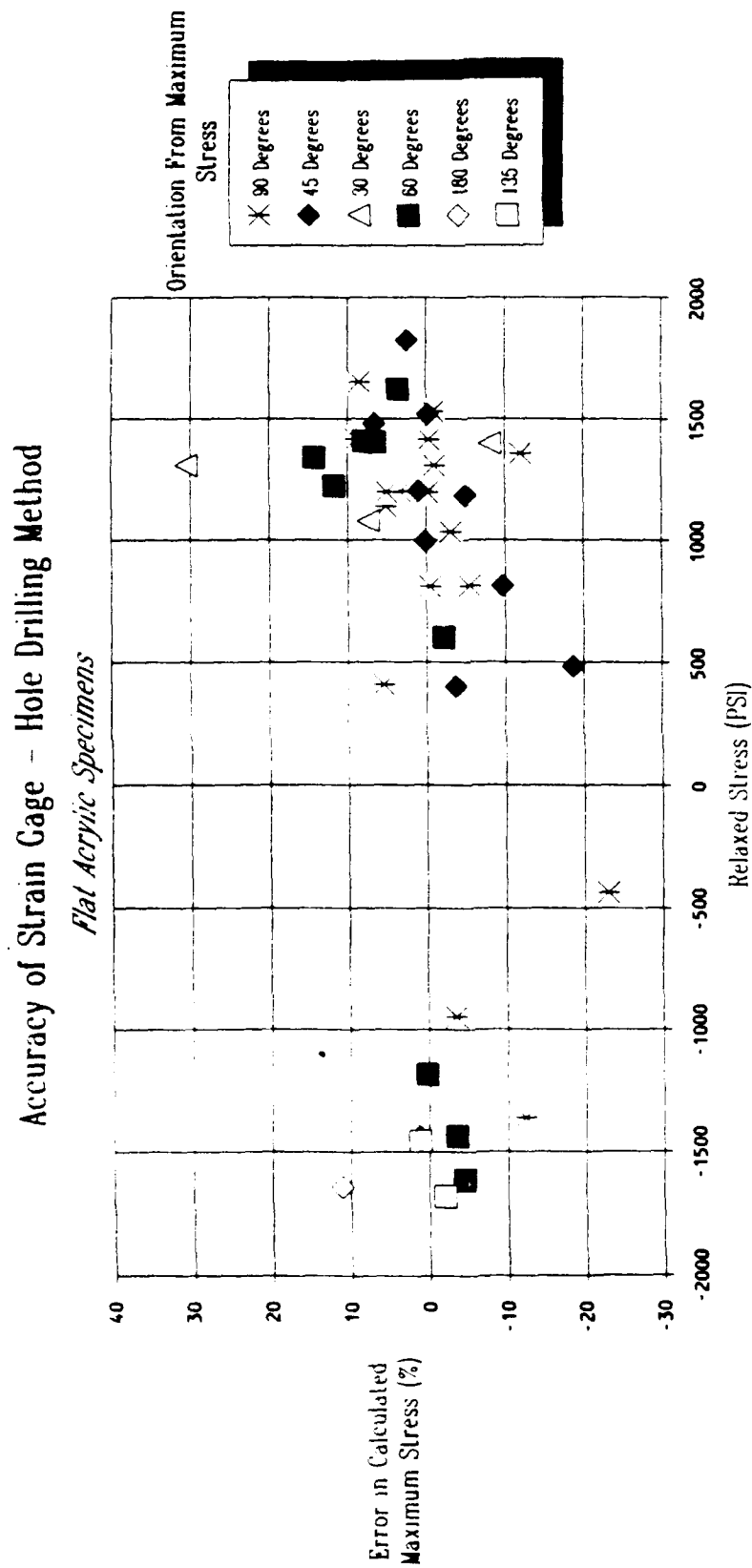


Figure 2.9. Uniaxial Verification Results.



Figure 2.10. Compression Verification Tests.

For 92% of the holes drilled, the error remained within  $\pm 12\%$ . The scatter shows no preferential toward positive or negative error, nor any increase in error with a particular rosette orientation. The inability of the material to relax in compression tests, due to friction from the antibuckling fixture, most likely accounts for the high error at -460 psi. Inaccurate centering of the drill accounted for the 30% error in the 30° rosette at 1300 psi. In addition, error below 500 psi appears no greater than error at high stress levels.

#### 2.4.2 Uniaxial Tension - Transversely Curved Surface

The curvature of an F-16 canopy surface imposes a possible additional source of error in residual stress measurement since the method is theoretically based on stress in a flat plate. Hole drilling tests on specimens with transverse curvature provided information to assess this error. Specimens cut lengthwise from a 10-inch ID acrylic tube (0.125-inch wall thickness) permitted application of test loads transversely to the direction of curvature, hence avoiding bending in the specimen. Specimen dimensions were identical to the tension/compression samples, except that the 1.500-inch width pertained to the width of a projection of the specimen onto a flat surface and not the distance across the actual specimen.

The results in Figure 2.11 demonstrate that transverse curvature does not affect the accuracy of the calibration constants. The hole drilling method maintains  $\pm 10\%$  accuracy over a 1500 psi range of uniaxial stress. Because the curvature of the specimens was greater than any curvature in the F-16 canopy geometry, these data indicate that field tests on actual canopies can neglect any curvature-induced error.

#### 2.4.3 Biaxial Stress - Curved Surface

Hole drilling on a pressurized 8-inch-diameter acrylic cylinder, Figure 2.12, permitted validation of the calibration constants for a curved surface under biaxial stress. This configuration most closely resembles the stress state in the canopy. Butyl rubber strips provided an air tight seal between the acrylic and rigid aluminum end plate. The combination of air pressure and compression on the end plates resulted in tensile hoop stresses and compressive longitudinal stresses. The maximum pressure in the cylinder imparted a 3.1% theoretical decrease in hoop stress through the thickness of the cylinder, resulting in an essentially uniform stress with depth. A maximum radial (Z direction from the surface) stress of -37 psi was negligible. Trimming with a precision dial indicator, Figure 2.13, ensured

# Accuracy of Residual Stress Determination on Transversely Curved ( $k=0.2$ ) Surfaces

*Constants From Flat Calibration Specimens.*

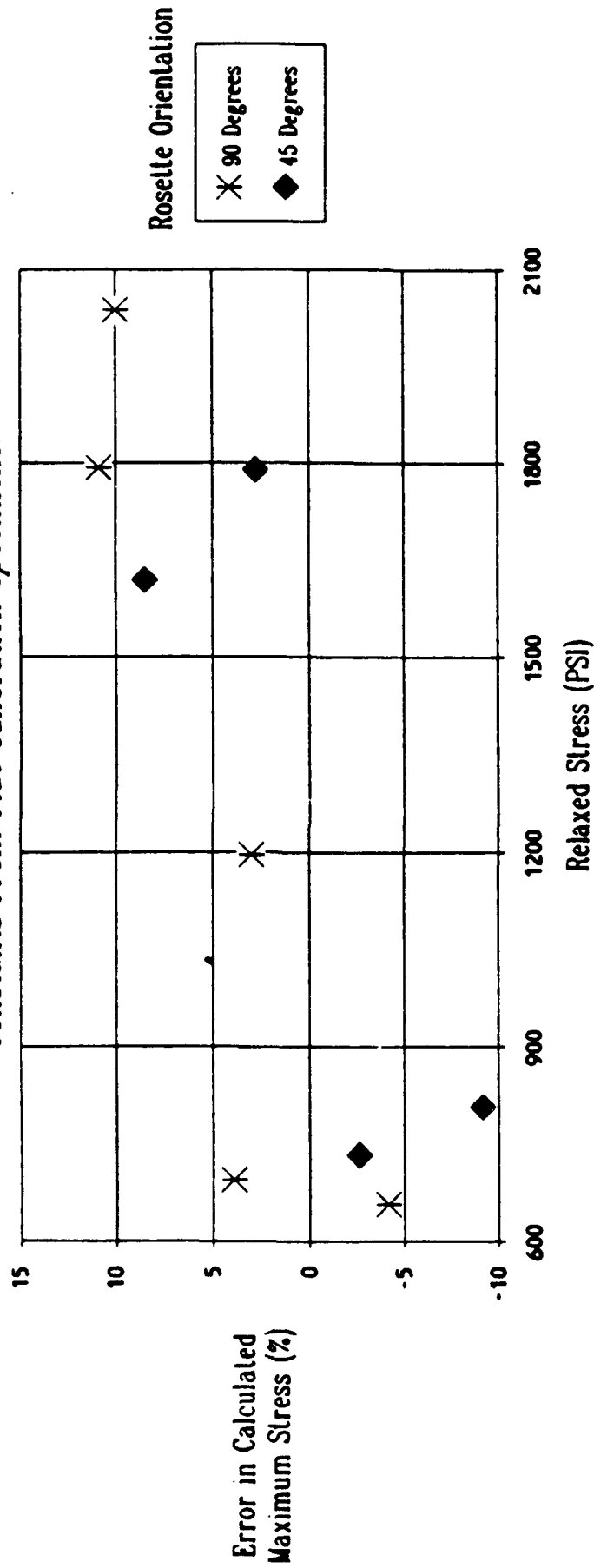


Figure 2.11. Curved Surface Uniaxial Verification Results.

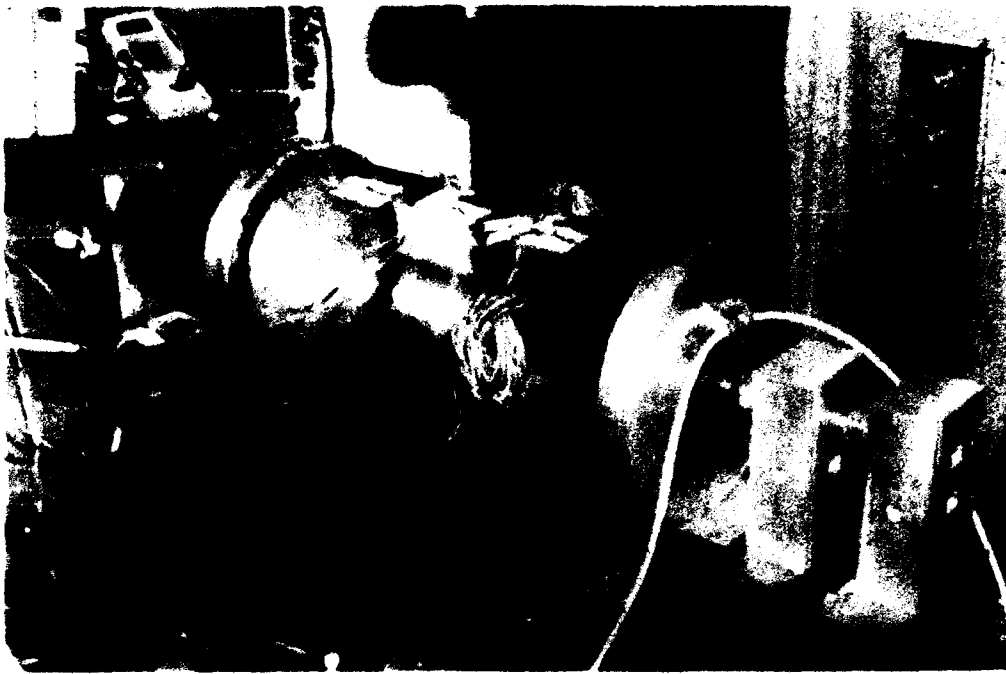


Figure 2.12. Curved Surface Biaxial Verification Test.



Figure 2.13. Tramming to Locate the Normal in Biaxial Verification Tests.

perpendicularity of the drill with the tube surface. A thin sheet of rubber attached to the inner surface of the tube prevented air from escaping after the hole was drilled.

Table 2.5 lists biaxial stress curved surface results. The accuracy shown is generally acceptable. Higher uncertainty (and hence error in the measurement) exists on the actual stress because the loading modes are mixed: pressure exerts a constant hoop stress, (and to some extent a constant longitudinal stress, due to the pressure balancing some of the load applied by the end plates), while the loading bolt induces a constant compressive displacement. Holes drilled without the aid of a microscope and without tramming produced the greatest errors in  $\sigma_{\max}$ . The constant pressure loading modes would produce the most error in the compression longitudinal stresses since constants were evaluated under specific constant strain ("stress relaxed") conditions. Table 2.5 shows this to be the case.

#### 2.4.4 Uniaxial Tension on Laminated Transparency Material

The final series of verification tests evaluated possible inaccuracies in hole drilling due to the laminated construction of the F-16 canopy. The tests involved two samples from each of two groups: untested acrylic/polycarbonate/urethane interlayer beams (from a previous study which evaluated candidate cross sections); and acrylic/polycarbonate/silicone interlayer beams sectioned from the top aft portion of an actual canopy. Table 2.6 shows the accuracy in measured stress is well within the 10-12% error band generated during the previous verification tests.

During these tests, the drill penetrated through the outer acrylic layer and partially into the soft interlayer. While this procedure apparently produces a "blind hole" (to which the calibration constants do not apply), previous work [6,13] has shown that drilling into the top 0.031 inch (for a 1/16-inch-diameter hole) of the surface produces the majority of the relieved strain. In addition, the soft interlayer is sufficiently compliant to allow expansion or contraction of the acrylic layer in a manner similar to that of a through hole in a thin sheet of monolithic acrylic. As these results demonstrate, the calibration constants are valid for the hole drilled through the acrylic outer ply of an F-16 canopy.



TABLE 2.5

## BIAXIAL/CURVED SURFACE HOLE DRILLING SUMMARY

Rosette	$\sigma_{\max}$ (psi)			$\sigma_{\min}$ (psi)			$\beta$ (degrees)	
	Actual	Meas.	% Error	Actual	Meas.	% Error	Actual	Meas.
A*	1000	998	-0.2	- 336	-88.5	163.0	0	5.91
B*	1000	1159	13.7	- 258	-316	22.5	90	94.3
C* <sub>+</sub>	1000	774	-22.6	- 535	-866	61.9	0	1.85
D** <sup>+</sup>	750	992	32.3	- 650	-655	0.78	135	134.0
E*	927	813	-12.3	- 799	-1652	106.0	0	1.31
F	1000	1053	5.3	-1032	-1277	23.8	0	3.25
G	750	873	16.4	-1186	-1352	14.0	90	88.3
H	800	916	14.5	- 851	-937	10.1	0	1.48
I	1200	1289	7.4	- 764	-962	27.0	135	134.0

\*Perpendicularity of drill with tube surface estimated.

<sup>+</sup>Drilled without aid of centering scope.

TABLE 2.6

## LAMINATED BEAM HOLE DRILLING SUMMARY

Rosette	SIGMAX (psi)			SIGMIN (psi)		BETA (deg)	
	Actual	Meas	%Err	Actual	Meas	Actual	Meas
A	2260	1990	12	0	173	90	88.6
B	1000	932	6.8	0	58	90	87.1
C	2000*	1840	7.9	0	63.7	90	89.1
D	1550*	1380	10	0	44.9	90	91.8

\*Stress calculated analytically to account for bending in specimen.

## 2.5 SUMMARY

A series of calibration tests for the strain gage hole drilling technique produced the following calibration constants:

$$A = -1.4712 \times 10^{-7} \frac{\text{in}^2}{\text{lb}}$$

$$B = -3.5215 \times 10^{-7} \frac{\text{in}^2}{\text{lb}}$$

for use in determining residual stress in laminated aircraft transparency outer plies.

Verification tests on various specimen geometries under various load conditions showed the calibration technique to yield accurate residual stress measurements down to 200 psi (the lowest stress level tested).

## SECTION 3

### DESIGN OF A PORTABLE DRILLING UNIT FOR USE ON COMPOUND CURVED SURFACES

Commercially available strain gage hole drilling hardware lacks several key features considered critical in applying the technique to aircraft transparencies. This section discusses these features and their implementation in a new device designed to drill holes in the acrylic ply of aircraft transparencies.

#### 3.1 SYSTEM REQUIREMENTS

Because the hole drilling method relies on accurate measurement of stress gradients in a small area, the means of introducing the hole must adhere to several critical requirements. These include the following:

- ***Accuracy of aligning the hole in the center of the rosette.*** Previous work has shown that holes must be drilled within  $\pm 0.0015 d$  ( $d$  is the diameter of the gage pattern) to ensure accurate results. A 1/16-inch-diameter hole must be drilled within 0.001 inch to avoid significant error.
- ***Accuracy in aligning the hole normal to the surface.*** Little work in the literature addresses the issue of the accuracy in stress measurement for holes not drilled perpendicular to the surface. Nonperpendicular drilling creates holes that become "off-center" with depth, and results in elliptical holes. While no work could be found which addresses this issue, an error of  $0.5^\circ$  from perpendicular for a 0.0625-inch-diameter drill creates a hole with a major axis of 0.062502 inch. This is within uncertainty for the drill itself and represents acceptable error. The system requirement for perpendicularity was therefore chosen to be  $\pm 0.5^\circ$ . Angles greater than this result in rapidly increasing error.

- ***Drilling stress free.*** Stresses produced in the material by introduction of the hole will induce error in residual strain readings since the rosette responds to strain relieved from all sources of stress. Figure 3.1 shows the theoretical error produced in residual stress readings as a function of nominal uniaxial stress and extraneous strain induced in the rosette (this strain may come from any source, including drill induced stress). As the figure presents, the drilling operation must induce less than 12µε in each gage to retain an uncertainty of less than 10% at 500 psi.

Figure 3.2 presents results of a preliminary study to determine the optimum means of introducing the hole into acrylic in a stress free manner. The methods which were tested corresponded to those suggested by ASTM E837-85 and other references. A precision jig borer provided accurate speed and feed control for introducing holes into samples of "pre-shrunk" (annealed) cast acrylic under zero load. Measurements Group, Inc., type TEA-06-062RK-120 rosettes proved most convenient for these tests. A P3500 Strain Indicator and SB10 Switch and Balance Unit (also from Measurements Group, Inc.) displayed the relieved strain.

Reverse cone carbide cutters and end mills are frequently used in hole drilling metals. They proved ineffective in the acrylic. The use of lubricants with the carbide cutter resulted in a decrease in residual strain, but not to a sufficient degree to warrant its use. High speed (100,000 rpm) drilling using the carbide cutter (another method widely employed in metals), conducted in unloaded preshrunk acrylic, resulted in enormous residual strains (Figure 3.3). This likely generated enough friction heat to degrade the polymer, resulting in high drill-induced stress. As the figure demonstrates, ordinary high speed steel twist drills produced the lowest "machining induced" strains.

Figure 3.4 displays a portion of the results of additional jig borer tests and demonstrates the desirable feature of automatically controlled feed and speed. The jig borer on which tests were conducted drilled automatically at various rates and at 0.001 inch/rev or 0.003 inch/rev feed rate. Drill retraction occurred automatically at the same rate as penetration, or manually at much faster rates. Since the feed rate was directly proportional to speed on the jig borer, effects of speed and feed rates are indistinguishable. However, for the drill speeds being

# Effect of Error in Measured Strain on Residual Stress Measurement

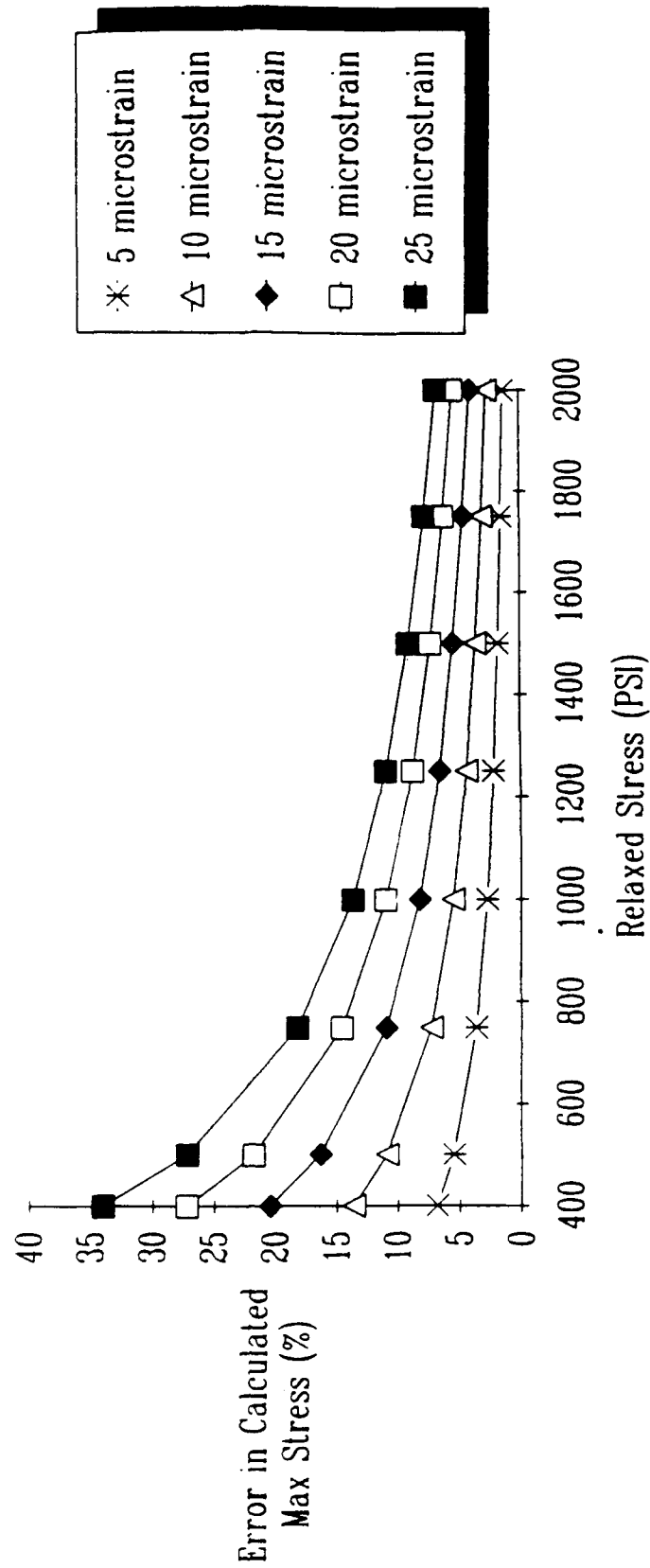


Figure 3.1. Theoretical Residual Stress Error.

# Machining Induced Microstrain

## Averaged Absolute Values

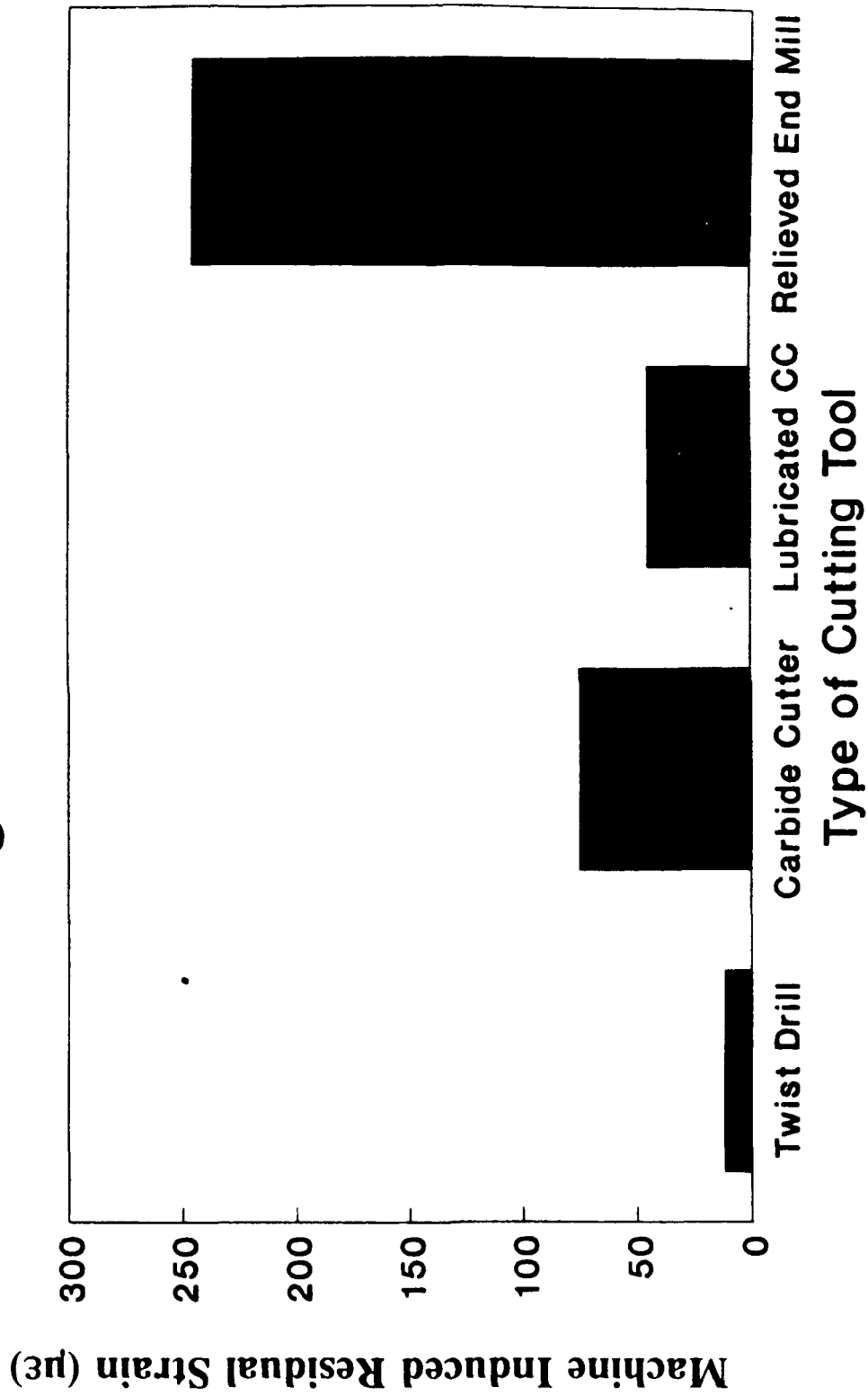


Figure 3.2. Optimal Machining Methods for Acrylic.

### Strain Gage Output of Rosette C (Test 3)

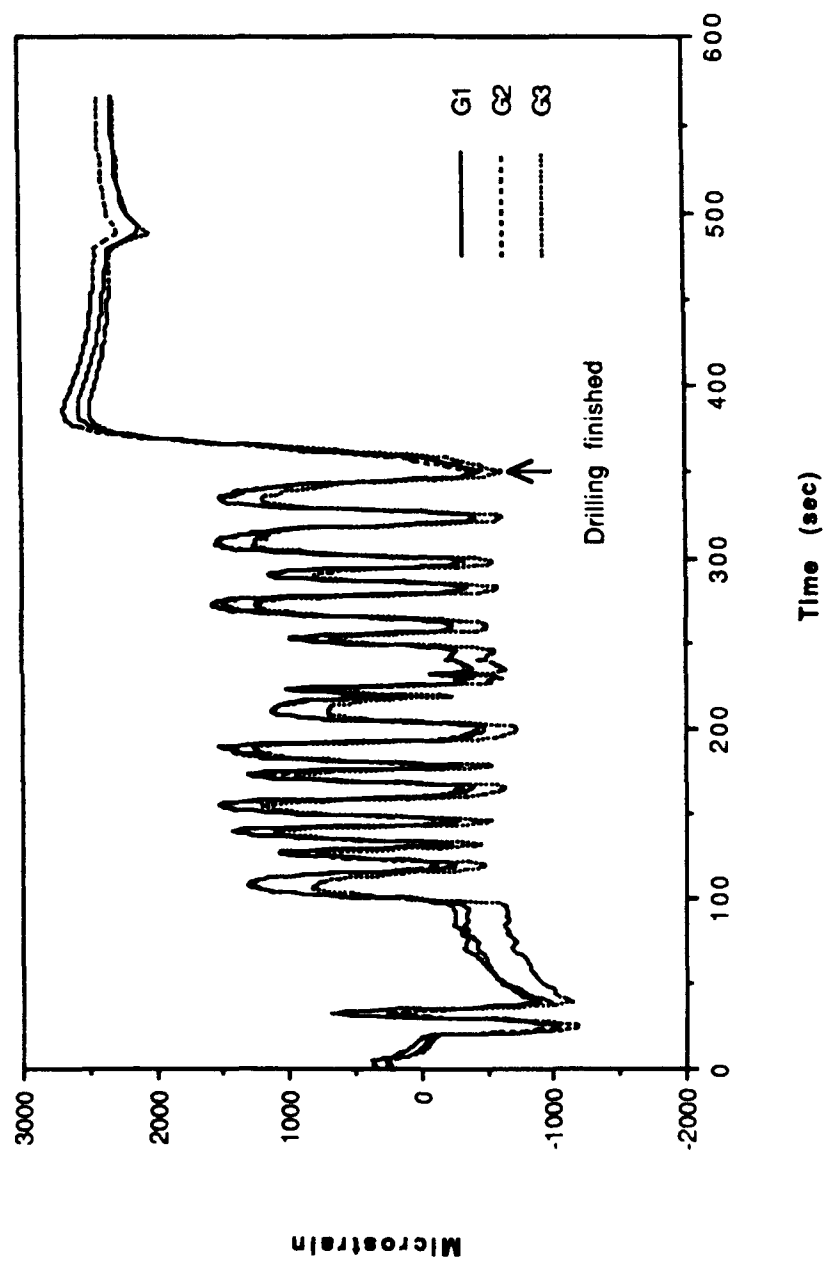


Figure 3.3. High Speed Air Turbine Machining Induced Stress.



## Drill Induced Strain

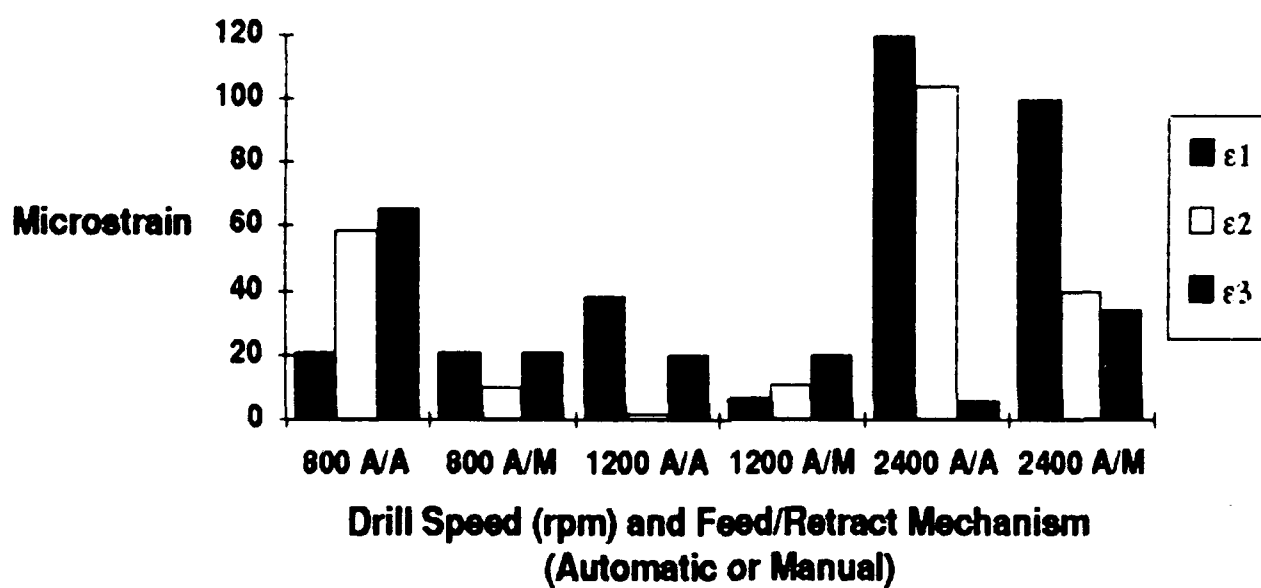


Figure 3.4. Optimal Drilling Parameters.

considered, the pressure of the tool on the acrylic, and hence the feed rate, most likely influences residual strain levels to a greater degree than the drill speed. The desire to reduce both drill pressure and drill time led to a compromise selection of 1200 rpm and 0.001 inch/rev as the optimal speed and feed for drilling. Based on these tests, rapid drill retraction was also required.

### 3.2 DRILLING DEVICE, DESIGN DRIVERS, AND FEATURES

The above system requirements led to the design and fabrication of the device pictured in Figure 3.5. Described by the acronym VALAPODD (Vacuum Attached Laser Aligned Portable Drilling Device), the unit consists of a base, alignment and drilling components, a control unit, and an external drill motor. The components were built with three design drivers in mind: portability, X-Y and  $\Theta$  adjustability, and the ability to automatically drill in a stress-free manner. These design drivers, and the components which satisfy them, are briefly discussed below.

- **PORTABILITY.** The desire to use the device to quickly collect data from in-service transparencies required the device to be portable. Figure 3.6 highlights vacuum cups at the bottom of the base's swivel feet, which allow quick and convenient attachment. Vacuum lines run from a central manifold positioned on the base. A low consumption venturi type vacuum pump, housed in the control unit, supplies 25-in hg vacuum at 60 psi, thus requiring only a compressed air source to secure the unit. The vacuum is sufficient to firmly attach the unit to the side of the canopy, oriented 90° to the upright position.

- **X-Y AND  $\Theta$  ADJUSTABILITY.** The base of the unit is essentially an optical translation stage with a 2-inch-diameter hole through the center. Micrometers, Figure 3.6, permit smooth and accurate x-y motion used to center the base over the rosette target. Each leg consists of a threaded canister portion, vacuum cups, and locks. Spherical bearings connecting the vacuum fittings to the threaded canister portion allow the feet to rotate as the canister heights are adjusted to bring the base perpendicular to the rosette surface. Locking rings on the canisters and jamming rods on the bearings rigidly fix the orientation of the base.

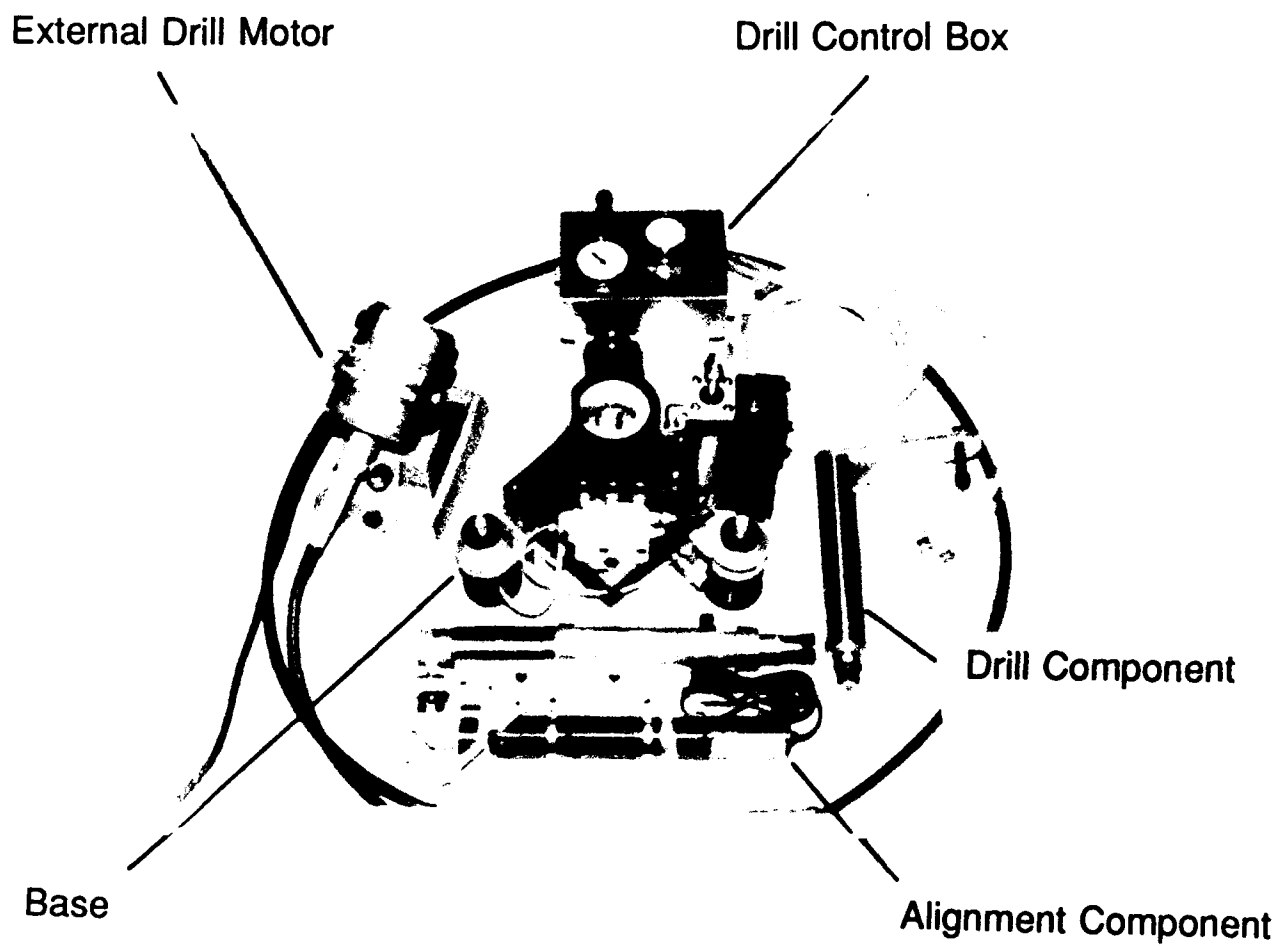


Figure 3.5. Vacuum Attached Laser Aligned Portable Drilling Device.

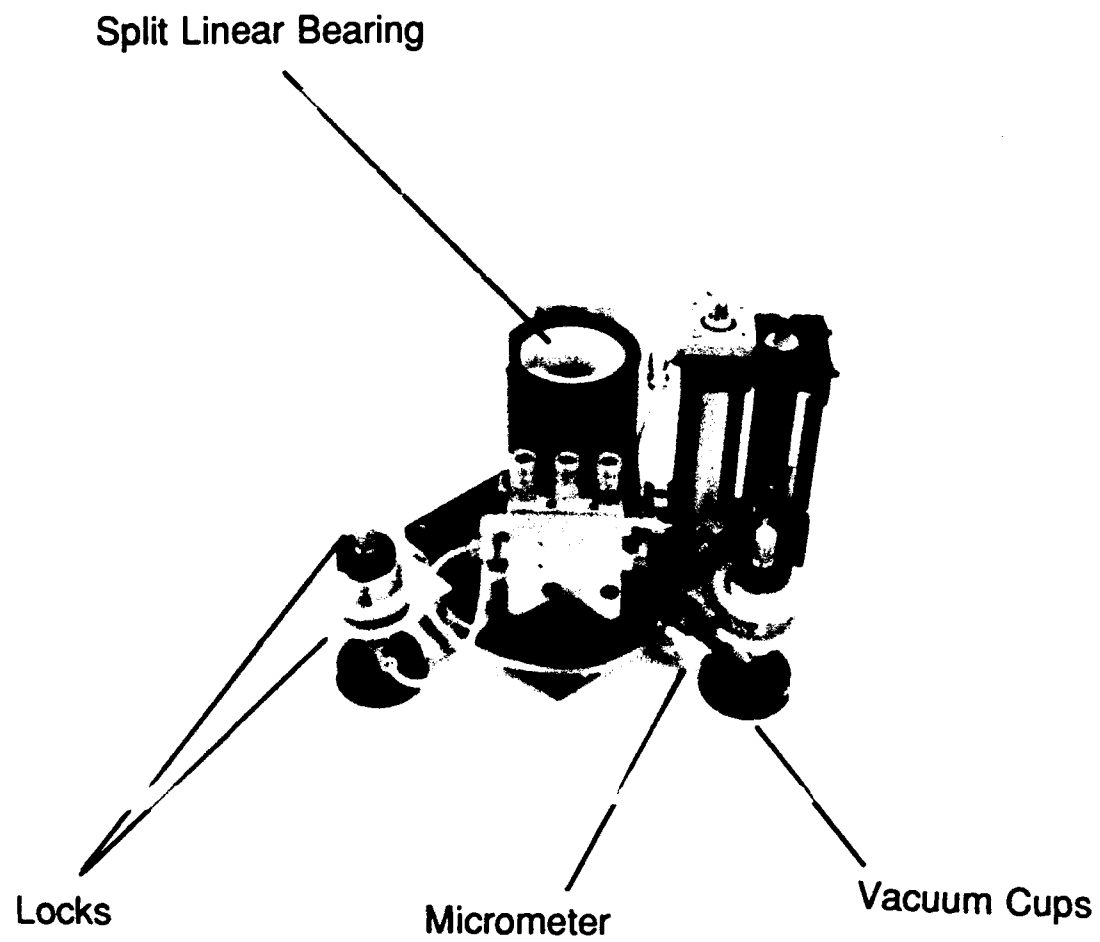


Figure 3.6. Front View of VALAPODD Base.

The alignment component consists of a 40x microscope for centering and a 0.5-mW HeNe laser for aligning normal to the surface. A cylindrical collar, mounted to the base, houses a split linear bearing which serves as an aligning journal for the device (see Figure 3.6). The microscope portion of the alignment unit, Figure 3.7, slides into the bearing. Centering of the unit is achieved by adjustment of X-Y micrometers in the translation stage so the microscope cross-hair reticle is centered on the rosette target.

The laser portion serves as the mechanism for aligning the device normal to the surface, as a laser reflection back along its original path indicates that the laser is perpendicular to the surface. Figure 3.8 displays a schematic of the microscope and laser in tandem. A series of beam splitters directs the polarized laser beam to a path collinear with the optic path of the microscope. The optic components then direct the laser reflection from the surface to a target mounted alongside the laser. Perpendicularity is achieved by adjusting the threaded canisters so that the reflection falls on the target cross-hairs. Perpendicularity can be aligned to within  $\pm 0.25^\circ$  using this system.

Centering with the micrometers may initially move the device away from a perpendicular orientation, just as adjusting the orientation throws the unit off center. Complete adjustment of the unit to center the journal over the rosette target and align the device normal to the drilled surface is therefore an iterative process. Two to three iterations usually suffice.

- **AUTOMATIC STRESS-FREE DRILLING.** Figure 3.9 displays the drilling component inserted into the alignment bearing. The component consists of a steel sleeve around a handpiece from a flexible shaft electric drill. A connecting bar attaches the drill component to an air cylinder and an adjustable viscous damper. The cylinder and damper, mounted to the base, serve to power the drill feed and control the drill feed rate, respectively. The damper is adjusted to feed the drill component at 1.2 ipm with 60 psi pressure in the air cylinder. Compressed air inlet and outlet lines run from the cylinder through the manifold mounted on the base. A three-way valve in the control unit, Figure 3.10, directs the air flow, and therefore specifies the "drill" or "retract" motion of the drill component.

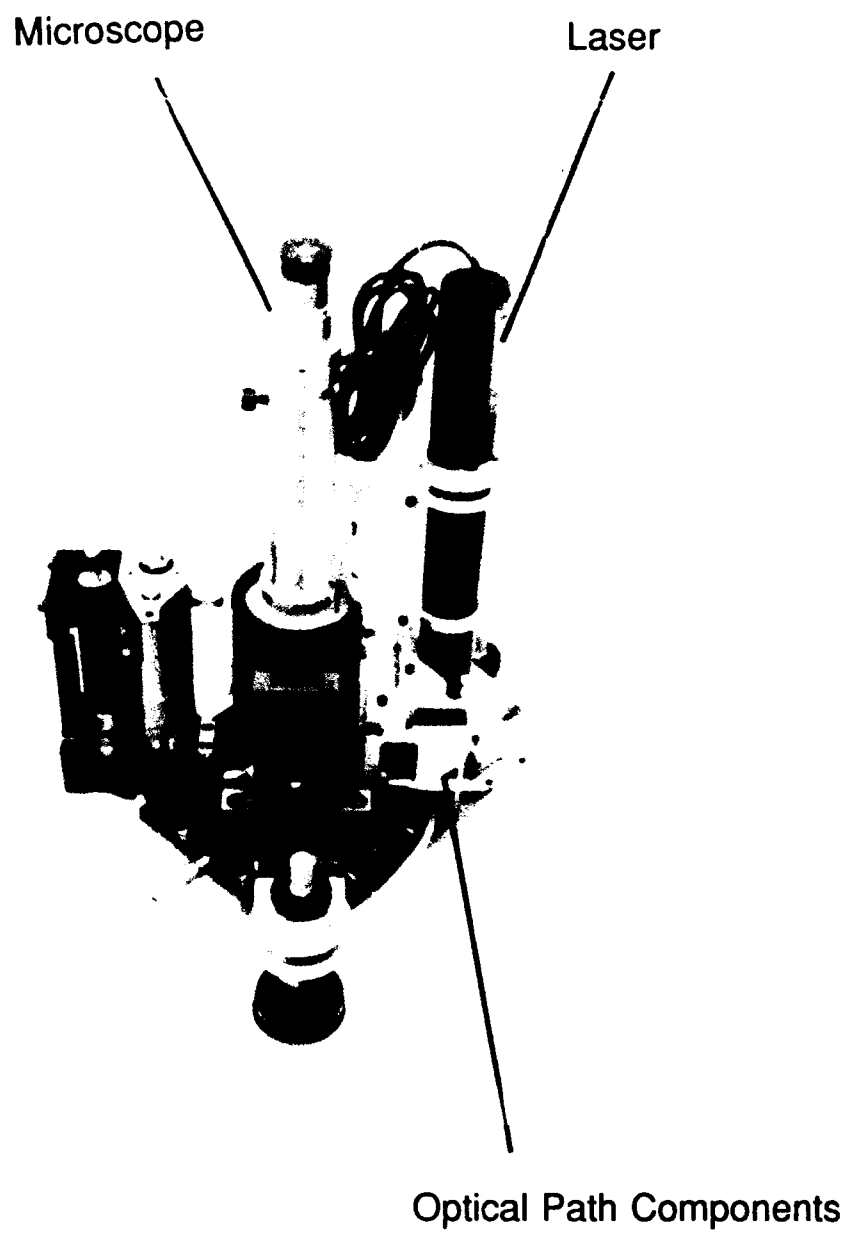


Figure 3.7. VALAPODD Alignment Configuration.

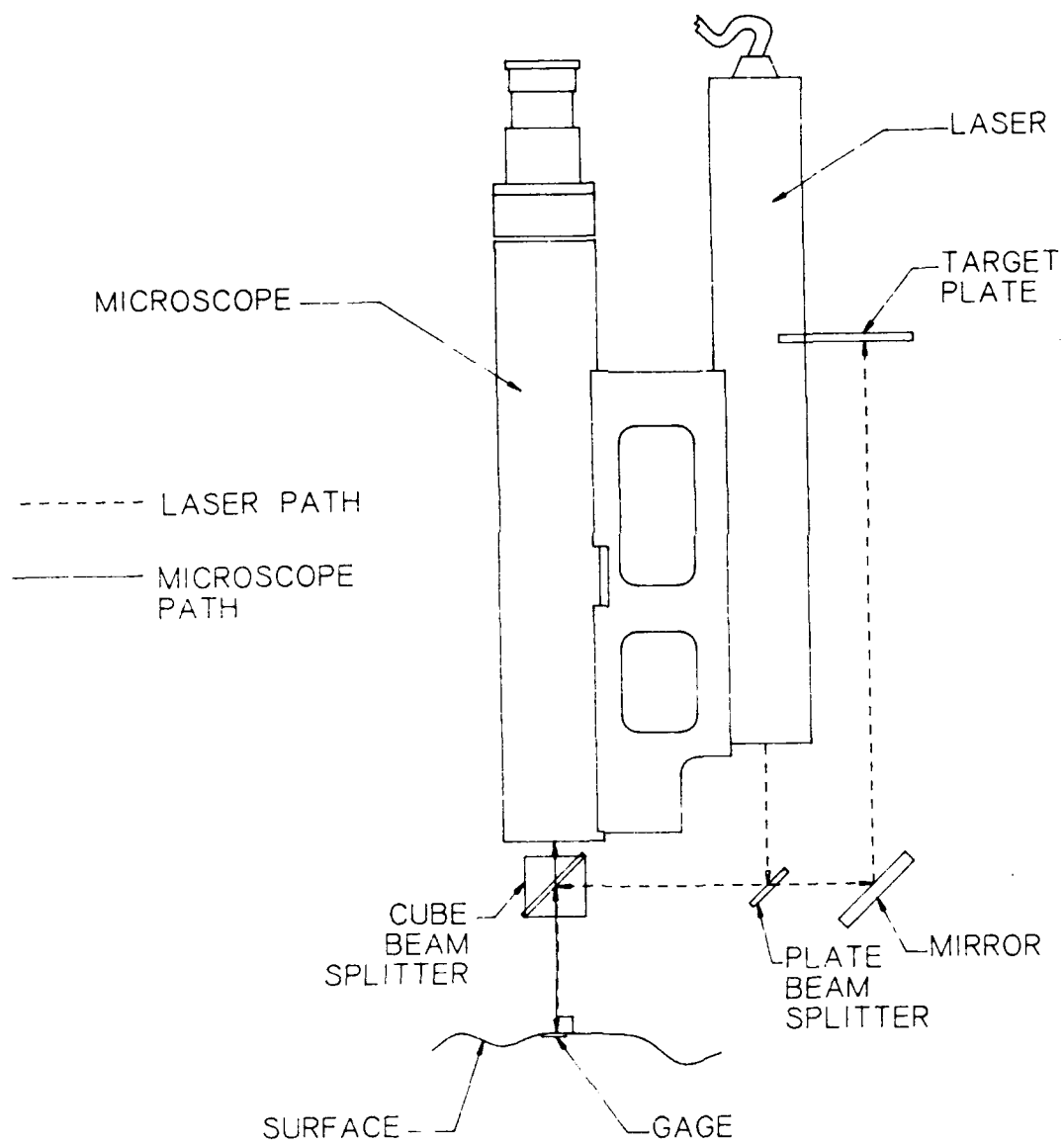


Figure 3.8. Optical Paths in Alignment Components.

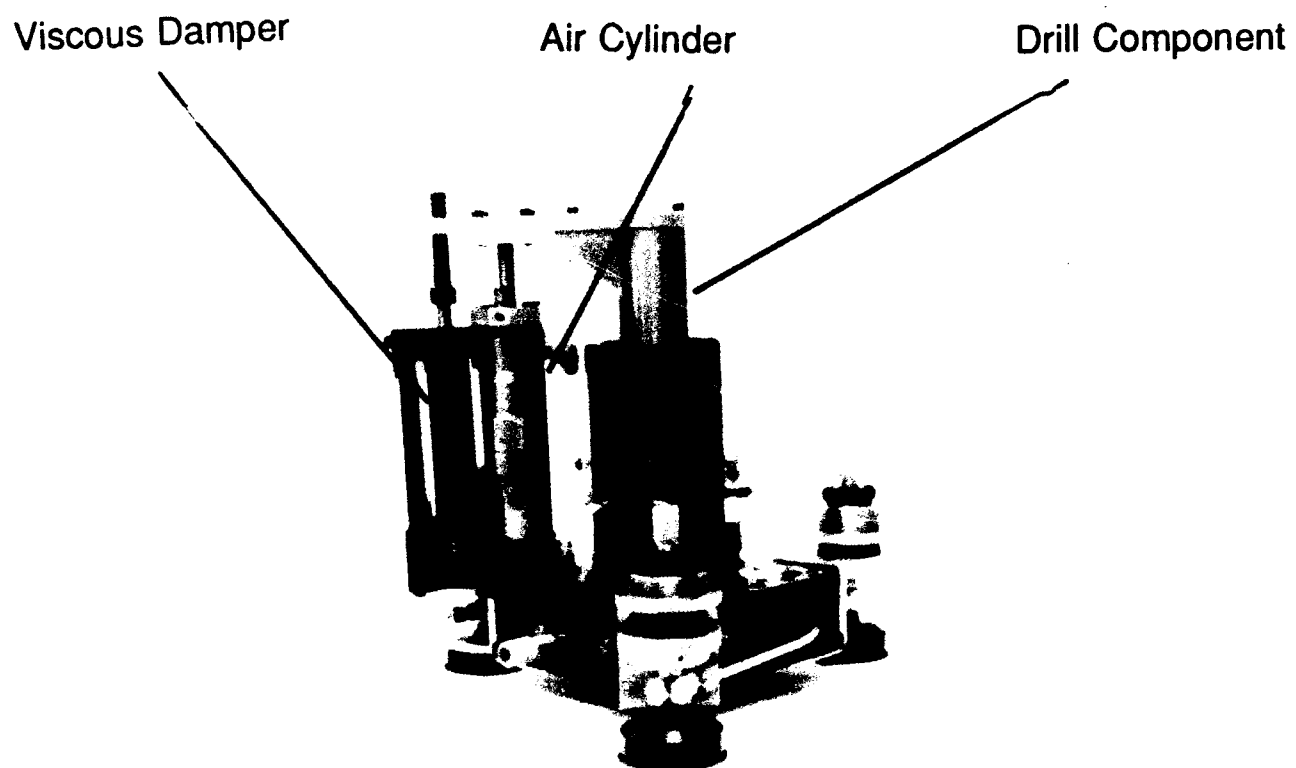


Figure 3.9. VALAPODD Drilling Configuration.



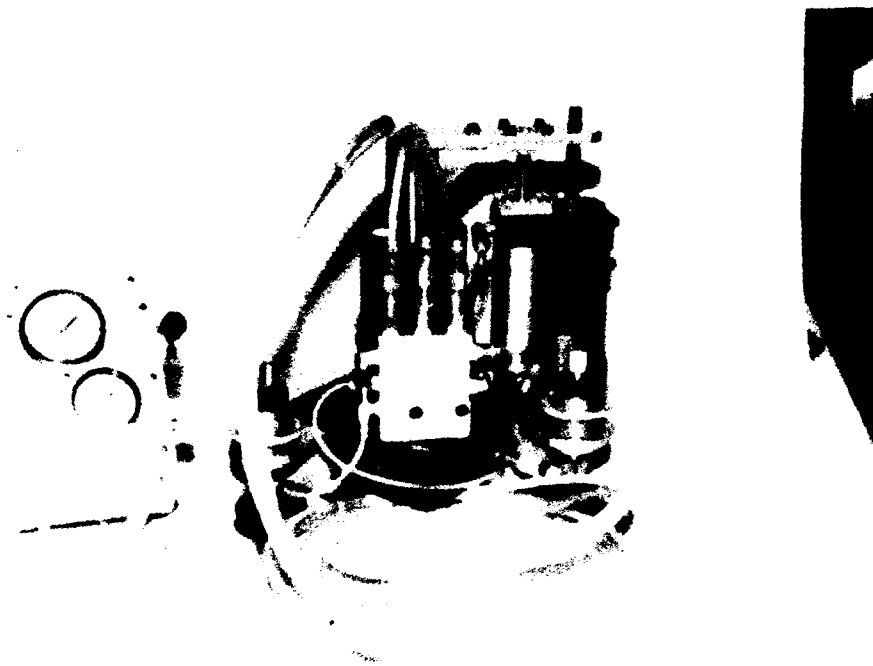


Figure 3.10. Vacuum, Air Feed Lines, and Control Box.

The flexible shaft, Figure 3.11, extends into the steel sleeve and connects the external drill motor to the drill component. A micrometer mounted on the air cylinder and butted against the connecting bar allows control of the depth the hole is drilled.

### 3.3 STRESS FREE DRILLING VERIFICATION AND PERFORMANCE

Hole drilling tests on instrumented samples loaded to known stress levels provided a means for verifying that the device would introduce holes in a stress free manner. Annealed acrylic samples were loaded in a small tension fixture equipped with load cell instrumentation. Holes drilled at various uniaxial stress levels gave an indication of the machining induced stress. Table 3.1 displays the results of these tests, based on the stress measured compared to the known stress. A large discrepancy between measured stress and actual stress would indicate high drilling induced stress. The error band of less than 10% indicates the device performed within the required limits and specifications for stress over 500 psi. Note the high percentage errors are due to the low absolute values of the stresses which are being measured.

The device performed well in measurements in all areas of the canopy, including those in which the device was mounted 90° to the vertical (Figure 3.12). Measurements taken after drilling of free state canopies (Section VI) showed the hole misalignment to average 0.00104 inch, with 47 of the 60 holes misaligned less than 0.0006 inch (the resolution of the micrometer).

Appendix A contains a step-by-step procedure for use of the VALAPODD. Appendix B contains mechanical drawings of the VALAPODD components.

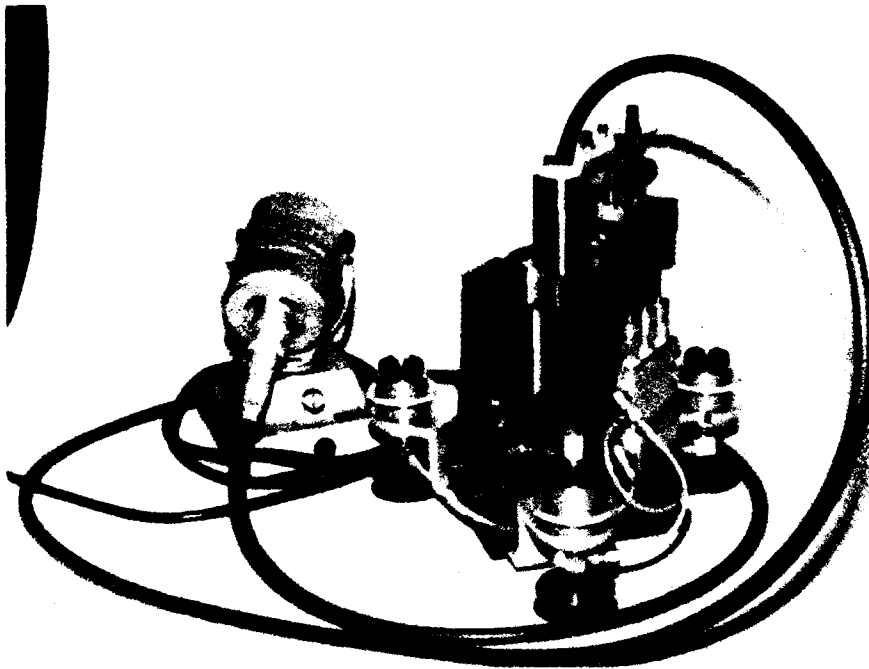


Figure 3.11. External Drill Motor and Flexible Shaft.

**TABLE 3.1**  
**VALAPODD VERIFICATION RESULTS**

Rosette	Measured Beta (deg)*	Measured $\sigma$ max (psi)	Measured $\sigma$ min (psi)	$\sigma$ Actual	% Error
VP1-1	91.93	51.71	-46.27	18.21	-64.78
VP1-2	85.51	55.39	15.37	33.96	-38.69
VP1-3	93.07	553.82	28.61	522.98	-5.57
VP2-1	87.28	1092.76	39.44	1110.17	1.59
VP2-2	91.4	1621.33	0.77	1613.22	-0.5
VP2-3	88.44	1988.51	79.93	1852.47	-6.84

\*Actual angle is 90°.

Strain Indicator



F-16 Tabletop Pressure Fixture

Figure 3.12. Hole Drilling on Installed and Pressurized F-16 Canopy.

## SECTION 4

### SECTIONING METHOD

#### 4.1 INTRODUCTION

Although calibration and verification tests indicated that hole drilling could produce acceptable residual stress data, a second method of determining these stresses on actual canopies would provide additional evidence to support the validation of hole drilling. The sectioning method is a well documented, although destructive, procedure for measuring residual stresses. Sectioning of two canopies after hole drilling and comparison of results provided confidence on the drill technique as well as a coarse mapping of stresses along the canopy surface.

Sectioning is a method closely associated with hole drilling in that removal of material around a strain gage rosette releases residual stresses resulting in strain changes in the material which the rosette can detect. The advantages are simplicity: ordinary rosettes are utilized in conjunction with simple coupon removal using any cutting mechanism. The disadvantages include uncertainty in the coupon size, since coupons must be cut as small as possible to relieve all the residual stress, while large enough so that cutting stresses do not influence readings; difficulty in cutting around gage lead wires; and the possible necessity of disconnecting gages from instrumentation and reconnecting, thus inducing resistance changes not attributable to mechanical load. These considerations led to the test techniques described in the following sections.

#### 4.2 CALIBRATION

The equations to reduce rosette strain data to principal stresses and directions are well known and documented [14]:

Maximum Principal Stress =

$$\sigma_p = \frac{E}{1-\nu^2} \left[ \frac{\epsilon_1[(1+\nu)\sin^2\phi + (1-\nu)] + \epsilon_2[(1+\nu)\cos^2\phi - (1-\nu)]}{(\cos^2\phi + \sin^2\phi)} \right] \quad (10)$$

Minimum Principal Stress =

$$\sigma_q = \frac{E}{1-\nu^2} \left[ \frac{\epsilon_1[(1+\nu)\sin 2\phi - (1-\nu)] + \epsilon_2[(1+\nu)\cos 2\phi + (1-\nu)]}{(\cos 2\phi + \sin 2\phi)} \right] \quad (11)$$

$$\text{Angle to Max Stress} = \phi = \frac{1}{2} \tan^{-1} \left( \frac{\epsilon_1 - 2\epsilon_2 + \epsilon_3}{\epsilon_1 - \epsilon_3} \right) \quad (12)$$

However, the mechanical properties necessary for these equations may vary widely from published data. A series of calibration tests provided mechanical property data to ensure accurate measurement of stresses in the canopy.

Recasting the strain gage equations in a form similar to the hole drilling equations provided a uniform means for calibration. Setting constants A and B to the following expressions:

$$\bar{A} = \frac{E}{1+\nu} \quad (13)$$

$$\bar{B} = \frac{E}{1-\nu} \quad (14)$$

and substituting into the above strain gage equations results in the following expressions:

$$\sigma_{\max} = \frac{\epsilon_1(A + B\sin 2\phi) - \epsilon_2(A - B\cos 2\phi)}{\cos 2\phi + \sin 2\phi} \quad (15)$$

$$\sigma_{\min} = \frac{\epsilon_2(A + B\cos 2\phi) - \epsilon_1(A - B\sin 2\phi)}{\cos 2\phi + \sin 2\phi} \quad (18)$$

The constants A and B may be determined by orienting a strain rosette with the number 1 gage aligned with the load in a uniaxial tensile test, taking strain data, and using the following equations:

$$\bar{A} = \frac{\sigma}{2(\epsilon_1 - \epsilon_2)}$$

$$\bar{B} = \frac{\sigma}{2\epsilon_2}$$

In this study, six rosettes bonded to a single 1/8-inch-thick acrylic specimen and pulled in tension with the same fixture used in calibrating hole drilling specimens furnished the stress/strain data for calculating A and B. The use of seven stress levels and a weighted least squares fit ensured average values for A and B (as in the hole drilling calibration). Figure 4.1 displays the results of the calibration as well as the A and B values obtained.



# Calibration Curve for Sectioning Rosettes

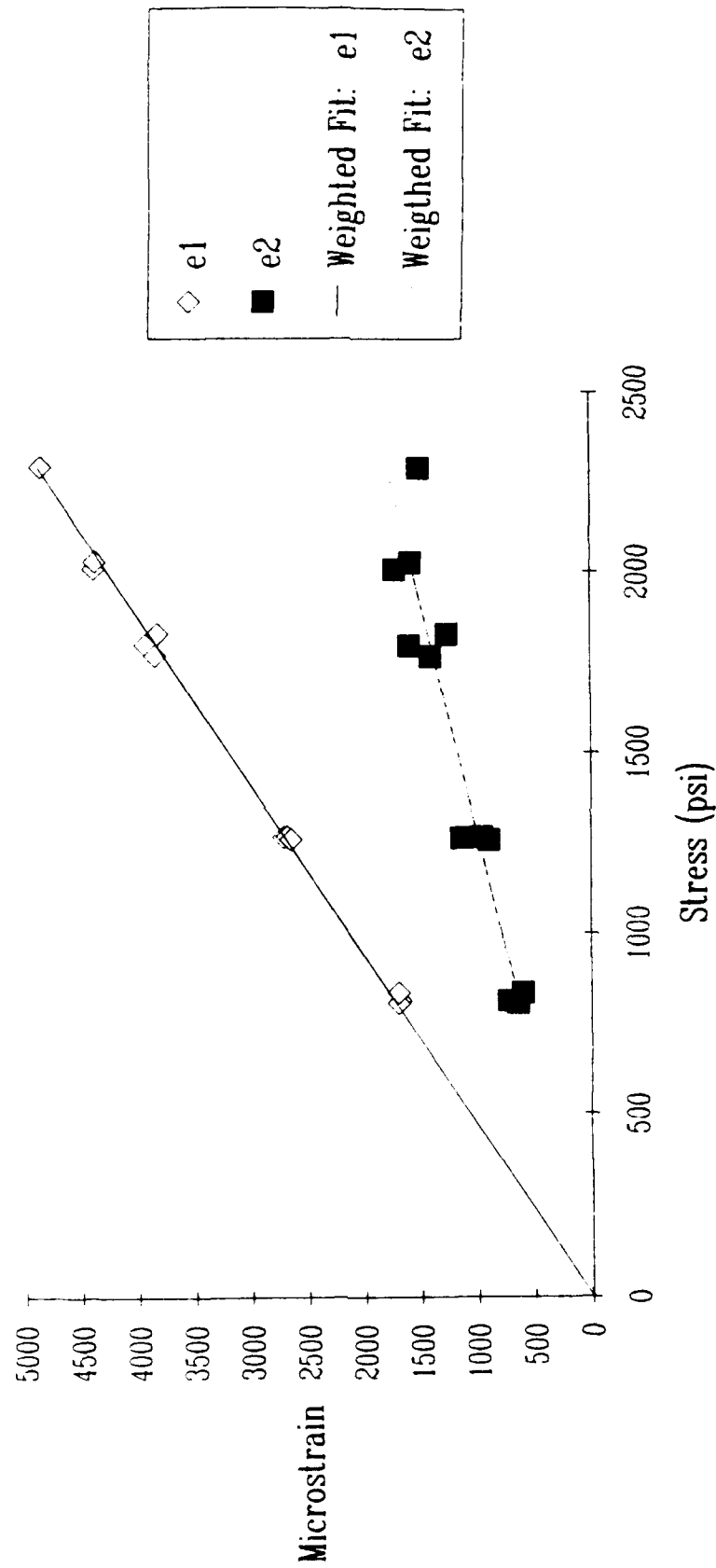


Figure 4.1. Strain Data from Regular Rosette Calibration.

## SECTION 5

### PRELIMINARY DETERMINATION OF STRESSES IN LAMINATED F-16 CANOPIES

#### 5.1 TEST SPECIMENS


The preliminary work consisted of instrumenting and testing two F-16 canopies: a Texstar canopy (removed from service) with two small crazing patches on the forward left side of the canopy, and a new, optically rejected Sierracin canopy. Both canopies were laminated with 0.125 inch nominal acrylic face plies. The canopies were designated T1 (Texstar) and S1 (Sierracin).

#### 5.2 ALIGNMENT FACILITY/GAGE LAYOUT

Figure 5.1 shows the gage types used for the sectioning work. The use of either particular type depended greatly on availability from the manufacturer at the time the gages were ordered. The preattached terminal wires on the EA-06-125RA-120 provided lead wire attachment points sufficiently far from the rosette to prevent solder heat damage from migrating into the gage grid area. The encapsulation of CEA-06-125UR-120 also prevented this damage. Although the gages were thermally matched to steel, the use of a compensation gage in the bridge circuit eliminated thermal strain errors.


Lead wires attached to these gages terminated in bullet type connectors (Figure 5.2). Short lead wires which could be easily folded permitted easier machining of specimens. The use of connectors resulted in rapid sweeping of the rosettes during readings (each rosette required attaching and unattaching the leads to the strain instrumentation). However, since the connection was in series with the gages, and the initial connection could never be exactly repeated, the change in resistance due to contact changes induced an uncertainty of  $\pm 15\mu\epsilon$  in the strain readings. Bullet connectors appeared to be the best compromise between convenience and repeatability in a series of tests with various connectors which included hook, miniclips, banana jacks, and screw type binding posts.

The layout and orientation of rosettes posed a problem due to a lack of reference points on the canopy and the curvature of the surface. The reference frame formed from waterline and fuselage stations coordinate axes appeared the most convenient and easily understood basis for orientation and positioning of rosettes. Figure 5.3 displays a modified

<b>125RA</b>			
			
GAGE LENGTH	OVERALL LENGTH	GRID WIDTH	OVERALL WIDTH
0.125 ES	0.275 CP	0.062 ES	0.424 CP
<b>3.18 ES</b>	<b>6.99 CP</b>	<b>1.57 ES</b>	<b>10.77 CP</b>
<i>Matrix Size</i>		0.39L x 0.46W	9.9L x 11.7W

# 125UR

## 'C' FEATURE



GAGE LENGTH	OVERALL LENGTH	GRID WIDTH	OVERALL WIDTH
0.125 ES	0.300 CP	0.060 ES	0.560 CP
<b>3.18 ES</b>	<b>7.62 CP</b>	<b>1.52 ES</b>	<b>14.22 CP</b>
<i>Matrix Size</i>		0.42L x 0.62W	10.7L x 15.7W

Figure 5.1. Gage Types Used for Sectioning [16].



Figure 5.2. Typical Sectioned Sample with Bullet Connectors.

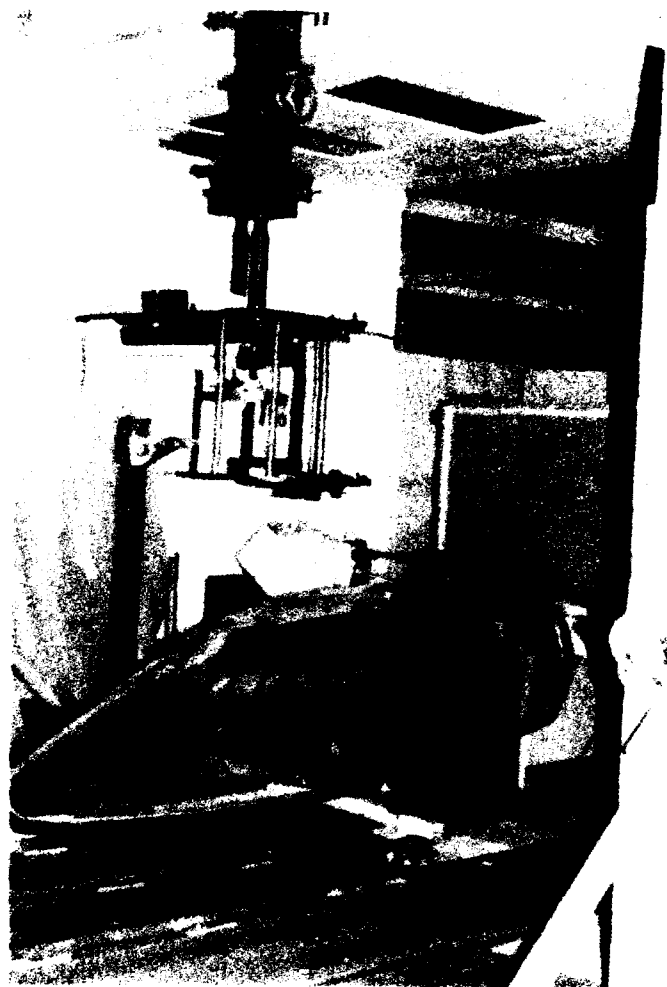


Figure 5.3. Rosette Alignment and Layout Facility.

photoelastic test rig (detailed in WRDC-TR-89-3099) which generated layout lines for gage positioning and orientation. A "three point" support frame positioned the canopy in the same orientation (with respect to a level plane) as it would be installed in an aircraft. V-grooved casters attached to the support frame allowed horizontal movement along a "track" constructed from steel angle iron and I-beams. A scale in 1/16-inch increments along the length of the track (Figure 5.4) indicated the fuselage station position of the points on the canopy centered under the test rig. A vertical scale with adjustable/retractable pointer arms indicated the waterline measurement of points on the canopy surface centered under the test rig.

A 5-mW helium/neon laser and associated mirrors directed a collimated beam of light onto the portion of the canopy centered under the rig. A cylindrical lens placed between the laser and canopy created a directed light sheet normal to the fuselage station axis. The light became visible as a line cast across the canopy surface, at the intersection of the light sheet and the canopy surface (Figure 5.5). The line trace generated vertical gage layout lines, which were traced onto cellophane tape on the canopy surface. The vertical scale and pointer indicated the correct waterline (along the length of the laser line) to place the gage.

The use of AE-10 two part epoxy adhesive in the Texstar canopy prevented any adhesive induced craze. The lack of a convenient or efficient heat source (and a desire not to change the residual stress state by heating) required an extended cure at room temperature. Vacuum clamps supplied sufficient clamping pressure on the gages to ensure proper curing. The low stress results from the Texstar canopy (Section 5.4) permitted the use of MBOND 200 on the Sierracin canopy. The use of this adhesive decreased installation time since it did not require the use of clamping pressure, extended cure times, or mixing.

Table 5.1 lists the positions of the sectioning rosettes on the two canopies. The Texstar canopy contained 29 rosettes concentrated toward the front of the canopy (the location of the crazes). An assumption of symmetry led to the instrumentation of the canopy's right side only. To obtain a better mapping toward the aft the Sierracin canopy was instrumented with 42 rosettes.

Table 5.2 lists the locations of hole drilling tests on these canopies. Gage type TEA-06-062RK-120 was used on all tests.

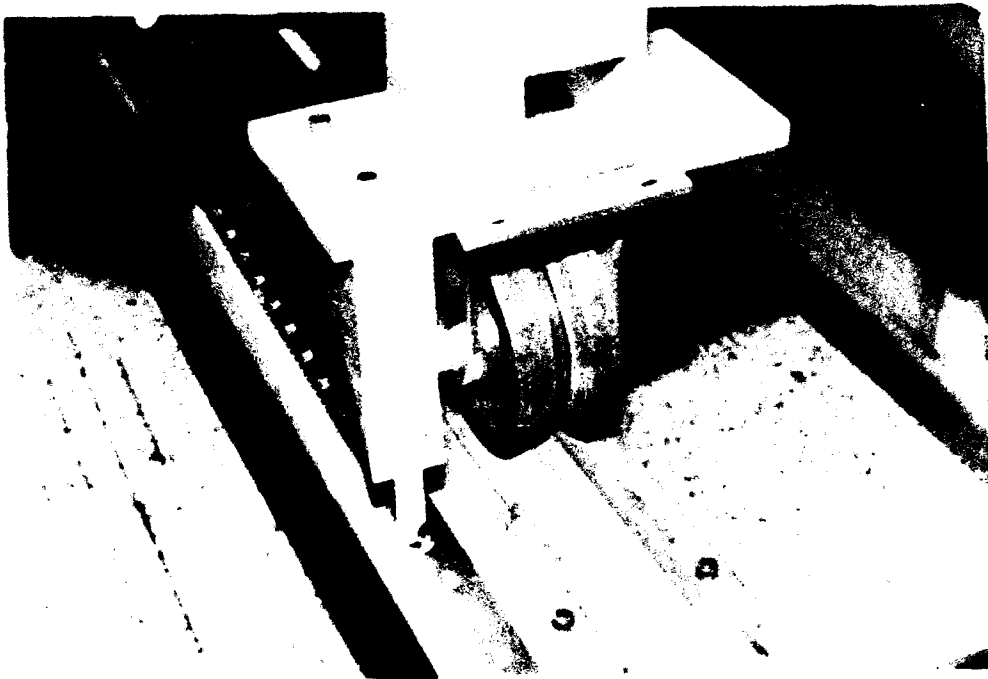


Figure 5.4. Fuselage Station Indicator.

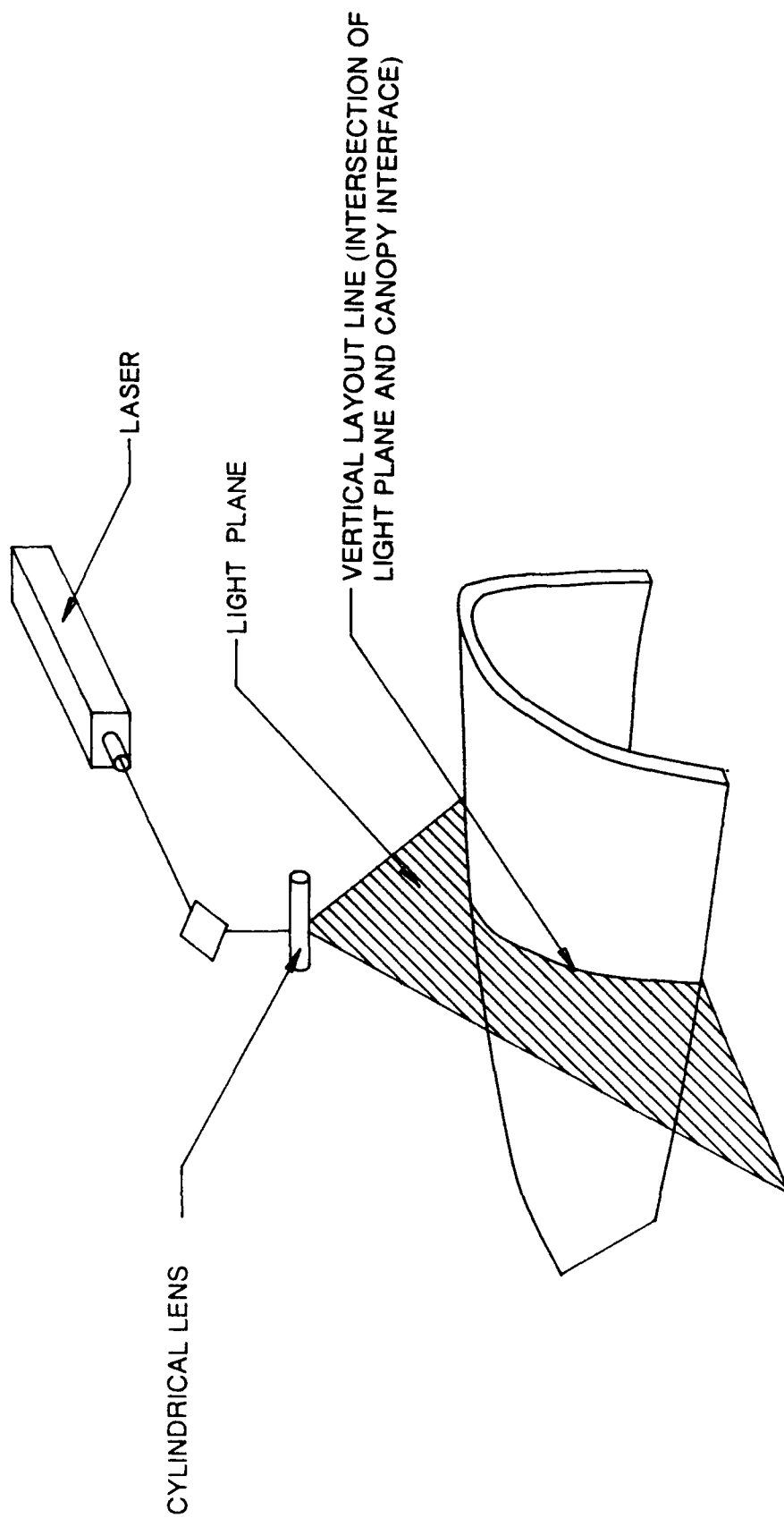


Figure 5.5. Use of Laser to Produce Rosette Layout Lines.



TABLE 5.1

## SECTIONING ROSETTE LOCATIONS

Rosette	Texstar		Sierracin	
	Fuselage Station (in)	Waterline (in)	Fuselage Station (in)	Waterline (in)
1	94.4	114.3	94	114.3
2	100.0	117.8	100	117.8
3	100.0	115.8	100	115.8
4	105.6	121.2	105.6	121.2
5	105.6	120.1	105.6	120.1
6	105.5	116.3	105.6	116.3
7	111.6	124.6	115	126.5
8	115.2	125.0	115	125.0
9	115.2	120.6	115	120.7
10	115.2	116.3	115	116.3
11	117.9	128.1	118	128.1
12	124.4	130.9	118	126.7
13	124.4	129.2	118	122.9
14	124.4	123.9	118	117.5
15	124.7	117.8	124	130.8
16	131.1	133.0	124	129.0
17	137.9	134.5	124	123.8
18	137.8	133.6	124	117.5
19	137.7	131.2	131	133.0
20	137.7	127.5	131	131.8
21	137.7	164.4	131	128.4
22	137.7	123.0	131	123.3
23	144.9	135.3	131	117.3
24	151.9	135.6	138	134.5
25	158.9	135.6	138	133.7
26	158.7	133.9	138	131.3
27	158.6	129.5	138	127.6
28	158.5	122.7	138	123.0
29	176.3	134.3	138	117.9
30			145	135.3
31			145	134.1
32			145	130.8
33			145	125.8
34			145	122.7
35			152	135.6
36			152	134.0
37			152	129.5
38			152	123.1
39			152	118.0
40			159	135.6
41			159	133.9
42			159	129.3

**TABLE 5.2**  
**LOCATIONS OF RESIDUAL STRESS HOLE-DRILLING TESTS**

**INSTALLED**

Rosette #	Texstar Canopy*		Sierracin Canopy+	
	Fuselage Station (in)	Waterline (in)	Fuselage Station (in)	Waterline (in)
1	103	118	100	117
2	109	122	110	121
3	119	127	120	128
4	131	131	136	132
5	148	133	157	131
6	102	119		
7	108	119		
8	109	122		
9	119	128		
10	120	121		
11	131	132		
12	141	128		
13	149	121		

\*Rosettes 1-5 starboard side, 6-13 port side

+starboard side

**PRESSURIZED**

Rosette #	Texstar Canopy*		Sierracin Canopy+	
	Fuselage Station (in)	Waterline (in)	Fuselage Station (in)	Waterline (in)
1	103	117	99	116
2	110	119	109	120
3	120	124	121	127
4	131	132	157	129
5	148	132	157	129
6	102	118		
7	108	118		
8	109	122		
9	131	132		
10	141	127		
11	149	118		

\*Rosettes 1-5 starboard side, 6-11 port side

+Starboard side

### 5.3 TESTING PROCEDURE

#### 5.3.1 Initial State

The test strains measured during this procedure were produced by three sources of stress: (1) deformation of the canopy during installation, (2) pressurization of the canopy during flight, (3) manufacturing induced residual stresses. After installation of the gages, all the gages were zeroed in the "free state." The position of the canopy while sitting on the gage layout frame defined the free state. As Figures 5.6 and 5.7 demonstrate, bolts at the canopy forward edge and restraining collars on the left and right aft attaching points placed the canopy in a fixed "displacement state." Lifting the Texstar canopy at the front and aft edges and allowing it to assume a "natural" state when placed on the collarless cross members of the frame determined the position of the collars for future canopies. Therefore, this procedure may have induced some small strain in the Sierracin canopy, since the two canopies were not identical. This method of defining the free state, although apparently arbitrary, suffices because the canopies are compliant enough that their own weight causes some small deflection no matter how they are sitting. Defining a fixed "free state configuration" gave a repeatable zero point configuration for each individual canopy.

#### 5.3.2 Installation

A full-scale F-16 tabletop fixture, Figure 5.8, provided to UDRI by USAF WL/FIBT and originally used in pressure/thermal testing, furnished a means for imparting installation deformations into the canopy. Installation followed T.O. 16W 2-5-2, with one exception. In place of 5601 sealing compound, butyl rubber was utilized along the inside edges of the canopy. The butyl rubber possessed easier handling characteristics, decreased installation time, and was more easily obtained than 5601.

Upon completion of installation, each regular rosette was in turn connected to the strain indicator, the balance set to the zero point recorded in the free state, and the strain due to installation read for each of the three gages. Hole drilling tests were also conducted using the VALAPODD at positions specified in Table 5.2.

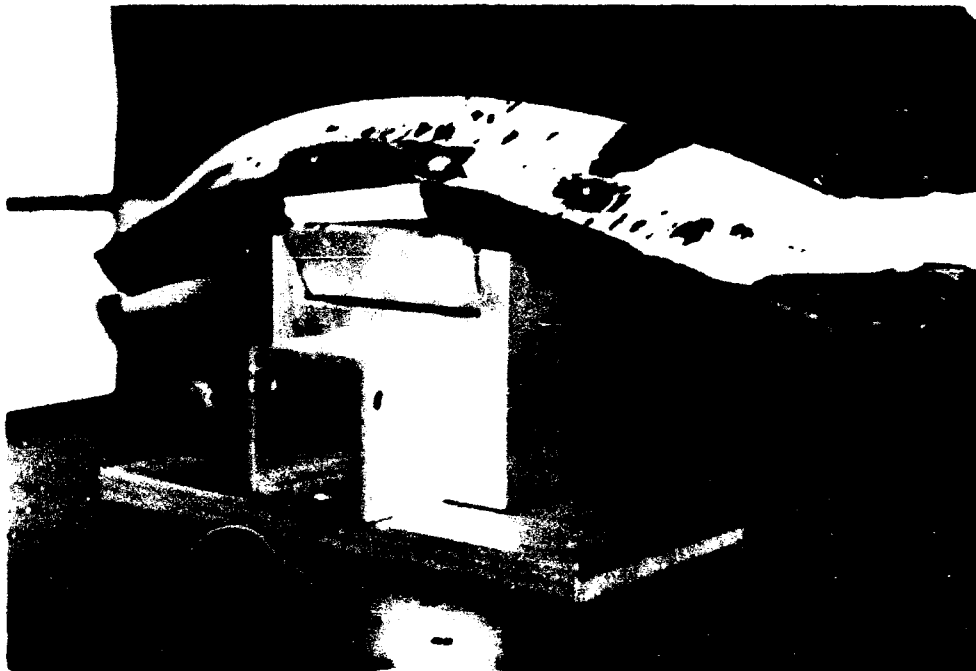


Figure 5.6. Forward Bolts on Canopy T-Frame.

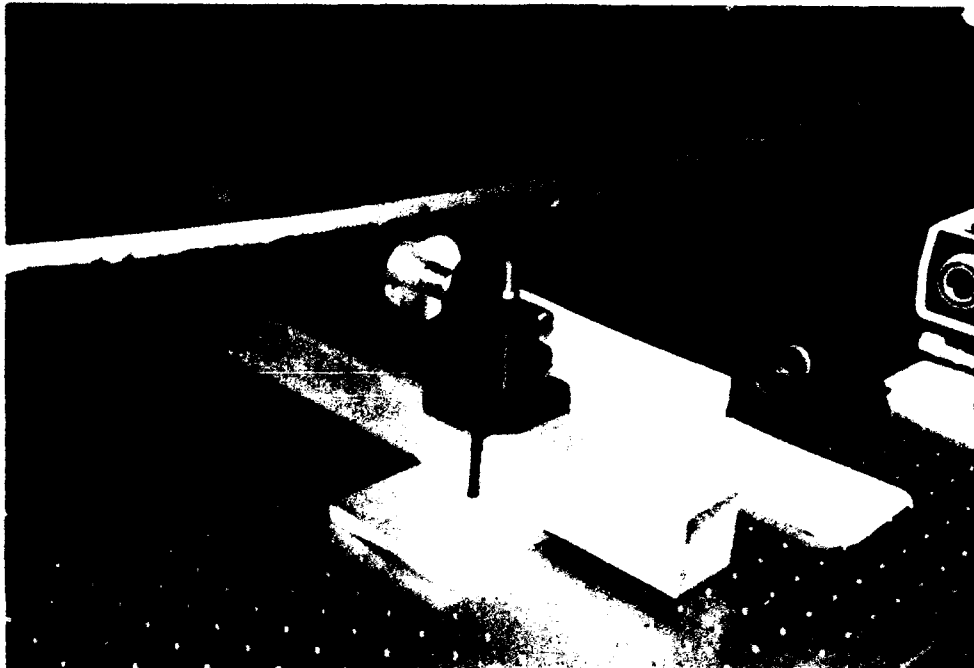


Figure 5.7. Aft Restraining Collars on Canopy T-Frame.



Figure 5.8. Full Scale F-16 Tabletop Pressure Fixture.

### 5.3.3 Pressurization

Pressurizing the mockup fixture with the canopy installed generated strain data comparable to what a typical canopy may see during high altitude flight due to the reduction in external atmospheric pressure. A shop air supply produced sufficient air flow to maintain 6 psig cabin pressure. The poor condition of the fixture required several repair operations, including removal and reinstallation of the aft canopy, sealing of sheet metal seams with 8802 sealing compound, and 1/2-inch-wide strips of butyl rubber placed adjacent to the inflatable seals along the entire perimeter of the cabin. (The butyl rubber required stripping and replacing after each opening of the cabin hatch.) A pressure gage ( $\pm 0.25$  psi accuracy, 15 psi range) mounted through the forward bulkhead fixture indicated cabin pressure.

Upon pressurization to 6 psig, each regular rosette was again connected to the strain indicator, the balance set to the zero point recorded in the free state, and the strain read. The strain noted in this manner represented a superposition of installation and pressure induced deformations. Hole drilling tests were conducted using the VALAPODD at positions specified in Table 5.2.

### 5.3.4 Residual Stresses

Sectioning of the canopy relieved "locked in" or residual stresses which induced strain in the rosettes. After depressurizing, the canopy was removed per T.O. 16W2-5-2 and replaced onto the "free state" frame. Sectioning work, using starter holes and a hand-held jigsaw commenced and produced 6 x 6 square specimens with the regular rosettes centered. The proximity of some gages to each other (especially toward the forward position of the canopy) prevented the removal of 6 x 6 specimens. These rosettes were removed as 5 x 5 specimens, or 4 x 4 where 5 x 5's could also not be obtained.

After removal, strains read from the 6 x 6 rosette (in a manner similar to installation and pressurization) indicated strains relieved by removal of the samples from the canopy. Since 6 x 6 specimens probably do not remove all of the residual stress, further reductions to 5 x 5 then to 4 x 4 (Figure 5.9), and finally to 2 x 2.5 ensured complete residual strain relief. This approach also generated relieved stress vs. coupon size data, which could possibly aid in specifying an optimum coupon size.

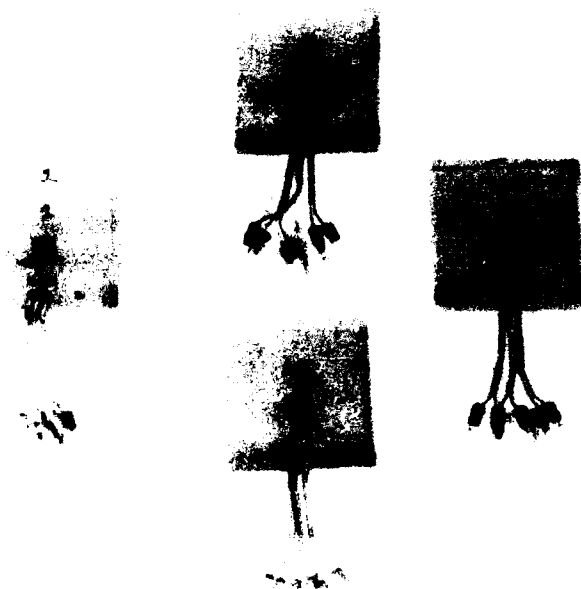


Figure 5.9. 4- x 4-inch Sectioning Specimens.



The sectioning of coupons relieves strains that are opposite in sign from the residual stress on the part. Consequently, the data reduction equations must incorporate negative signs to be correct.

$$\sigma_{\max} = \frac{\epsilon_2(A - B\cos 2\phi) - \epsilon_1(A + B\sin 2\phi)}{\cos 2\phi + \sin 2\phi}$$

$$\sigma_{\min} = \frac{\epsilon_1(A - B\sin 2\phi) - \epsilon_2(A + B\cos 2\phi)}{\cos 2\phi + \sin 2\phi}$$

$$\tan 2\phi = \frac{-\epsilon_1 + 2\epsilon_2 - \epsilon_3}{\epsilon_3 - \epsilon_1}$$

The sectioning calibration constants,  $\bar{A}$  and  $\bar{B}$ , remain the same.

#### 5.3.5 Sierracin Canopy Procedure Alterations

The testing of the Sierracin canopy (S2) proceeded in a manner similar to the Texstar canopy with the following exceptions:

- (a) With the strain indicator set at a fixed balance point, the first readings taken in the "free state" provided initial "strain" readings as opposed to "zero" points. Subtraction of the initial readings from subsequent readings (installation, pressurization, etc.) resulted in the actual strain for that step. This process reduced the time to take measurements.
- (b) The repeatability of the connectors caused some uncertainty in the Texstar canopy strain readings. Averaging of multiple readings at each step (after installation, during pressurization, etc.) by disconnecting and reconnecting the rosettes provided more accurate data. Subtraction of the average initial strain (free state) from the average at each step gave the actual strain at that step.
- (c) Coupon size increments consisted of 6- x 6-inch, 4- x 4-inch and 2- x 2-inch specimens.

## 5.4 TEST RESULTS

In the following discussion, "Maximum principal stress" refers to the algebraically largest stress. A principal stress of 75 psi (tension) is a maximum compared to -100 psi (compression).

### 5.4.1 Sectioning Method

#### 5.4.1.1 Installed State

Figures 5.10 through 5.15 display stress results from the regular rosettes due to installation in both canopies. Maximum and minimum principal stresses are plotted separately. The curves are plotted parametrically, with fuselage station serving as the second independent spatial variable.

Comparison of Texstar and Sierracin results show the maximum principal stresses to be primarily tensile in the Texstar canopy and compressive in the Sierracin canopy. The large tolerances in the manufacture of canopies and the mounting frames most likely produce this effect. Wide variation in installation stresses will most likely occur from canopy to canopy and from aircraft to aircraft. The stress will depend on whether the canopy must be deflected inward or outward from an initial state to be installed.

In general, the trends on the results show greater variation in stress with waterline level for fuselage stations away from the forward and aft edges. For a given fuselage station, maximum stresses are greatest near the centerline (waterline 136) and near the lower edges (waterline 116); probably representing greatest bending (deflection) and clamping stresses, respectively. Minimum stresses generally increase from the lower edge toward the canopy center.

The Texstar canopy shows the greatest maximum and minimum principal stresses at the forward and aft fuselage stations, with stresses in between generally decreasing from the forward to the aft. The Sierracin canopy shows the same general behavior, except that the aft fuselage station (159) possesses generally lower stresses than other fuselage stations.

#### 5.4.1.2 Pressurized State

Figures 5.16 through 5.21 display stress results from regular rosettes obtained during cabin pressurizing to 6 psig. Maximum and minimum

# Maximum Installation Stresses Canopy T1

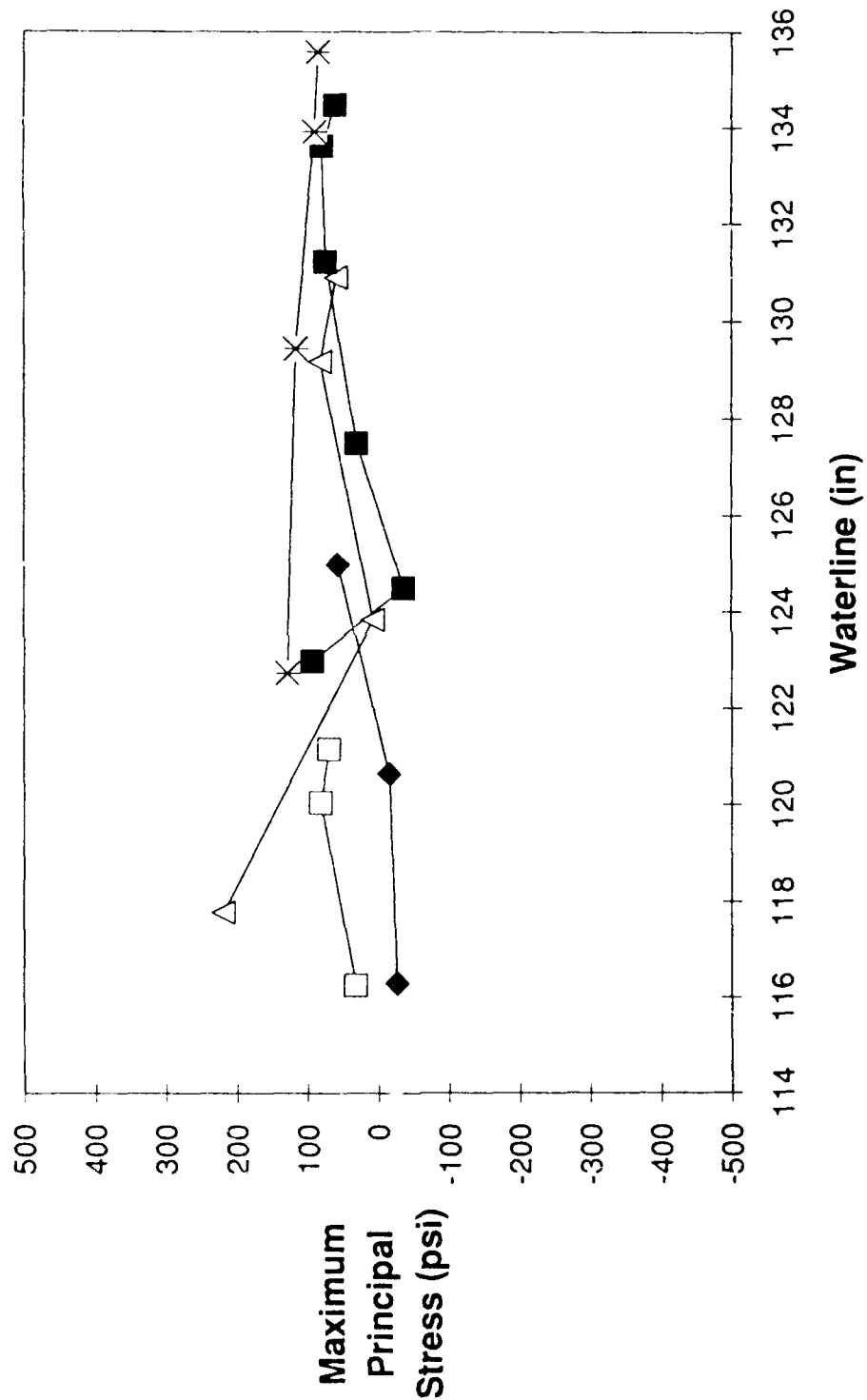


Figure 5.10. Maximum Installation Stresses - Canopy T1.

## Maximum Installation Stresses Canopy S1: Forward

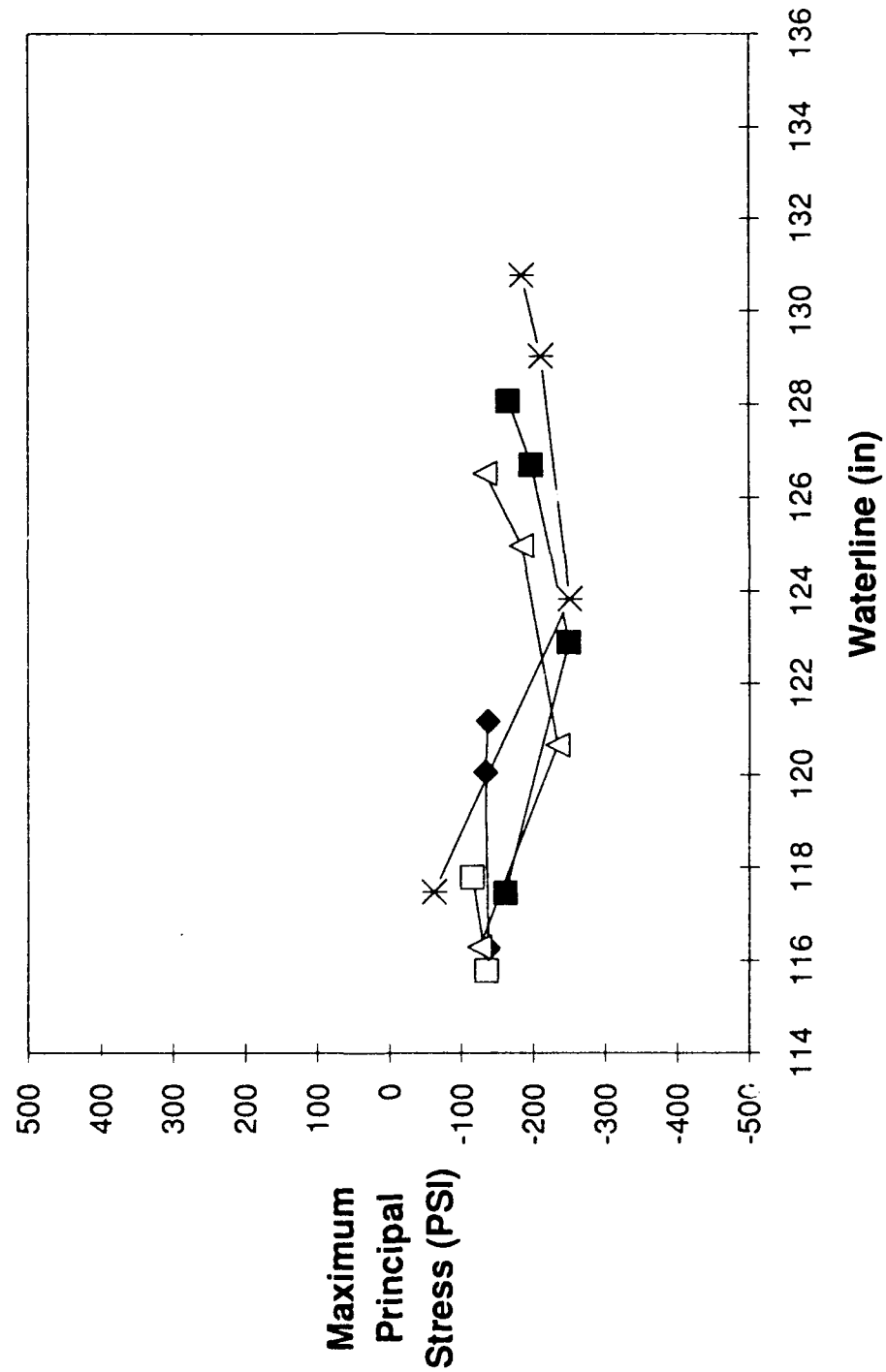


Figure 5.11. Maximum Installation Stresses - Canopy S1: Forward.

## Maximum Installation Stress Canopy S1: Aft

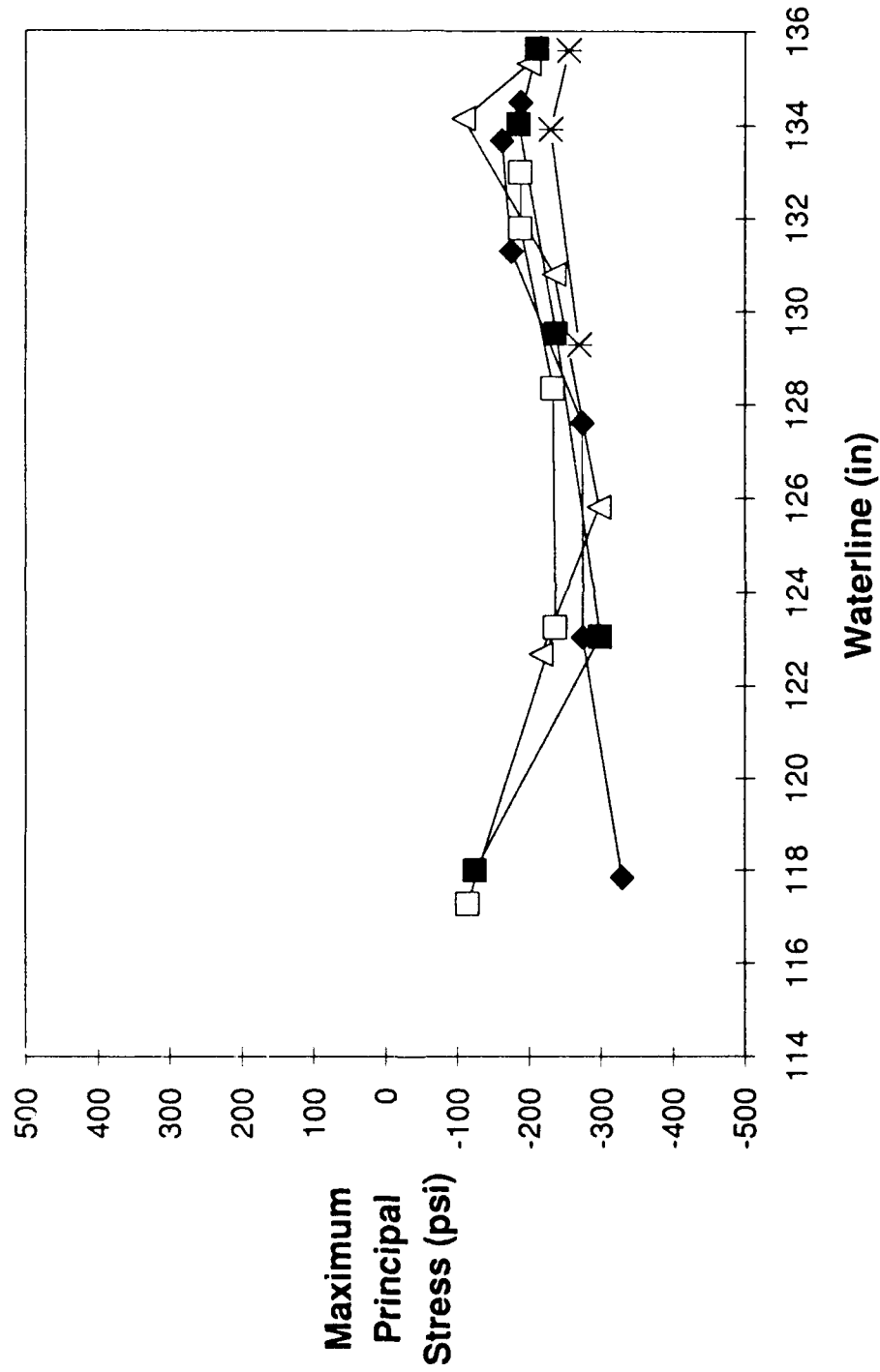


Figure 5.12. Maximum Installation Stresses - Canopy S1: Aft.

# Minimum Installation Stresses Canopy T1

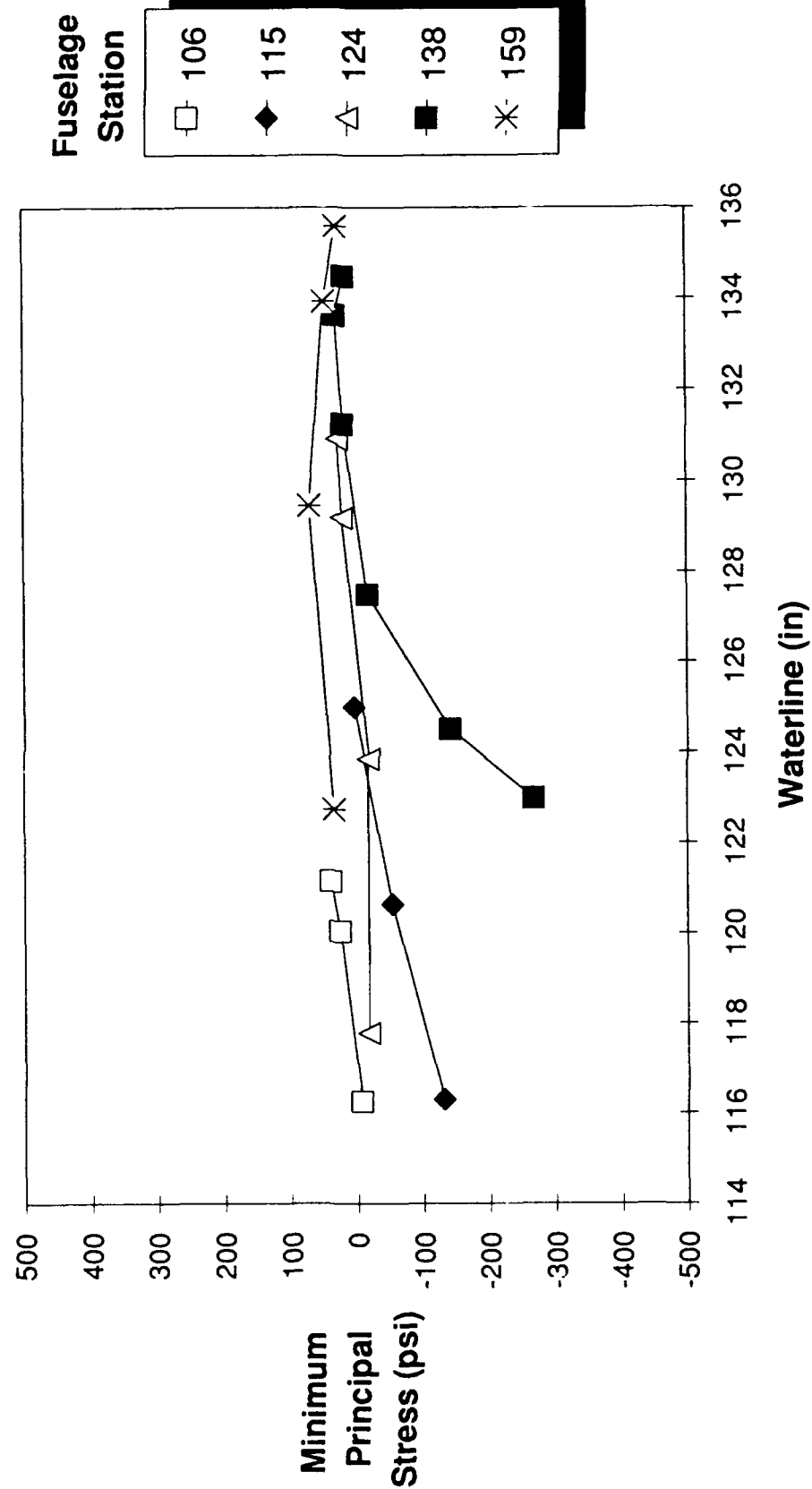


Figure 5.13. Minimum Installation Stresses - Canopy T1.

# Minimum Installation Stresses Canopy S1: Forward

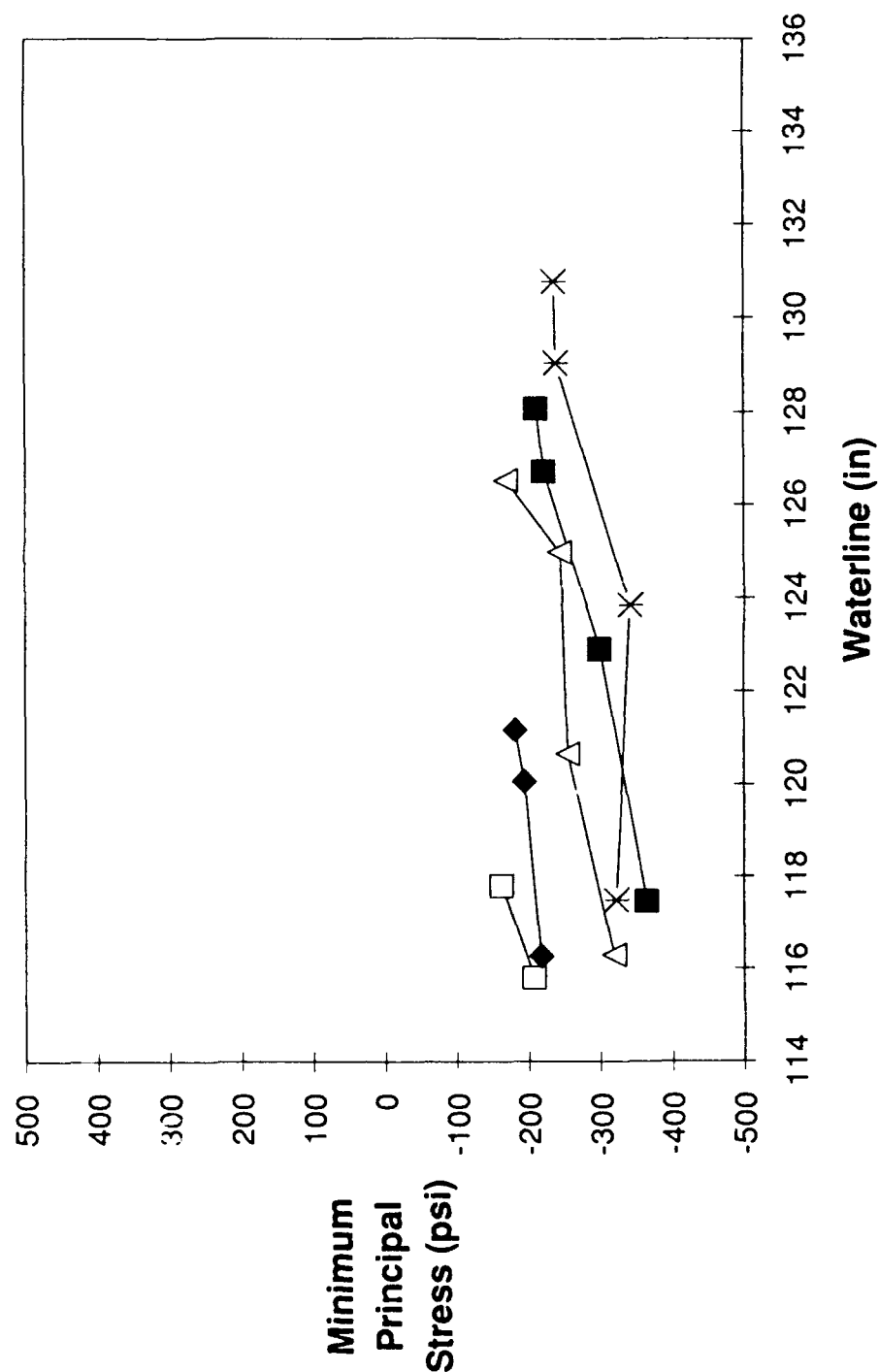


Figure 5.14. Minimum Installation Stresses - Canopy T1: Forward.

# Minimum Installation Stresses Canopy S1: Aft

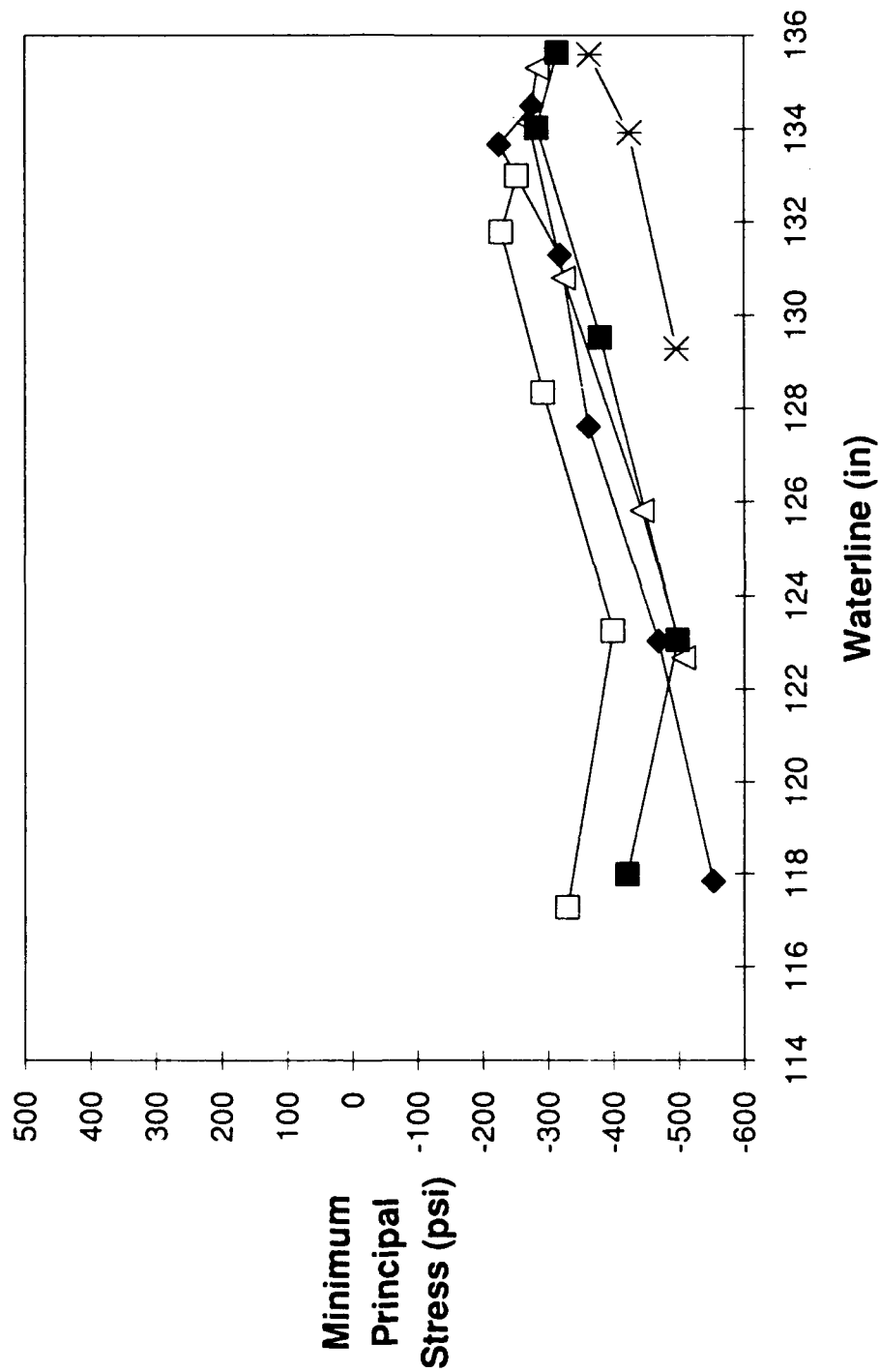


Figure 5.15. Minimum Installation Stresses - Canopy S1: Aft.



## Maximum Pressure Stress Canopy T1

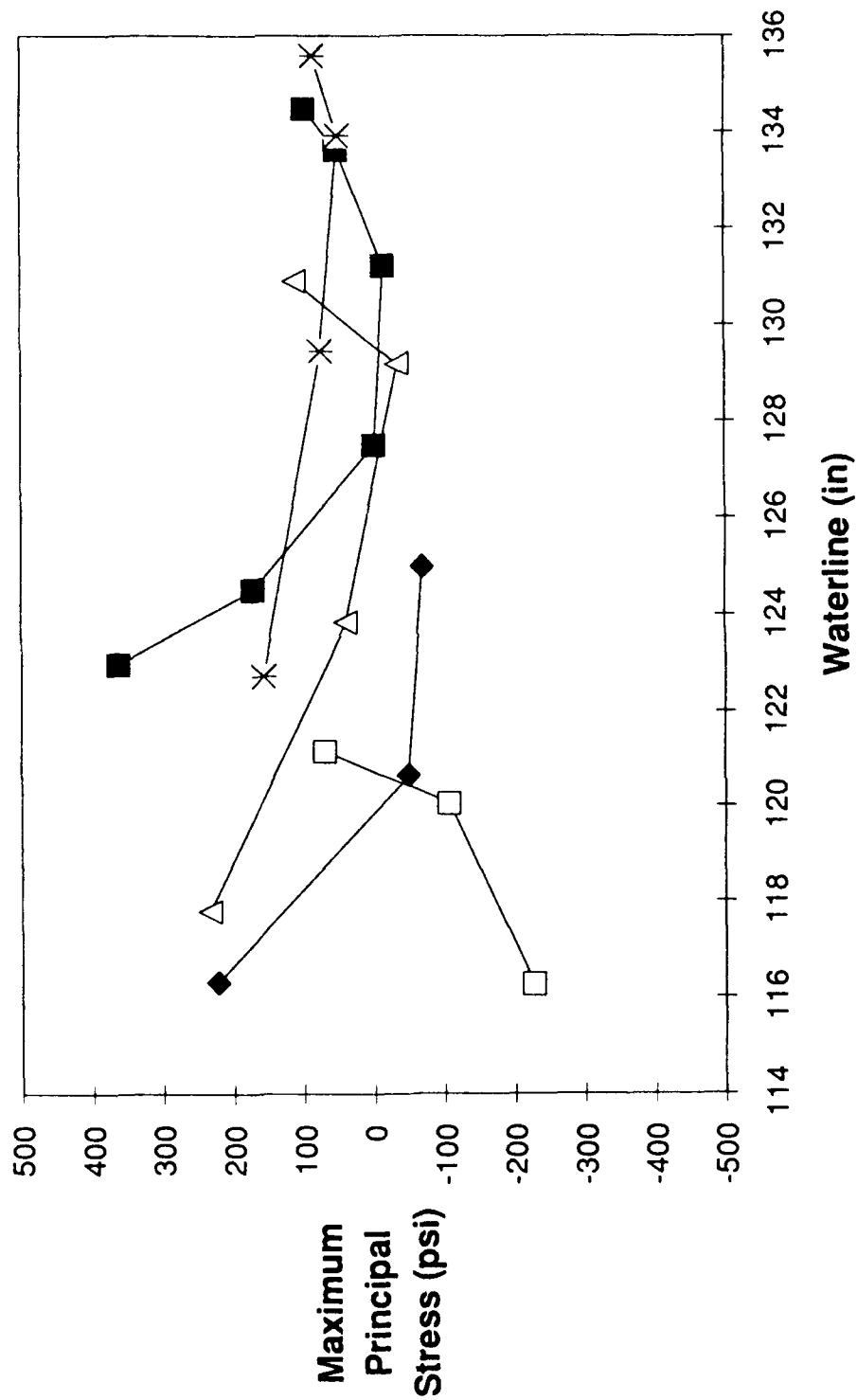


Figure 5.16. Maximum Pressure Stress - Canopy T1.

# Maximum Pressurization Stress Canopy S1: Forward

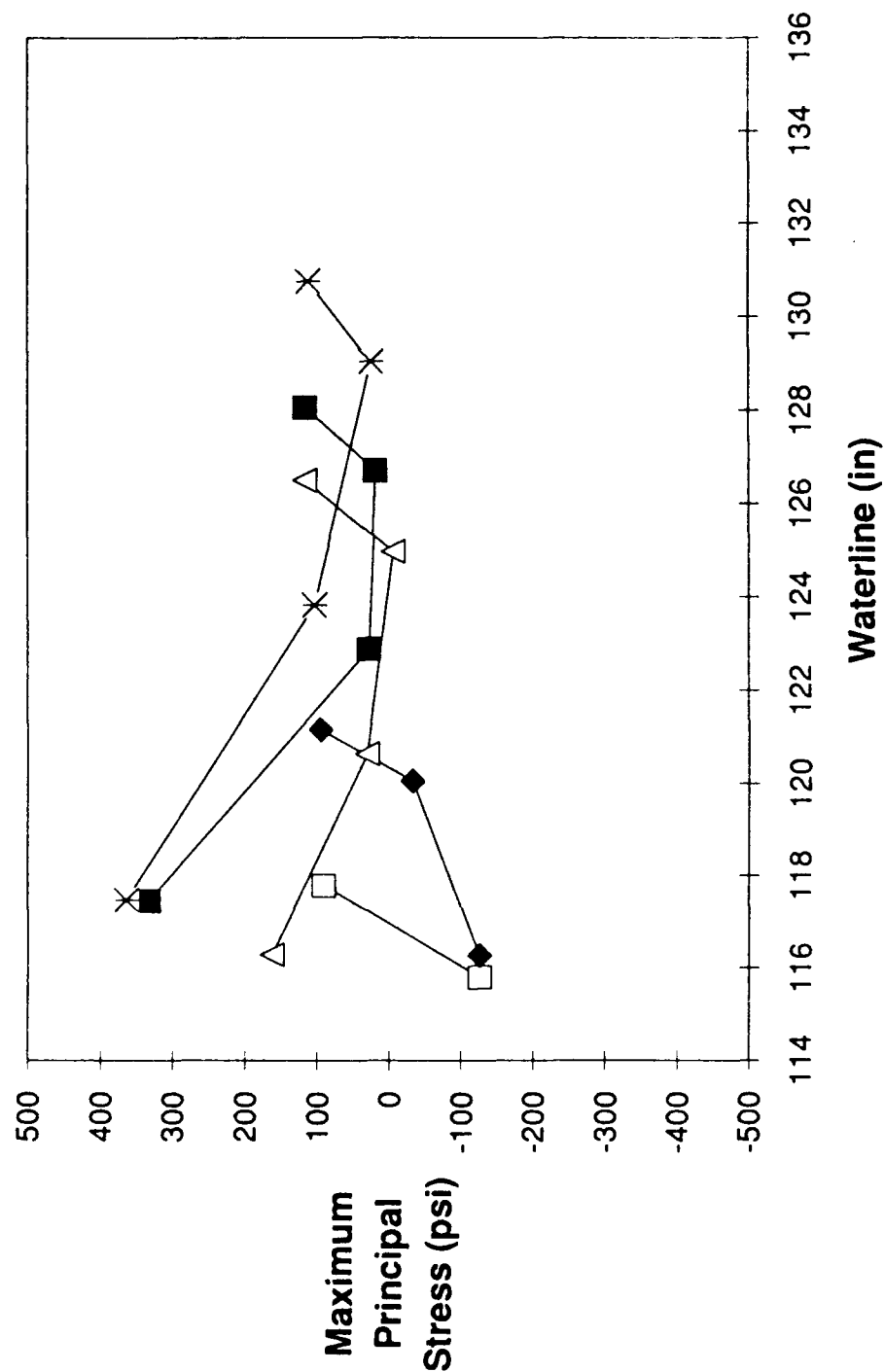


Figure 5.17. Maximum Pressurization Stress - Canopy S1: Forward.

## Maximum Pressurization Stress Canopy S1: Aft

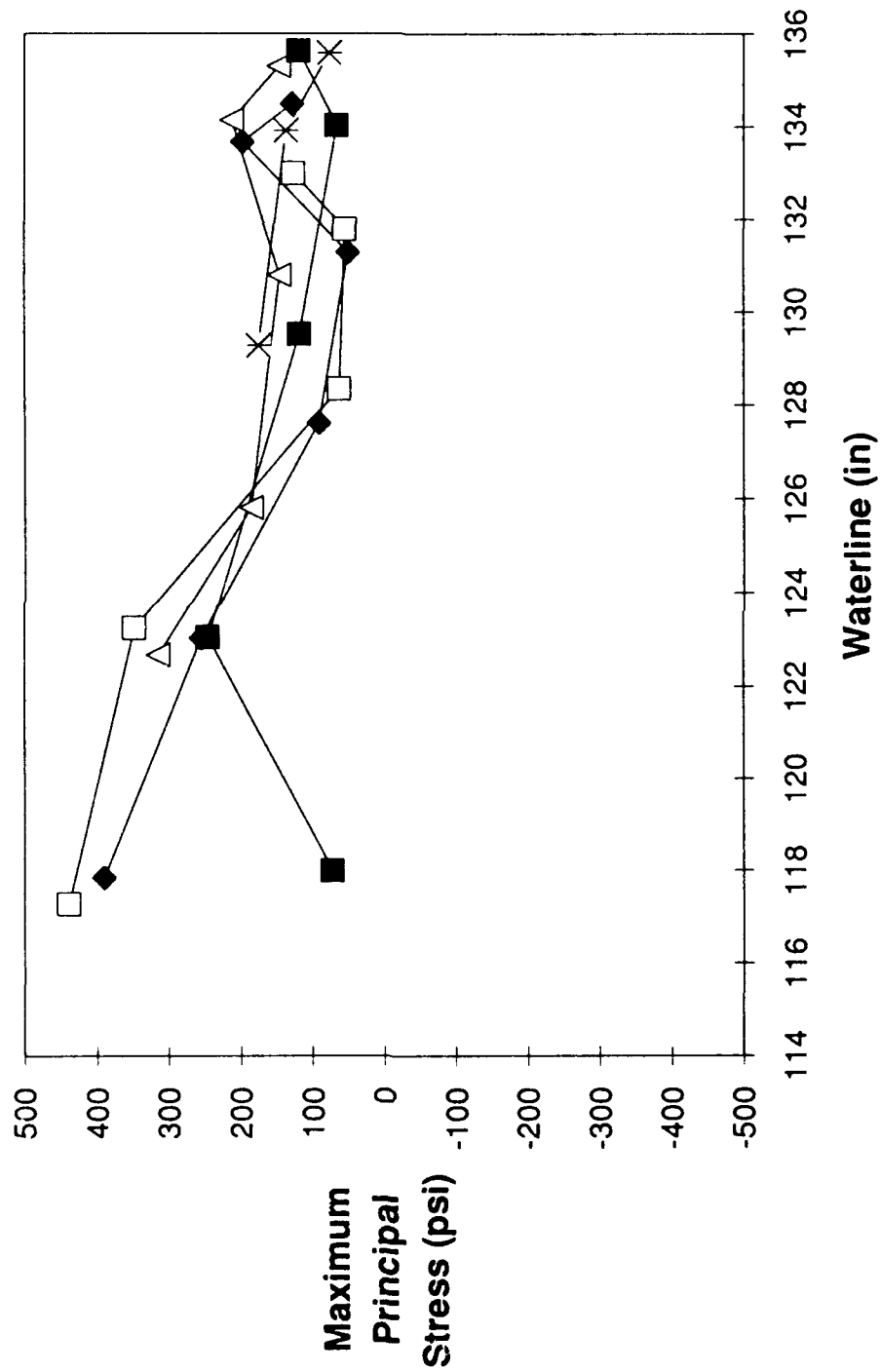


Figure 5.18. Maximum Pressurization Stress - Canopy S1: Aft.

## Minimum Pressure Stress Canopy T1

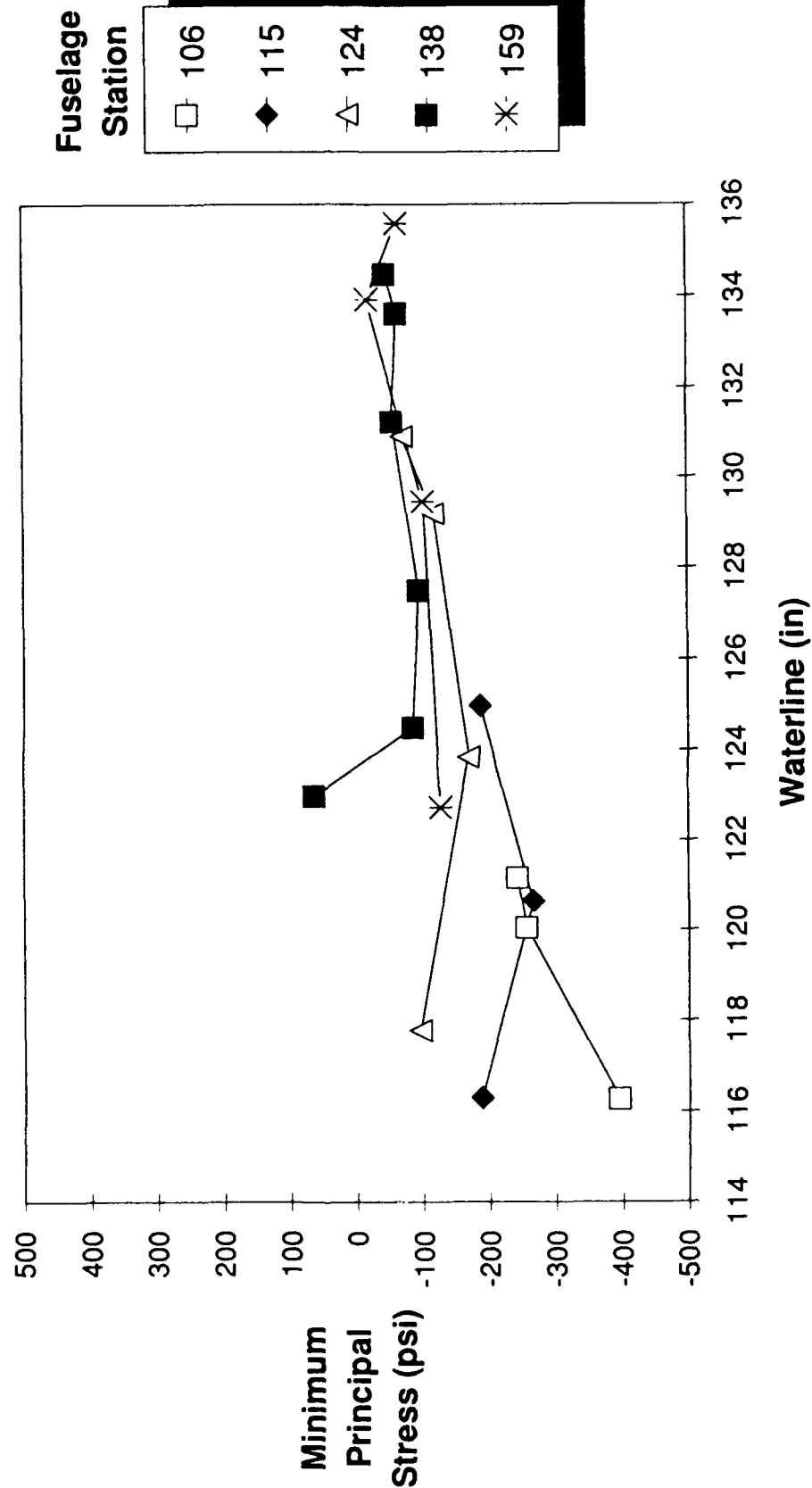


Figure 5.19. Minimum Pressure Stress - Canopy T1.

## Minimum Pressurization Stress Canopy S1: Forward

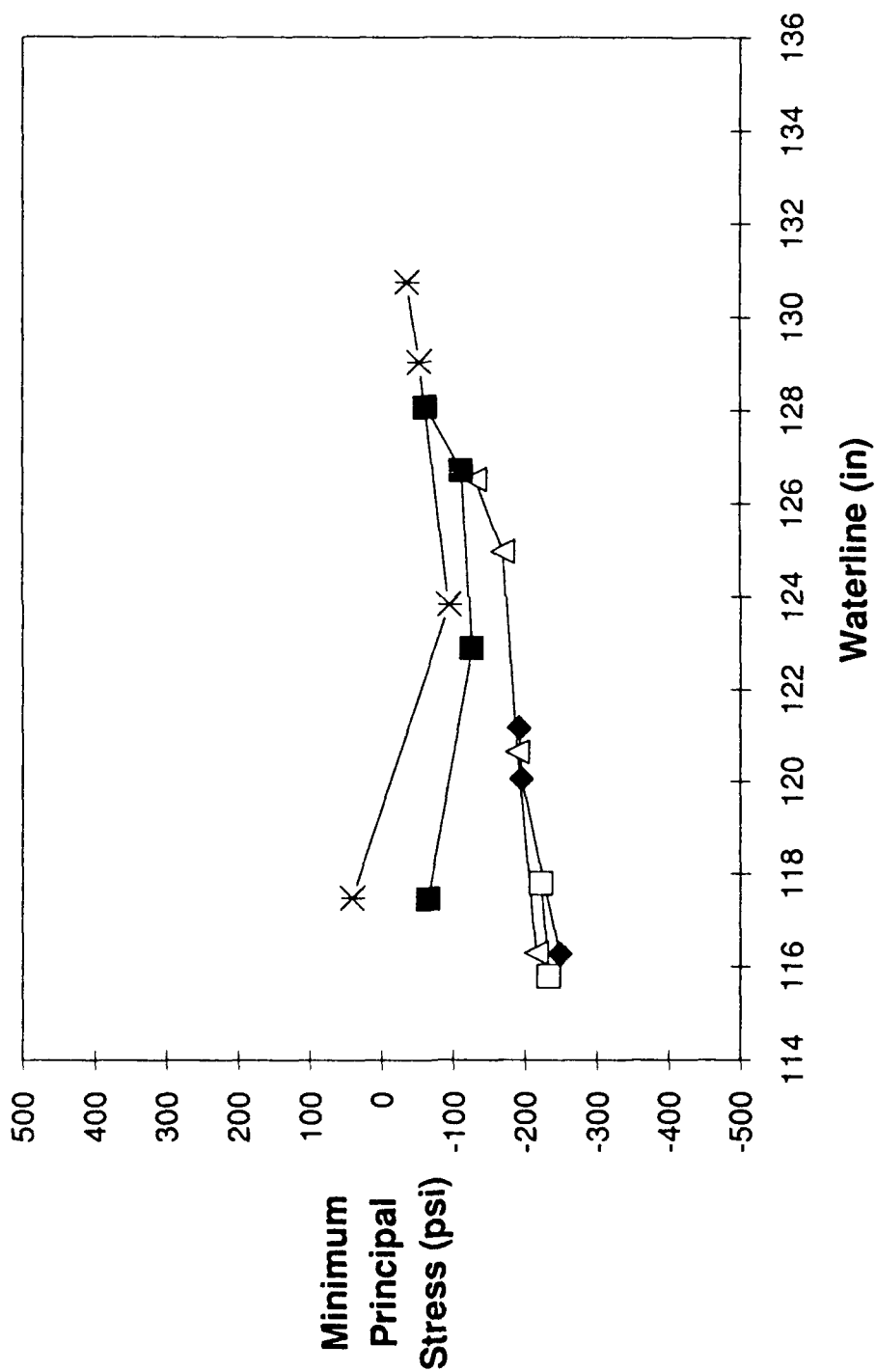


Figure 5.20. Minimum Pressurization Stress - Canopy S1: Forward.

# Minimum Pressurization Stress Canopy S1: Aft

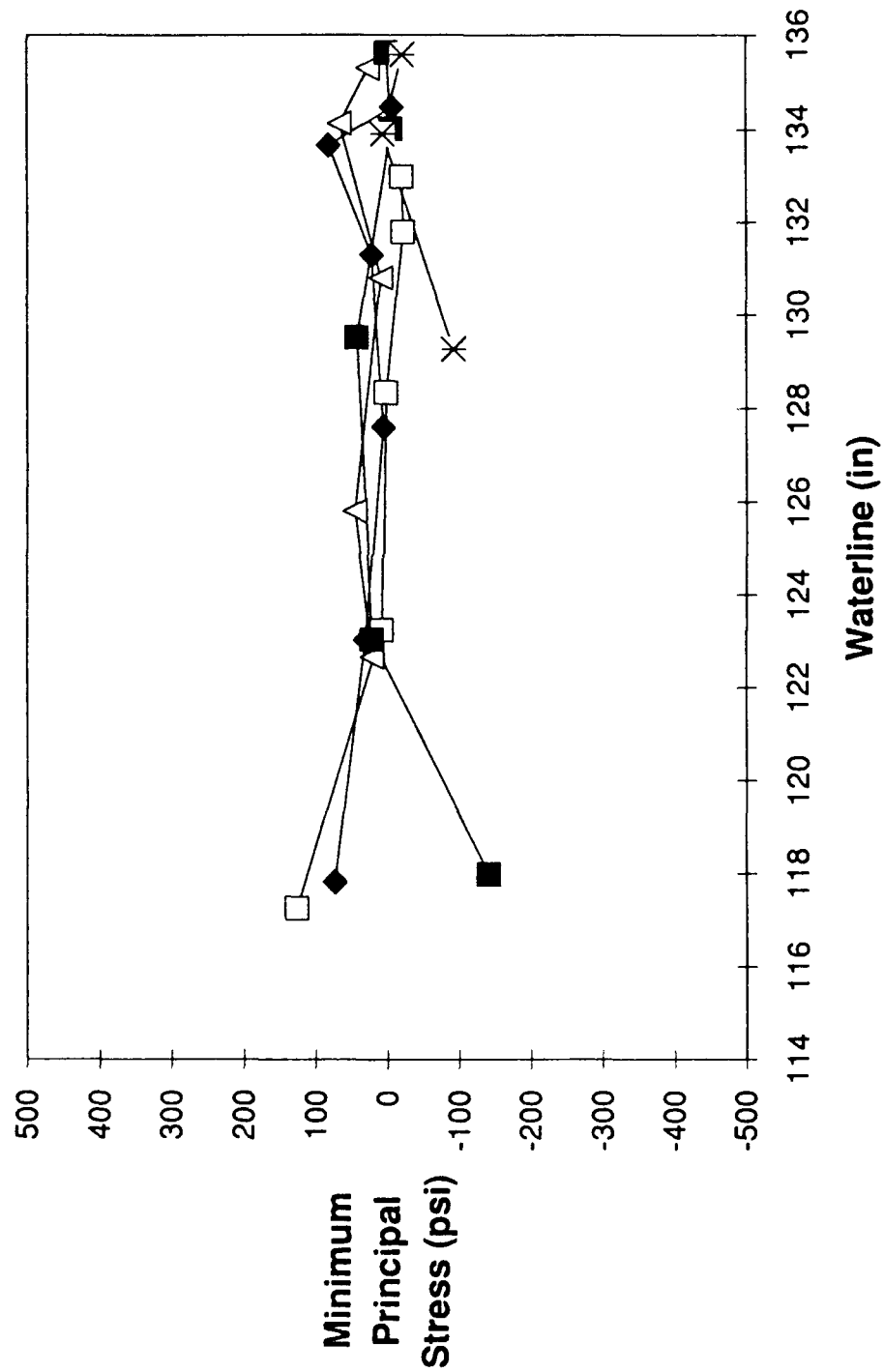


Figure 5.21. Minimum Pressurization Stress - Canopy S1: Aft.

principal stresses are again plotted separately on parametric curves using fuselage station as the second variable.

As expected, pressure loads induced primarily tensile type maximum principal stresses in both canopies. The Sierracin canopy produced the higher maximum principal stresses, while both canopies possessed minimum principal stresses of roughly equal magnitude. All the graphs display a typical behavior for a given fuselage station: higher stresses near the lower edge, decreasing as the waterline increases, and then increasing again as the waterline approaches the centerline of the canopy. The fuselage stations near the aft section show generally greater stresses, most likely due to the greater radius at these points. In comparing maximums and minimums for each canopy, several positions reveal that the minimum is numerically larger than the maximum ( $|\sigma_{\min}| > |\sigma_{\max}|$ ).

It is also interesting to note that installed and pressurized maximum stresses are of roughly the same magnitude for the Texstar canopy, while the minimums for the pressurized state are much more compressive in nature. The Sierracin canopy also shows installed and pressurized maximums of similar magnitude, but of opposite sign.

#### 5.4.1.3 Residual Stresses

Figures 5.22 through 5.27 display results of residual stresses measured on the Texstar and Sierracin canopies by the sectioning method. Chart formats are identical to those for the installed and the pressurized state.

In comparing residual stress to installation and pressure induced stress, the Texstar results indicate the manufacturing process induces the higher maximum principal stresses. The Sierracin canopy showed similar results on the forward section, while the aft section possessed higher pressure induced stresses. The minimum stresses on the Texstar canopy indicate large tensile stresses. The Sierracin canopy shows smaller tensile minimums in the forward section, and both tensile and compressive stresses aft.

Although these results indicate the Texstar canopy produces the highest residual stresses, the difference in service lives makes the results of such a comparison difficult to interpret. Section 6 will examine residual stresses in more detail through hole drilling tests in 20 in-serviced canopies.

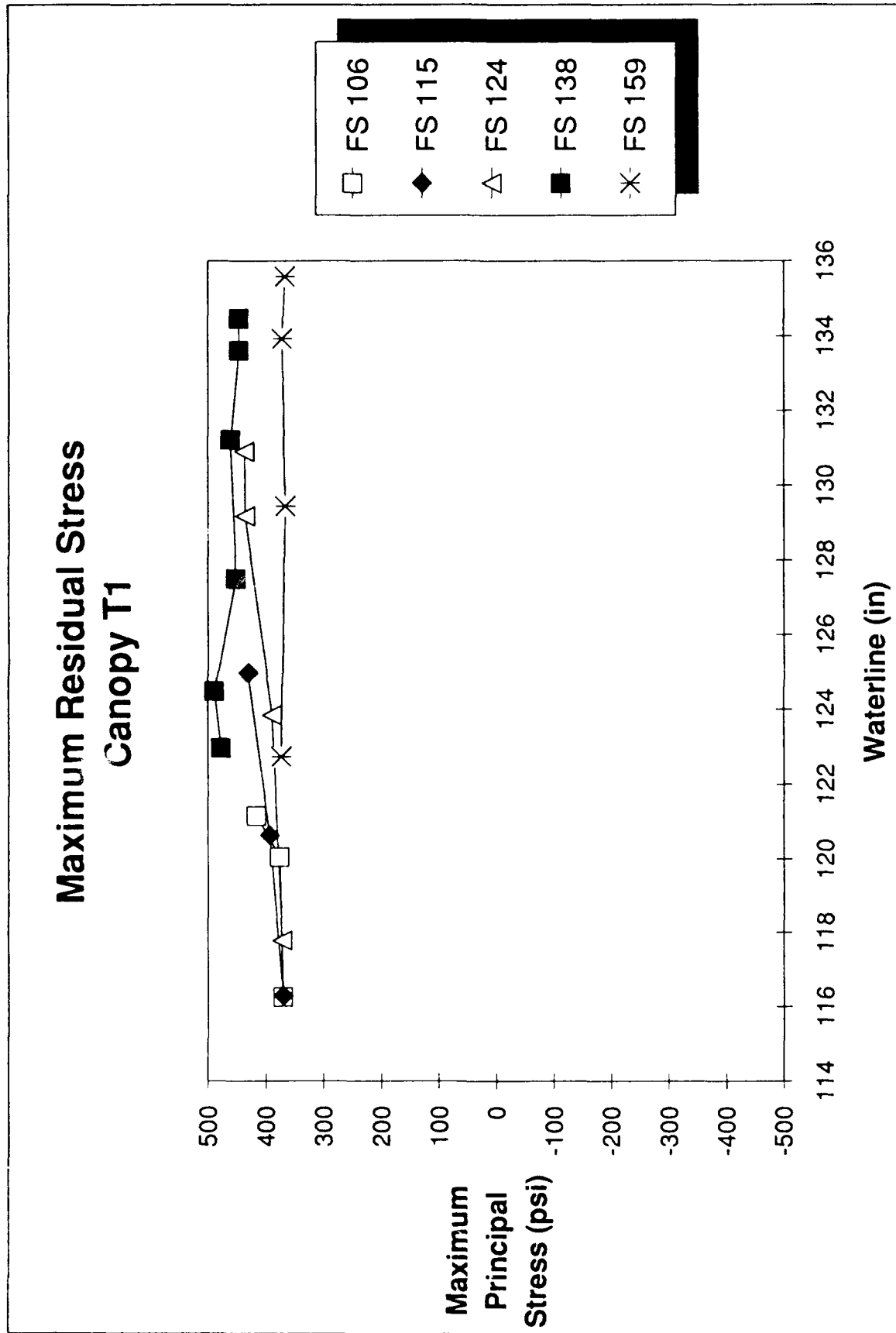


Figure 5.22. Maximum Residual Stress - Canopy T1.



## Maximum Residual Stress Canopy S1: Forward

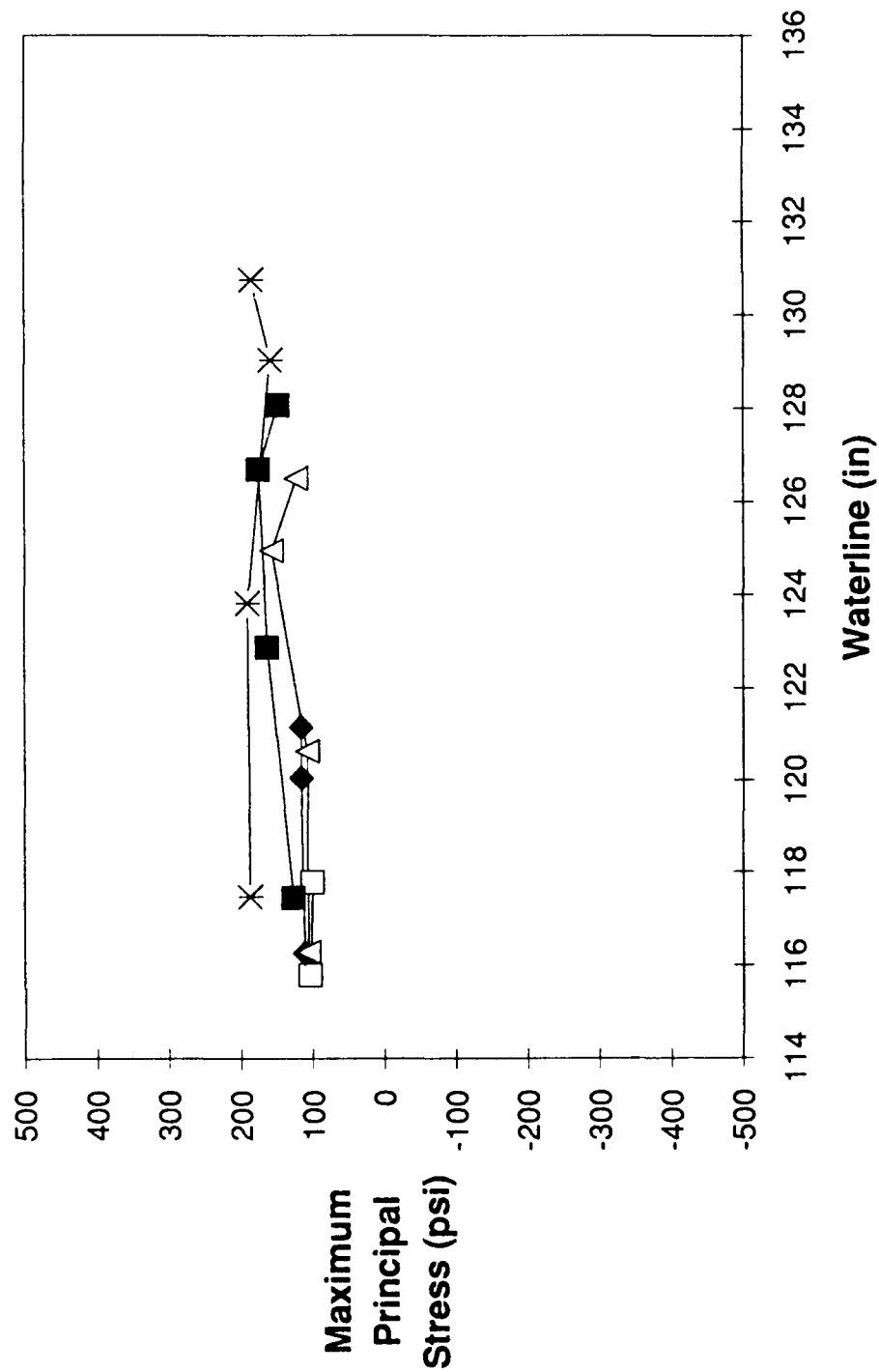


Figure 5.23. Residual Stress Using Initial Strain Baseline - Canopy S1: Forward.

# Maximum Residual Stress Canopy S1: Aft

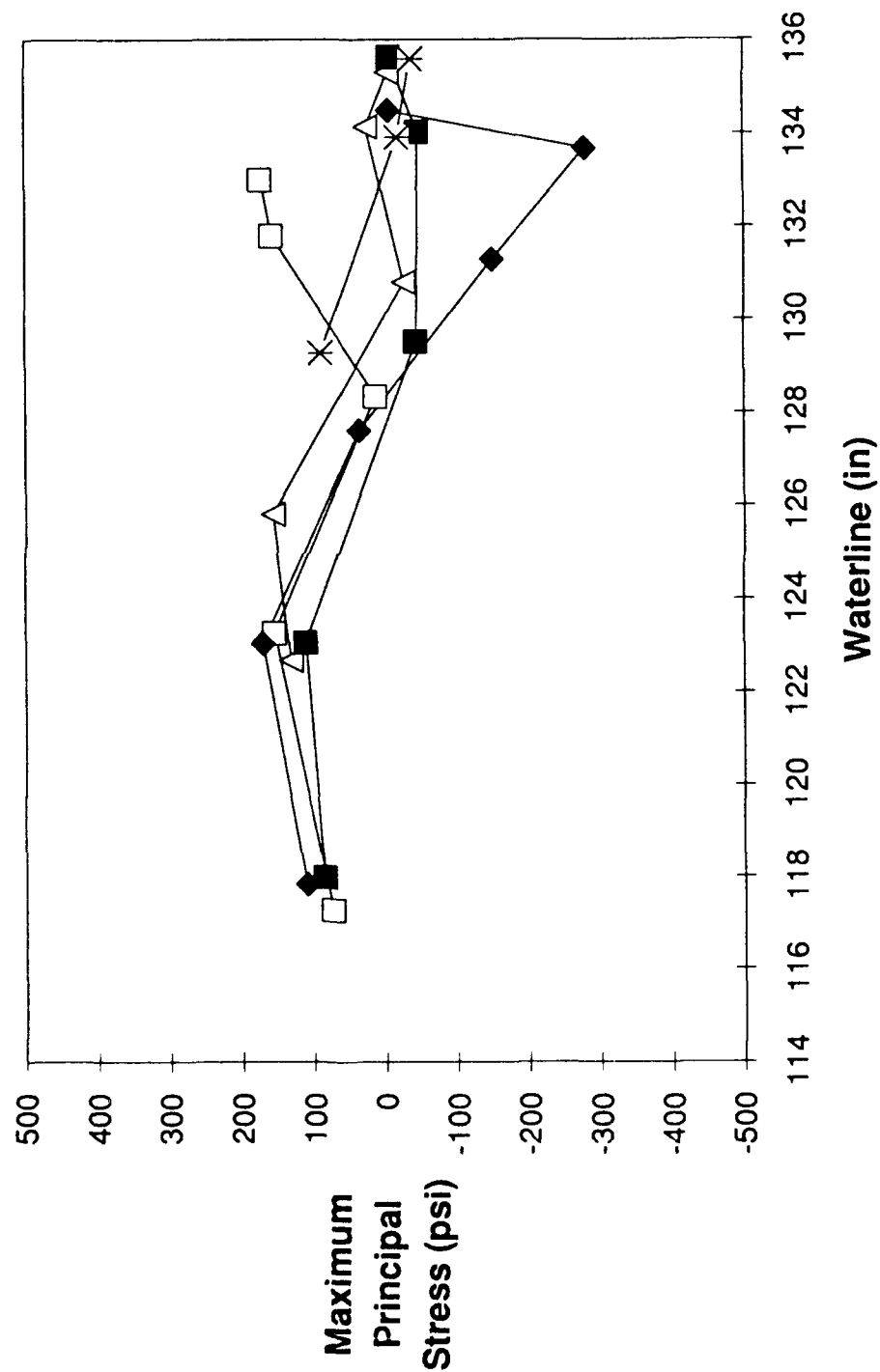


Figure 5.24. Residual Stress Using Initial Strain Baseline - Canopy S1: Aft.

## Minimum Residual Stress Canopy T1

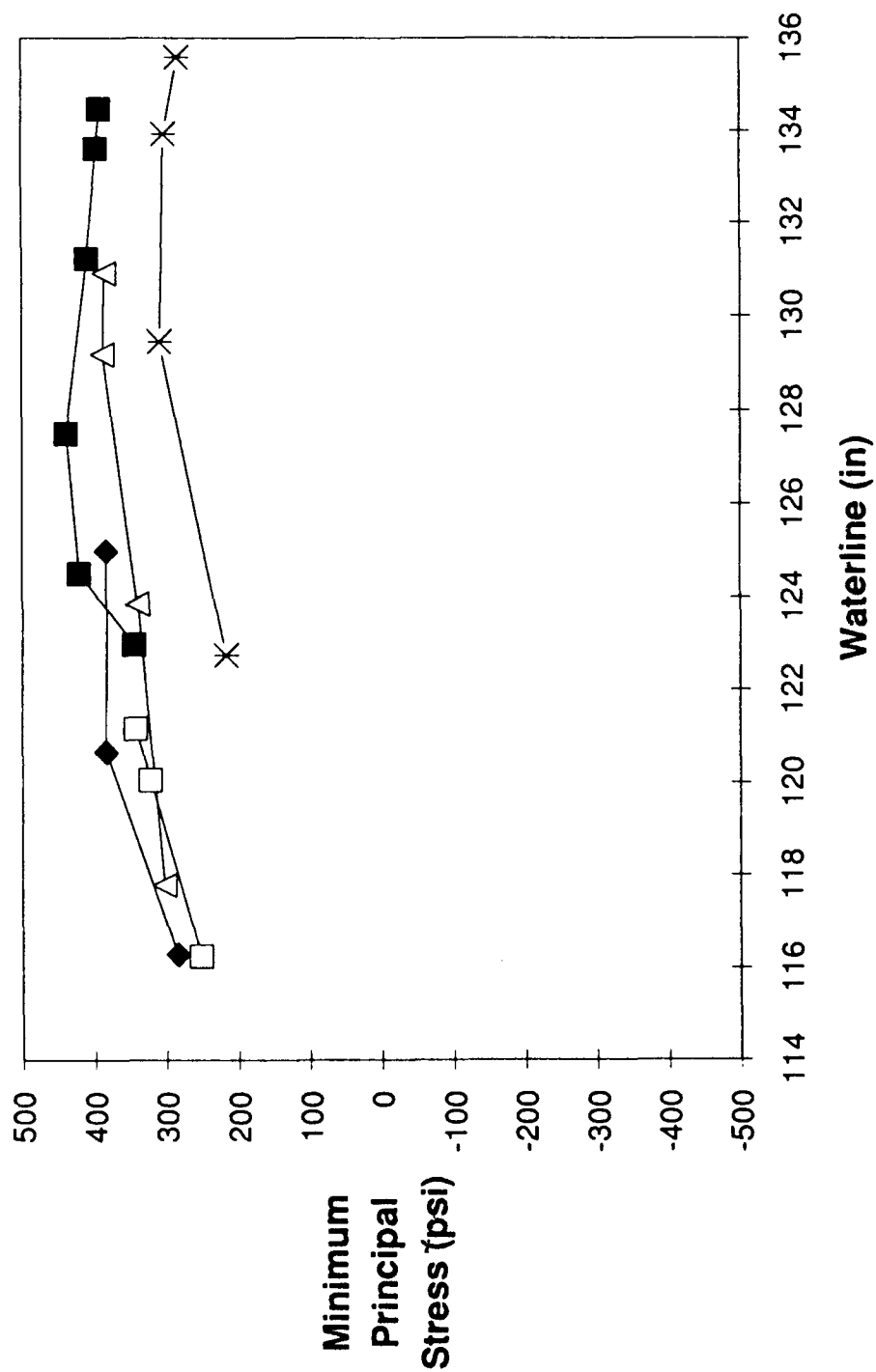


Figure 5.25. Minimum Residual Stress - Canopy T1.

# Minimum Residual Stress Canopy S1: Forward

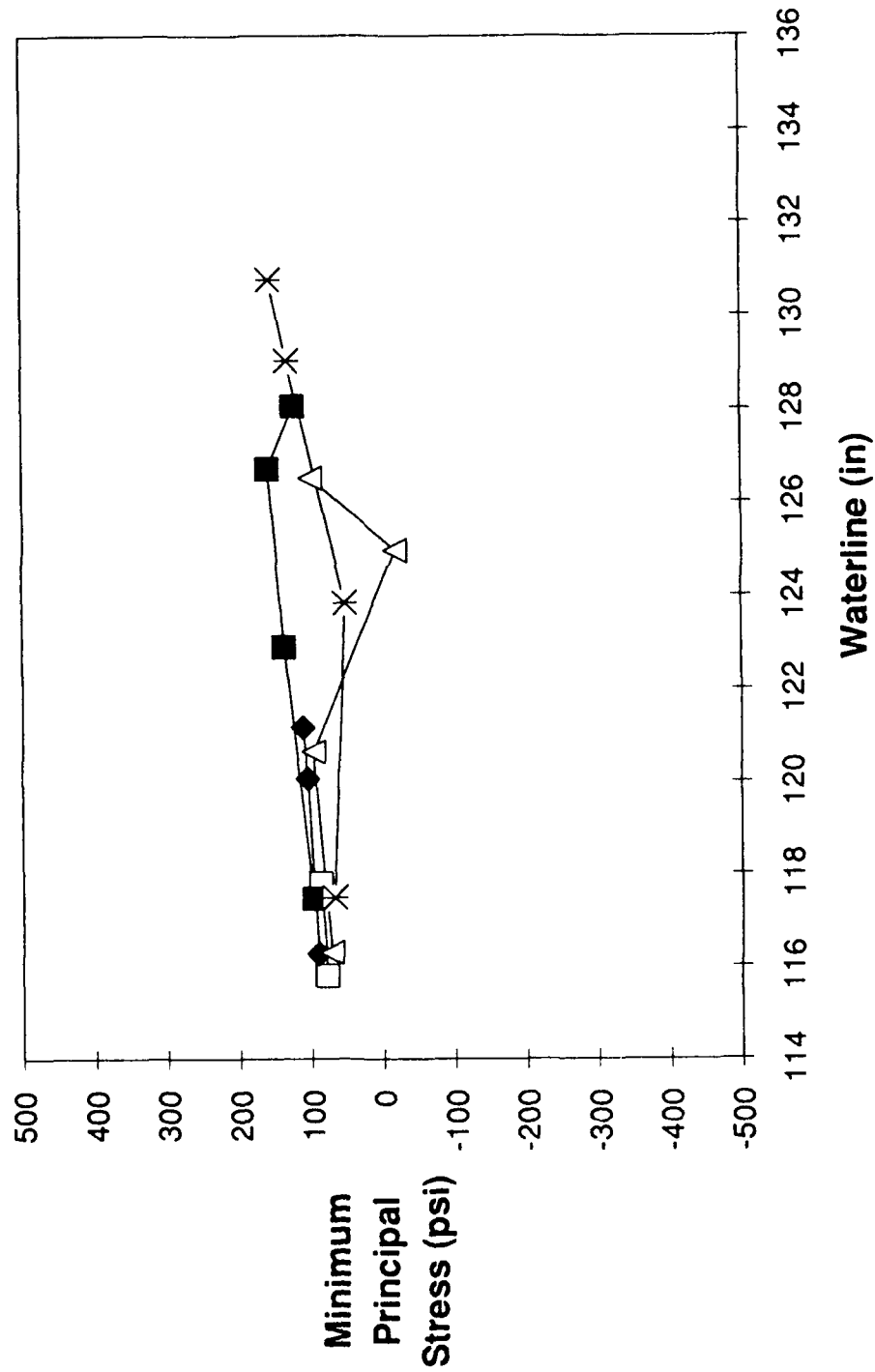


Figure 5.26. Minimum Residual Stress - Initial Strain Baseline - Canopy S1: Forward.

# Minimum Residual Stress Canopy S1: Aft

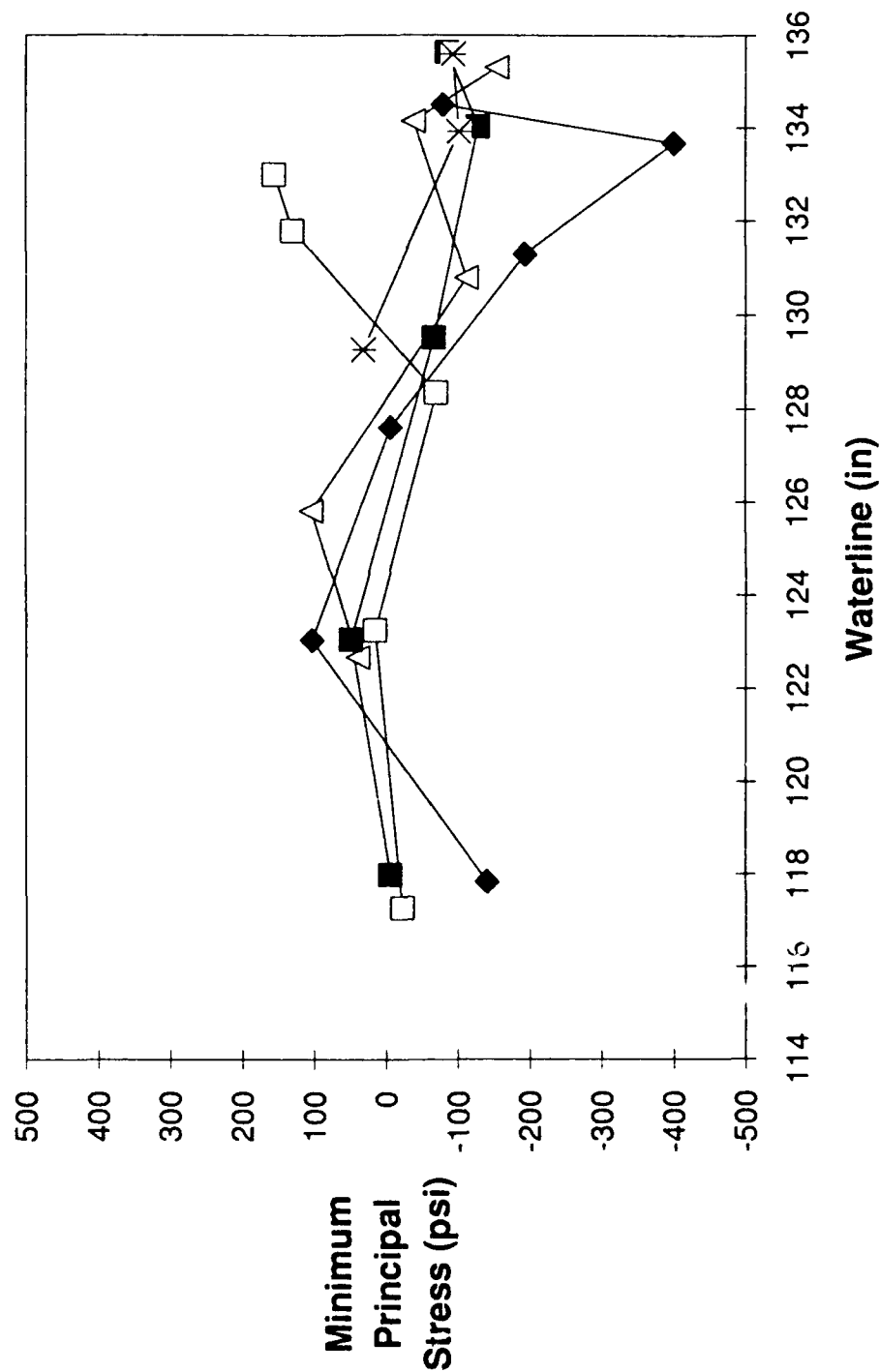


Figure 5.27. Minimum Residual Stress - Initial Strain Baseline - Canopy S1: Aft.

#### 5.4.2 Hole Drilling and Superimposed Regular Rosette Results

Because the hole drilling method measures relieved strain due to the stress on the component, it does not distinguish between stress inducing mechanisms. Hole drilling tests on installed canopies measure stress due to installation and residual stresses, and on pressurized canopies measure the superposition of installation, pressure, and residual stresses. The following results and discussion, therefore, superimpose the above regular rosette results to compare to hole drilling results.

##### 5.4.2.1 Hole Drilling on Installed Canopies

Table 5.3 shows results for both canopies in the installed state. It is interesting to note that the Texstar stresses (installation plus residual) are predominately tensile/tensile while the Sierracin stresses are mainly compressive/compressive.

In comparing Table 5.3 to the sectioning results (obtained by superimposing installed and residual stresses), Figures 5.28-5.30, the two methods yield essentially the same results. Variations between the two methods come from two sources: (1) the two methods are not conducted at the exact same locations in the canopies, and (2) the installation induced stress is applied through a constant displacement which may relax slightly over time. The hole drilling method, which responds to stress in the material, would measure the relaxed stress. The sectioning rosettes, however, respond to the installation displacements which remain constant as the stress relaxes. The sectioning method would therefore tend to yield higher installation stresses than the hole drilling method.

##### 5.4.2.2 Hole Drilling on Pressurized Canopies

Table 5.4 shows hole drilling results for both canopies while the canopies were being pressurized to 6 psig. Figures 5.31-5.33 show sectioning results for installation, pressurization, and residual stresses superimposed. In comparing the hole drilling and sectioning results, the two methods roughly agree in maximum stress measurements. It is also interesting to note that the Texstar measurements show some degree of symmetry between L/H and R/H measurements. Discrepancies are again due to the error in the measurement techniques and slight differences in hole locations. Differences in deflection

TABLE 5.3

HOLE DRILLING RESULTS: INSTALLED CANOPIES  
CANOPY T1

$$A = -1.5E-07$$

$$B = -3.5E-07$$

FS	WL	$\sigma_{\max}$ (psi)	$\sigma_{\min}$ (psi)	$\beta^*$ (deg)
R/H				
103.00	117.70	147.90	84.50	135.00
109.00	121.90	509.20	438.20	136.50
119.00	126.60	602.90	536.60	169.30
130.70	131.20	424.30	339.90	167.60
148.30	132.70	437.10	300.20	132.30
L/H				
102.00	118.50	200.40	103.50	148.80
107.70	118.70	55.60	-11.30	135.00
109.10	122.20	236.00	135.00	140.90
118.90	128.40	337.70	270.00	3.17
120.10	120.90	100.55	-15.65	168.20
131.40	132.00	359.20	302.20	150.80
141.30	128.00	266.80	202.50	147.90
149.40	121.40	309.40	262.60	149.30

CANOPY S1  
(All measurements L/H side)

FS (in)	WL (in)	$\sigma_{\max}$ (psi)	$\sigma_{\min}$ (psi)	Theta (deg)
99.90	116.80	157.09	124.44	-74.52
109.70	120.50	-201.46	-352.66	16.45
120.20	127.70	-231.67	-371.60	-6.55
136.20	132.40	-160.98	-281.42	-9.50
156.70	131.00	-446.77	-607.84	-22.03

# Maximum Stress (Installed Plus Residual) Canopy T1

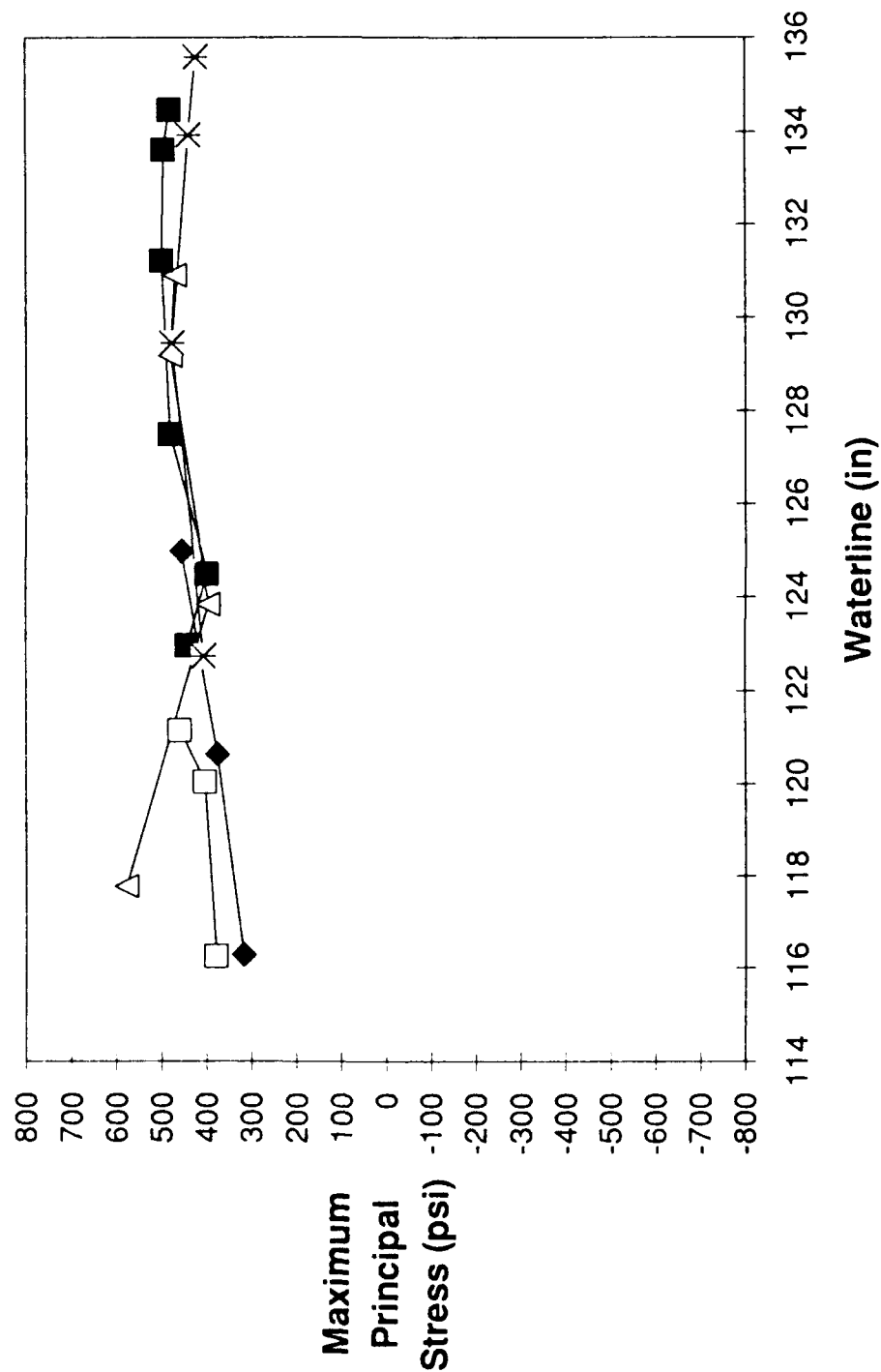


Figure 5.28. Maximum Stress (Installed Plus Residual) Canopy T1.



# Maximum Stress (Installed Plus Residual) Canopy S1: Forward

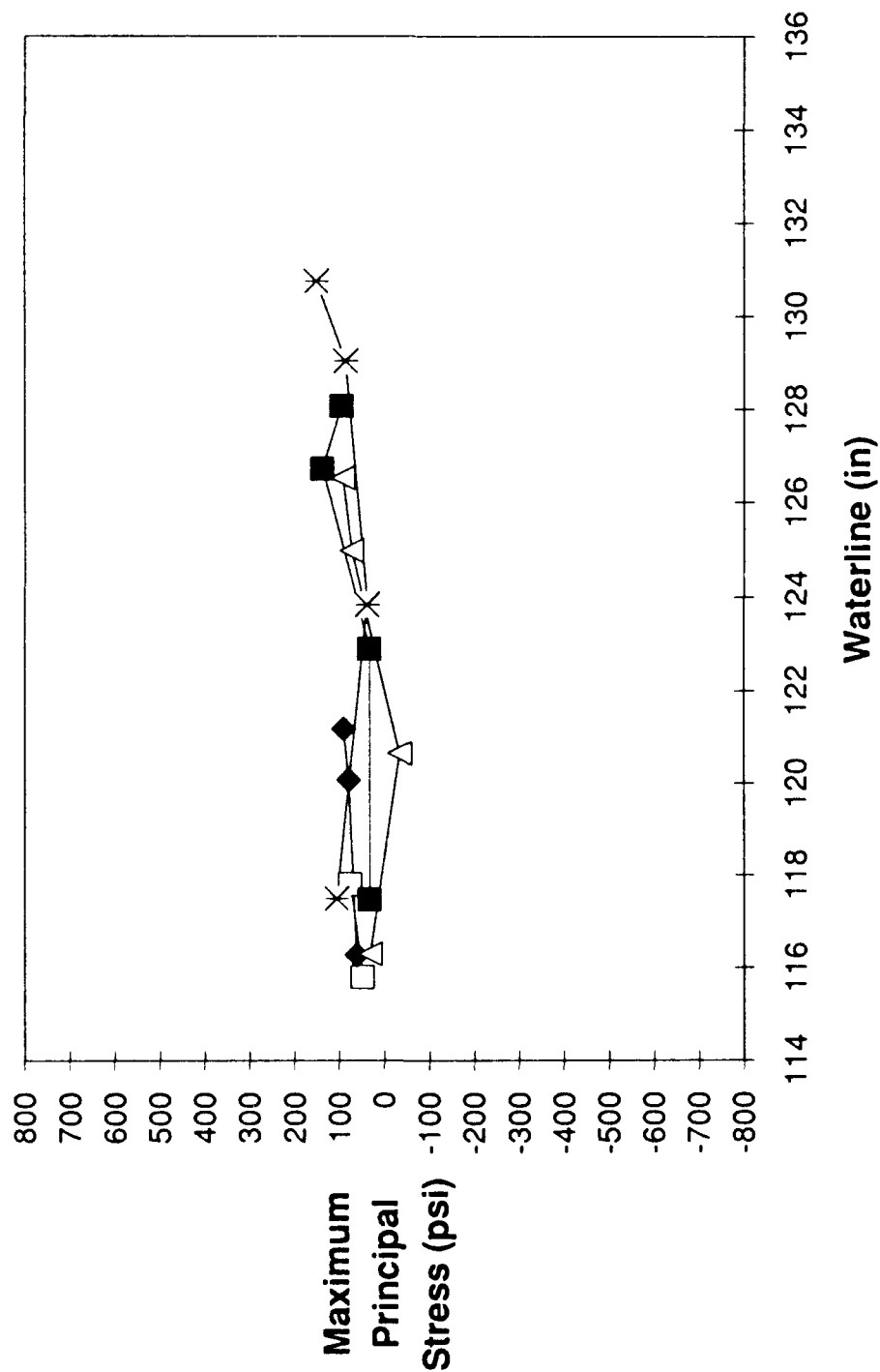


Figure 5.29. Maximum Stress (Installed Plus Residual) Canopy S1: Forward.

# **Maximum Stress (Installed Plus Residual)** **Canopy S1: Aft**

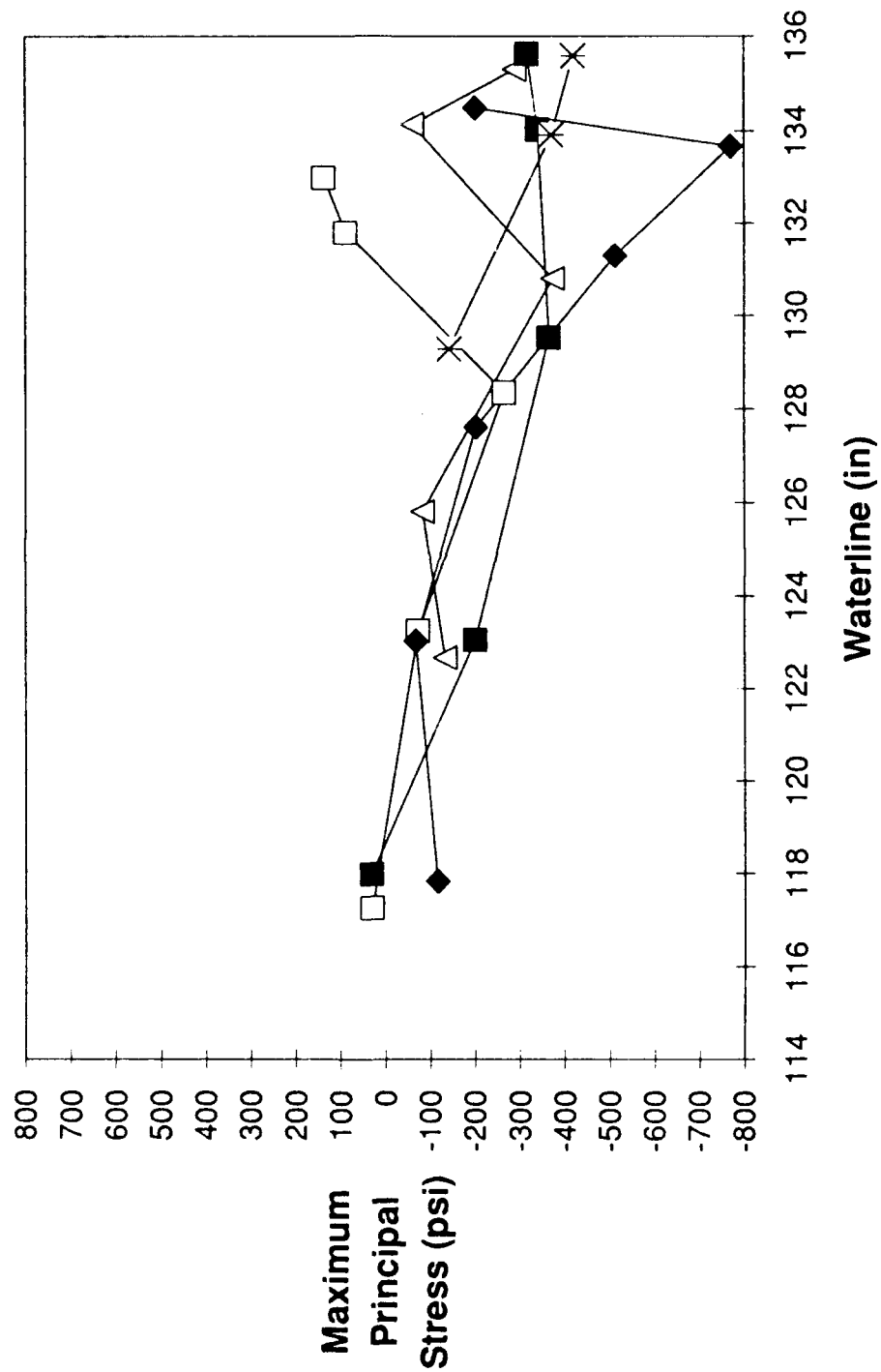


Figure 5.30. Maximum Stress (Installed Plus Residual) Canopy S1: Aft.

TABLE 5.4

## HOLE DRILLING RESULTS: PRESSURIZED CANOPIES

CANOPY T1				
FS	WL	$\sigma_{\max}$ (psi)	$\sigma_{\min}$ (psi)	$\beta^*$ (deg)
R/H				
102.70	117.10	17.93	-125.18	143.20
110.00	119.20	-92.55	-264.95	5.36
120.10	123.80	29.17	-87.26	65.50
130.76	130.60	381.47	311.17	47.50
148.30	131.90	367.33	334.20	3.75
L/H				
102.30	118.10	132.60	-29.80	161.20
107.90	118.10	-206.80	-499.20	122.50
109.30	121.80	62.13	-182.80	151.90
131.40	131.50	462.80	270.05	164.20
141.40	126.70	468.70	389.30	110.60
149.40	118.20	615.40	546.50	38.74

CANOPY S1  
(ALL MEASUREMENTS L/H)

98.90	116.30	145.68	64.35	-4.62
108.80	120.00	-220.89	-294.52	-22.50
120.90	127.60	-110.86	-237.70	-23.69
136.20	130.70	-52.99	-197.26	5.22
156.70	129.20	-309.07	-611.48	-10.11

# Maximum Superimposed Stress Canopy T1

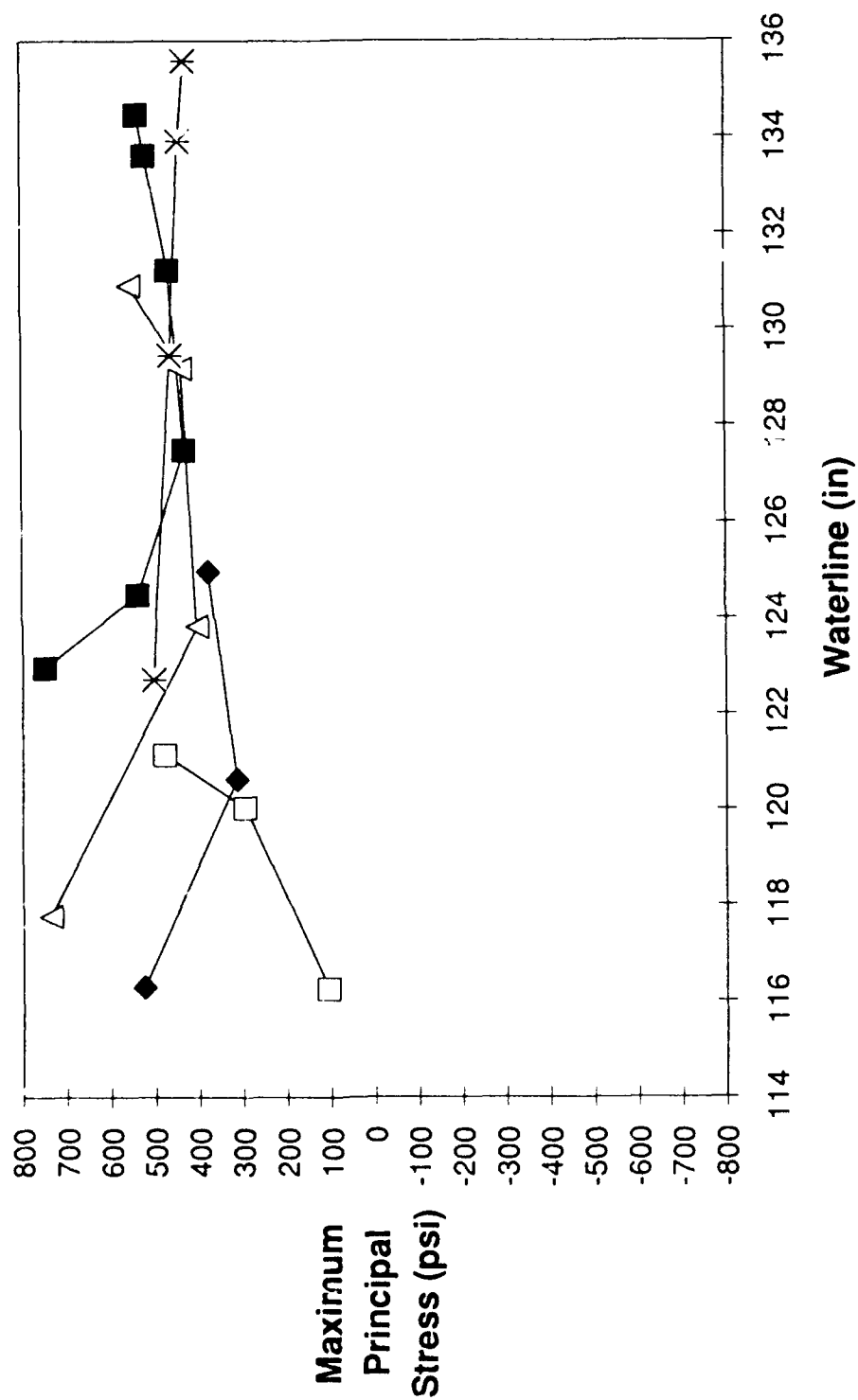


Figure 5.31. Maximum Superimposed Stress, Canopy T1.

# Maximum Superimposed Stress Canopy S1: Forward

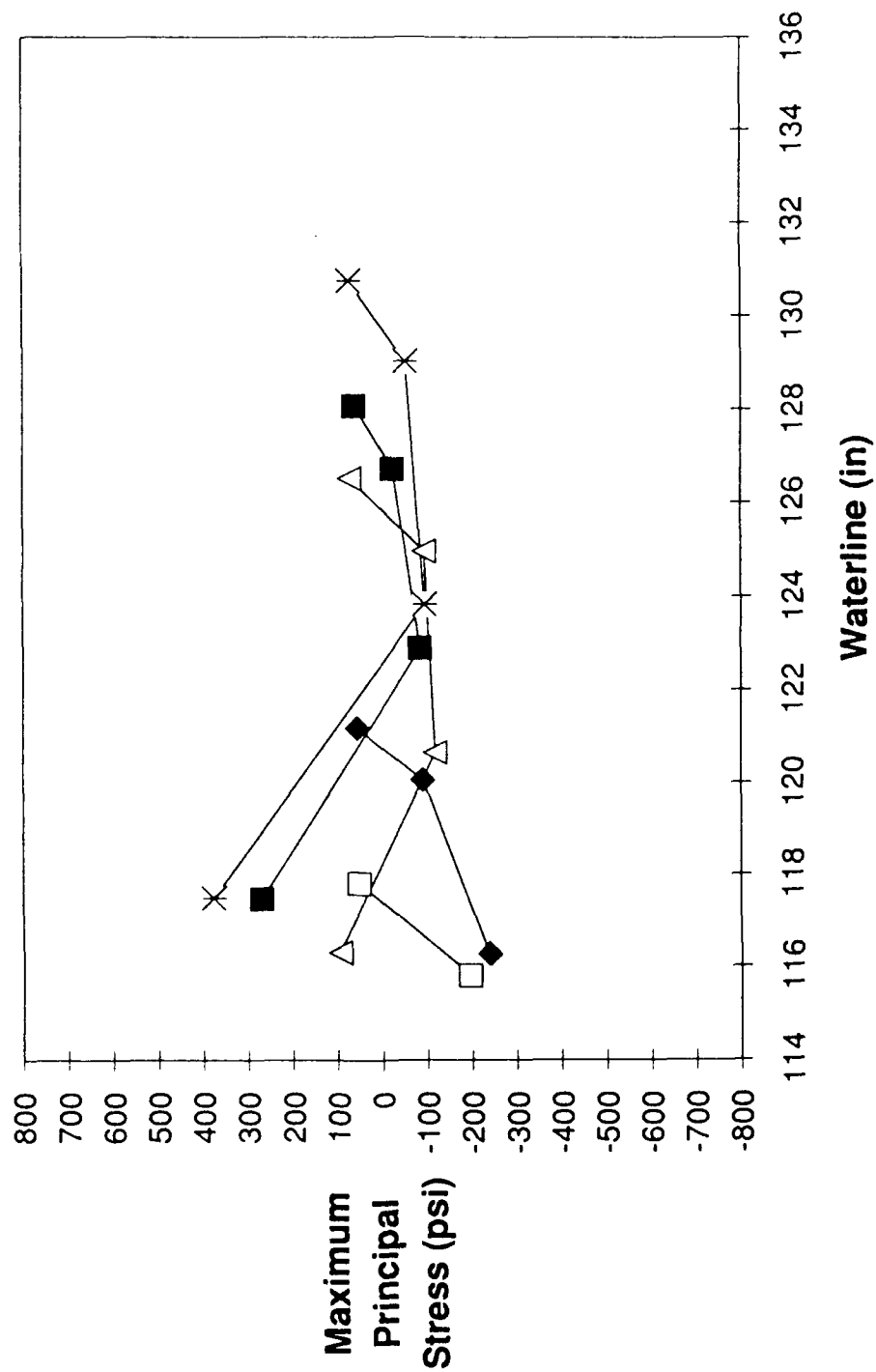


Figure 5.32. Maximum Superimposed Stress, Canopy S1: Forward.

# Maximum Superimposed Stress Canopy S1: Aft

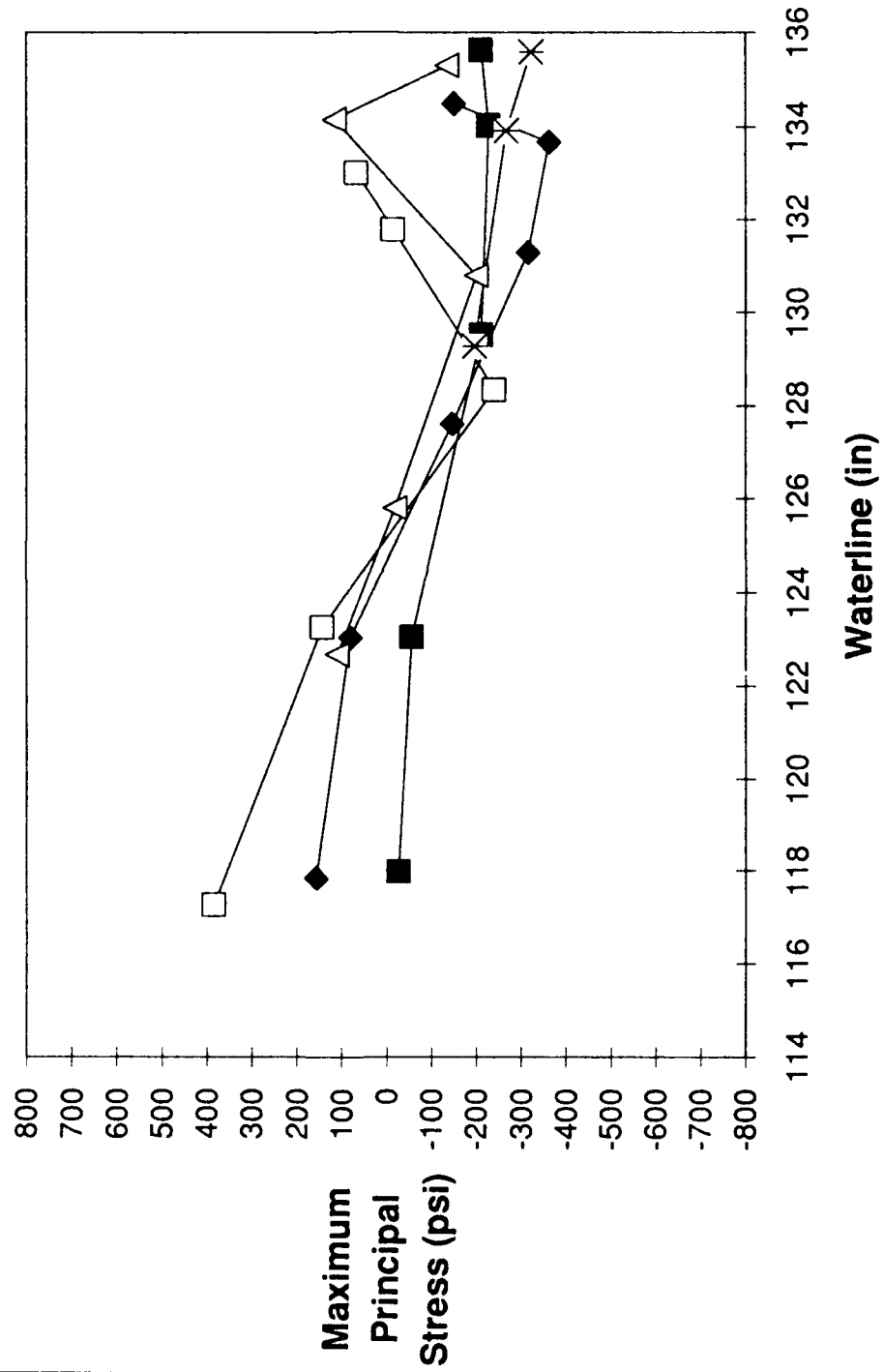


Figure 5.33. Maximum Superimposed Stress, Canopy S1: Aft.

between L/H and R/H during installation may also contribute to differences in stress measurement.

As stated previously, differences in service-life and age between the two canopies make comparisons difficult to interpret. However, it is interesting to note that both canopies show the same trend in maximum principal stresses for similar fuselage stations. Forward fuselage stations show increasing stress with increasing waterline. Mid-section fuselage stations show a decrease with waterline and then increase again with waterline as the centerline is approached. Aft fuselage stations show stable or decreasing maximum stresses with increasing waterline. The difference is in the magnitude of the maximum principal stresses: the Texstar canopy shows all positive (tensile) stress while the Sierracin shows a mixture of lower positive stress and compressive stress.

## SECTION 6

### DETERMINATION OF RESIDUAL STRESSES BY THE HOLE DRILLING METHOD

With hole-drilling techniques and hardware developed and validated, full-scale testing was undertaken to determine the residual stress levels in in-service canopies.

#### 6.1 TEST SPECIMENS

Table 6.1 describes the 20 full-scale F-16 canopies tested. As noted, the degree of crazing varied greatly from canopy to canopy. Some showed no visible sign of crazing during inspection prior to testing despite indications to the contrary on the appropriate "measle" charts. The canopies were manufactured by either Texstar or Sierracin. Several canopies, as indicated on Table 6.1, were forward canopies from F-16C aircraft.

Because of the limited number of canopies tested, dependence of stress or crazing on canopy age could not be established. It also does not appear from the limited data that the specific USAF base influenced crazing. However, of the 12 Texstar canopies, 11 were crazed, while only 2 of 8 Sierracin canopies were crazed.

#### 6.2 STRAIN GAGES/ALIGNMENT FACILITY

In general, each canopy was instrumented with three hole drilling gages: one inside a crazed region, one in an uncrazed region adjacent to the crazed region, and a third in an uncrazed region distant from the crazed region. The most notable exception was the four holes drilled in test #17 (S/N 283), which possessed numerous highly crazed regions. The specific locations are listed along with stress results in Section 6.4. Appendix B gives schematic drawings of rosette locations.

All tests utilized Measurements Group, Inc. rosette type CEA-06-062UM-120. A set of calibration tests conducted on flat preshrunk acrylic samples (identical to those used to



TABLE 6.1  
FULL SCALE TEST SPECIMEN PROFILE

SPECIMEN NO.	S/N	DOM	DOR	BASE	MANUFACTURER	<u>CRAZE STATE</u>
1	473	1-86	N/A	Shaw	Sierracin	None
2*	184	10-87	3-90	MacDill	Sierracin	None
3	373	10-85	4-90	Kunsan	Texstar	Small locally dense
4*	218	10-85	N/A	N/A	Texstar	Small locally dense
5	1476	9-87	2-89	Luke	Texstar	Small locally dense
6	289	7-85	4-89	Nellis	Texstar	Small locally light
7*	138	7-87	11-89	MacDill	Sierracin	None
8	612	5-86	3-90	Ramstein	Texstar	Small locally light
9	734	2-84	1-90	Kelly	Sierracin	Small locally dense; others light
10	1483	12-87	N/A	Nellis	Sierracin	None
11	133	4-84	N/A	Nellis	Texstar	None
12	1358	10-87	4-90	MacDill	Sierracin	Locally very light
13	835	9-86	5-90	Ramstein	Texstar	Locally dense
14	869	9-86	1-90	Tinker	Texstar	General light
15	499	2-86	12-89	Ramstein	Sierracin	Locally very light
16*	019	1-85	N/A	N/A	Sierracin	None
17	283	9-85	4-90	Shaw	Texstar	Locally dense
18	504	2-86	12-89	Ramstein	Texstar	Light deep local craze
19*	401	9-87	N/A	MacDill	Texstar	Locally light
20	279	7-85	3-90	Shaw	Texstar	Locally light, deep craze

\*F-16C forward canopies

DOM denotes date of manufacture

DOR denotes date of removal

calibrate and validate type TEA and EA rosettes) yielded coefficients of  $\bar{A} = -9.5 \times 10^{-8}$  in<sup>2</sup>/lb and  $\bar{B} = -5.1 \times 10^{-7}$  in<sup>2</sup>/lb. These calibrations were conducted exactly as the previous calibration tests, with the VALAPODD replacing the jig borer for drilling.

Rosettes were aligned and waterline and fuselage station measurements were taken using the same alignment/layout rig described in Section 5.2.

### 6.3 TEST PROCEDURE

After removal from the shipping crate, each canopy was placed on the T-frame under the alignment rig and, when required, the surface cleaned. In some instances the canopy required inward deflection to seat it within the restraining collars. After consulting the appropriate "measle" chart, sites for drilling were selected and rosettes installed. Waterline and fuselage station measurements were recorded for each rosette.

Hole drilling commenced at each site using the VALAPODD. Appendix A describes the exact procedure followed for using the device. To more accurately record results, an NCR PC-8 personal computer equipped with a Metrabyte DASH-8 analog-to-digital data acquisition board logged the strain data. Along with a Metrabyte EXP-16 multiplexer/amplifier, this data collection system allowed more precise collection of strain vs. time data. The DASH-8, a 12-bit A/D card, in conjunction with the EXP-16, had a resolution of  $\pm 2.4 \mu\epsilon$ .

### 6.4 RESULTS

Deflecting the canopy to fit into the T-frame presented concerns as to whether the deflection induced stress was high enough to affect residual stresses, hence inducing error in the hole drilling measurement. To investigate the possibility, Canopy S/N 133 (Test #11) was instrumented with a rosette on the canopy centerline at FS 144. This represented a position directly above a spreader bar, whose ends were positioned approximately 3 inches in and 3 inches up from the lower aft corner of the canopy. The canopy was then spread (as during installation or removal) in 0.5-inch increments and the resulting strains recorded. These readings gave an indication of the greatest stress which may be induced by deflecting the canopy to fit on the T-frame.

Figure 6.1 displays the results of the test. As shown, stresses induced during high deflection (as during installation) can be considerable at the point instrumented. However, none of the canopies which were tested during this program required more than 0.5 inch of deflection to fit inside the restraining collars. In addition, the position tested was considered the point to contain the highest deflection induced stress. For these reasons, and with the assumption (for small deflections) that inward and outward deflections of equal magnitude create equivalent stress (but with opposite sign), stresses produced by deflection during hole drilling were neglected.

Table 6.2 summarizes the results for all 20 canopies tested. All of the locations tested away from crazed areas displayed compressive maximum and minimum stresses. All locations which showed tensile stresses were in or near crazed regions. However, several regions which showed light crazing produced compressive stresses, as in test numbers 9, 12, 15, 19 and 20. Crazed regions very near the canopy edges, test numbers 4 and 5, produced highly compressive stress. However, the location of these regions required mounting the VALAPODD off the canopy via an extension plate, which may increase the uncertainty of the reading.

It is interesting to note the trend in positive stresses near crazed regions. Tests 3, 8, 13, 14, 18 and 20 show tensile stresses to be lower inside the crazed region than in regions immediately surrounding, and in some cases reducing to compression far away. This may be a result of the stress relieving mechanism of craze. This trend is not found, however, in crazed regions showing compressive stress. In these regions no particular trend can be distinguished.

Seven canopies (1, 2, 6, 7, 10, 11, 16) showed no signs of crazing and produced all compressive stresses. Canopies 2, 6, 7, 16 show the maximum principal stress becoming less compressive from forward to aft. Test number 1 shows the opposite trend, while 10 and 11 show no specific trend.

# Stress Induced by "Free State" Deflection

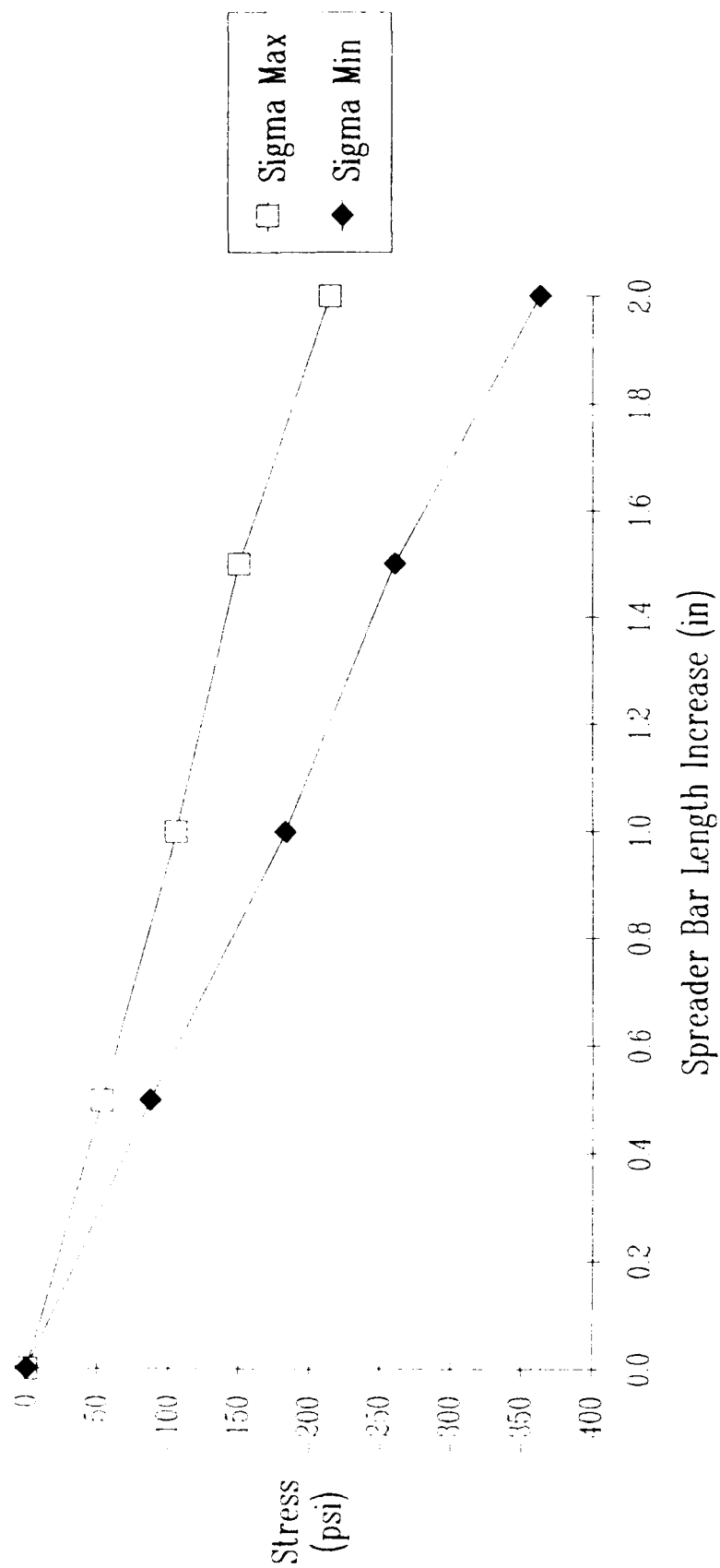


Figure 6.1. Stress Resulting from Deflection by the Spreader Bar.

TABLE 6.2  
FULL SCALE F-16 HOLE DRILLING RESULTS

A = -9.5E-08

B = -5.1E-07

TEST*	S/N	WL	FS	e1	e2	e3	SIGMAX	SIGMIN	BETA**	CRAZE STATE***
1A 1B 1C	473	132.2 129.2 115.2	161.9 130.9 98.9	280 188 188	302 209 159	273 162 140	-1426.5 -881.9 -837.4	-1477.2 -953.6 -885.3	3.6 10.3 -139	None None None
2A 2B 2C(L)	184	132.7 116.7 113.9	153.9 115.9 100.9	154 252 267	180 217 236	170 263 375	-832.4 -1310.3 -1586.1	-870.3 -1390.3 -1783.7	-12.3 -85.9 -73.7	None None None
3A 3B 3C(L)	373	132.2 129.2 113.4	159.4 130.9 95.2	182 126 -29	113 74 -118	190 181 68	-903.9 -722.4 41.6	-1047.1 -886.4 -244.7	-98.4 -80.3 -80.2	None None Small dense horizontal
4A 4B 4C	218	133.2 124.7 112.2	155.9 125.9 93.4	172 160 267	165 41 174	274 203 166	-1095.5 -813.1 -1070.9	-1248.6 -1094.3 1201.8	-69.5 -85.7 -114.9	None None Small dense vertical near edge
5A(L)  5B 5C	1476	118.0  128.2 115.4	168.4  126.9 97.4	174  235 229	200  130 113	392  210 224	-1349.7  -1075.2 -1076.8	-1619.6  -1259.5 -1301.4	-63.6  -93.6 -90.6	Small dense near edge None None
6A 6B 6C	289	132.7 128.7 113.6	165.9 136.9 101.7	105 160 259	97 106 308	228 209 142	-781.5 -888.0 -931.6	-964.3 -1050.4 -1171.6	-69.3 -81.3 14.2	None None Very light vertical
7A 7B 7C	138	129.2 129.5 114.9	157.4 124.9 97.4	233 269 293	210 209 263	266 253 293	-1268.3 -1318.3 -1509.2	-1353.5 -1422.1 -1567.7	-78.8 -94.2 -89.8	None None None
8A 8B 8C	612	131.3 115.8 114.9	170.5 123.8 98.8	401 82 30	295 -26 -81	369 86 -4	-1930.4 -331.9 25.9	-2110.2 -548.4 -161.3	-94.9 -89.5 -95.2	Light mixed  Light horizontal
9A 9B 9C	734	115.1 122.1 111.3	112.2 109.3 93.0	63 65 97	-16 -70 23	88 -23 113	-303.3 -10.7 -468.7	-485.1 -208.7 -630.5	-86.1 -102.9 -87.2	Light mixed Light horizontal Light vertical
10A 10B 10C(L)	1483	133.6 129.7 114.2	171.9 131.9 97.4	454 308 370	431 238 271	454 299 310	-2361.2 -1526.5 -1709.6	-2406.4 -1654.9 -1857.5	-89.9 -92.0 -101.8	None None None
11A 11B 11C(L)	133	134.2 123.5 115.5	144.4 227.5 98.5	185 162 310	120 117 235	197 141 286	-930.6 -761.5 -1501.9	-1070.8 -831.5 -1628.0	-87.6 -98.5 -95.3	None None None
12A 12B 12C	1358	132.4 128.4 113.0	161.9 127.2 94.0	227 209 246	214 143 155	210 178 209	-1136.8 -964.1 -1119.4	-1154.9 -1067.8 -1266.3	-121.7 -98.8 -97.2	None None Light Mixed

TABLE 6.2 (Continued)

TEST*	S/N	WL	FS	e1	e2	e3	SIGMAX	SIGMIN	BETA**	CRAZE STATE***
13A 13B(L) 13C(L)	835	133.9 117.8 116.7	141.5 102.2 100.7	26 -172 -55	-51 -203 -139	7 -152 -73	-20.3 891.5 409.3	-155.6 809.6 259.9	-94.0 -83.2 -93.5	None Adjacent to crazed region Heavily crazed, mixed
14A 14B 14C	869	125.3 119.0 114.9	114.9 107.9 97.2	-239 -176 -83	-259 -226 21	-256 -229 -202	1306.9 1098.3 920.1	1289.8 1028.6 578.0	-126.8 -114.6 15.0	Moderate; less than hole #2 Heavy; less than hole #3 Very dense; mixed
15A 15B 15C	499	116.3 125.3 114.9	143.2 114.9 97.2	377 148 175	258 121 169	489 113 170	-2091.5 -666.4 -899.7	-2454.0 -705.6 -908.1	-81.1 -121.1 -106.3	Very light craze mixed None None
16A 16B 16C	019	133.0 121.8 115.2	138.7 111.7 97.9	23 36 260	-72 -39 132	27 58 239	-36.4 -161.8 -1194.4	-227.7 -333.1 -1426.9	-89.4 -86.5 -92.5	None None None
17A 17B 17C 17D	283	128.1 119.7 114.7 113.1	123.7 105.2 100.4 98.5	7 146 212 232	-64 36 138 156	6 138 213 195	35.3 -640.9 -1042.0 -1062.2	-103.5 -849.2 -1188.2 -1182.2	-90.0 -91.0 -89.7 -98.8	Lightly crazed Crazed, small impact marks Outside crazed area Very dense local craze (from impact)
18A(L) 18B(C) 18C(L)	504	121.2 118.2 113.4	109.8 102.5 95.3	-45 -214 -157	-185 -276 -256	-144 -274 -152	597.4 1322.3 910.1	393.6 1236.0 710.3	-104.3 -111.6 -89.2	Heavy vertical Between holes #1 and #3 Heavy mixed
19A(L) 19B(L) 19C(L)	401	134.7 116.8 114.0	160.9 156.4 101.2	195 94 139	50 -9 143	98 94 159	-661.5 -391.9 -963.0	-874.4 -594.9 -1124.5	-103.2 -89.9 -66.5	Light horizontal Light mixed Very light vertical
20A 20B 20C	279	121.3 129.6 131.6	107.8 134.23 157.0	67 -78 130	-7 -92 -112	84 28 85	-315.2 213.9 -347.5	-478.4 46.4 -781.1	-87.1 -67.9 -92.9	None Light crazing mixed Light deep craze mixed

- \* (L) Left side of canopy
- (R) Right side of canopy
- (C) Centerline of canopy

\*\* Positive angle refers to CCW rotation from waterline axis to maximum algebraic stress.

\*\*\* Horizontal/Vertical refers to orientations of the majority of crazes in that region

## SECTION 7

### DISCUSSION AND RECOMMENDATIONS

Based on craze threshold stresses found in the literature, the stresses measured in the majority of transparencies appear too low to cause crazing, in a "uniform" environment (no large temperature changes; low moisture content; brief contact with crazing compounds). Although craze threshold values can be as low as 0 psi (for water saturated Plex-55 in ethylene glycol), typical uniaxial values are, for example, 930 psi for Plexiglas II in Dimethyl Formide [19], 1450 psi for plexiglass 201 in acetone, 2175 psi for Swedlow S-708 in acetone, 3190 for Polycast 76 in isopropanol [20], to 11,400 psi (or essentially ultimate strength) for dry Plex-55 in water. Many acrylic material/crazing agent combinations reveal crazing thresholds between 1000 and 4500 psi [21].

Bouchard [17] recently reported a crazing stress threshold of approximately 1150 psi for uniaxial laminated beam tests in 98% isopropanol. This value remained stable over 3 years of aging with no environmental exposure. However, the threshold dropped to 610 psi with 3 years of natural environmental exposure. Although none of the installed or pressurized canopy stresses were this high, several of the residual stress hole drilling measurements exceeded this value in and around crazed regions. This may indicate that craze could occur in these regions, especially with pressure and flight loads superimposed on the residual stresses. It should be noted, however, that this craze threshold applies to a uniaxially stressed specimen in contact with a crazing compound (98% isopropanol) for a 30-minute time period. Conditions in and around the transparency could be very different.

Based on measurements taken on 20 F-16 canopies, it is interesting to note that all of the tests conducted far away from crazed regions show compressive stresses. These areas of compression were primarily in the aft section of the canopy. The current craze criteria suggest craze should not appear in areas which contain compressive stress. In fact, no crazing was found in the aft portions with the exception of aft crazing near bolt hole edges.

It should be understood that the craze criteria being applied to this study is maximum stress. The material is thought to craze when in contact with a crazing solution and when the maximum stress exceeds a certain critical level. This may not be the best criteria for crazing

in acrylic. Other criteria, such as strain energy density, may better describe the crazing threshold. If the stress data were recast in another form to match another criteria, more information might be gained. This area should be pursued in conjunction with other crazing criteria.

A second point, somewhat related to the previous one, is the biaxial nature of the stress states in the canopies. A uniaxial criterion does not sufficiently predict craze onset in biaxial stress states, because the criterion does not state how the second stress field affects crazing in the first stress field. For example, Read, Dean, and Duncan [22] reported increases in craze resistance for a tensile/tensile biaxial stress field compared to an equivalent uniaxial stress field. This increase makes sense in terms of a maximum strain criteria, since Poisson's effects cause the strain to decrease in one direction as tension is applied in the other. However, other biaxial tests conducted at UDRI have shown "threshold values" (stress at which crazing does not occur until 30 minutes after application of solution) in the range of 1400/2000 psi, somewhat lower than corresponding uniaxial tests. This might correspond to a stress criteria or strain energy criterion. A fundamental biaxial craze criteria needs to be developed to accurately correlate canopy craze to stress states.

It would appear from the data that other mechanisms which by themselves may not cause craze must be considered in gaining a fundamental understanding of the craze problem. Such mechanisms could cause the transparencies to craze when superimposed on residual and pressure stresses. Among those that deserve attention are:

- Moisture deportation from the surface. Quick ascent from a hot/wet field location to cold/dry atmospheric conditions can cause desorption of water from a thin surface layer of the canopy. This results in high tensile stresses in laboratory scale tests [18]. Accurate mission profiles for aircraft stationed at bases in hot/wet environments and surface stress laboratory data are necessary to pursue this possibility.
- Cyclic loading. Previous tests [22] have shown that cyclic biaxial loading with load-on/load-off ratios near unity produce more crazing than higher values of the ratio (10:1 or greater). Like fatigue, this indicates craze is sensitive to the nature in which the load is applied and should be investigated.



- Cyclic exposure to crazing solutions. No work has been done on the decrease in craze resistance which may occur if a crazing agent is applied to the acrylic, but removed before crazing occurs. The material may be less craze resistant the next time the agent is applied to the surface. Just as fatigue cycles are additive despite long time gaps between sets of cycles, the time under craze may be additive despite long time gaps between application of the craze agent. This possibility should also be investigated.

## REFERENCES

- (1) Raju, B., Nondestructive Measurement of Residual Stresses in Aircraft Transparencies, WRDC-TR-89-3099, Wright-Patterson Air Force Base, Ohio, 1989.
- (2) Timoshenko, S. P., and Goodier, J. N., Theory of Elasticity, Third Edition, McGraw-Hill, Inc., New York, 1970.
- (3) Measurements Group, Inc., Measurement of Residual Stresses by the Hole-Drilling Strain Gage Method, Tech Note TN-503-3, Raleigh, North Carolina, 1988.
- (4) Gupta, B. P., "Hole Drilling Technique: Modifications in the Analysis of Residual Stress," Experimental Mechanics, Vol. 13, No. 1, January 1973.
- (5) Schajer, G. S., "Applications of Finite Element Calculations to Residual Stress Measurement," Journal of Engineering Materials and Technology, American Society of Mechanical Engineers, Vol. 103, April 1981.
- (6) Kabiri, M., "Toward More Accurate Residual Stress Measurement by the Hole-Drilling Method: Analysis of Relieved Strain Coefficients," Experimental Mechanics, Vol. 26, No. 1, March 1986.
- (7) Flaman, M. T., Mills, B. E., and Boag, J. M., "Analysis of Stress-Variation-With-Depth Measurement Procedures for the Center-Hole Method of Residual Stress Measurement," Experimental Techniques, Vol. 11, June 1987.
- (8) Chow, C. L., and Cundiff, C. H., "On Residual-Stress Measurements in Light Truck Wheels Using the Hole-Drilling Method," Experimental Mechanics, Vol. 25, No. 1, March 1985.
- (9) Plotkowski, P. D., and Kowalski, H. C., "Residual Stress Determination on Nasty Surfaces," Experimental Techniques, Vol. 12, No. 3, March 1988.
- (10) Nelson, D. V., and McCrickerd, J. T., "Residual Stress Determination Through Combined Use of Holographic Interferometry and Blind-Hole Drilling," Experimental Mechanics, Vol. 26, No. 4, December 1986.
- (11) Beaney, E. M., "Accurate Measurement of Residual Stress on any Steel Using the Centre Hole Method," Strain, July 1976.
- (12) Gran, M. G., "Residual Stresses in F-16 Transparencies," Conference on Aerospace Transparency Materials and Enclosures, AFWAL-TR-89-4044, S. A. Marolo, editor, April 1989.

- (13) Lu, J., and Flavenot, J. F., "Applications of the Incremental Hole-Drilling Method for Measurement of Residual Stress Distribution," Experimental Techniques, November 1989.
- (14) Perry, C. C., Lisner, H. R., The Strain Gage Primer, McGraw-Hill, Inc., New York, 1962.
- (15) Dumore Corporation, "A Guide to Profitable Production Holemaking," technical brochure, Racine, Wisconsin, 1988.
- (16) Measurements Group, Inc., "Catalog 500 Part A - Strain Gage Listings," technical brochure, Raleigh, NC, 1989.
- (17) Bouchard, M. P., "Evaluation of the Effects of Artificial and Natural Environmental Exposure on Laminated F-16 Transparency Material," AFWAL-TR-88-3016, June 1988.
- (18) Burchill, P. J., and Stacewicz, R. H., "Effect of Water on the Crazing of a Cross-Linked PMMA," Journal of Material Science Letters, Vol. 1, 1982.
- (19) Hahan, K. I., "Environment Stress Cracking of Polymers," NASA Contract NSG-806, University of Southern Colorado report N80-18182.
- (20) Burchill, P. J., Mathys, G., and Stacewicz, R. H., "Analysis and Properties of Some Commercial PMMA-Based Materials," Journal of Materials Science, Vol. 22, February 1987.
- (21) Kambour, R. P., "A Review of Crazing and Fracture in Thermoplastics," Journal of Polymer Science: Macromolecular Review, Vol. 7, 1973.
- (22) Read, B. E., Dean, G. D., and Duncan, J. C., "Characterization and Influence of Orientation and Internal Stresses in Acrylic Aircraft Materials," NPL Report DMA(A) 113, December 1985.

**APPENDIX A**  
**PROCEDURES FOR USE OF VALAPODD**

## PROCEDURES FOR USE OF VALAPODD

The following is a step-by-step procedure for using the VALAPODD to measure stress by the hole drilling method.

1. Remove device from transport case and loosen both bearing lock and elevating support locking ring.
2. Set elevating supports (three) at the middle of travel.
3. Set translation stage at center location.
4. Attach control box consisting of three supply lines (two air and one vacuum) into quick disconnects. Set air pressure at 60 psi. With the VALAPODD on a level flat surface and position feet so that vacuum engages. Check the vacuum gauge to ensure 25 mHg of vacuum. If the gauge reads less, check for leaks in the connectors and hoses, a clogged vacuum pump in the control box, or tears in the vacuum cups. **DO NOT USE THE DEVICE IF 25-IN. HG VACUUM CANNOT BE MAINTAINED!**
5. Choose gauge to be tested and install a 0.125-inch-dia. x 0.007-inch-thick disk of Lexan to improve the reflective surface necessary to achieve perpendicularity. On one side of a sheet of 0.007 inch Lexan, place a strip of double-sided cellophane tape. Using a standard hole punch, cut a 0.125-inch-diameter disk from the sheet. Gently place the disk, cellophane tape side down, over the rosette target with enough pressure to ensure the disk remains in place.
6. Position VALAPODD base over the gauge, visually centering the device over the center target of the rosette. Using the relief valve (located on the inside surface of the control manifold) will allow suction cup to slide on transparency surface, if initial placement is not satisfactory. Ensure that the feet are square on the transparency surface and that vacuum is fully engaged (25 in Hg) before letting go of the base.
7. Remove microscope/laser from transport case. Wipe the steel mating surface of the microscope with a clean cloth and insert into linear bearing column.
8. Employ light source with toggle switch.

9. Using translation stage micrometers, locate the telescope cross-hairs over the center of the target.
10. Using the elevation supports, visually adjust the device to a position approximately perpendicular to the rosette surface.
11. Connect power source to laser and open shutter located on the lower right portion of the laser, making sure not to view rosette with laser shutter open. Although the lower power of the laser and polarized optical component prevent eye damage, viewing the rosette with the laser on and the shutter open can be uncomfortable.
12. Using the elevation supports, adjust the device so as to center the laser beam reflection on the target adjacent to the laser. This will provide an orientation perpendicular to the rosette surface.
13. After establishing a normal position, close laser shutter and verify location with microscope. Adjusting the device to a perpendicular in the previous step may cause the device to lose its centered location. It will therefore require several iterations between micrometer adjustment and elevation adjustment to maintain both target locations and perpendicularity.
14. Satisfied that both center and normal are correct, engage the bearing and elevation support locks. Recheck centered position, as engaging support lock nuts could push the base off-center. Even if re-centering is necessary, perpendicularity will be maintained.
15. Remove microscope/laser component.
16. Install drilling depth gauge block on end of drill bit.
17. Insert drill component into linear bearing column.
18. With the air cylinder rod fully retracted, allow depth gauge block to rest on rosette.
19. Set drilling depth with micrometer adjacent to the air cylinder. This is accomplished by backing the micrometer away from the drill component crossbar a distance equal to the depth to be drilled + 0.075 inch. This will permit the drill bit to penetrate the surface so that the conical portion of the drill tip completely penetrates through the desired depth.
20. Set the adjustable screw above the viscous damper so that it just touches the viscous damper rod. Finger-tighten the nut.

21. Remove drill head.
22. Insert microscope/laser and verify location. If location and perpendicularity are not correct, repeat steps 9-21.
23. Remove microscope/laser. Adjust air cylinder rod with the control lever so that the rod is fully extended. Remove drilling depth gauge block from drill bit. Insert the drill component into the bearing and secure to air cylinder rod with lock nut. Gently remove the Lexan from the rosette surface with a probe or tweezers, being careful not to damage the gauges.
24. Install flexible drive shaft to inside center of drill component. It will be necessary to sight align key on end of shaft with key slot located inside the drill head. Slightly push until shaft snaps into position.
25. On the base of the external drill motor, set drill speed at top center position of speed range. This should be approximately 1200 RPM for acrylic.
26. Ensure strain gauge and instrumentation are in order. Ensure gauges are zeroed. Begin drilling by positioning drill control lever forward. Drill will proceed quickly until viscous damper is engaged.
27. Drilling process is complete when micrometer is engaged with stop surface. Immediately retract drill head by reversing control lever. Drill will retract quickly.
28. Turn drill off.
29. Record strain gauge data.
30. Remove flexible shaft from drill component. Remove drill component from the linear bearing column. Insert microscope and evaluate hole location and quality of hole.
31. If necessary, compute distance and direction from rosette center to hole center using x-y micrometers on base. Apply to data.
32. Remove microscope/laser.
33. Reset translation stage to center position.
34. Remove VALAPODD by depressing relief valve. Set on table and reset, beginning at step #2. If testing is complete, remove air lines at quick disconnect and loosen both elevating support locks, allowing suction cups to sit flat. Set elevation supports at minimum height and relock. Replace all components, base, drill, and control box into case.

## APPENDIX B

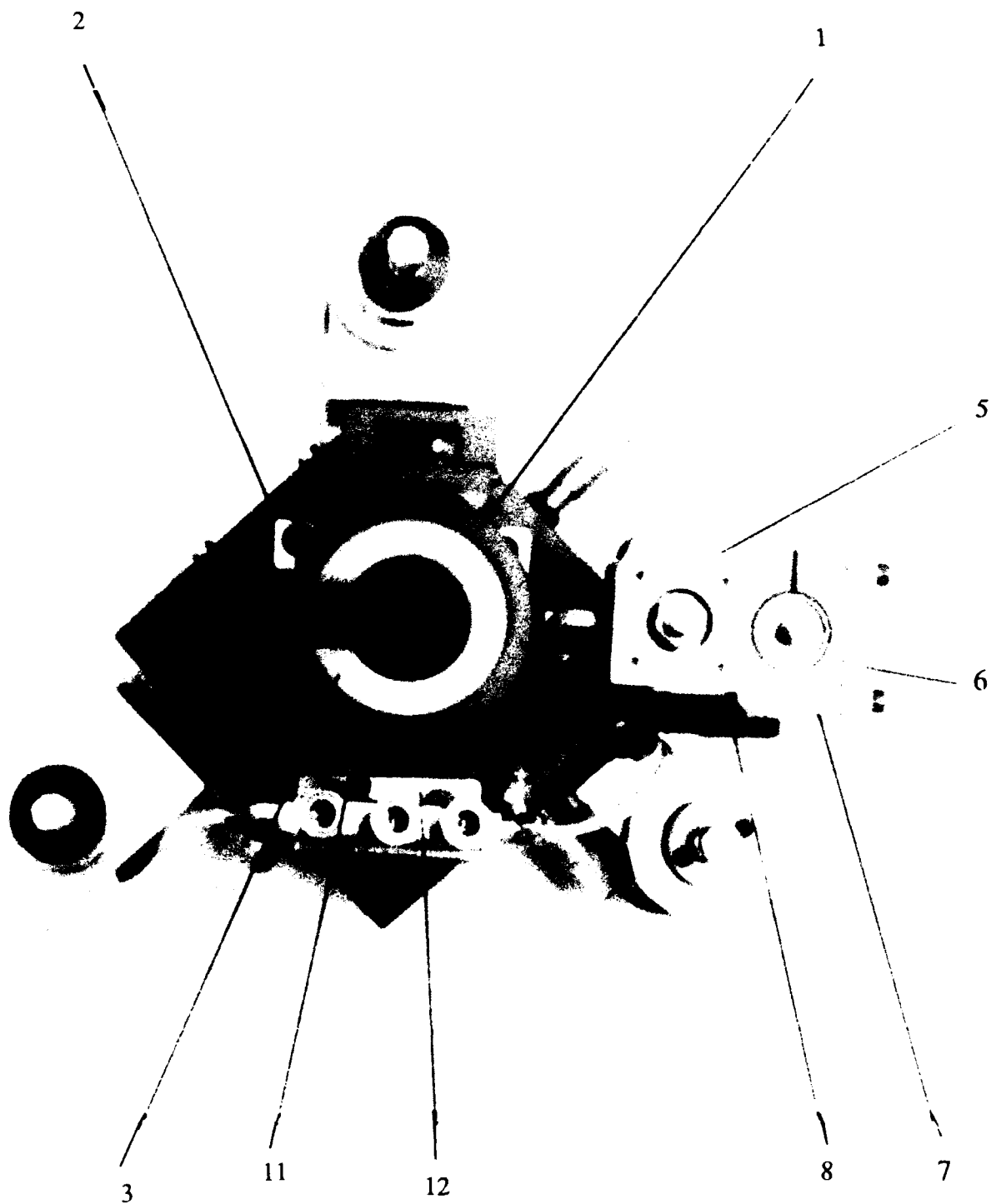
### DETAIL DRAWINGS OF HOLE DRILLING DEVICE

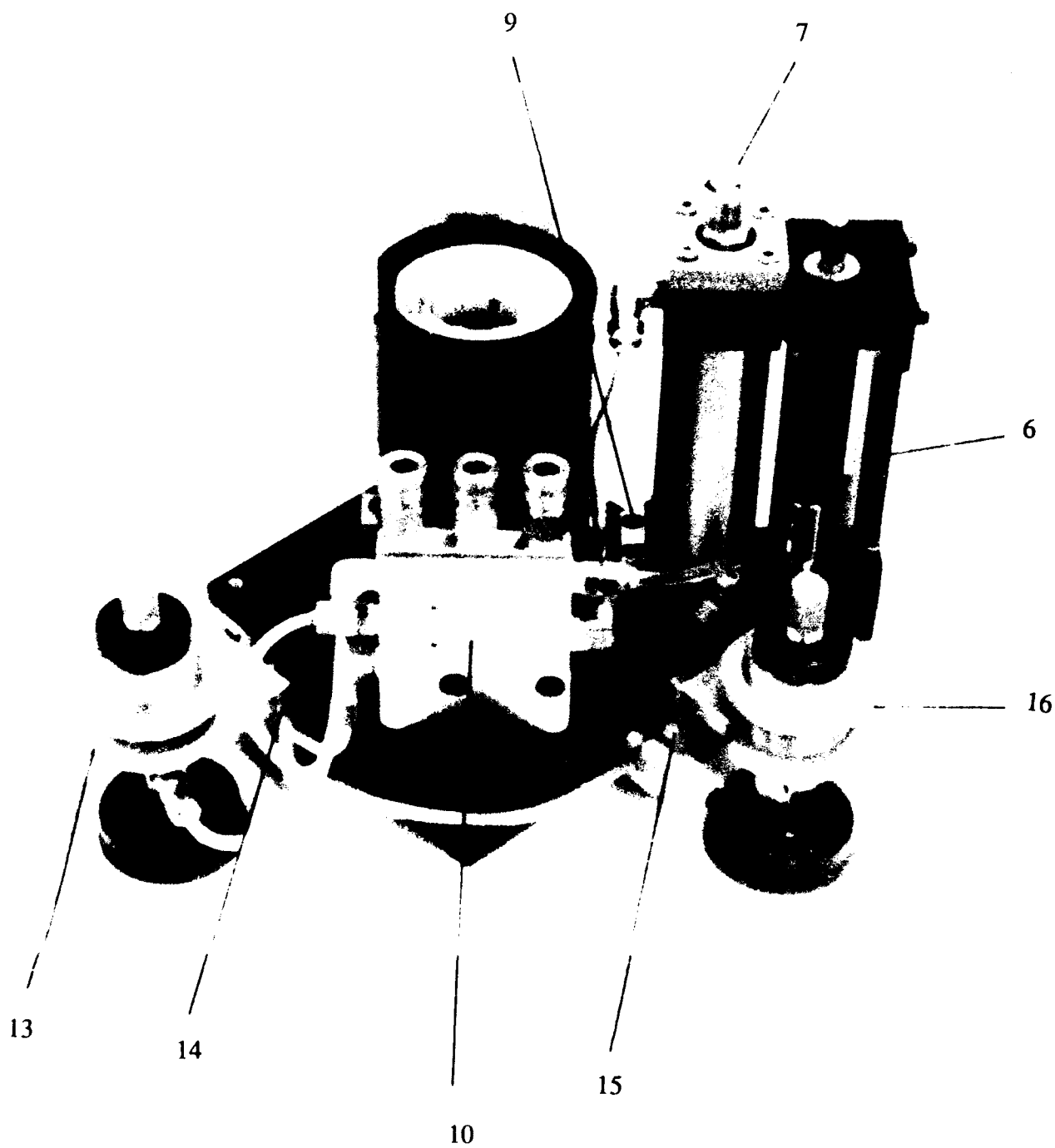


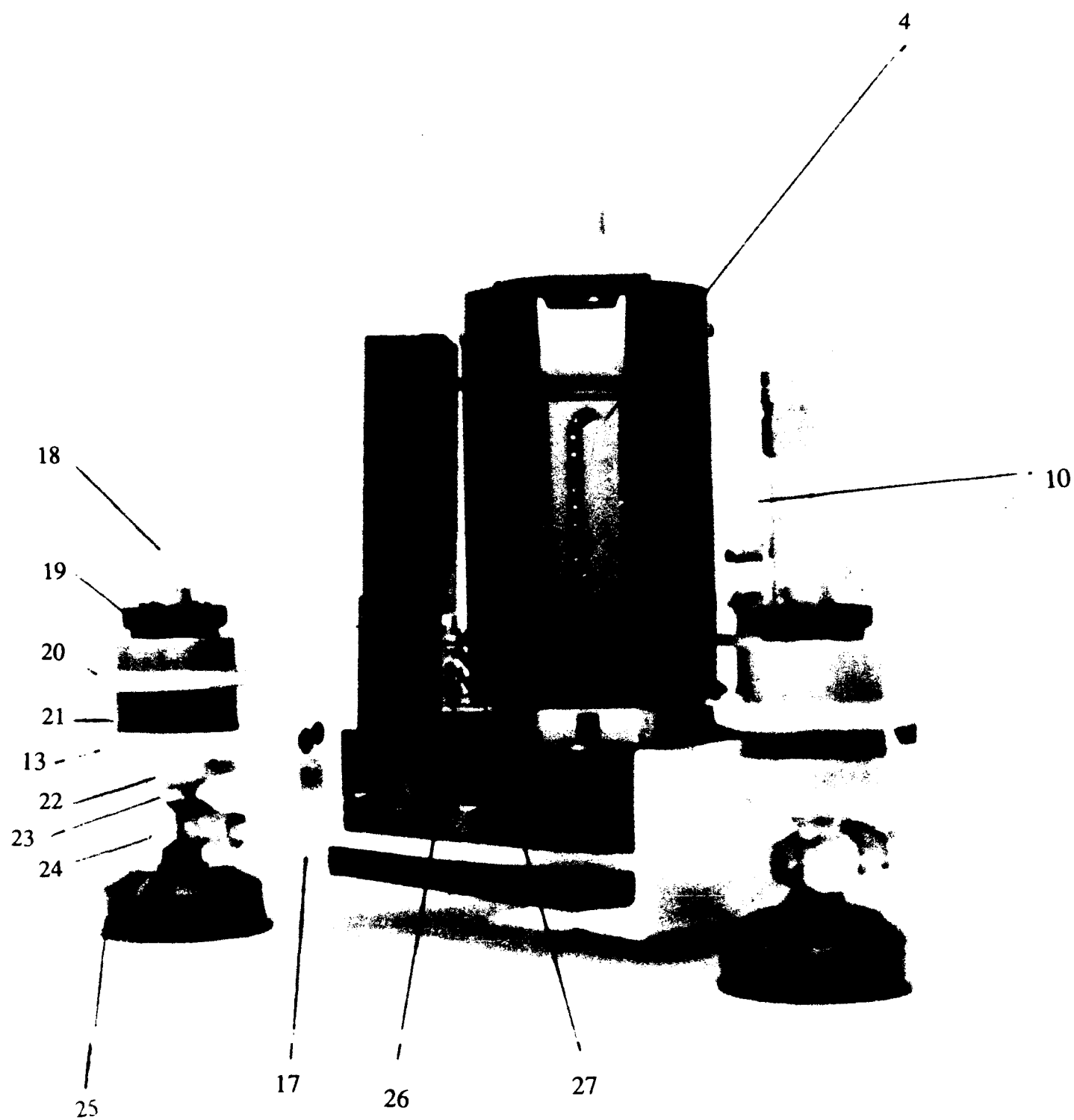
## ASSEMBLY NO. 1

### PARTS LIST

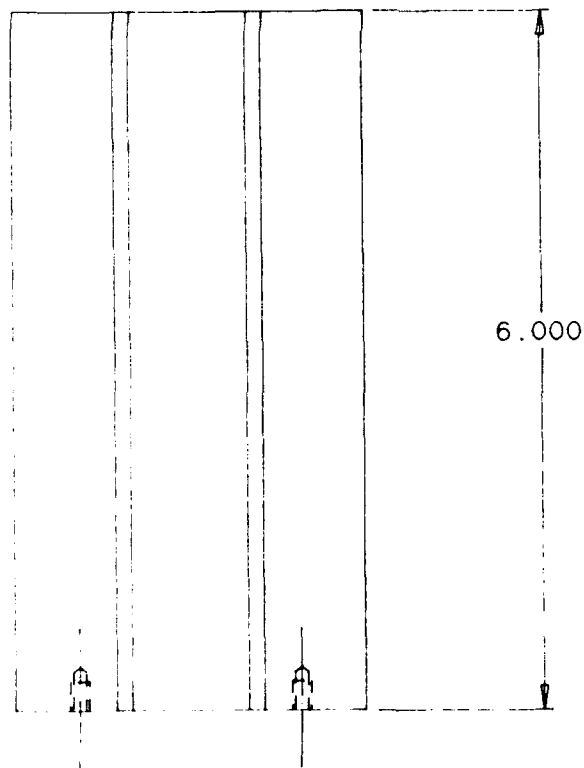
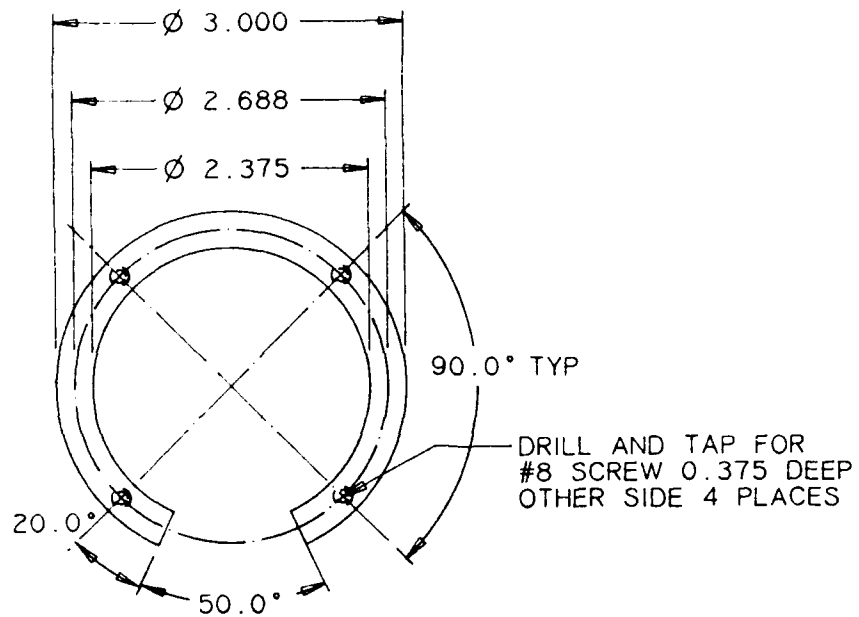
- 1 Linear Bearing Housing
- 2 Linear Bearing Base
- 3 Nylon Alignment Ring
- 4 Open Linear Bearing (1.5000-inch bore, 2.3750-inch housing bore) (not detailed)
- 5 Micrometer Mount
- 6 Feed Control Clamp Support Post
- 7 Feed Control Clamp
- 8 Feed Control Base Plate
- 9 Air Cylinder Mounting Block
- 10 Control Manifold
- 11 Vacuum Release Lever
- 12 Manifold Bracket
- 13 Adjustment Post Support #4
- 14 Adjustment Post Support #2
- 15 Adjustment Post Support #3
- 16 Adjustment Post Support #5
- 17 Adjustment Post Support #1
- 18 Swivel Bearing Locking Post
- 19 Adjustment Post Knob
- 20 Adjusting Post Locking Ring
- 21 Attachment Adjusting Post
- 22 Spherical Bearing (0.500-inch bore) (not detailed)
- 23 Bearing Shaft
- 24 Vacuum Cup Fitting
- 25 Vacuum Cup Rigidizer
- 26 Light Tube
- 27 Light Pack Bracket





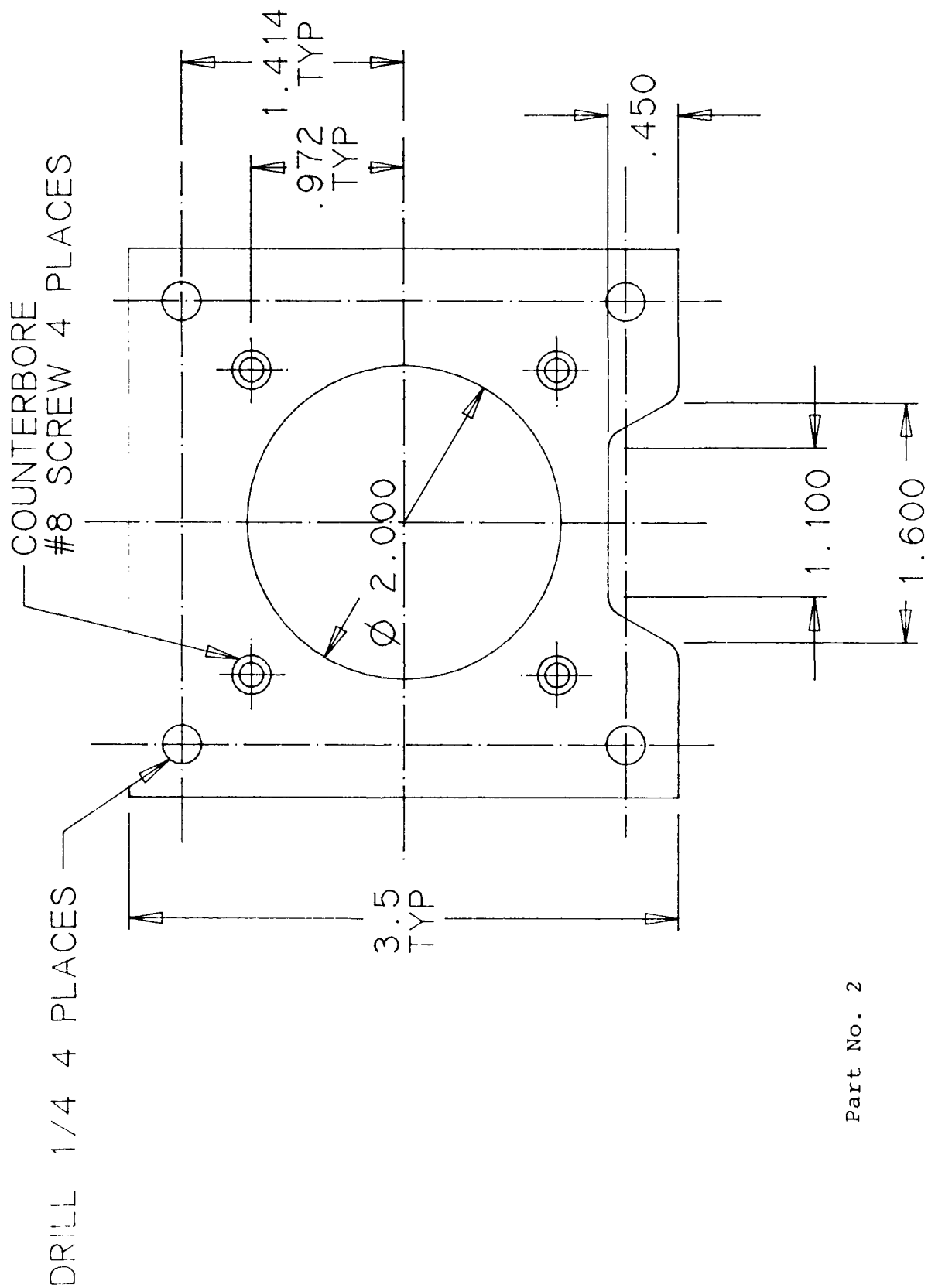


LINEAR BEARING HOUSING  
MATERIAL: ALUMINUM



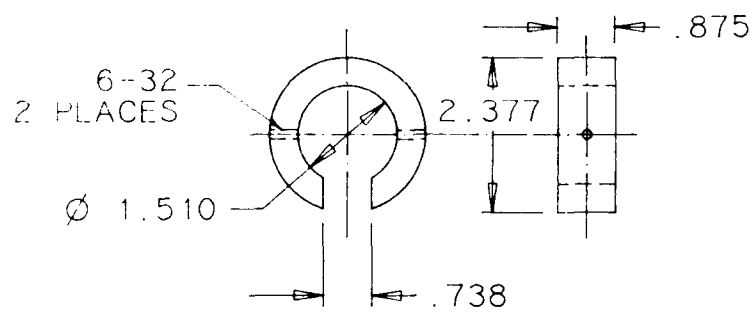
Part No. 1

LINEAR BEARING BASE  
1/4" ALUMINUM PLATE



Part No. 2

TITLE: NYLON ALIGNMENT RING  
MATERIAL: NYLON



Part No. 3

8-32  
D & T

0.375

0.437

2.250

0.501

0.750

1.500

DRILL AND COUNTERBORE  
.080 DEEP #10 2 PLACES

DRILL AND COUNTERBORE  
.125 DEEP #10 2 PLACES

0.25  
TYP

0.75  
TYP

1.500

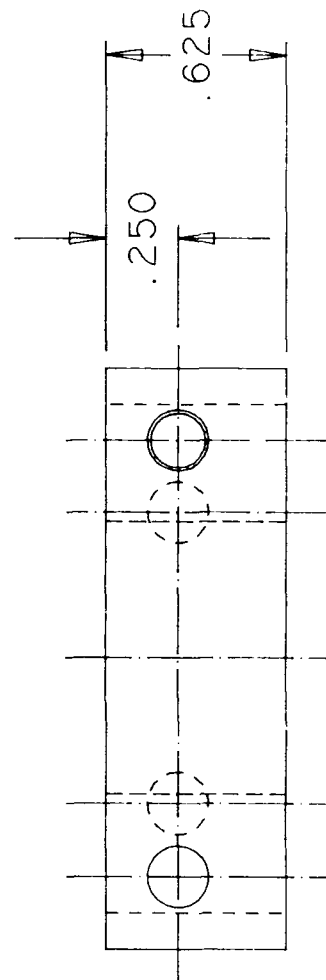
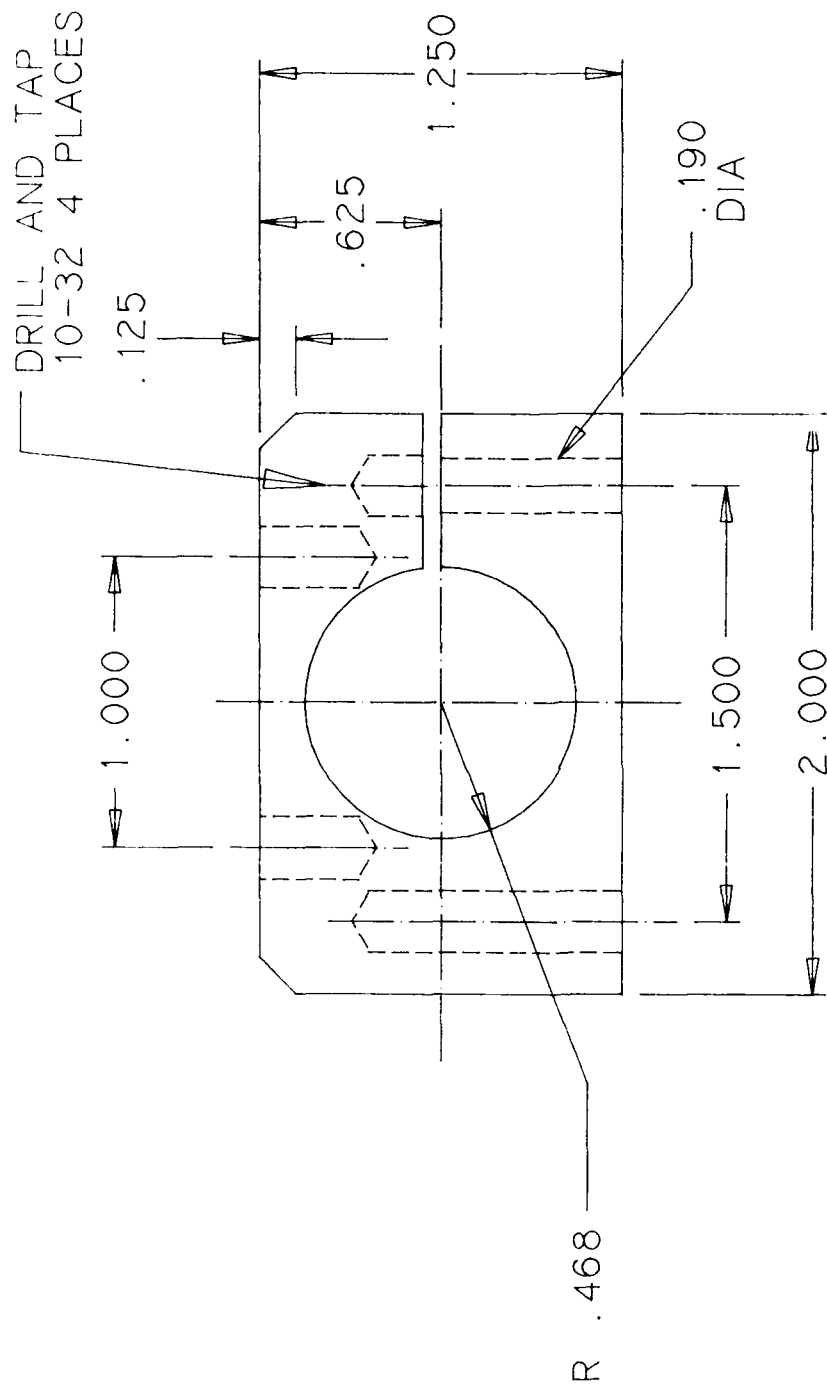
Part No. 5

125



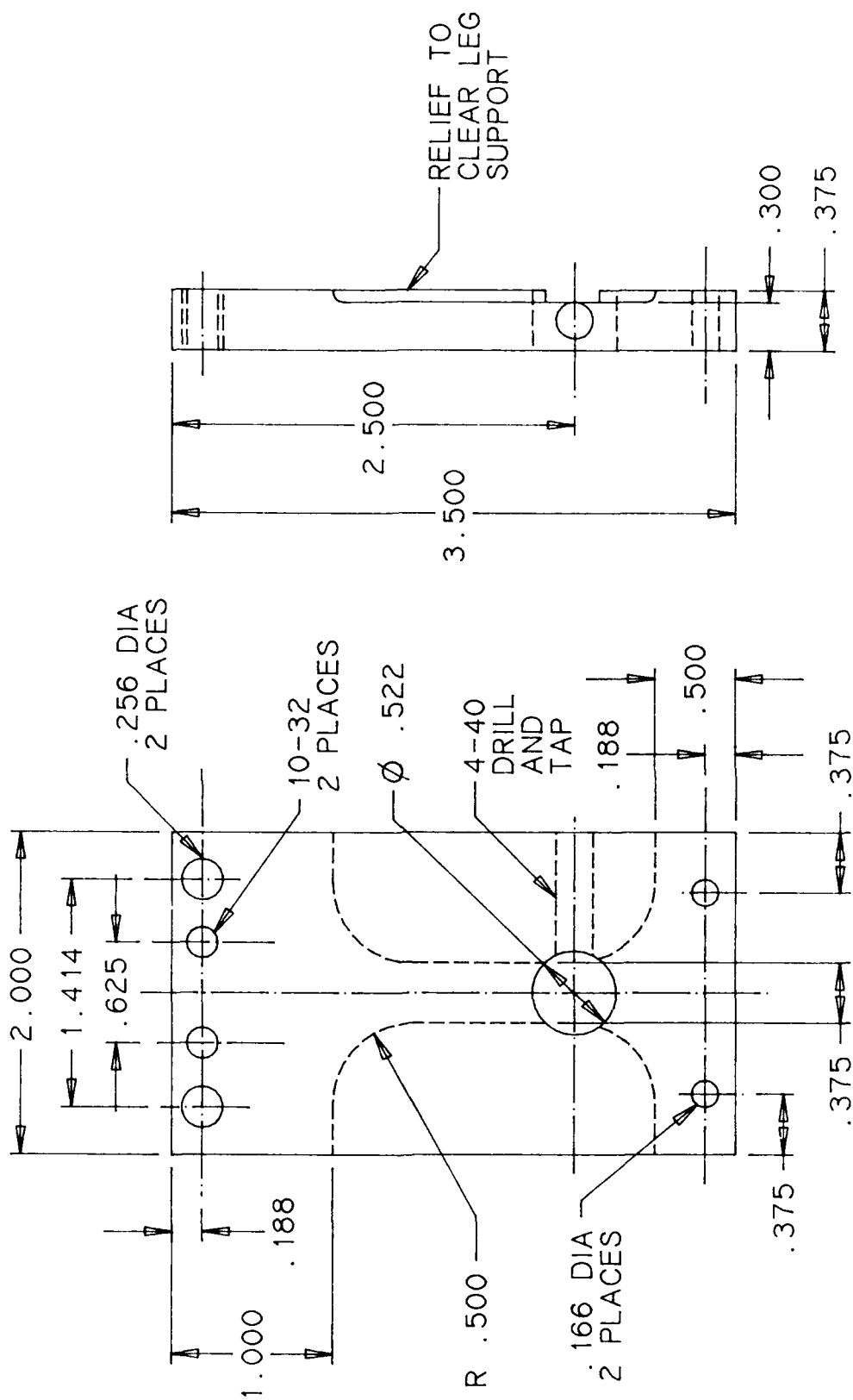


# FEED CONTROL CLAMP ALUMINUM



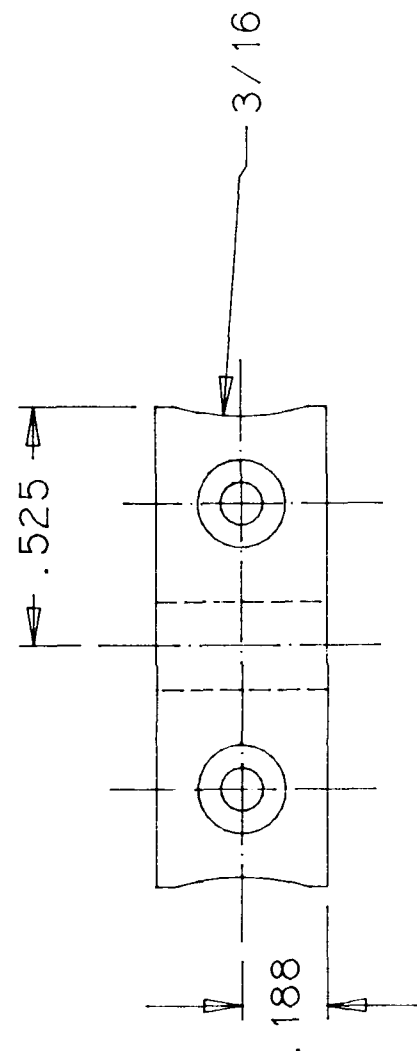
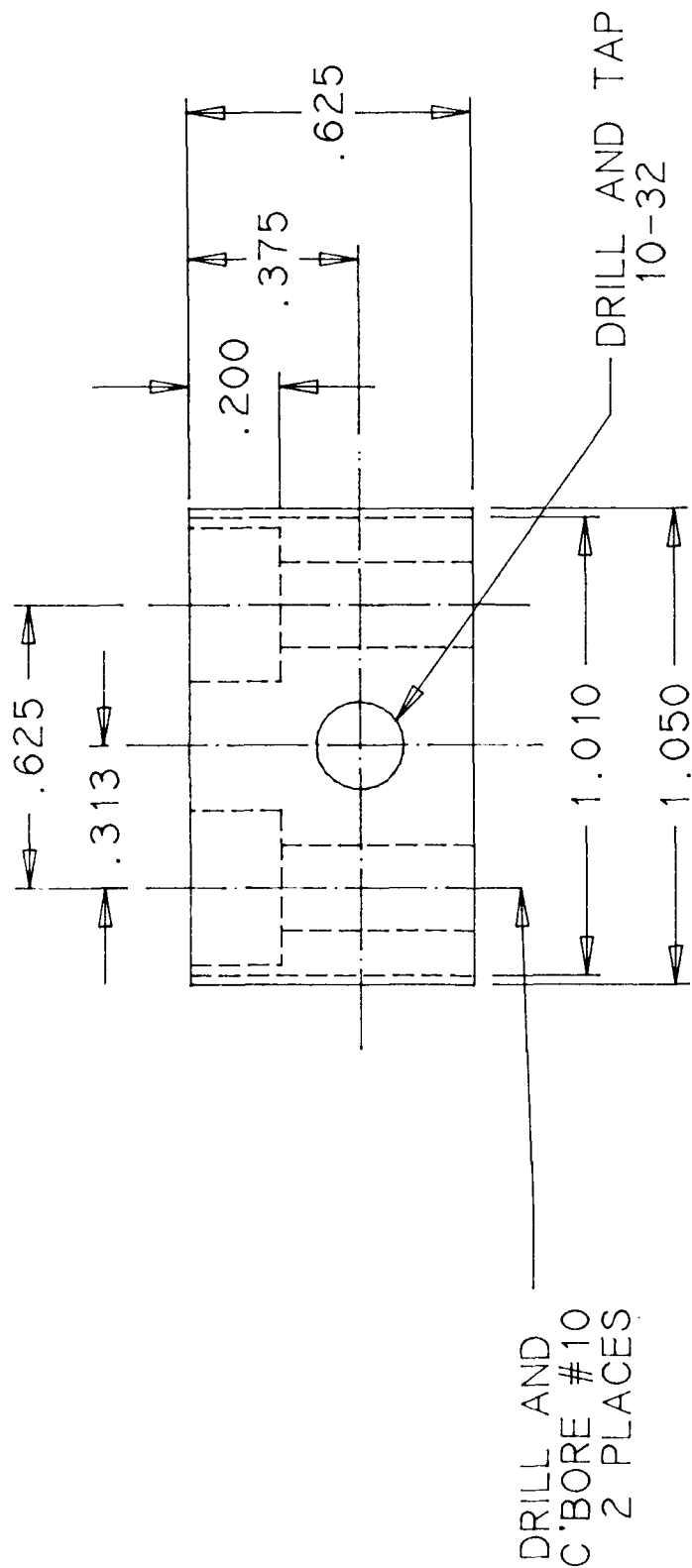
Part No. 7

TITLE: FEED CONTROL BASE PLATE  
MATERIAL: ALUMINUM



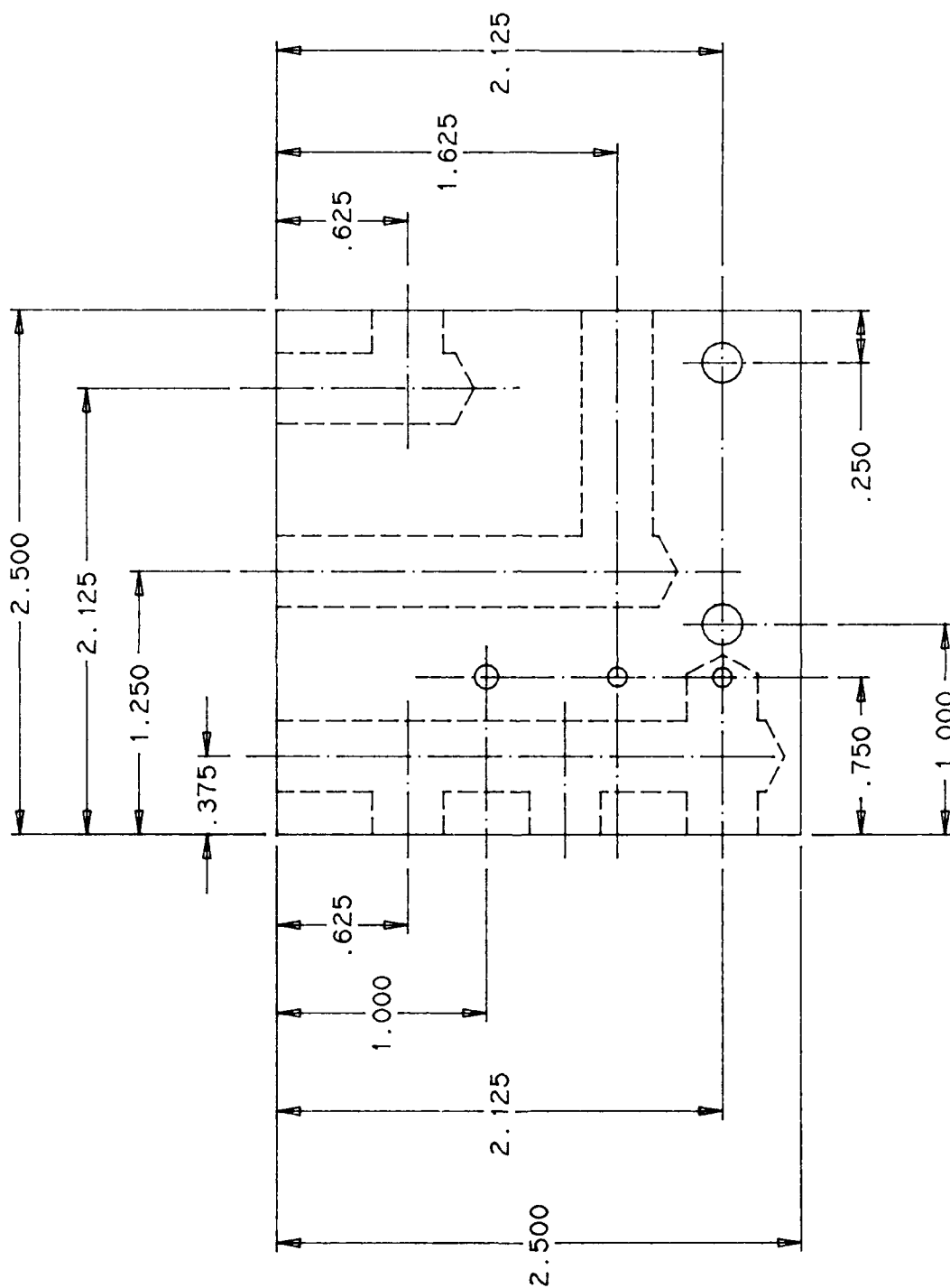
Part No. 8

TITLE: AIR CYLINDER MOUNTING BLOCK  
 MATERIAL: ALUMINUM



Part No. 9

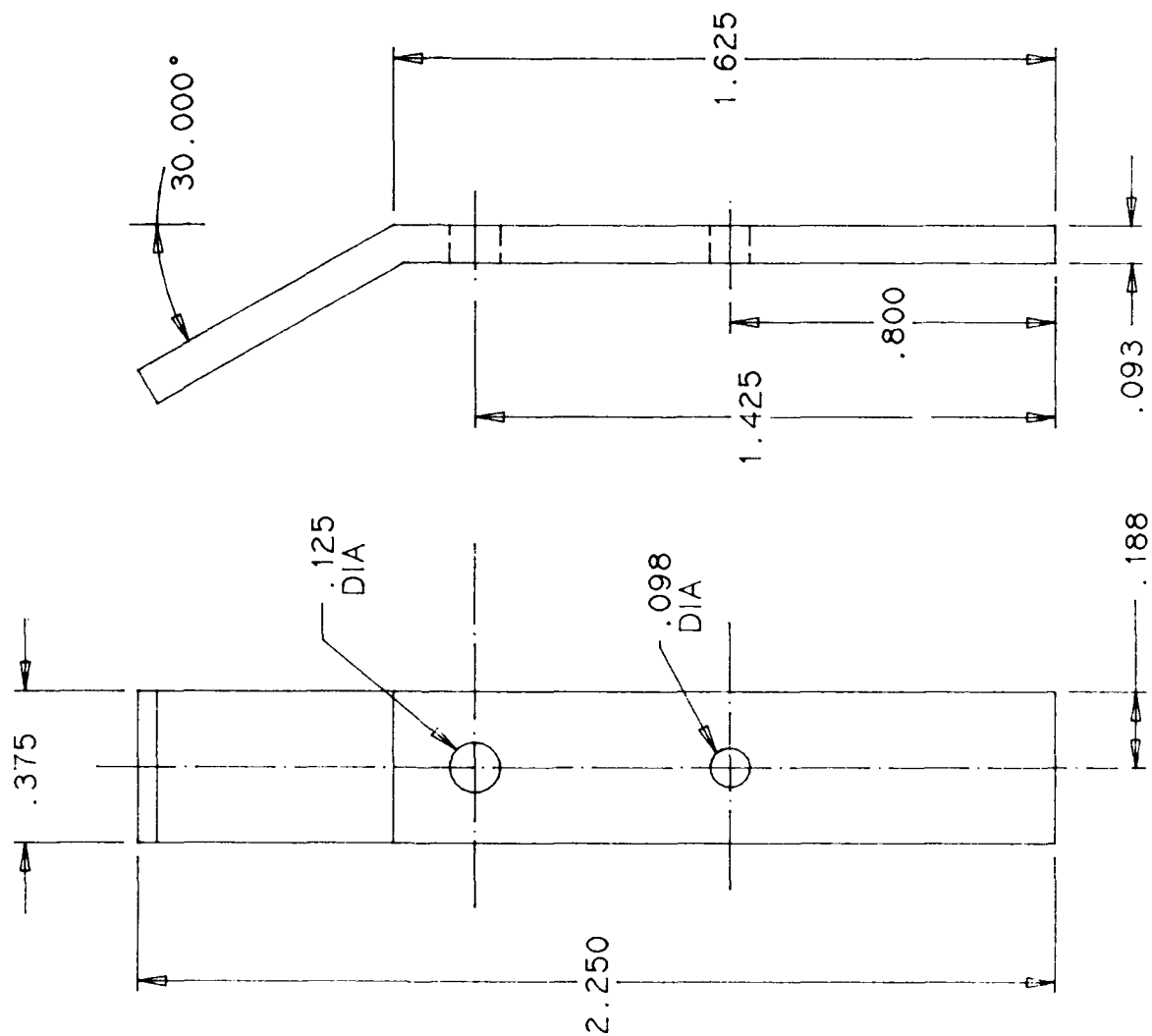
CONTROL MANIFOLD  
1/2" ALUMINUM



NOTE : DRILL INTERSECTING HOLES  
WITH LETTER "R" DRILL TAP 1/8  
TAPER PIPE

Part No. 10

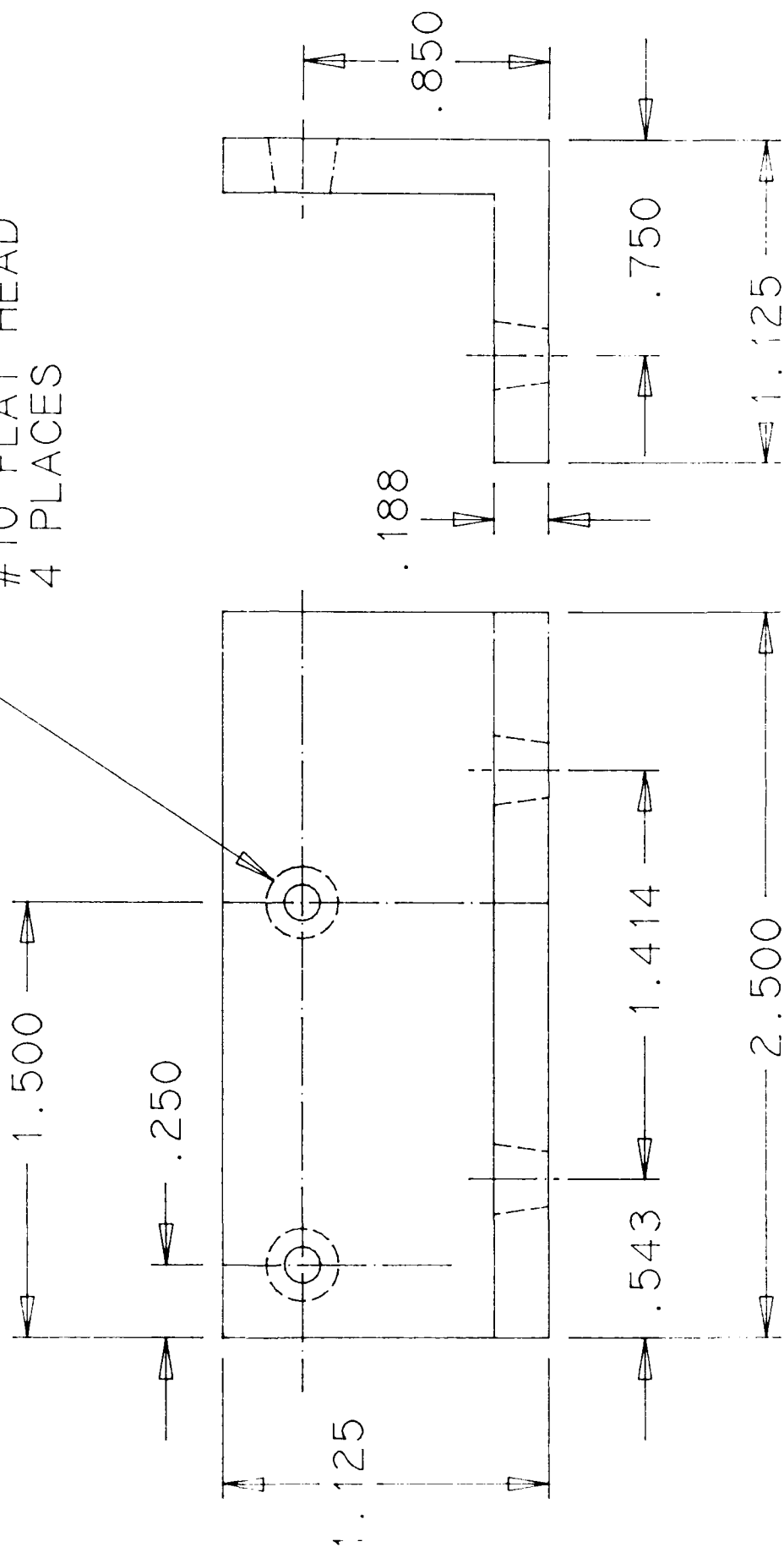
TITLE: VACUUM RELEASE LEVER  
MATERIAL: ALUMINUM



Part No. 11

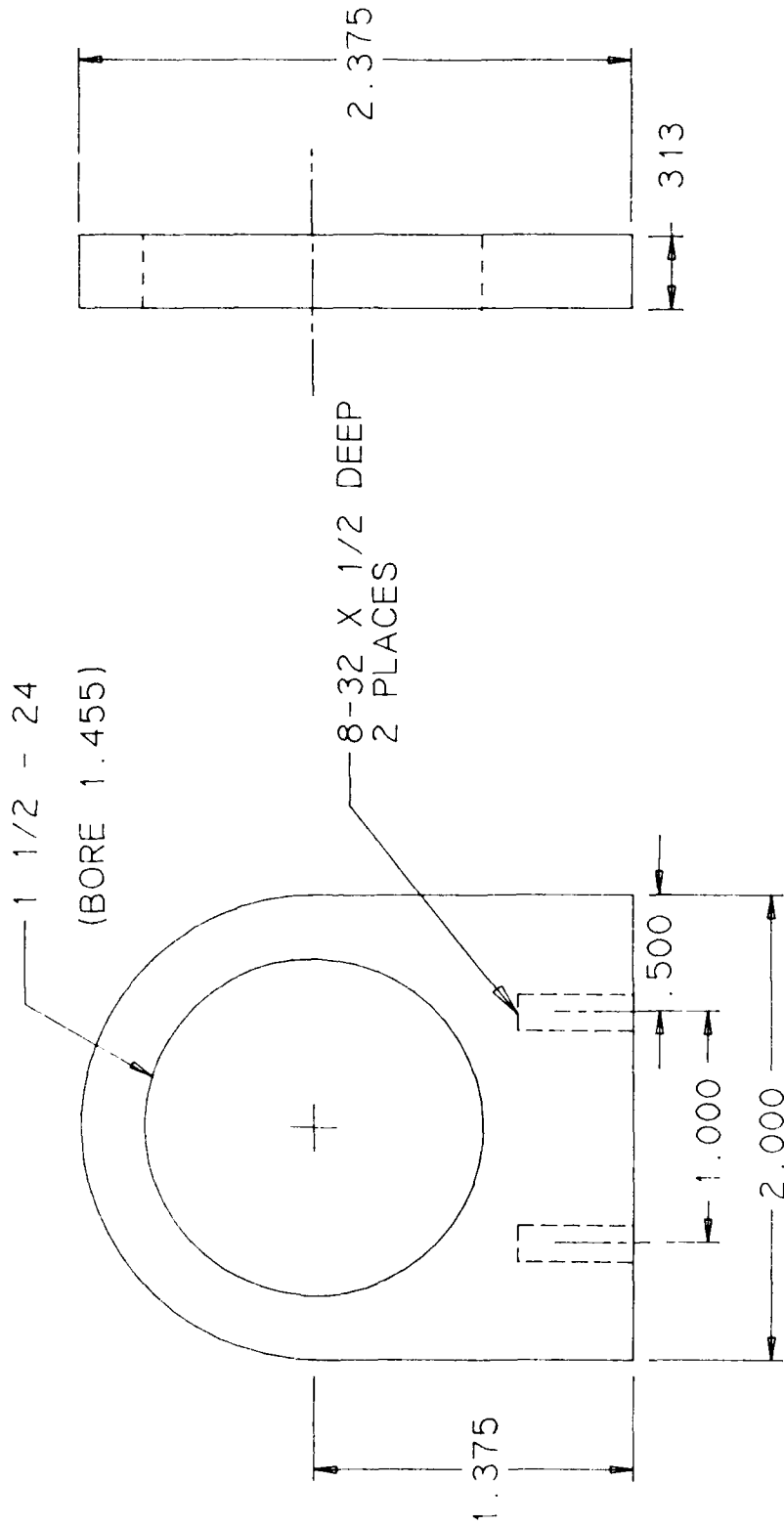
TITLE : MANIFOLD BRACKET  
 MATERIAL : ALUMINUM ANGLE

DRILL AND SINK  
 #10 FLAT HEAD  
 4 PLACES



Part No. 12

TITLE : ADJUSTMENT POST SUPPORT #4  
MATERIAL : ALUMINUM





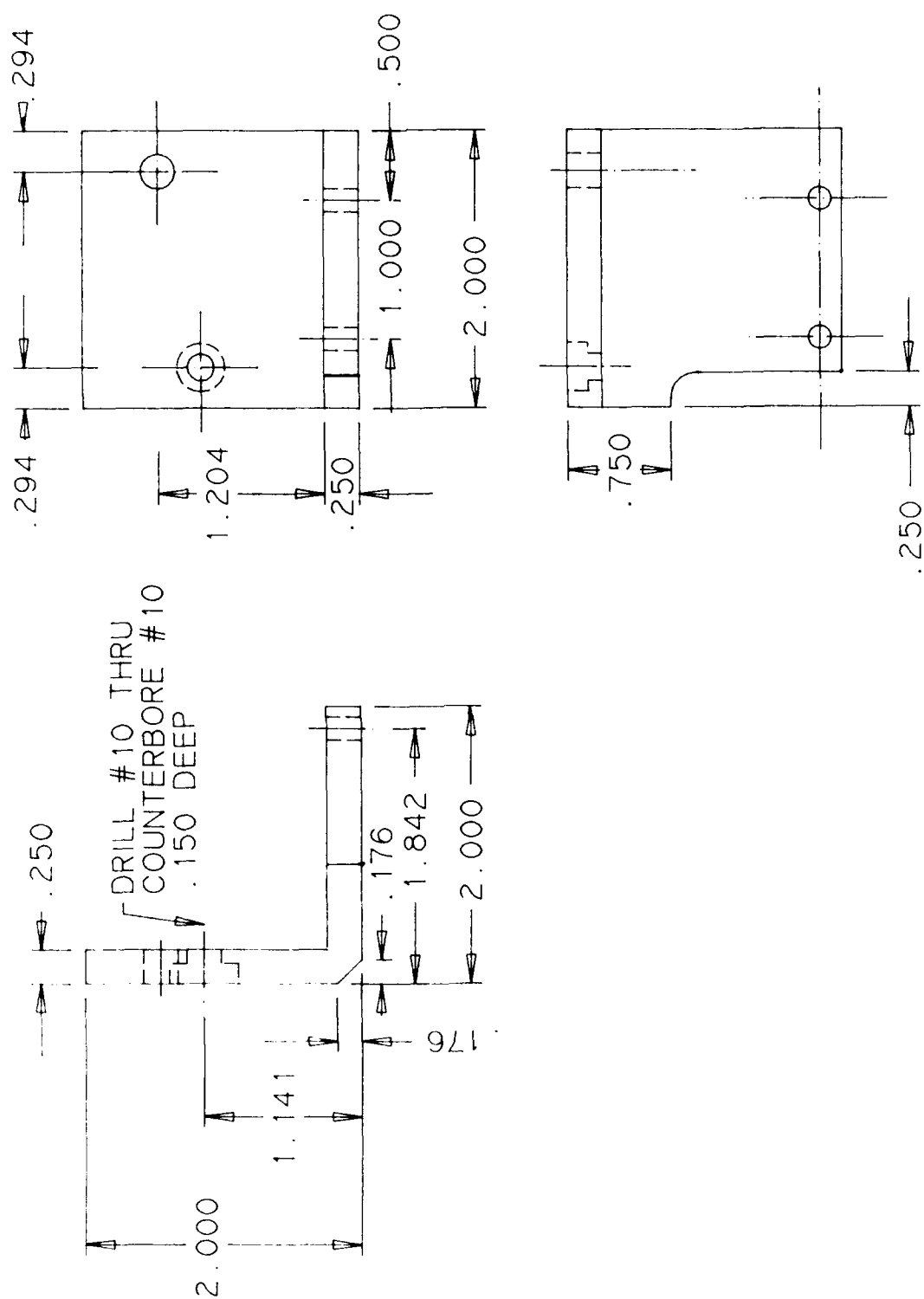
Technical drawing of a mechanical part, likely a bracket or plate, showing dimensions and features:

- Dimensions:**
  - Overall width: 2.000
  - Overall height: 2.000
  - Top horizontal segment: 1.842
  - Bottom horizontal segment: 1.141
  - Left vertical segment: 1.204
  - Right vertical segment: 1.500
  - Top-left corner radius: .294
  - Bottom-left corner radius: .294
  - Top-right corner radius: .176
  - Bottom-right corner radius: .176
  - Central vertical slot width: .250
  - Central horizontal slot width: .250
- Features:**
  - Top-left corner: DRILL #10 THRU COUNTERBORE #10 .150 DEEP
  - Top-right corner: 1/4-20 D & T
  - Central slot: .166 DIA THRU

1 PIECE ALUMINUM

Part No. 14

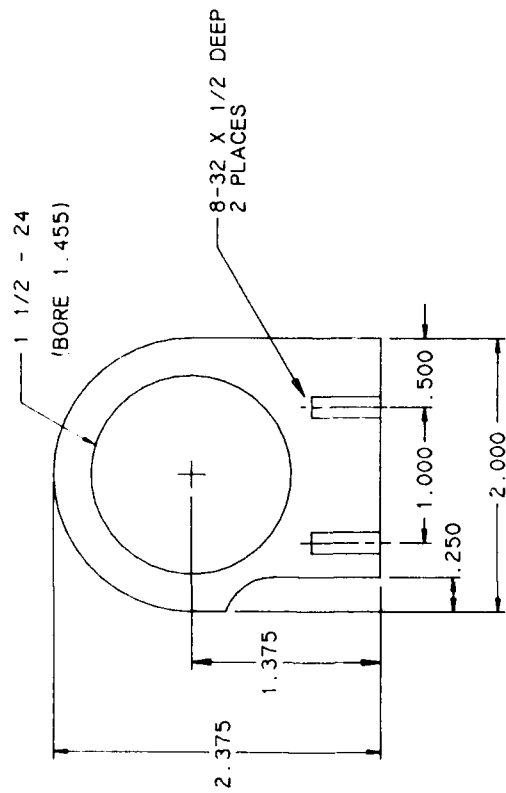
## FILE : ADJUSTMENT POST SUPPORT #3



Part No. 15

1 PIECE ALUMINUM

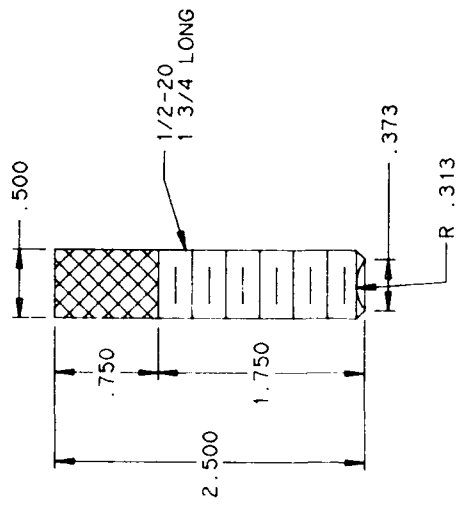
TITLE : ADJUSTMENT POST SUPPORT #5  
 MATERIAL : ALUMINUM



2 PCS  
 ALUM 6061-T651

Part No. 16

SWIVEL BEARING LOCING POST  
 3 PIECES  
 ALUMINUM

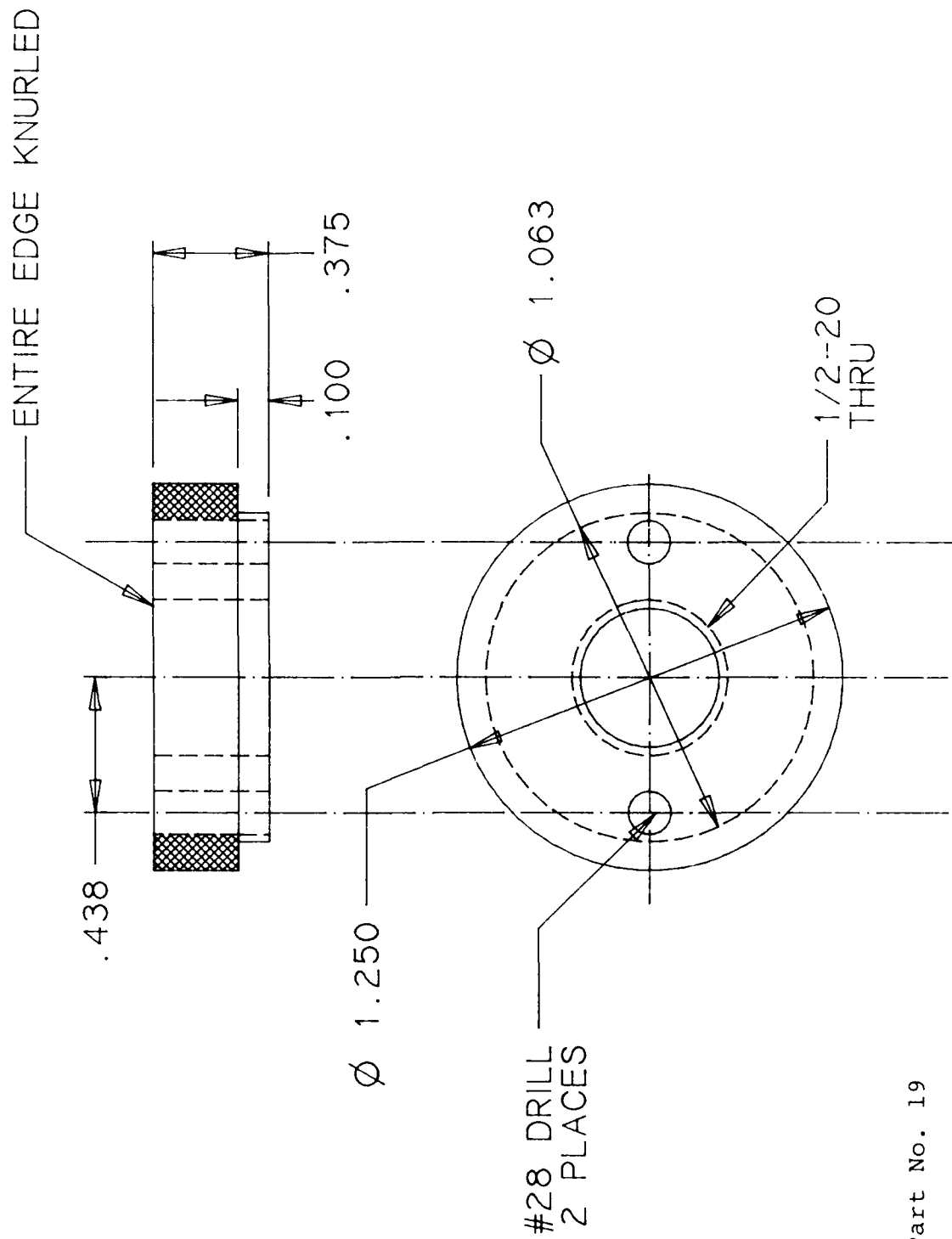


Part No. 18

[illegible]

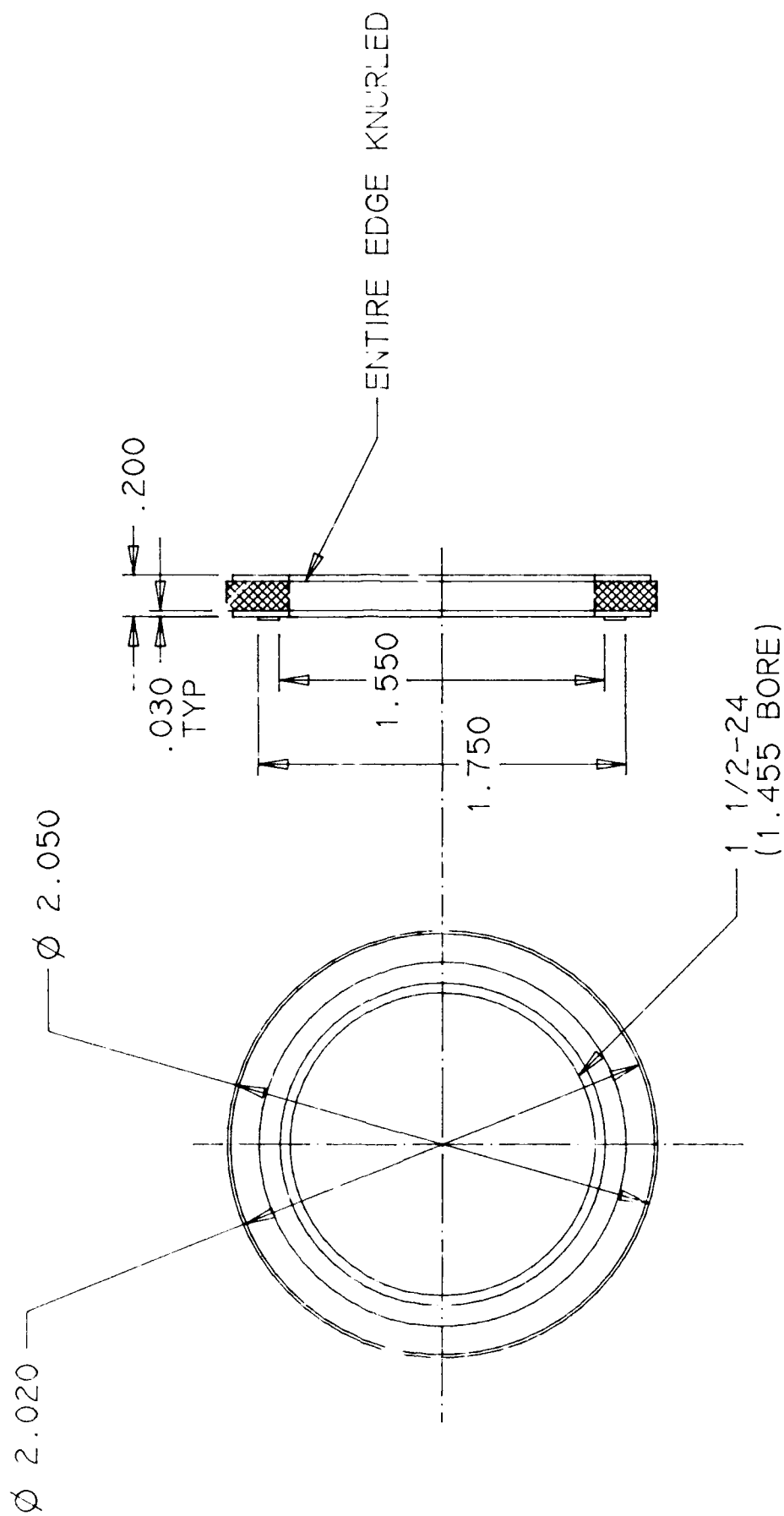
Part No. 17

# ADJUSTING POST KNOB 3 PIECES ALUMINUM



Part No. 19

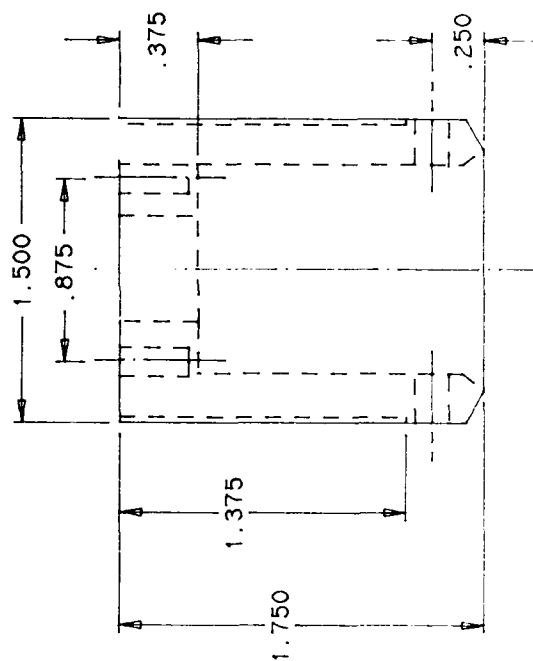
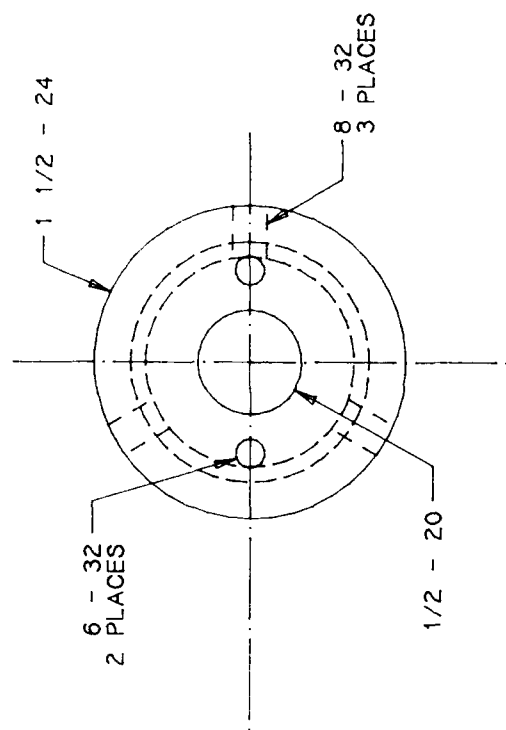
TITLE: ADJUSTING POST LOCKING RING



ALUMINUM 3 PIECES

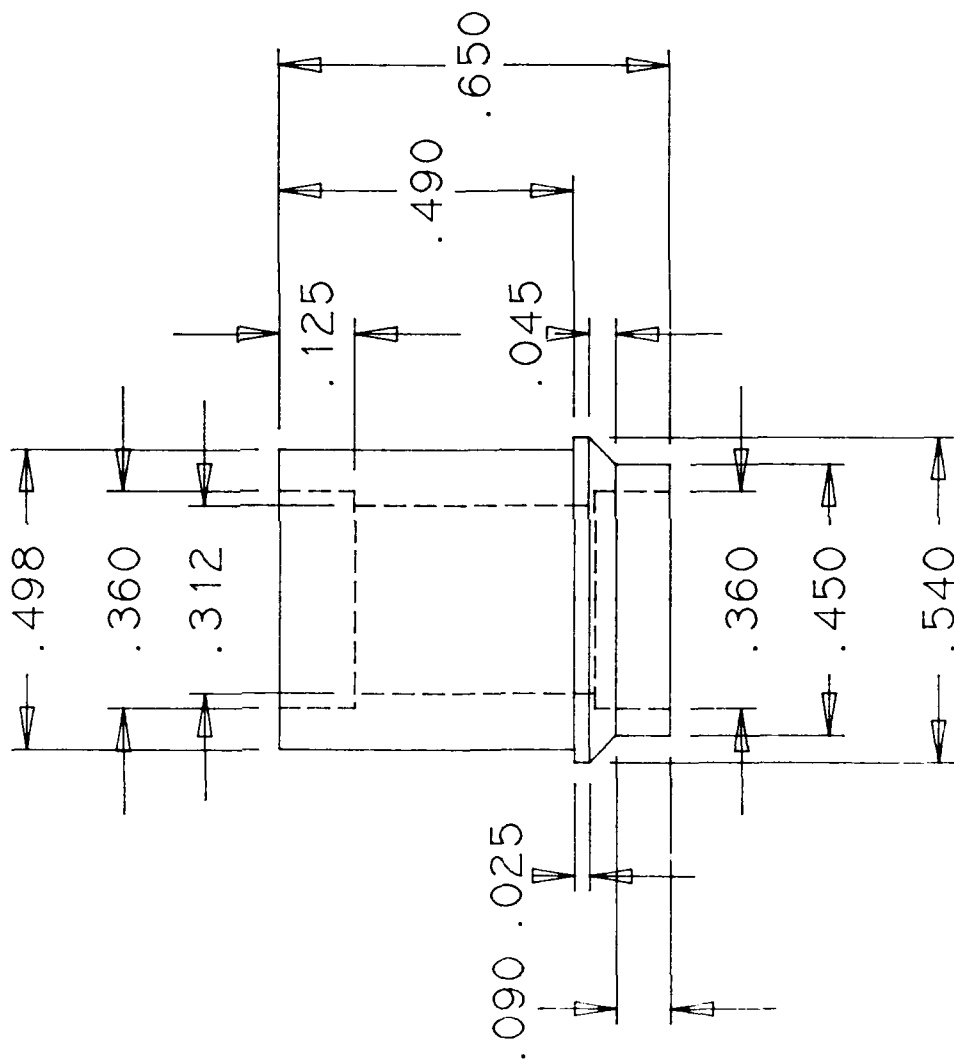
Part No. 20

ATTACHMENT ADJUSTING POST  
3 PIECES  
ALUMINUM: 6061-T051



Part No. 21

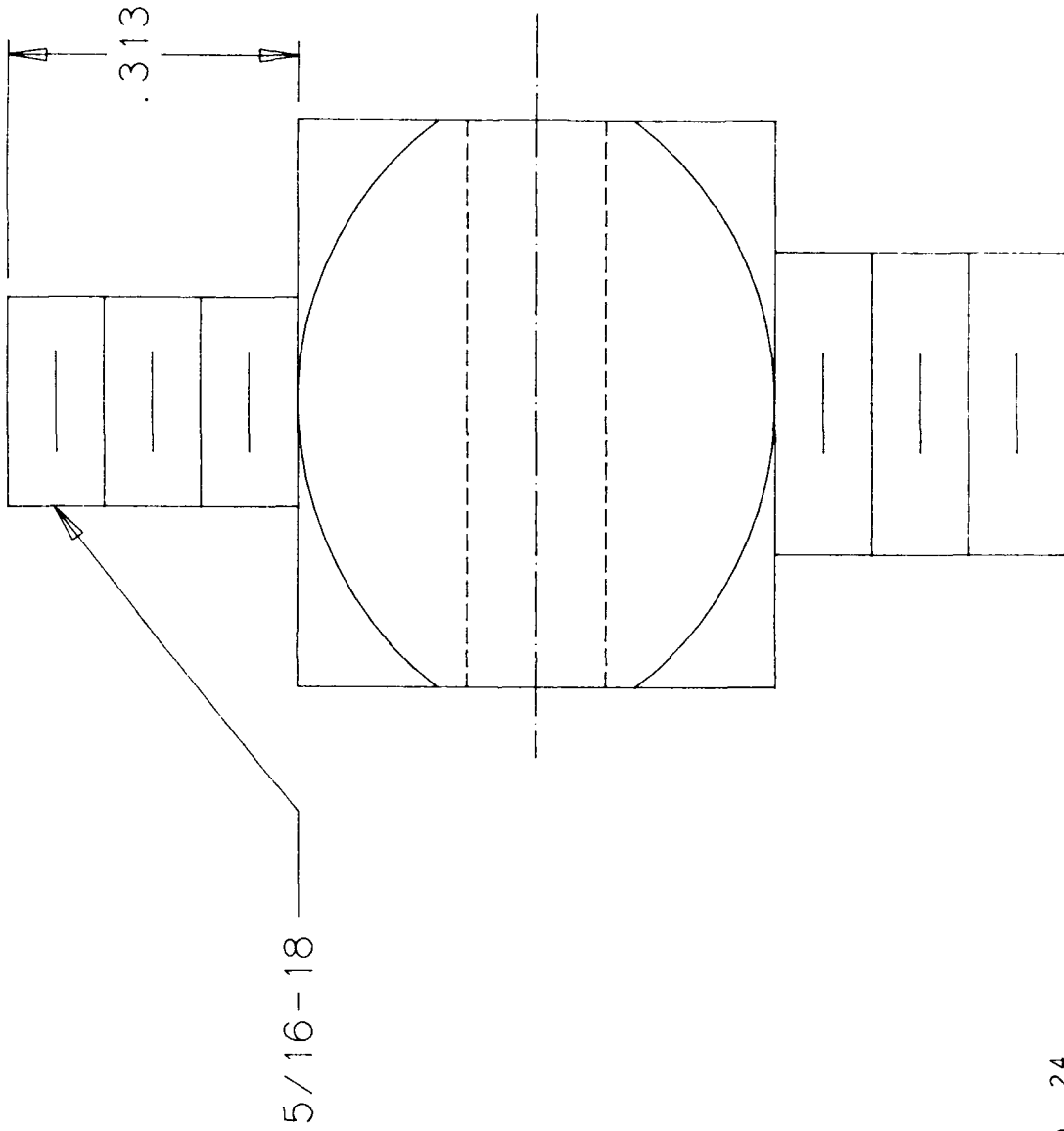
TITLE: BEARING SHAFT  
 3 PIECES  
 ALUMINUM: 6061-T651



Part No. 23

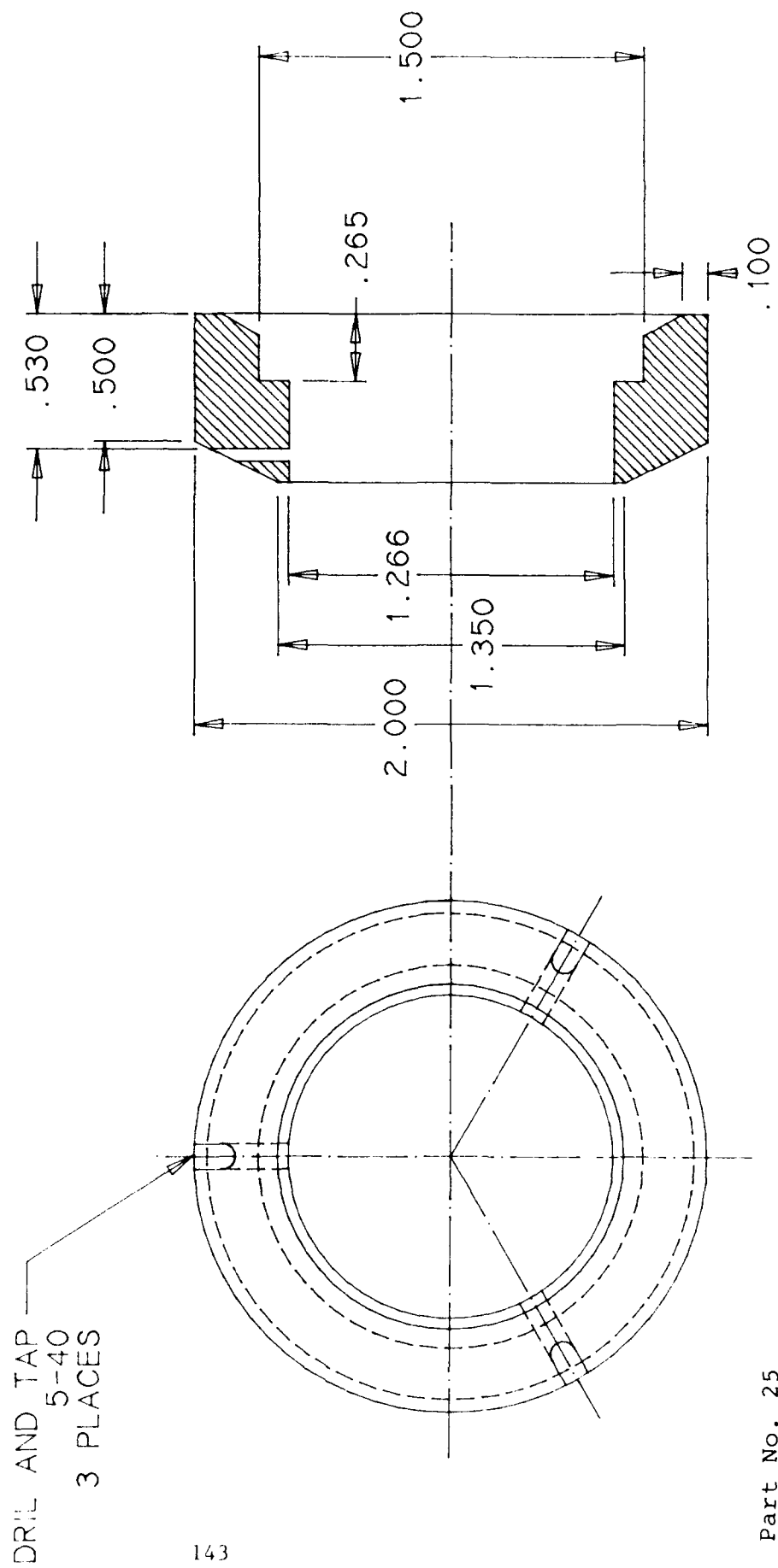


# VACUUM CUP FITTING (ALTERED)

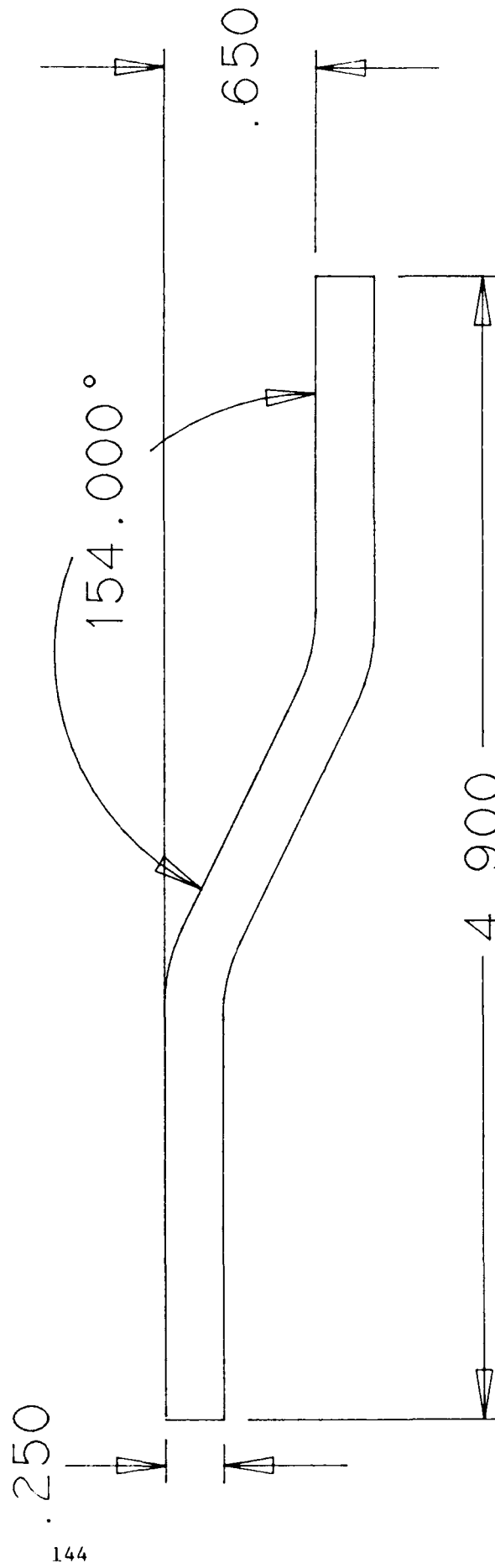


Part No. 24

VACUUM CUP RIGIDIZER  
ALUMINUM  
3 PIECES

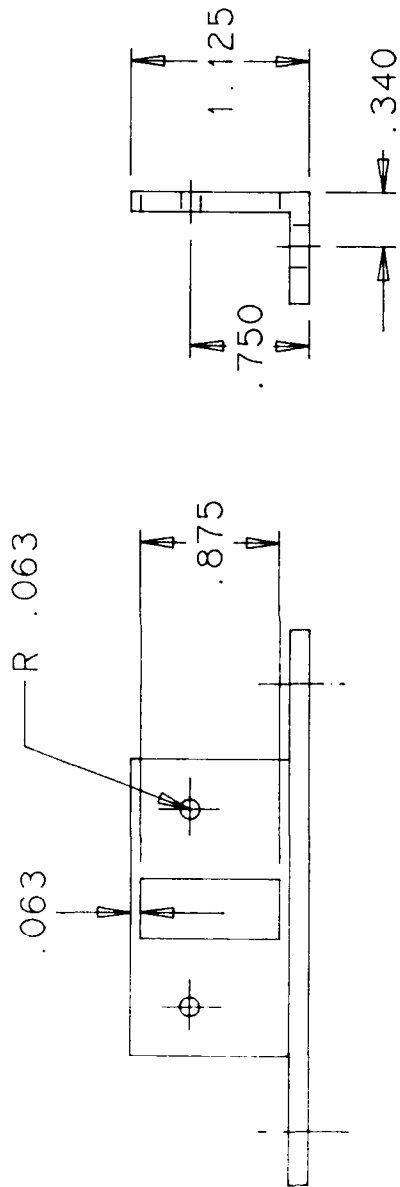


LIGHT TUBE  
1/4" DIA ACYCLIC ROD

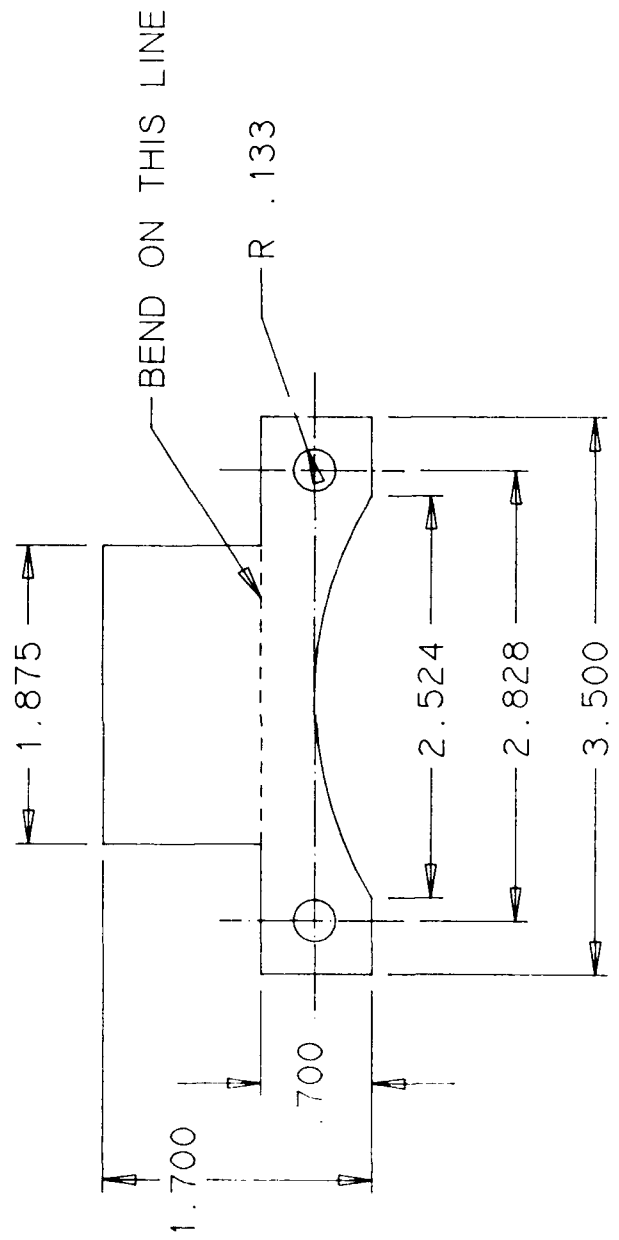


Part No. 26

LIGHT PACK BRACKET  
1/8" ALUMINUM SHEET METAL



BLANK CUT-OUT

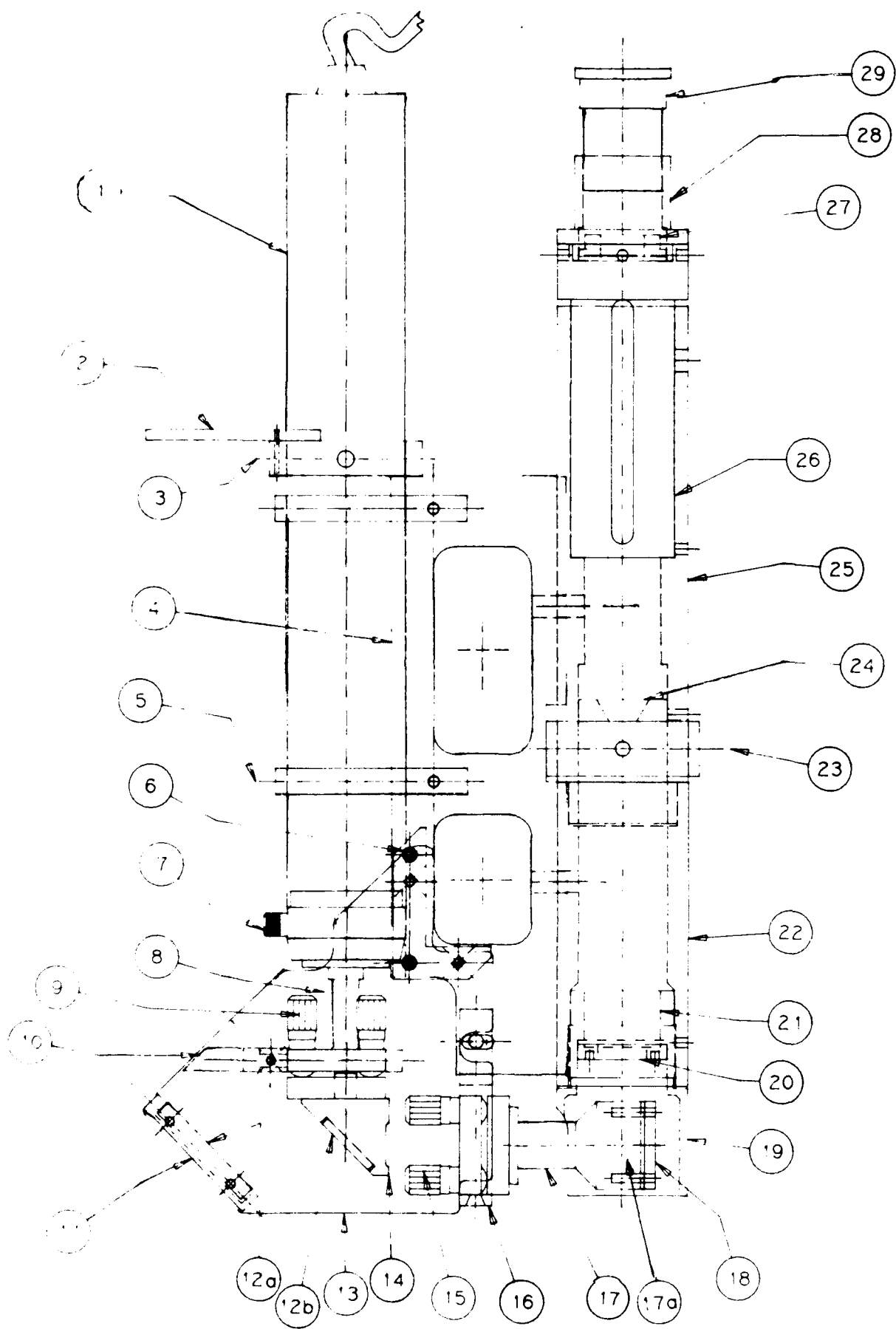


Part No. 27

## ASSEMBLY NO. 2

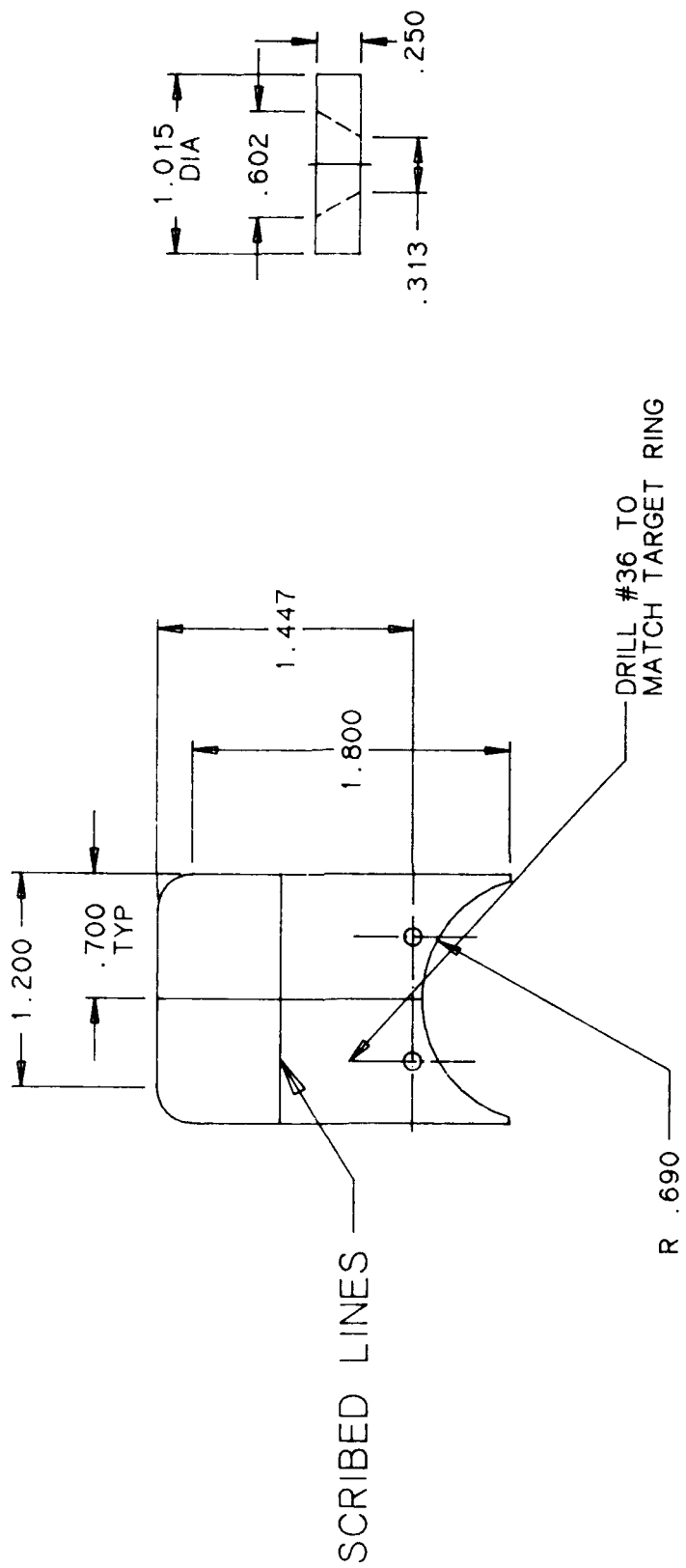
### PARTS LIST

- 1 Aerotech, Inc. 0.5 mW He Ne Laser (not detailed)
- 2 Laser Target
- 3 Laser Target Ring
- 4 Scope/Laser Main Frame
- 5 Laser Clamp
- 6 Optics Shield Mount Blocks
- 7 Aerotech, Inc. MSA Series Mechanical Shutter (not detailed)
- 8 Laser Tube Extender
- 9 MM-1 Modification #2
- 10 Target Mirror Support
- 11 End Plate (made to fit Aluminized Mirror) (not detailed)
- 12a 25mm x 35mm Aluminized Mirror (not detailed)
- 12b 15mm x 20mm Beam Splitter Plate (not detailed)
- 13 Optics Shield
- 14 Beam Plate Holder
- 15 MM-1 Modification #1
- 16 MM-1 Lower Mount
- 17 Beam Splitter Cube Holder
- 17a 0.5 in x 0.5 in x 0.5 in Beam Splitter Cube (not detailed)
- 18 Holder Cover
- 19 Beam Splitter Cube Cover
- 20 Objective Lens Holder/Adjustment Ring
- 21 Objective Lens Holder/Adjustment Ring
- 22 Scope Lower Body Bearing Surface
- 23 Microscope/Laser Positioning Ring
- 24 Aperture
- 25 Scope Upper Body
- 26 Eyepiece Adjustment Housing
- 27 Eyepiece Retainer
- 28 Eyepiece Mount
- 29 Rolyn Optics 20X Eyepiece (not detailed)



LASER TARGET  
1/8" ACRYLIC  
(MILKY WHITE)

APERTURE  
ALUMINUM

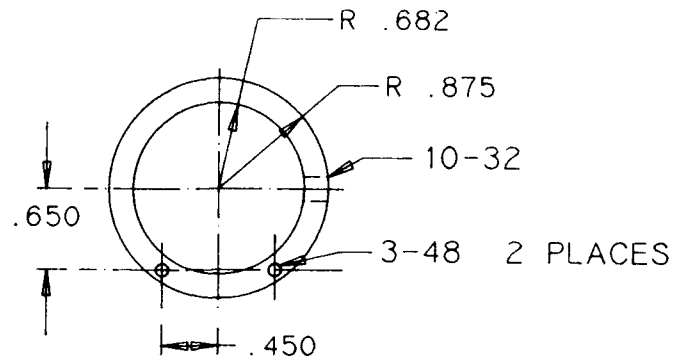


Part No. 24

Part No. 2

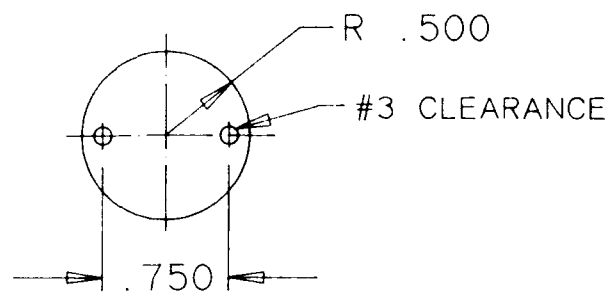
LASER TARGET RING  
MATERIAL: ALUMINUM

Part No. 3



HOLDER COVER

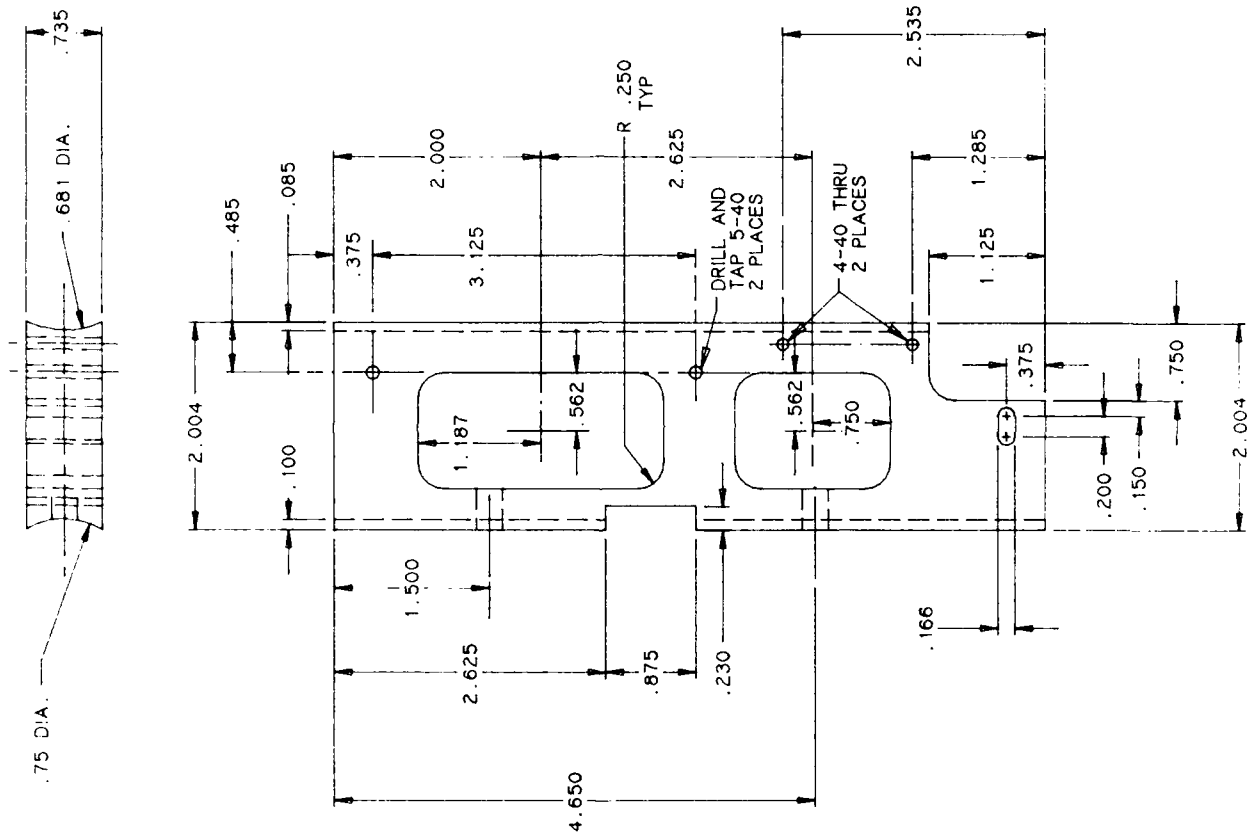
Part No. 18



1 PIECE  
1/8" ALUMINUM



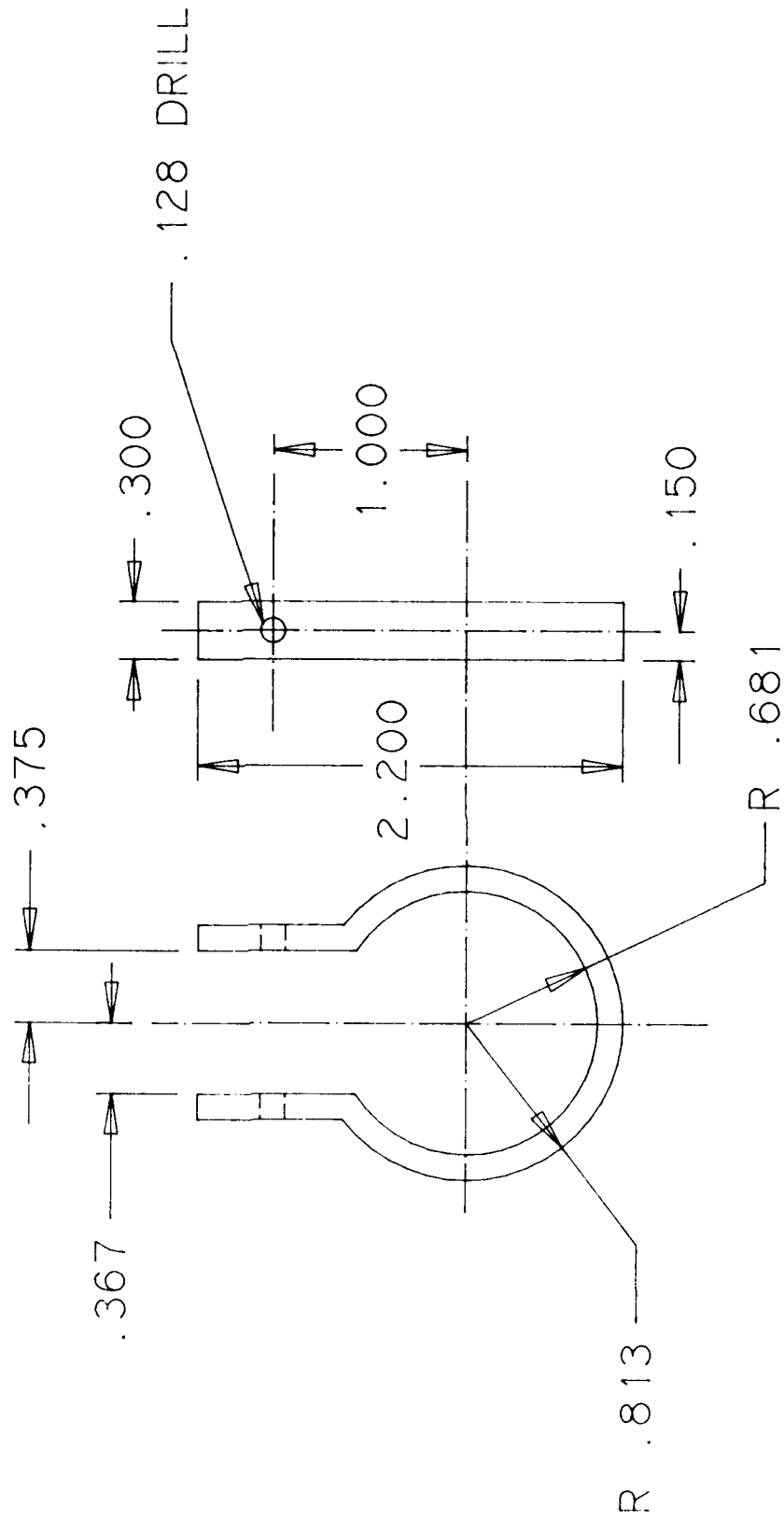
SCOPE/LASER MAIN FRAME  
ALUMINUM  
1 PIECE



Part No. 4

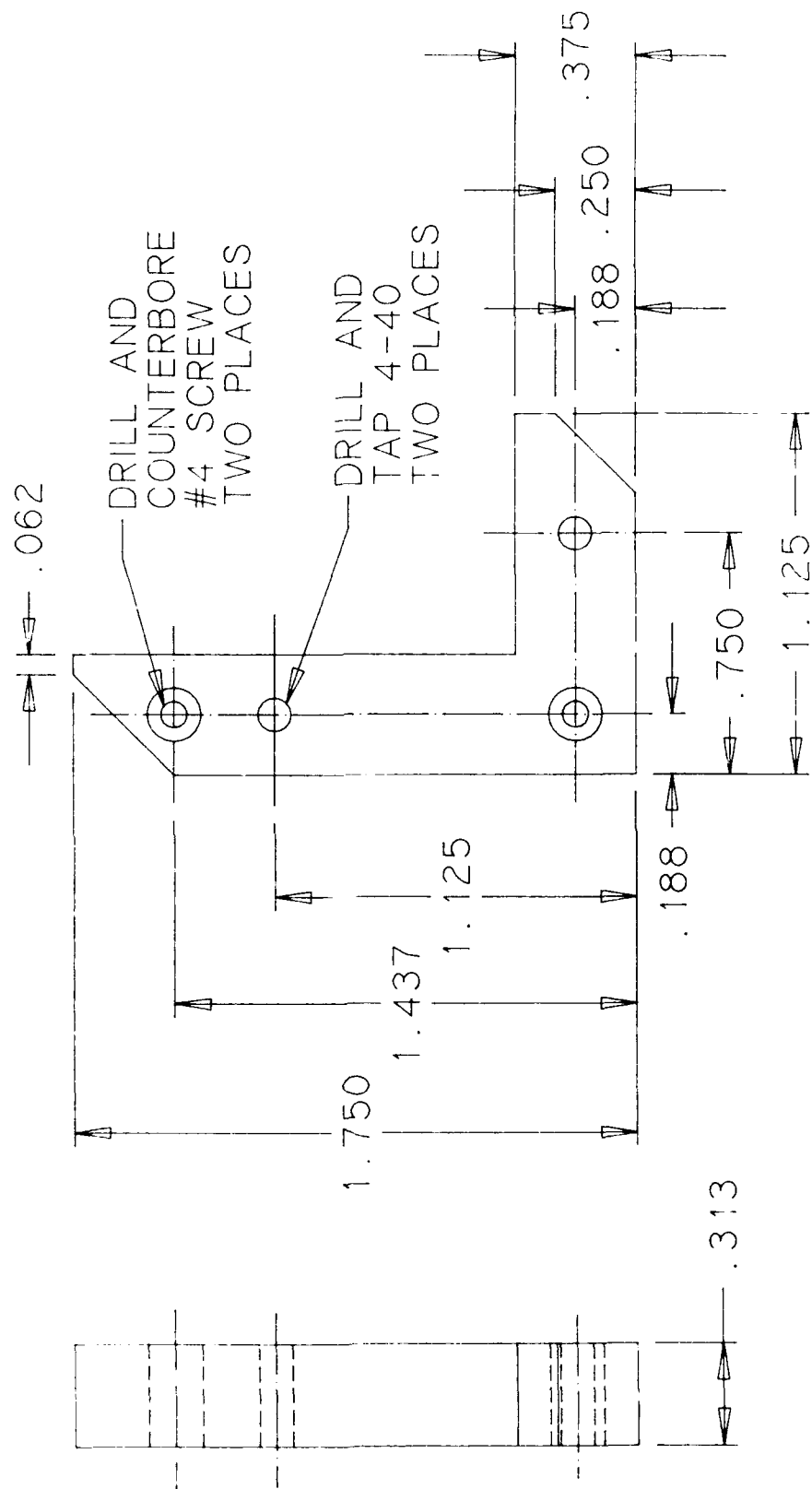
# LASER CLAMP

MATERIAL: 2024-T3 ALUMINUM  
2 PIECES



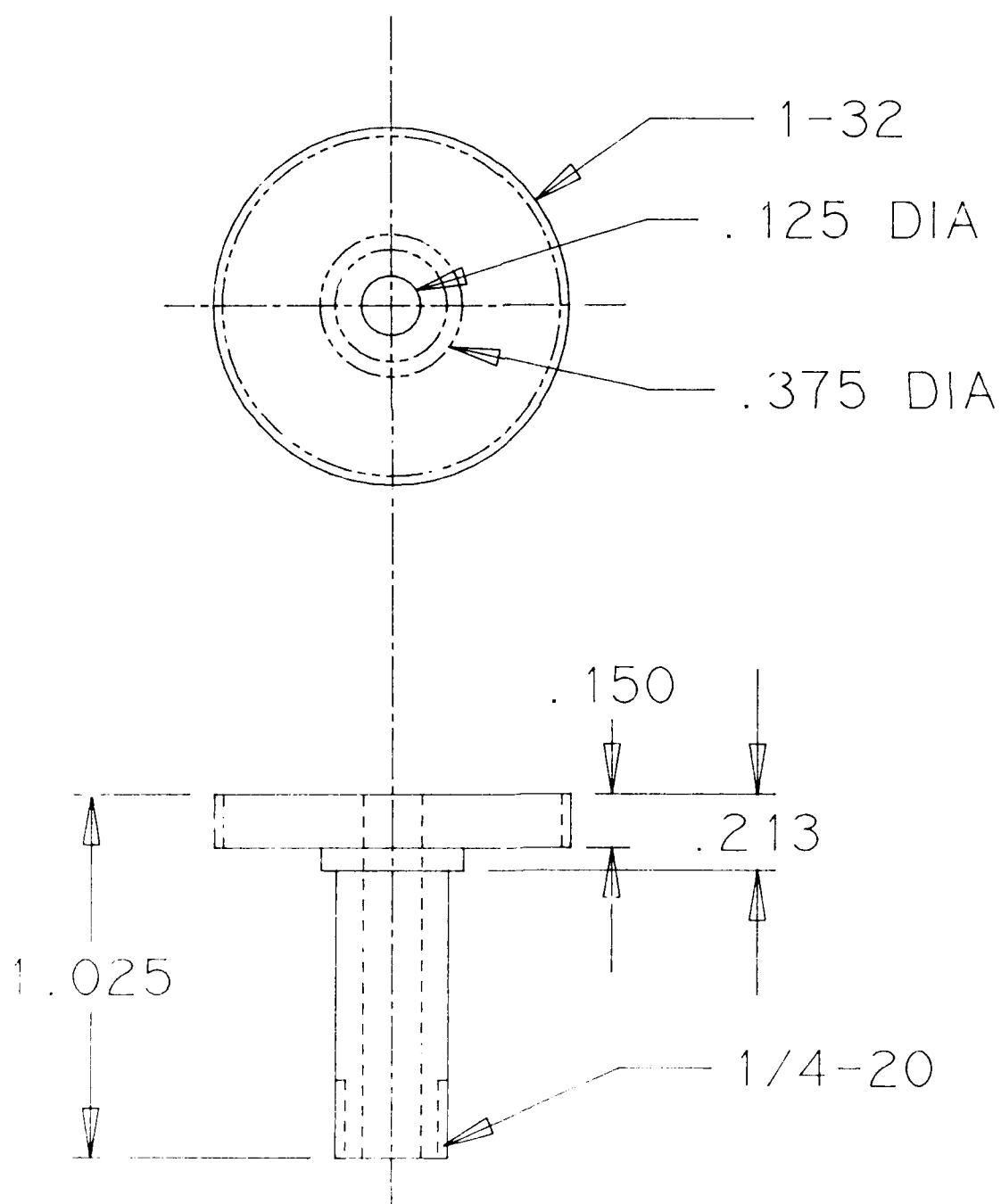
Part No. 5

OPTICS SHIELD MOUNT BLOCKS  
ALUMINUM TWO PIECES  
ONE PIECE MIRROR IMAGE



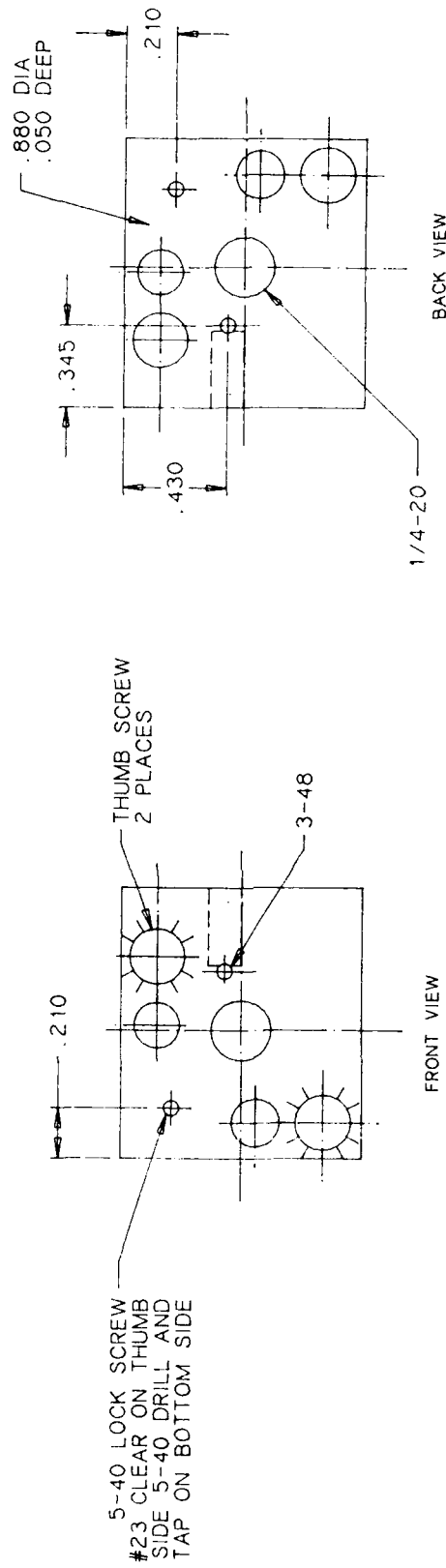
Part No. 6

TITLE: LASER TUBE EXTENDER  
ALUMINUM ONE PIECE



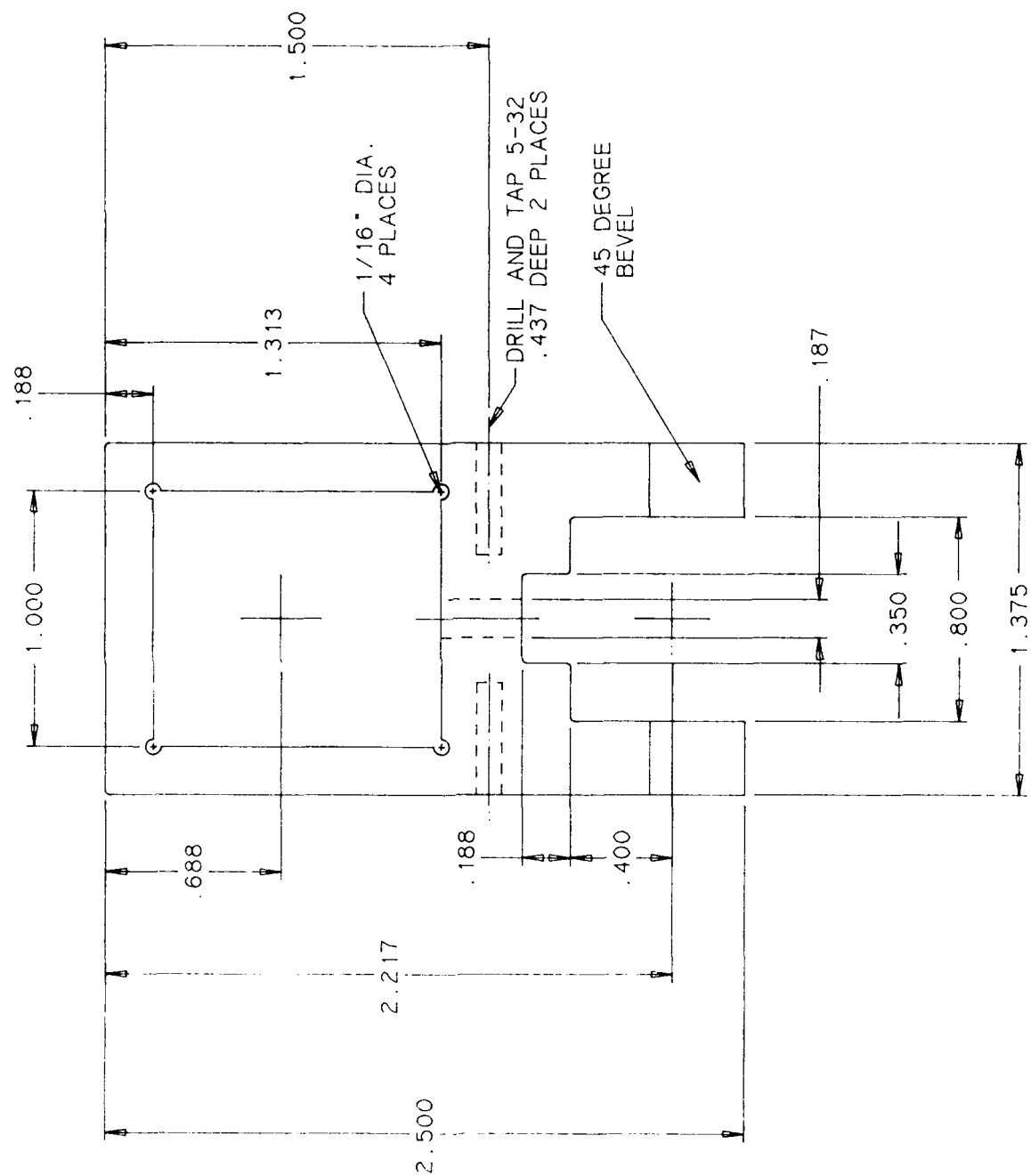
Part No. 8

MM-1 [MIRROR MOUNT] MODIFICATION #2



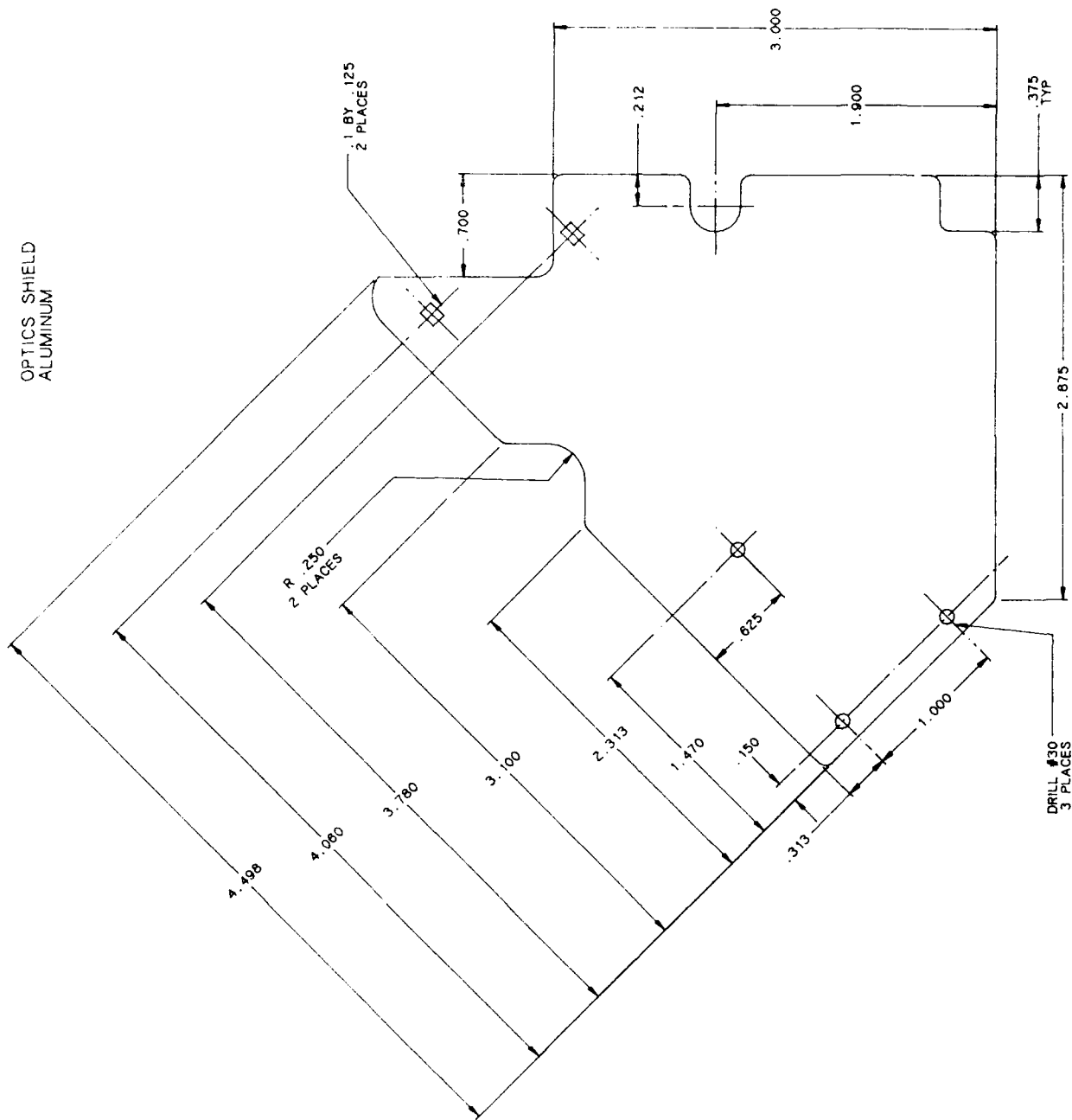
Part No. 9

TARGET MIRROR SUPPORT  
1 PIECE 1/4" ALUMINUM



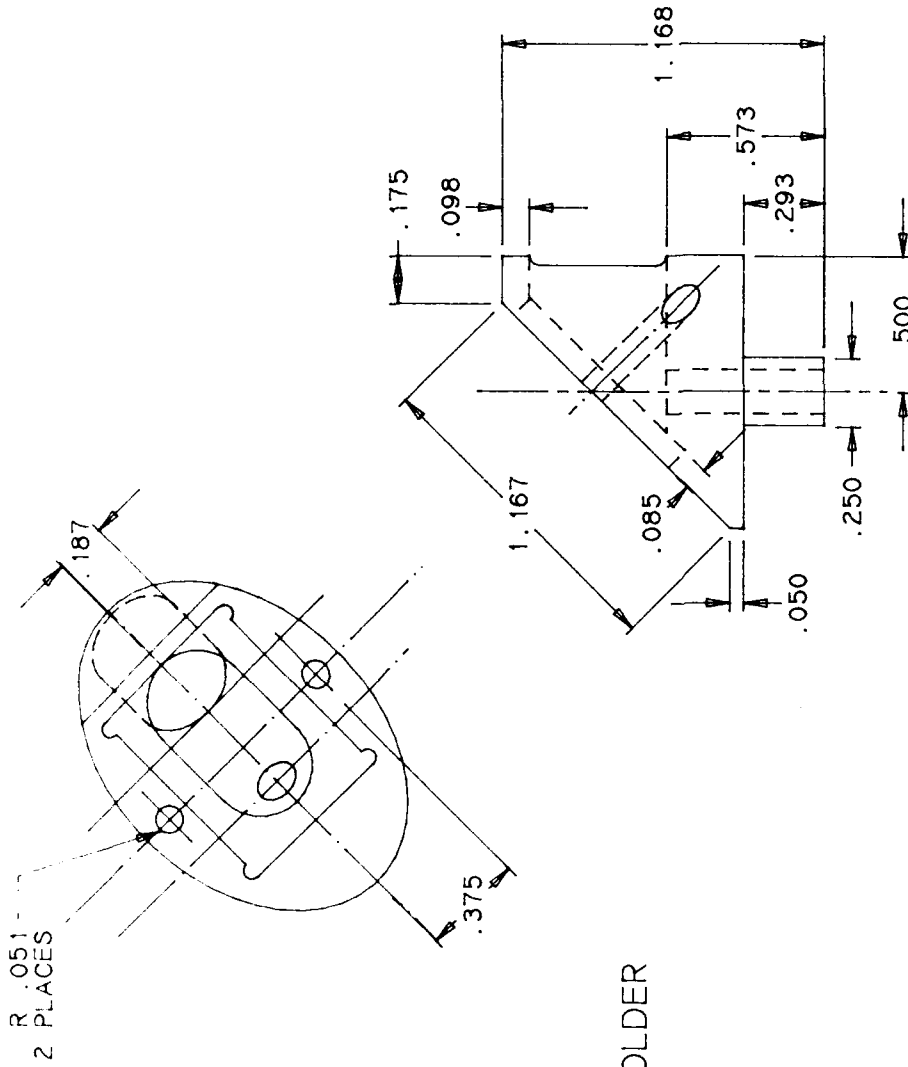
Part No. 10

OPTICS SHIELD  
ALUMINUM

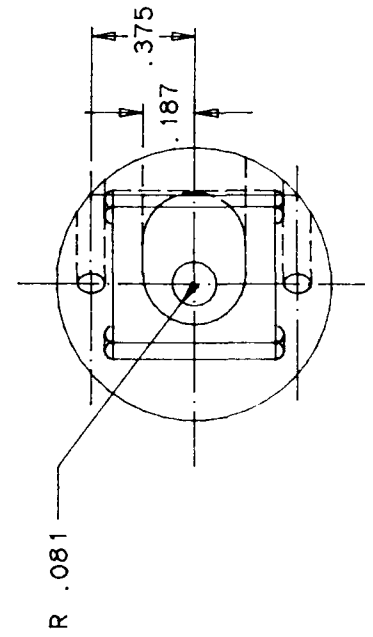


2 PIECES, 1 PIECE MIRROR IMAGE

Part No. 13



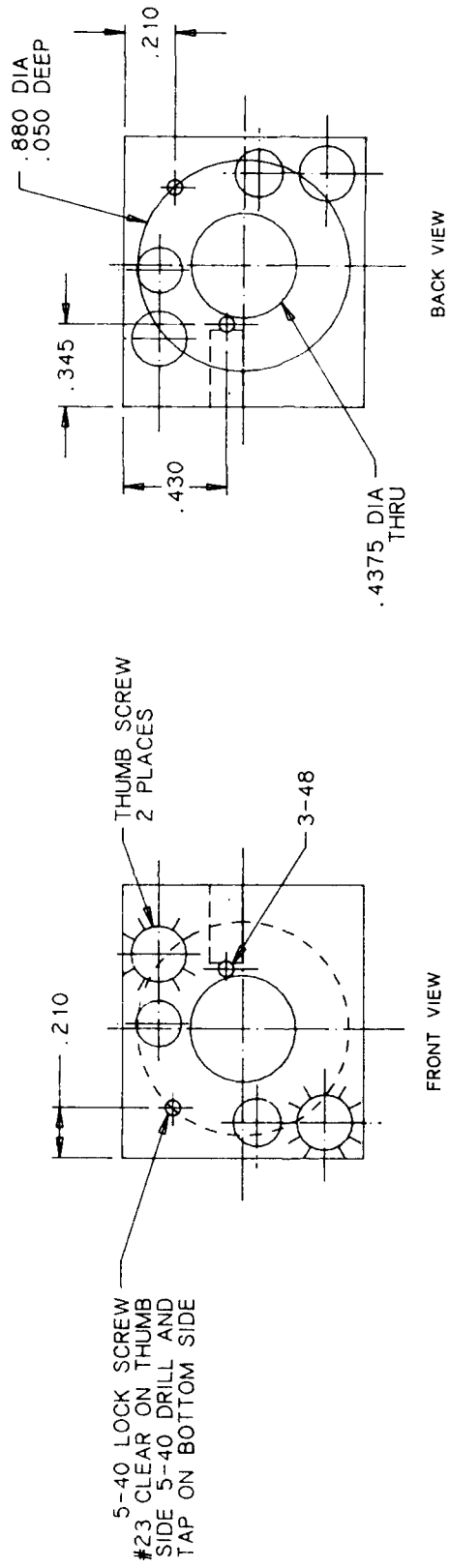
BEAM PLATE HOLDER  
ALUMINUM  
1 PIECE



Part No. 14

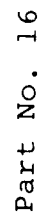


MM-1 [MIRROR MOUNT] MODIFICATION #1

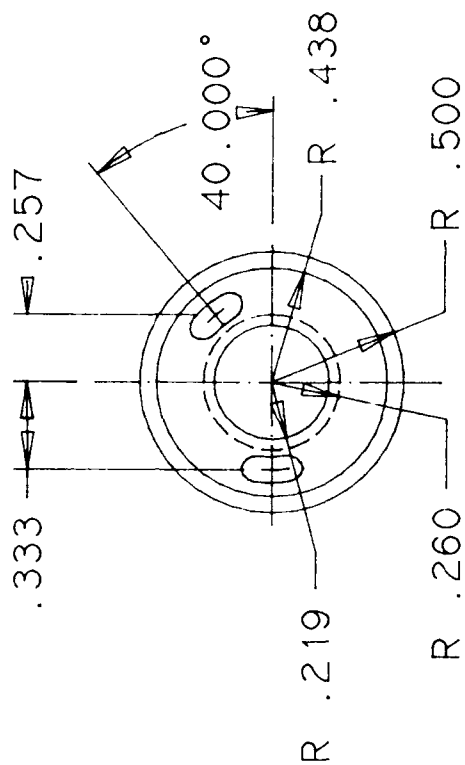
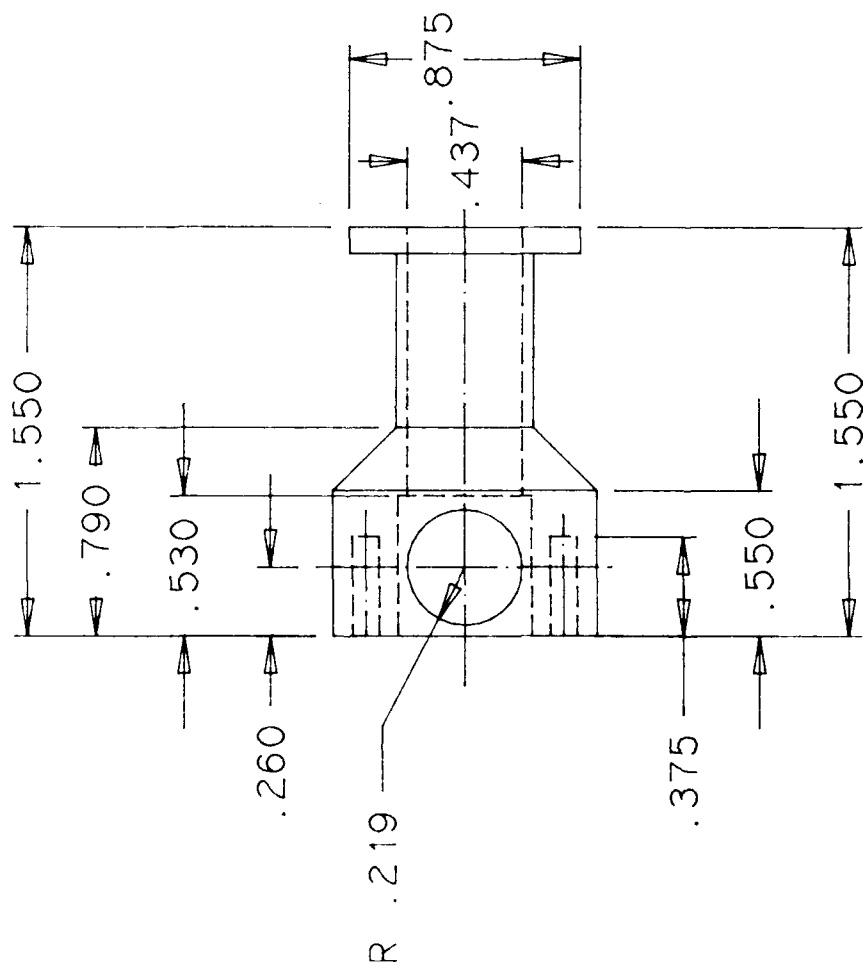


Part No. 15

## 159

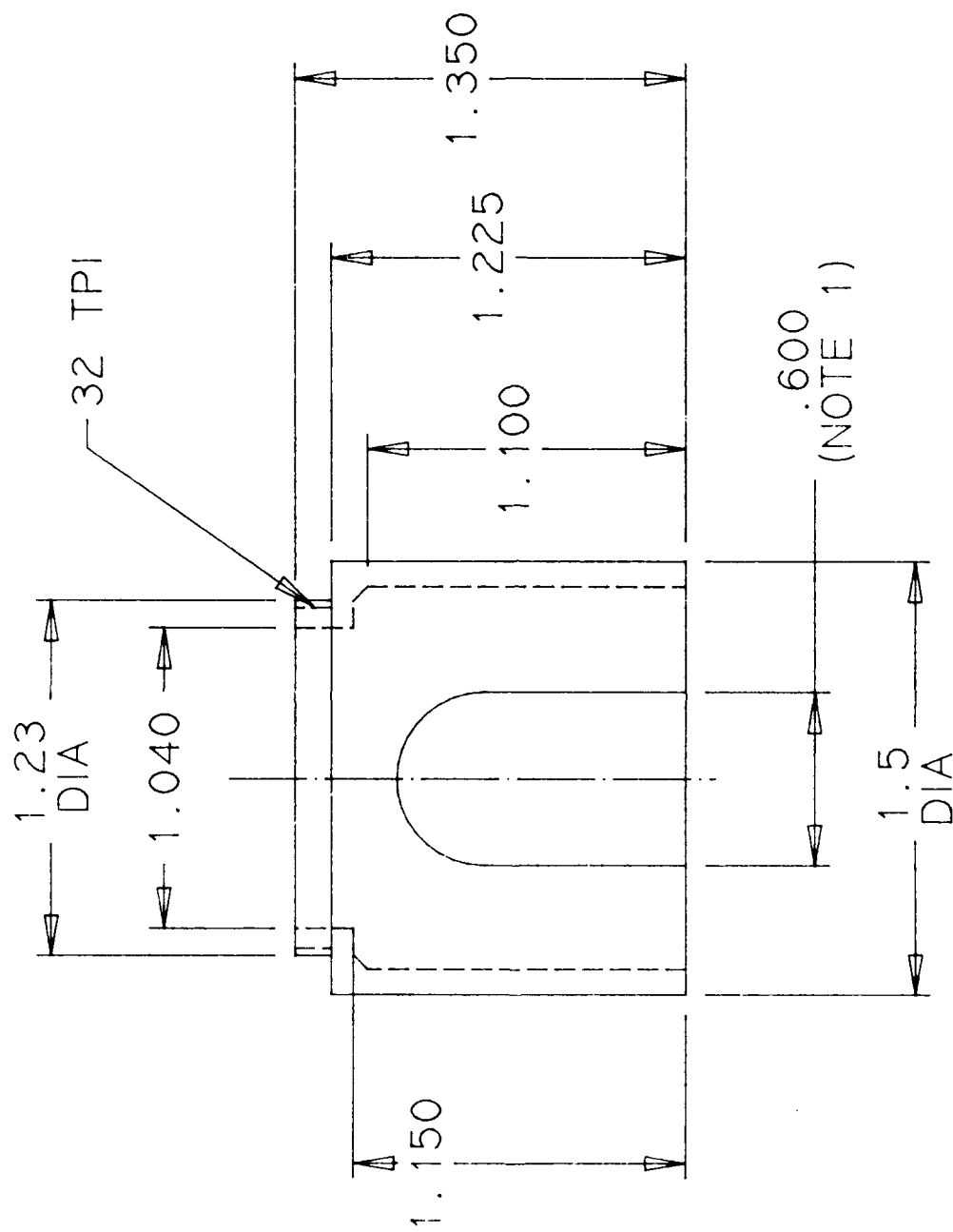


# BEAM SPLITTER (CUBE) HOLDER 1 PIECE ALUMINUM



Part No. 17

TITLE: BEAM SPLITTING CUBE COVER  
MATERIAL: ALUMINUM



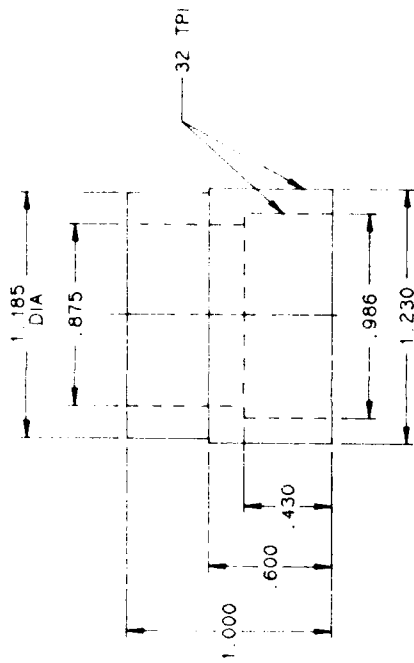
Part No. 19

NOTES:

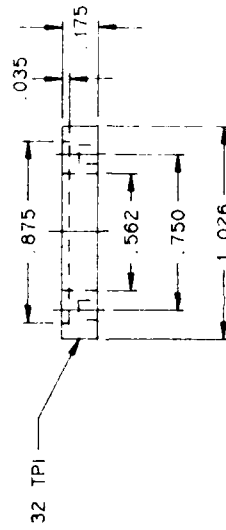
- 1.) SLOT POSITION TO BE DETERMINED AFTER THREADING INTO ASSEMBLED TELESCOPE BODY

# OBJECTIVE LENS HOLDER/ ADJUSTMENT RING

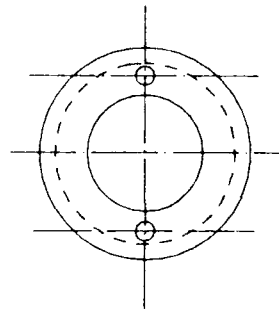
MATERIAL : ALUMINUM



Part No. 21

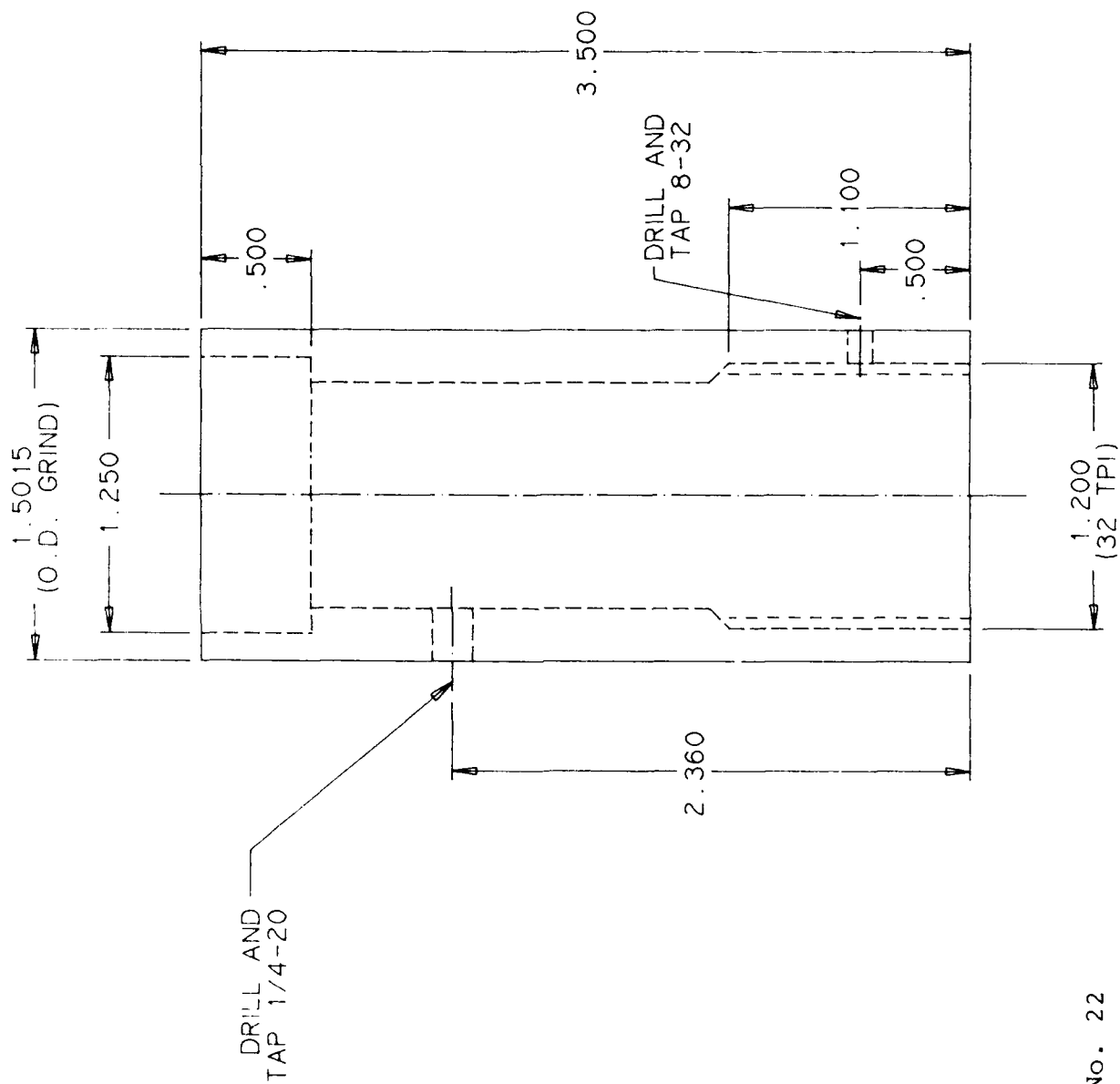


Part No. 20



NOTE : THIS ASSEMBLY IS POSITIONED  
AT .100 BELOW FACE OF TELESCOPE  
BEARING FACE

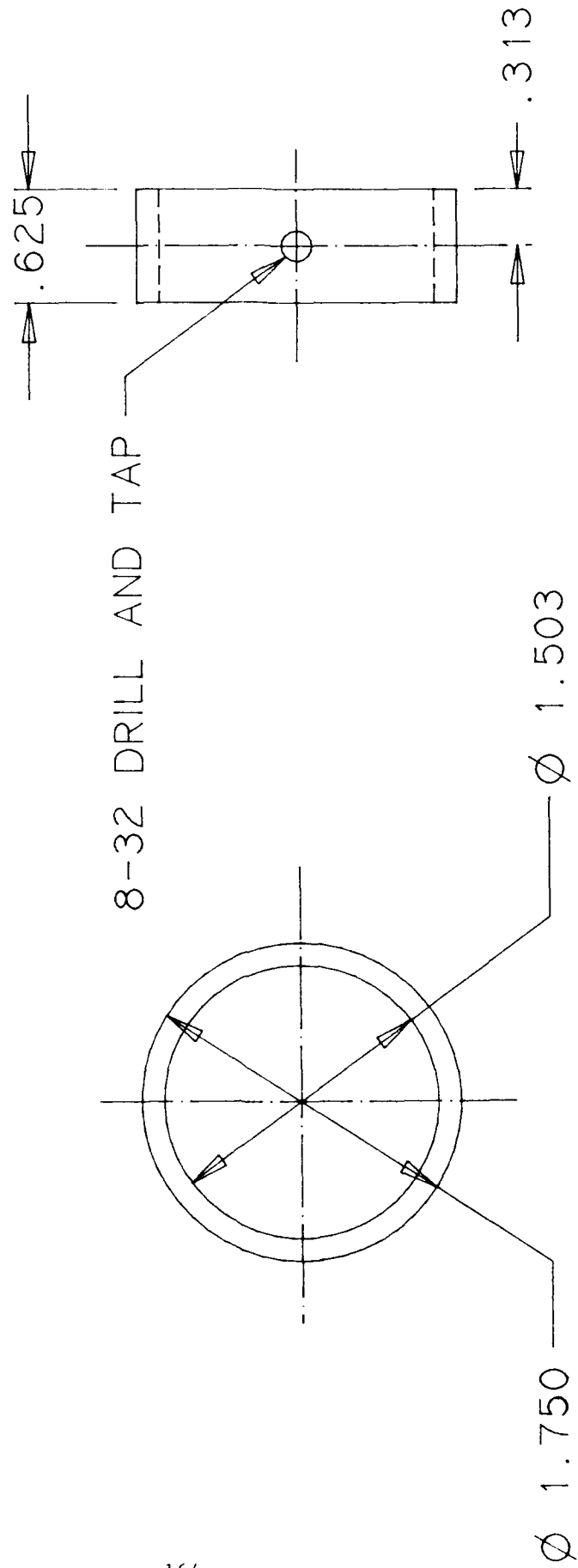
TITLE : SCOPE LOWER BODY BEARING SURFACE  
 MATERIAL : 52100 STEEL R/C 62



Part No. 22

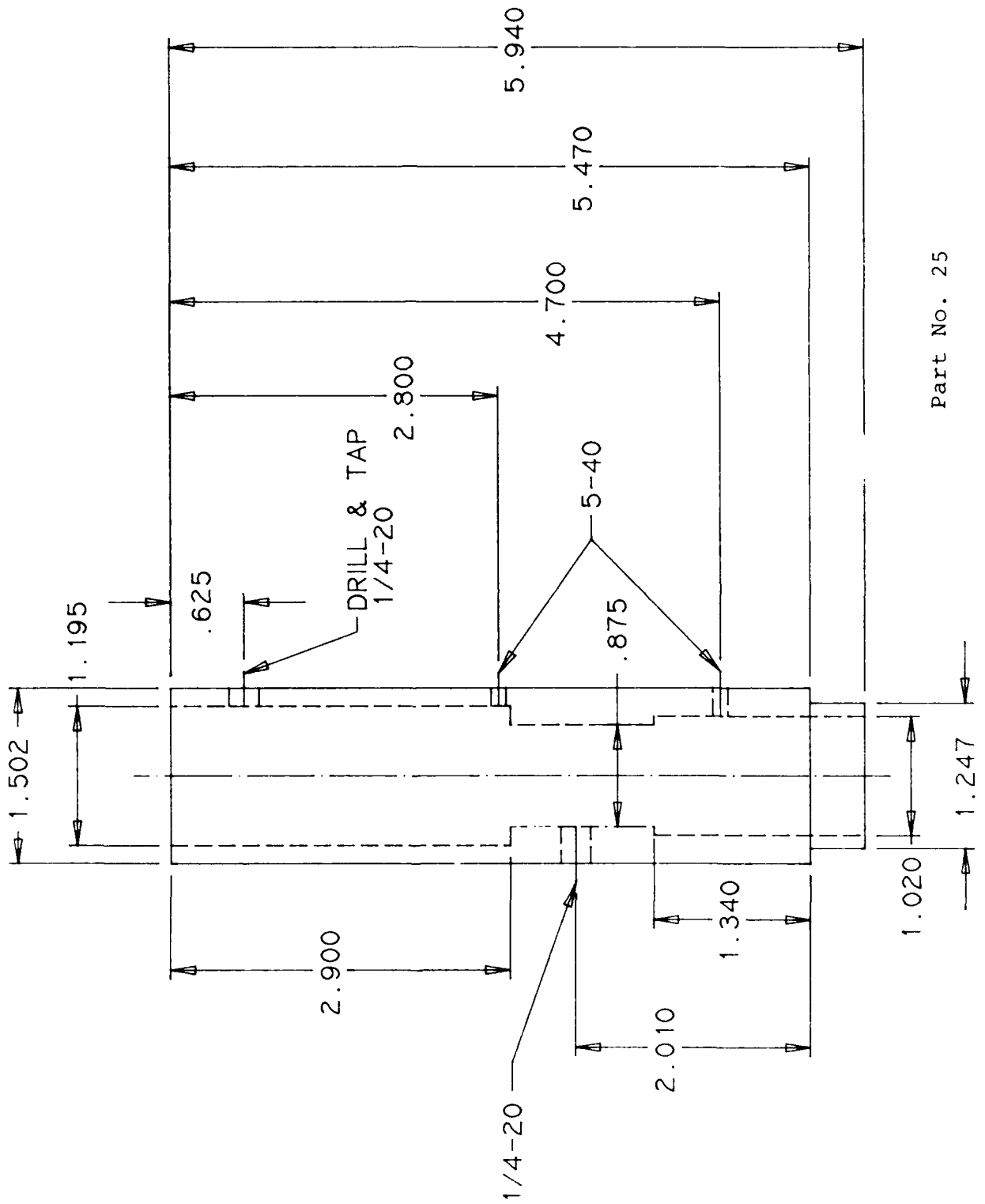
# MICROSCOPE/LASER POSITIONING RING

MATERIAL: ALUMINUM



Part No. 23

SCOPE UPPER BODY  
MATERIAL : ALUMINUM

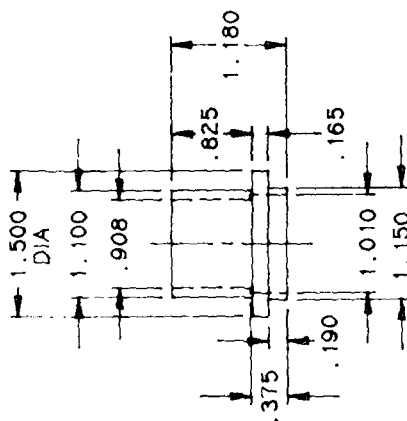


Part No. 25



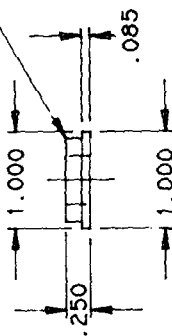
EYEPiece MOUNT/EYEPiece RETAINER/ADJUSTMENT HOUSING  
MATERIAL : 6061 ALUMINUM

Part No. 28

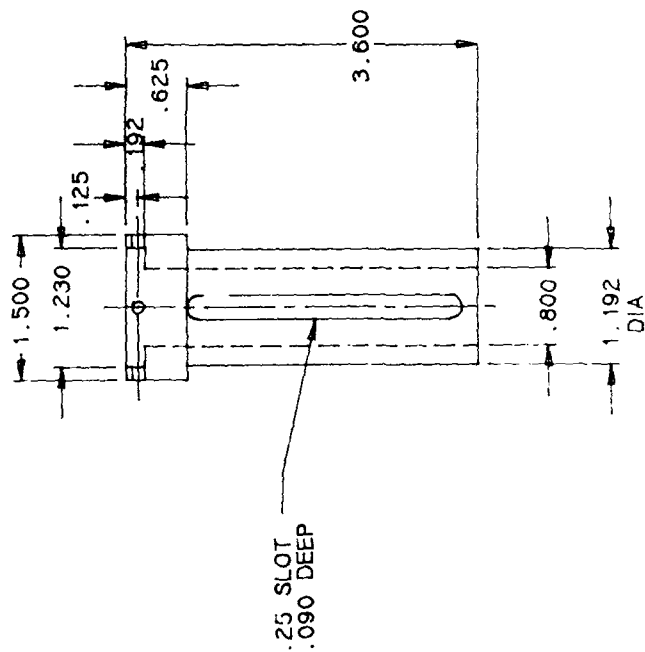


.860 DIA X 36 TPI (MACHINE FIT TO EYEPiece)  
.500 HOLE THRU CENTER

Part No. 27



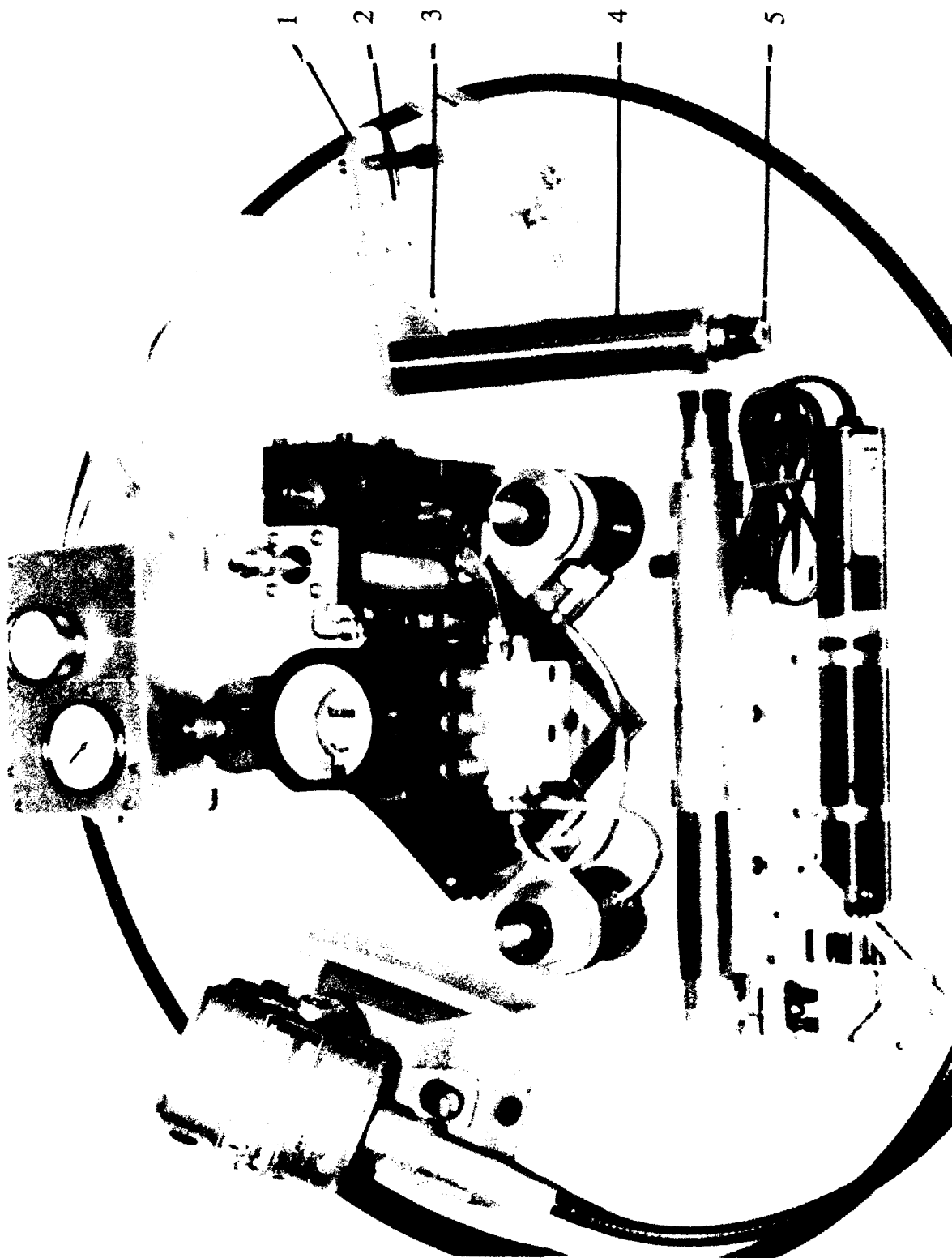
Part No. 26



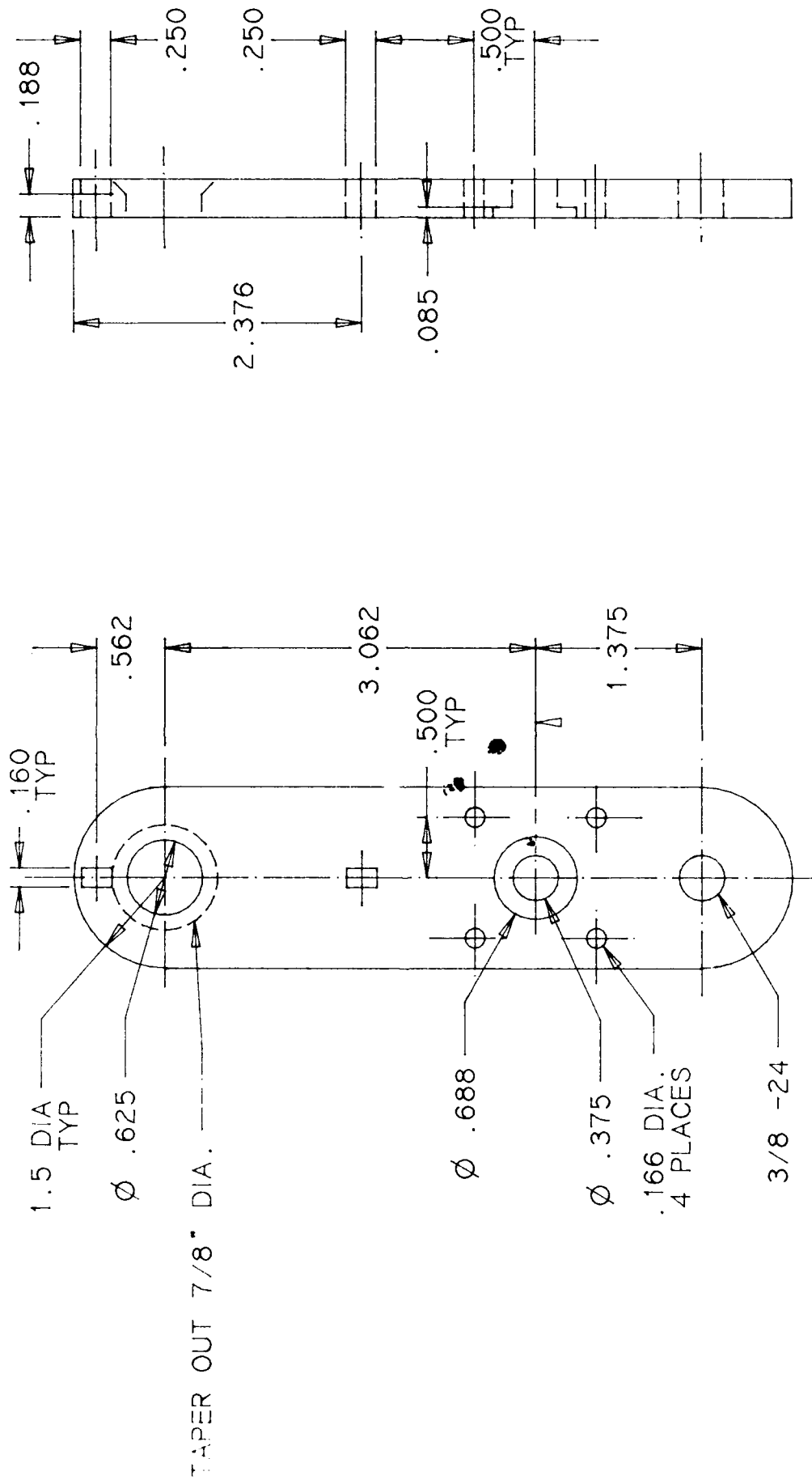
## ASSEMBLY NO. 3

### PARTS LIST

- |   |                                     |
|---|-------------------------------------|
| 1 | Upper Acuating Arm                  |
| 2 | Micrometer Stop Bracket             |
| 3 | Acuating Arm Support Block          |
| 4 | Drill Motor Housing                 |
| 5 | Drill Motor Collet Nut Modification |



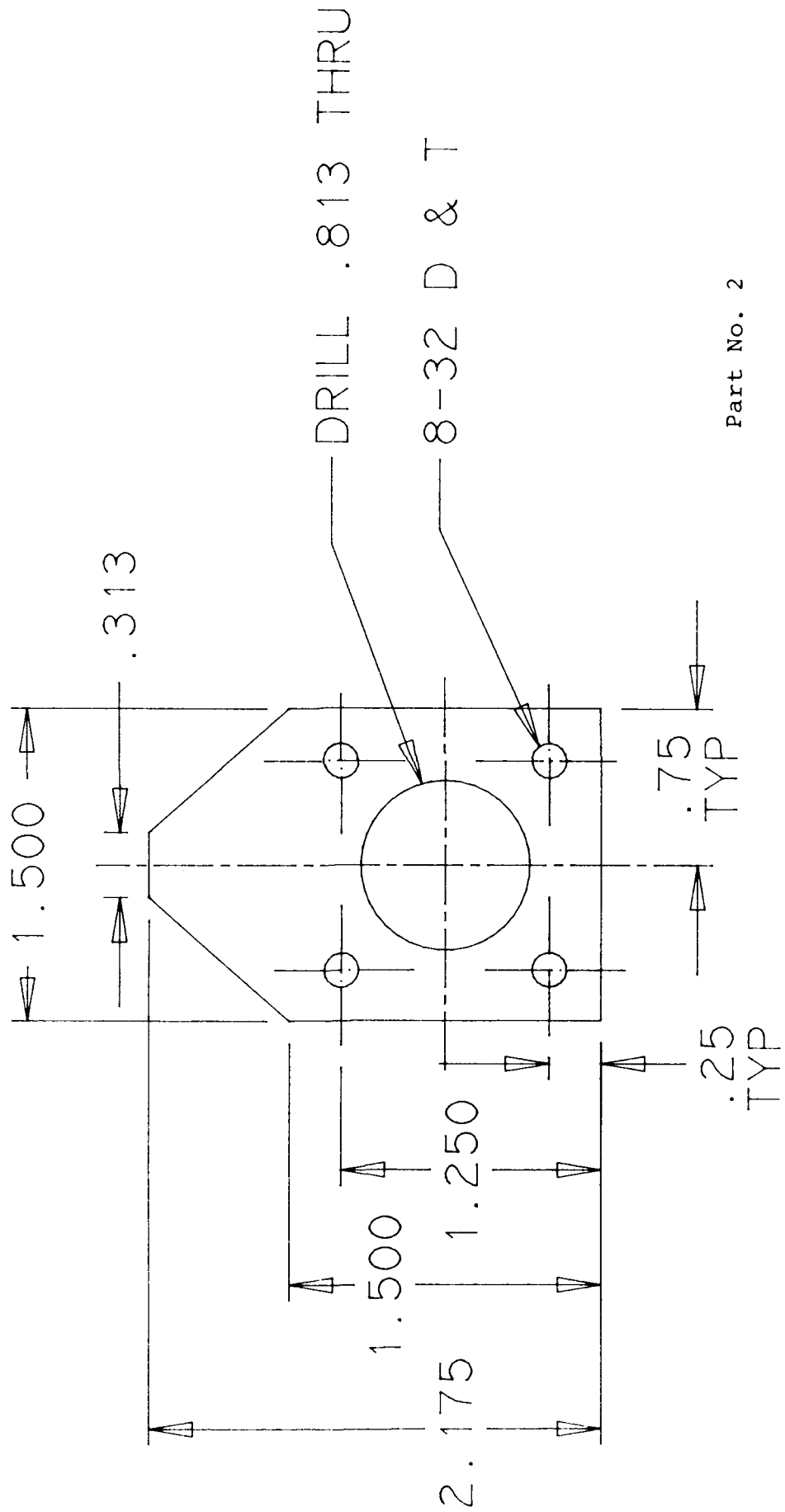
# TITLE: UPPER ACUATING ARM



Part No. 1

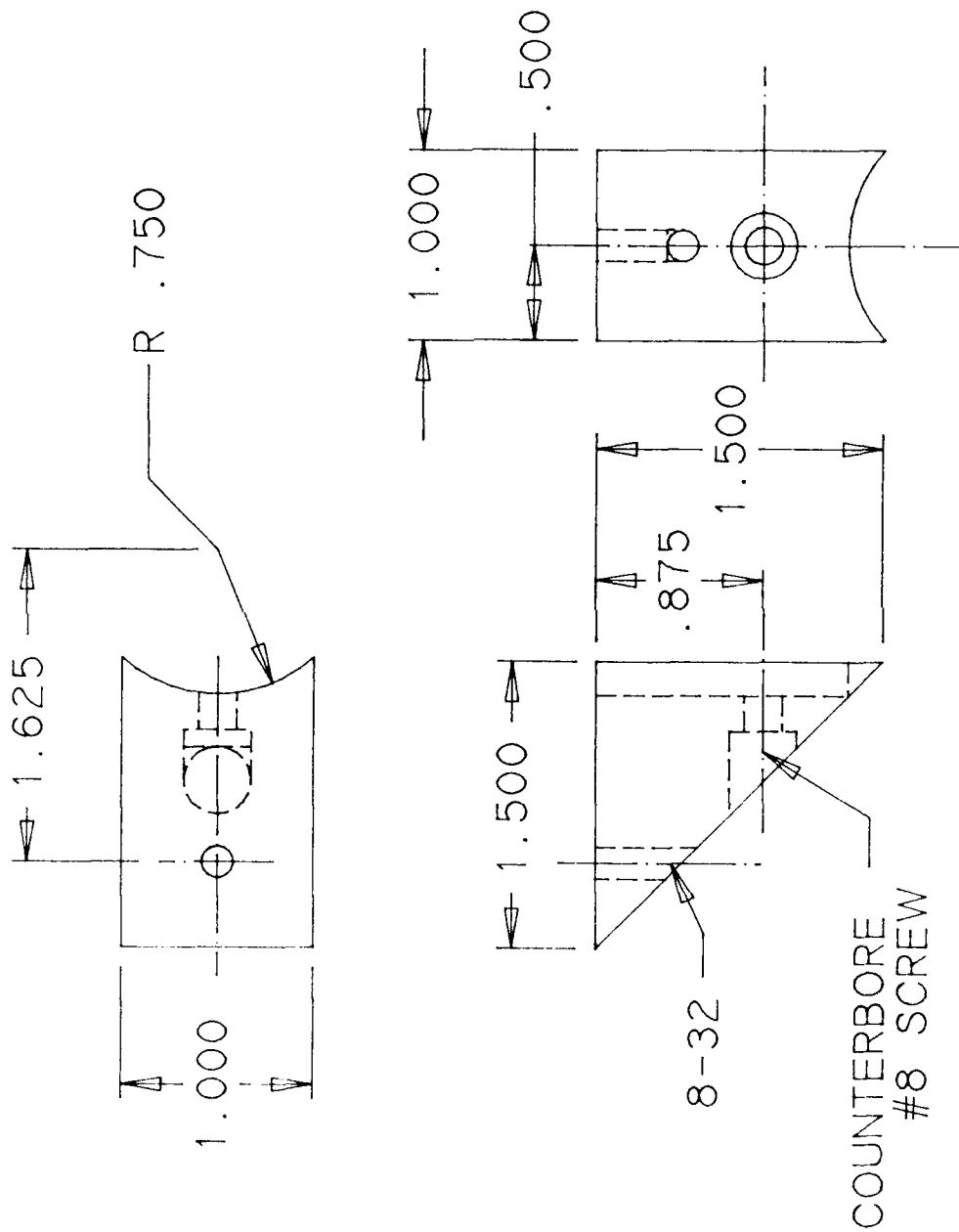
ALUMINUM 5/16 THICK BY 1 1/2 WIDE 1 PIECE

TITLE: MICROMETER STOP BRACKET  
 MATERIAL: 1/4" THICK 6061-T6 ALUMINUM



Part No. 2

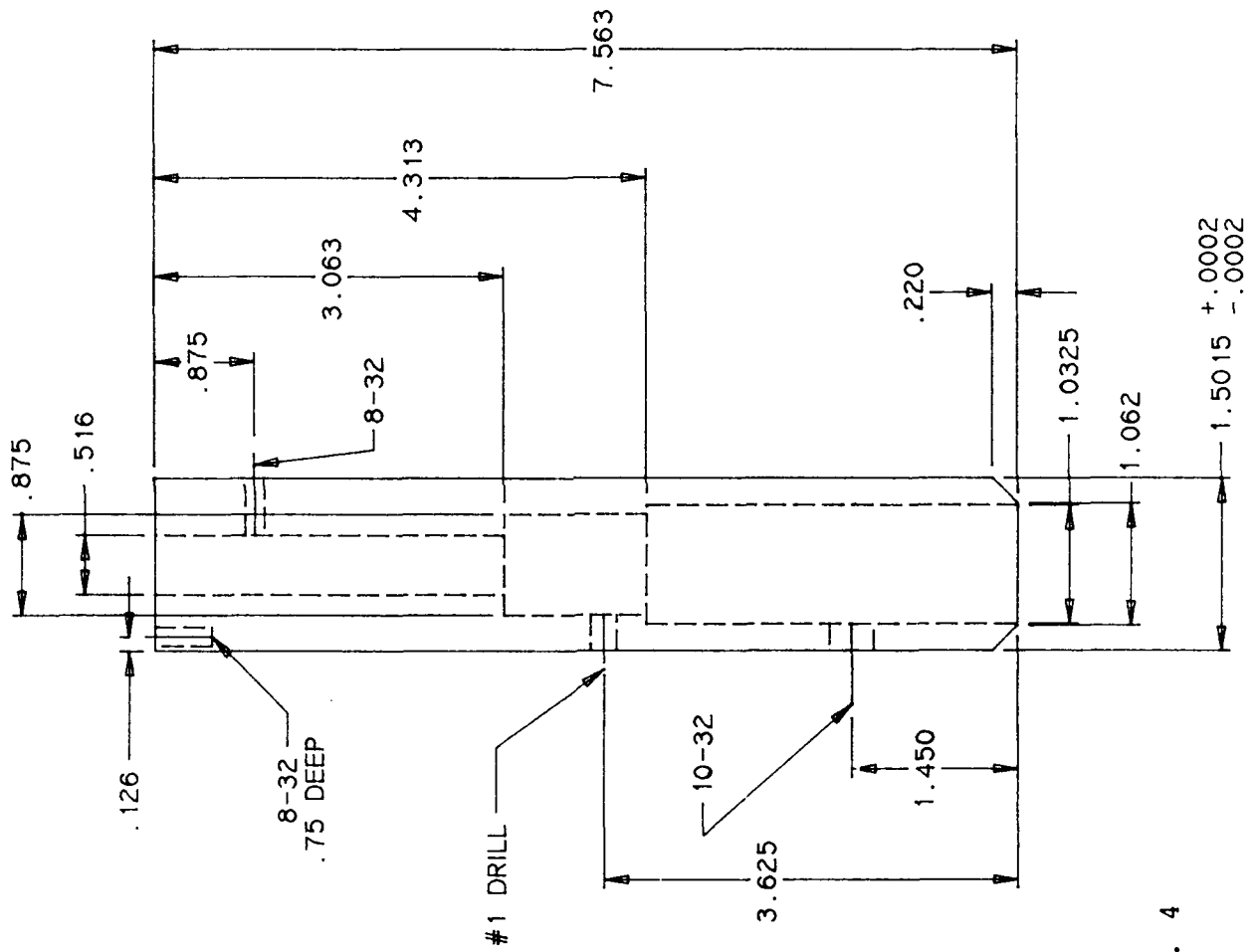
# ACUATING ARM SUPPORT BLOCK



Part No. 3

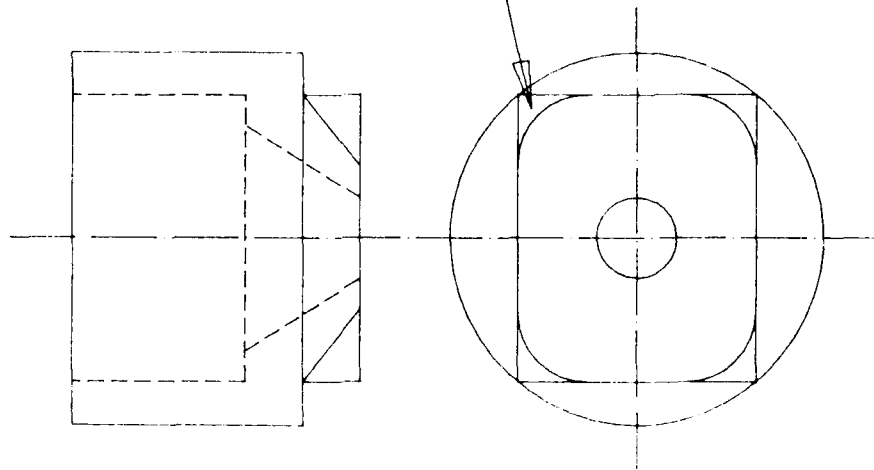
ALUMINUM 1 PEICE

# DRILL MOTOR HOUSING



Part No. 4

DRILL MOTOR COLLET  
NUT MODIFICATION



TURN TAPER ON SQUARE TO  
ALLOW CLEARANCE FOR LIGHT ROD

Part No. 5



## APPENDIX C

### HOLE DRILLING LOCATIONS FOR IN-SERVICED CANOPIES

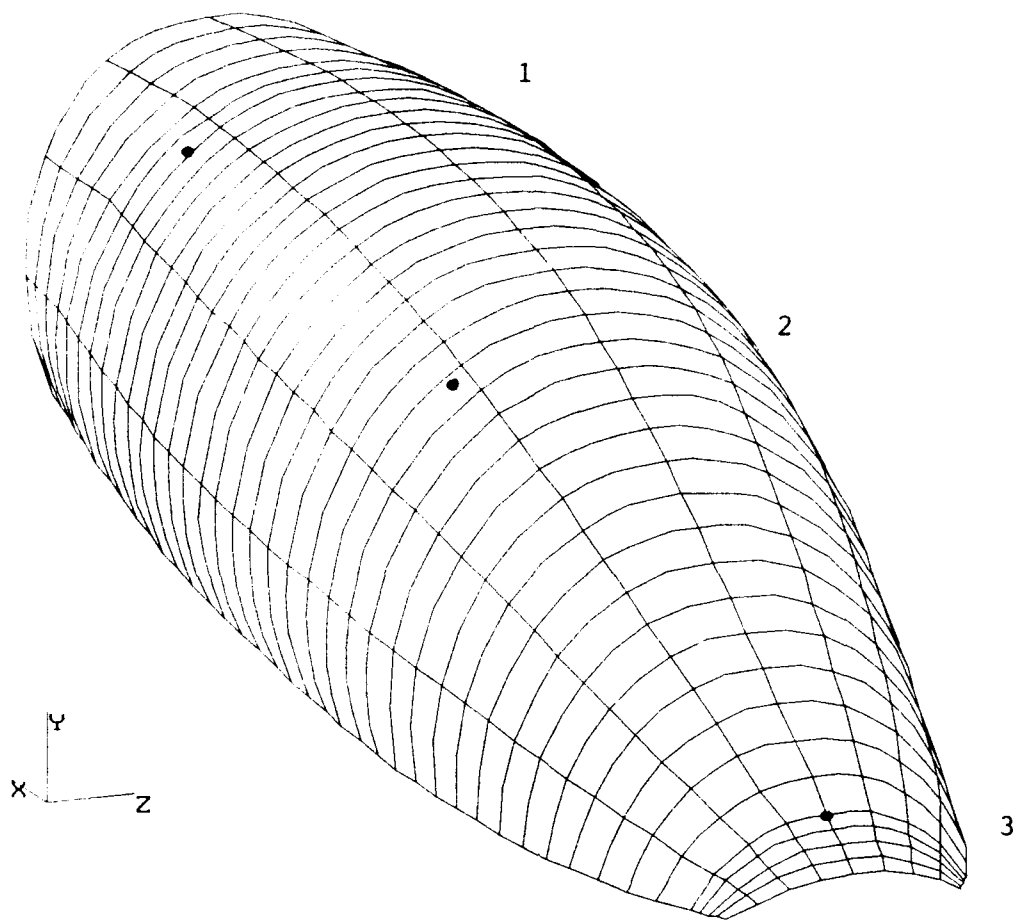


Figure C1. Rosette Locations for Canopy #1 (SN 473).

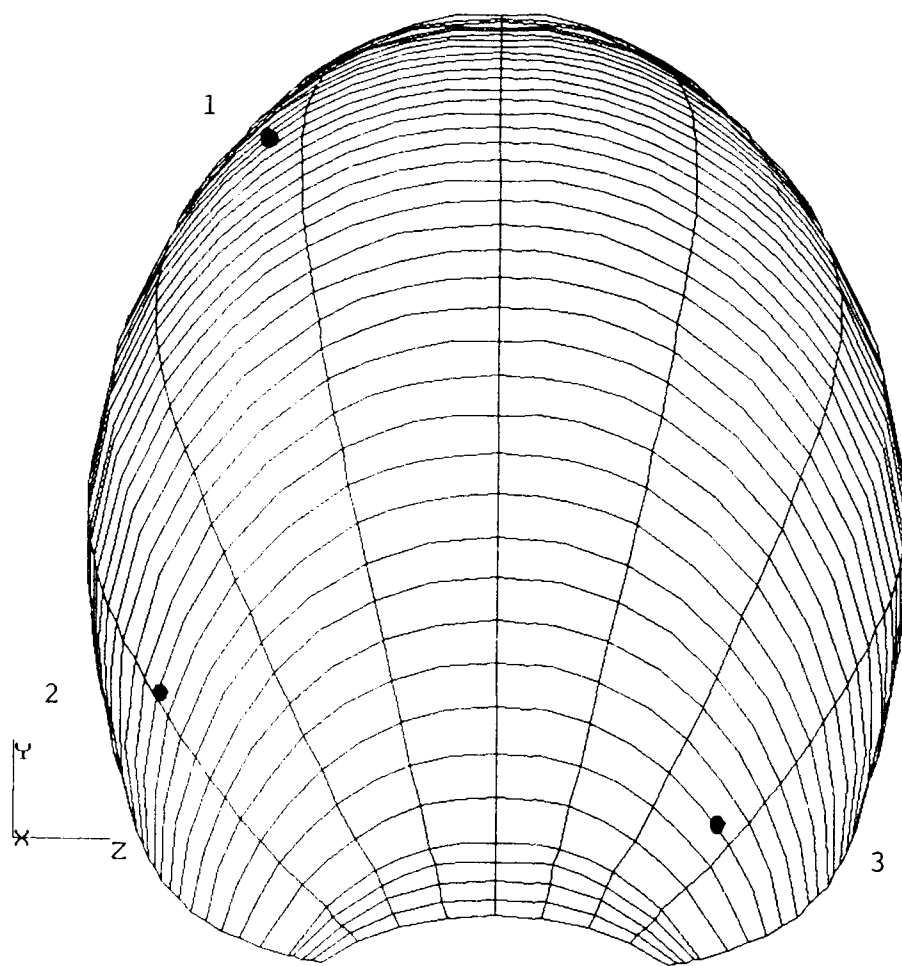


Figure C2. Rosette Locations for Canopy #2 (SN 184).

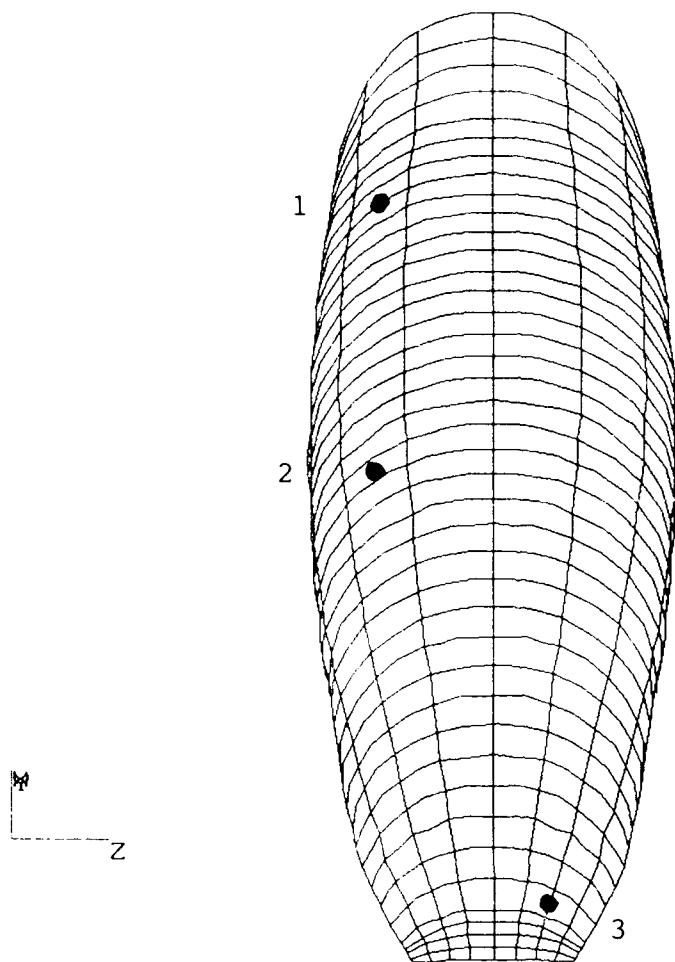


Figure C3. Rosette Locations for Canopy #3 (SN 373).

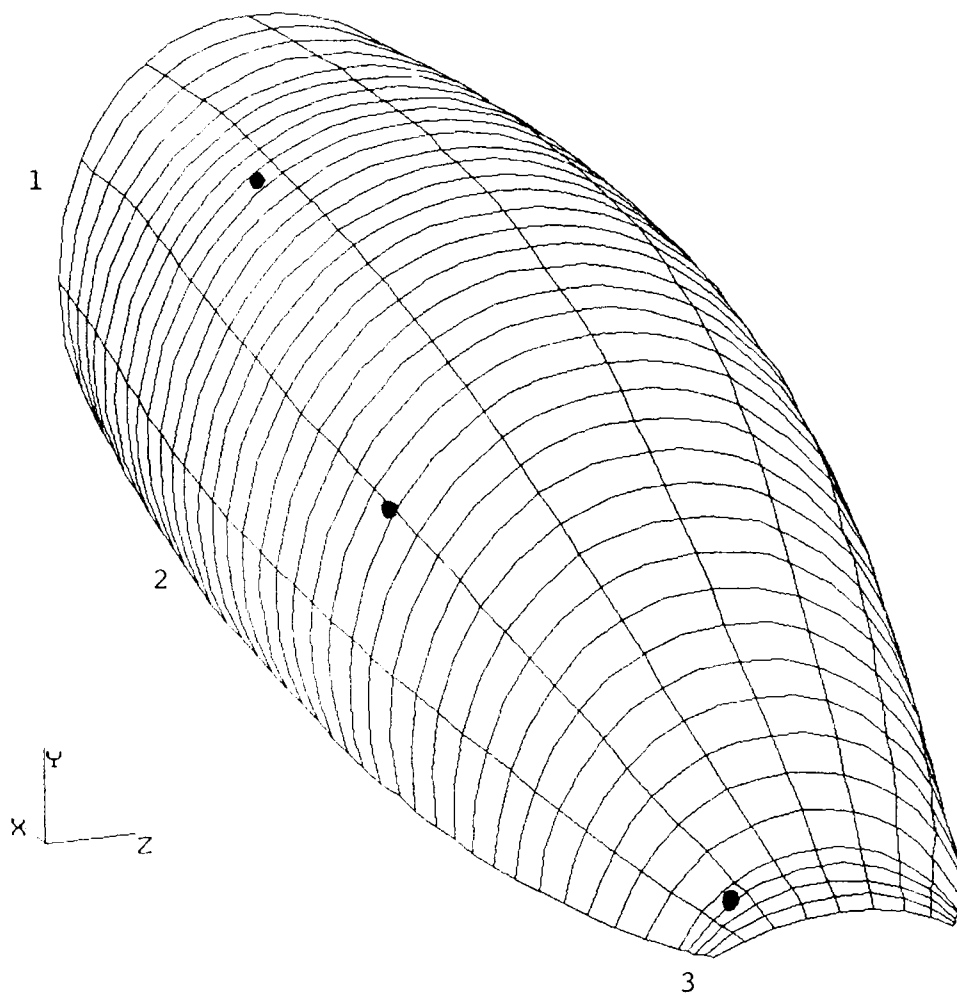


Figure C4. Rosette Locations for Canopy #4 (S/N 218).

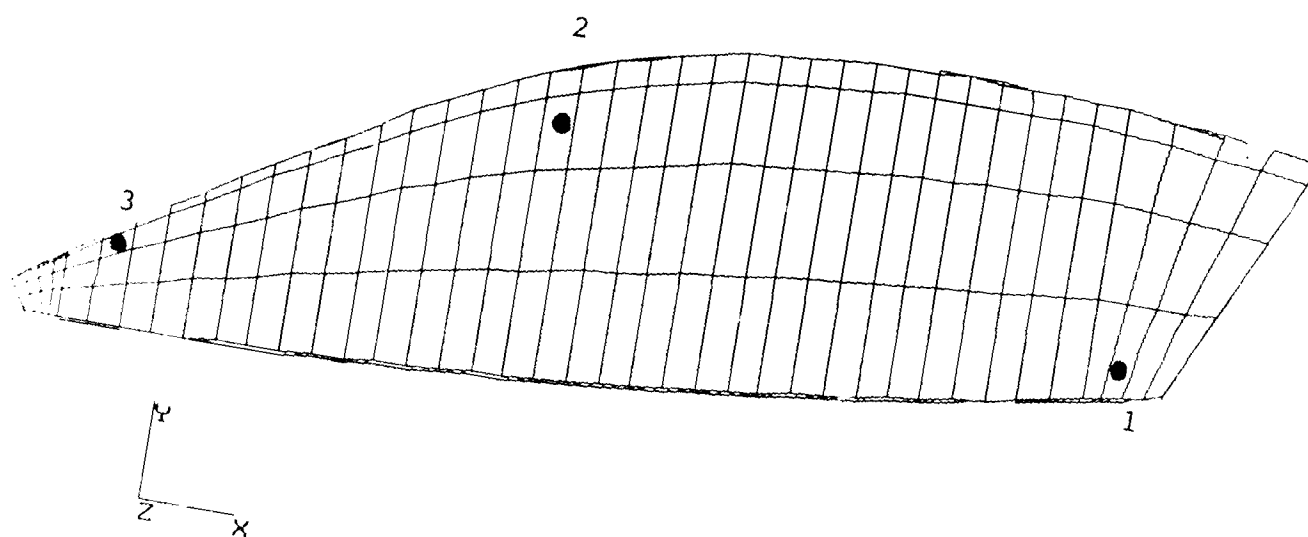


Figure C5. Rosette Locations for Canopy #5 (S/N 1476).

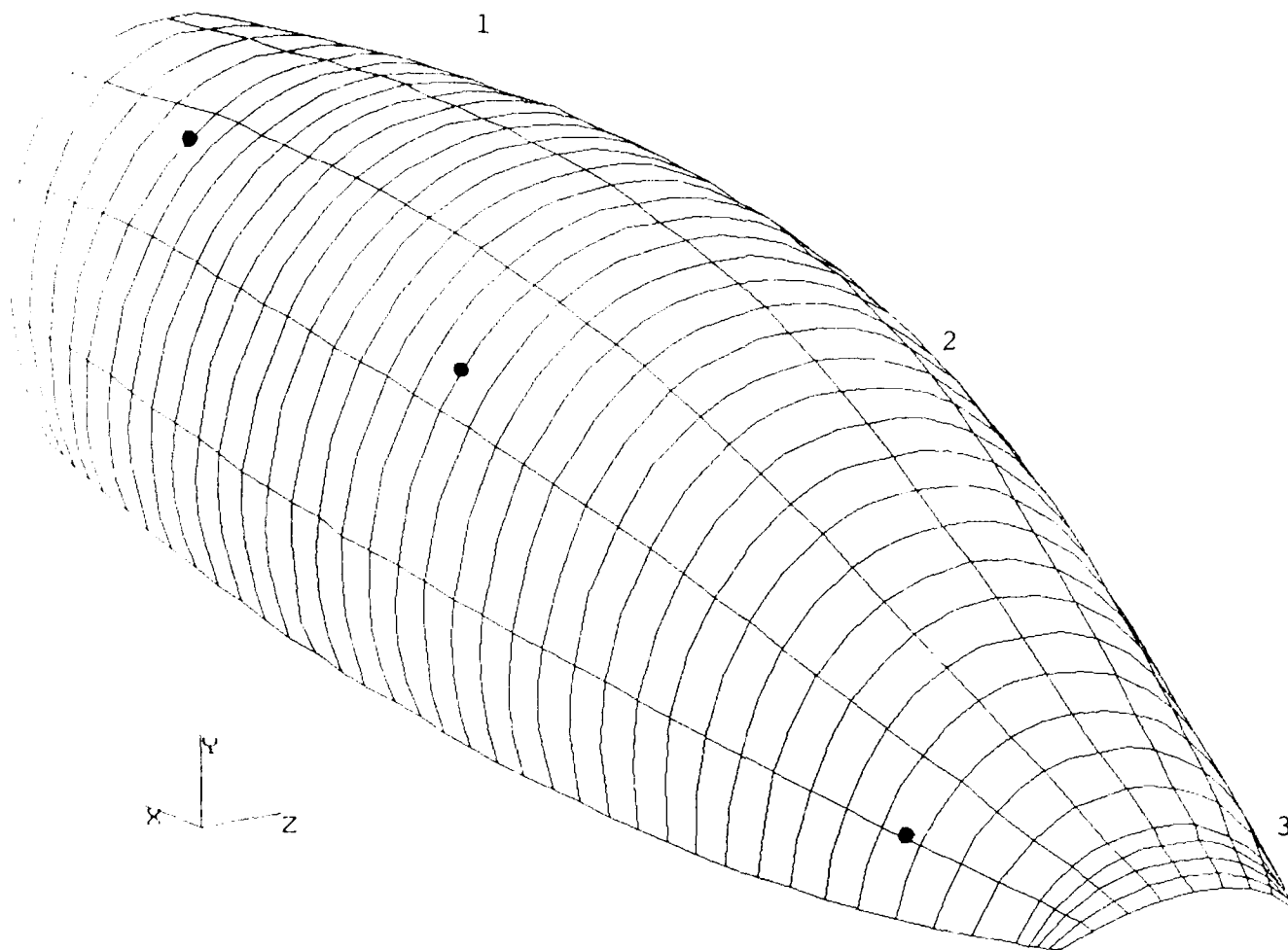


Figure C6. Rosette Locations for Canopy #6 (S/N 289).

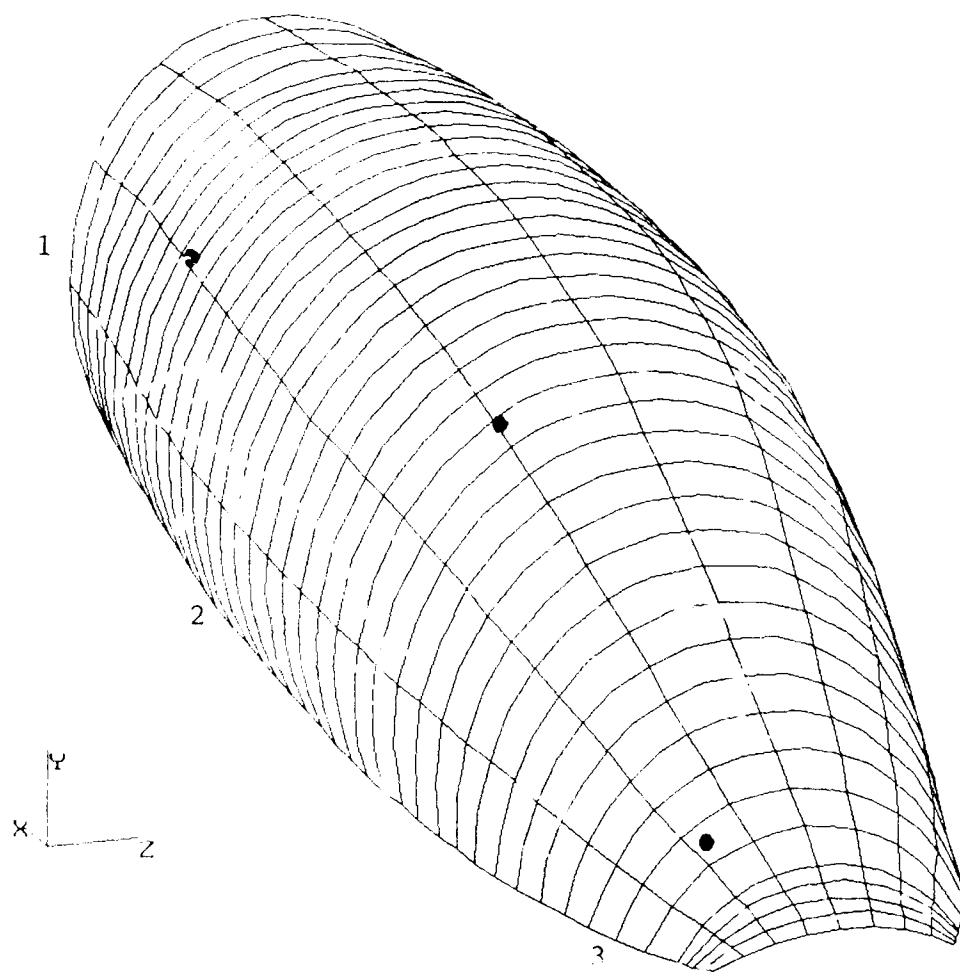


Figure C7. Rosette Locations for Canopy #7 (S/N 138).



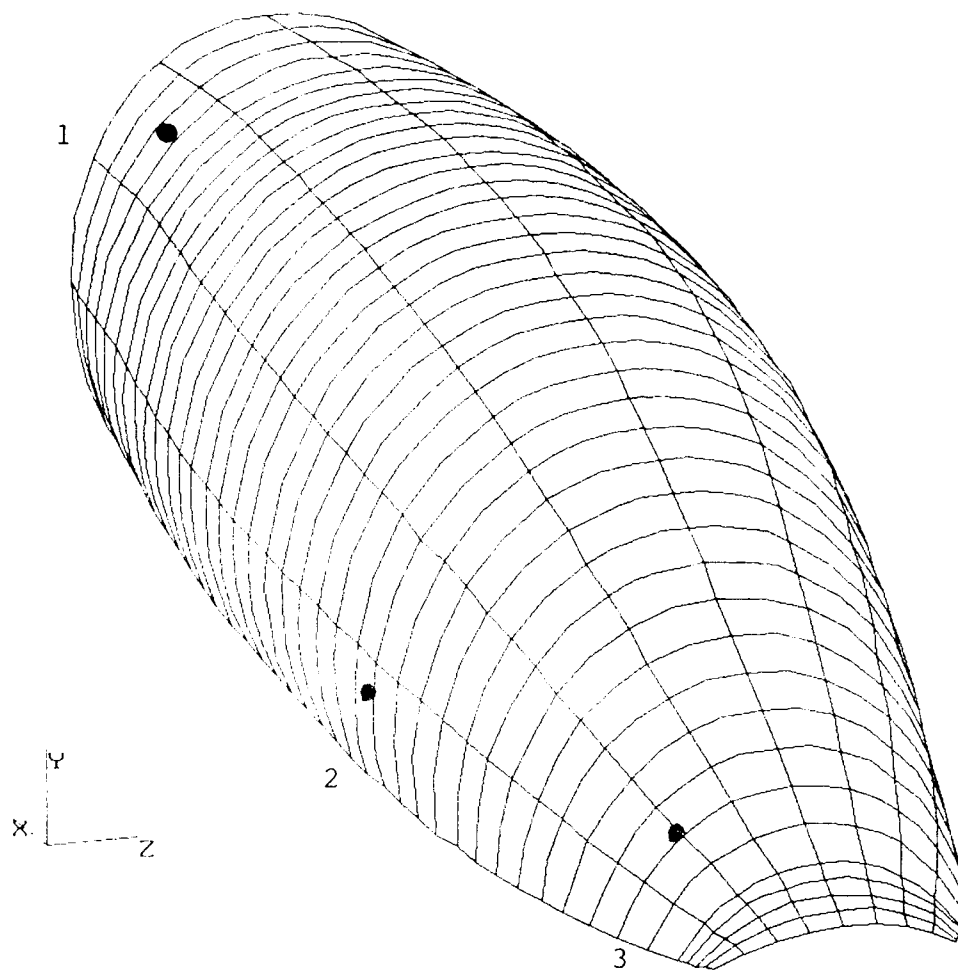


Figure C8. Rosette Locations for Canopy #8 (S/N 612).

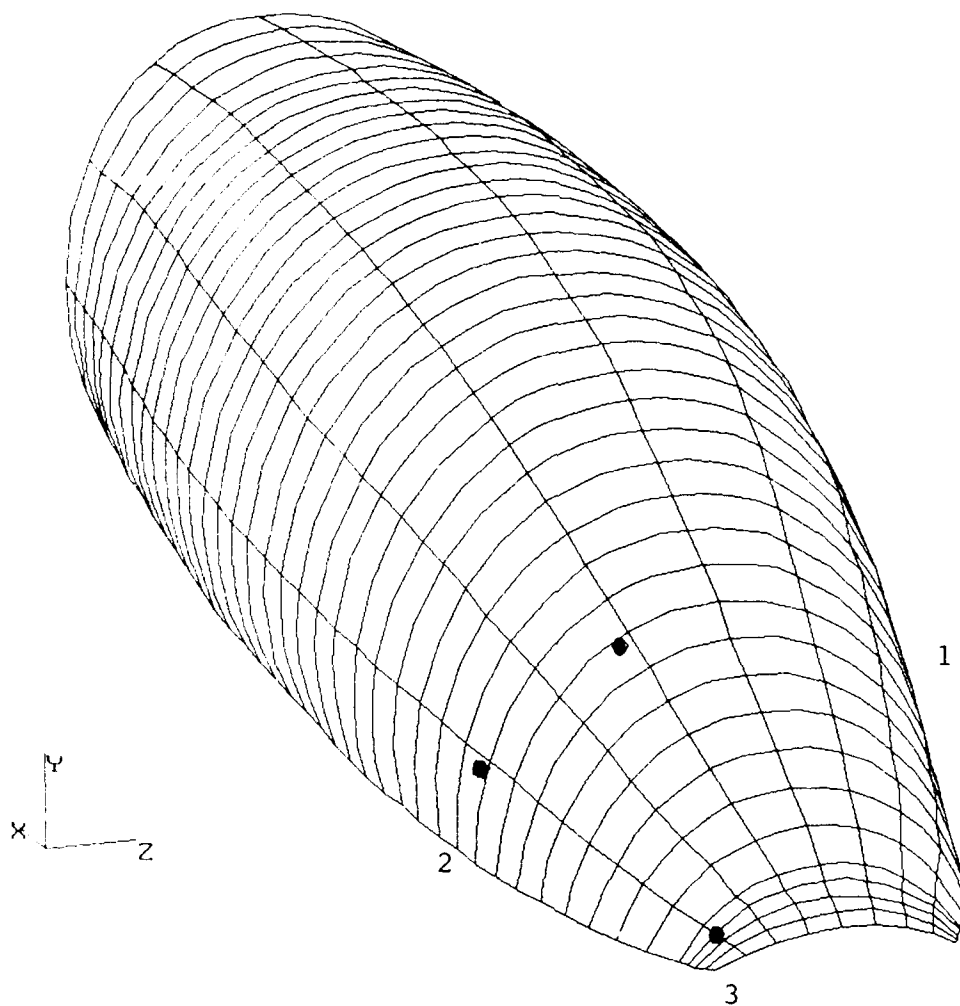


Figure C9. Rosette Locations for Canopy #9 (S/N 734).

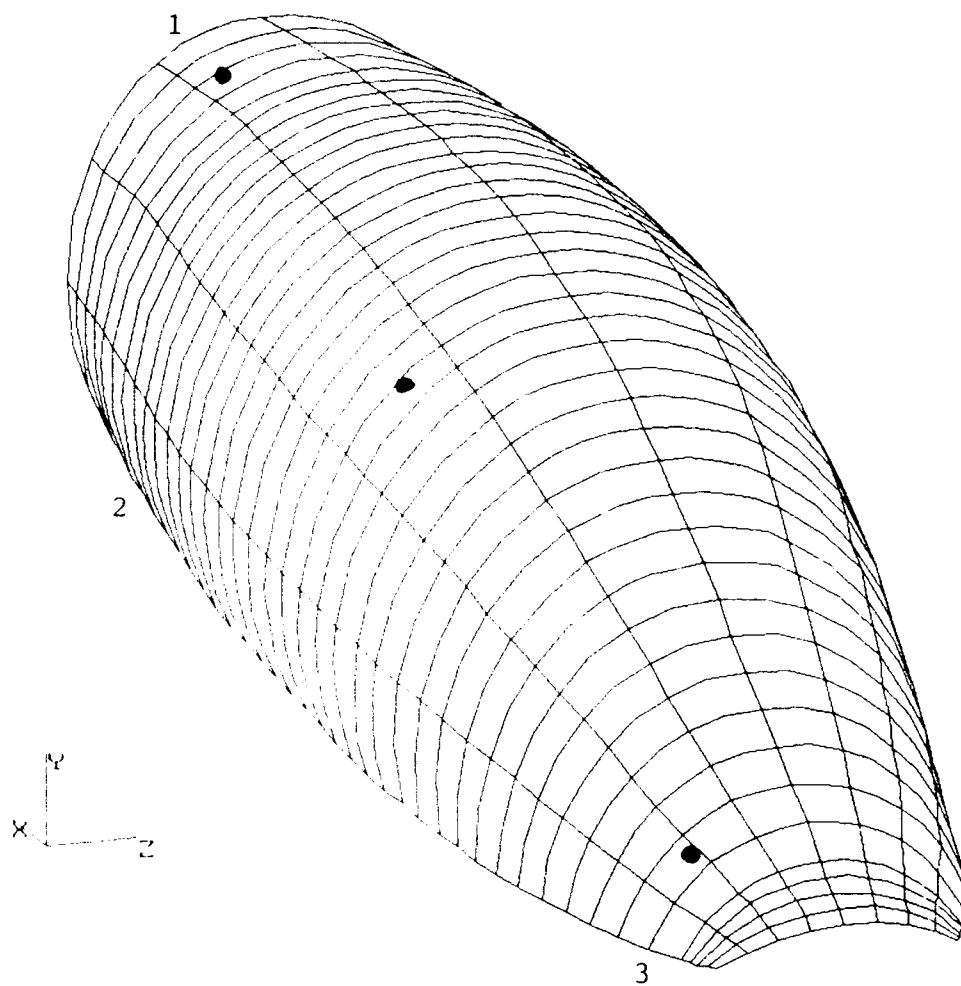


Figure C10. Rosette Locations for Canopy #10 (S/N 1483).

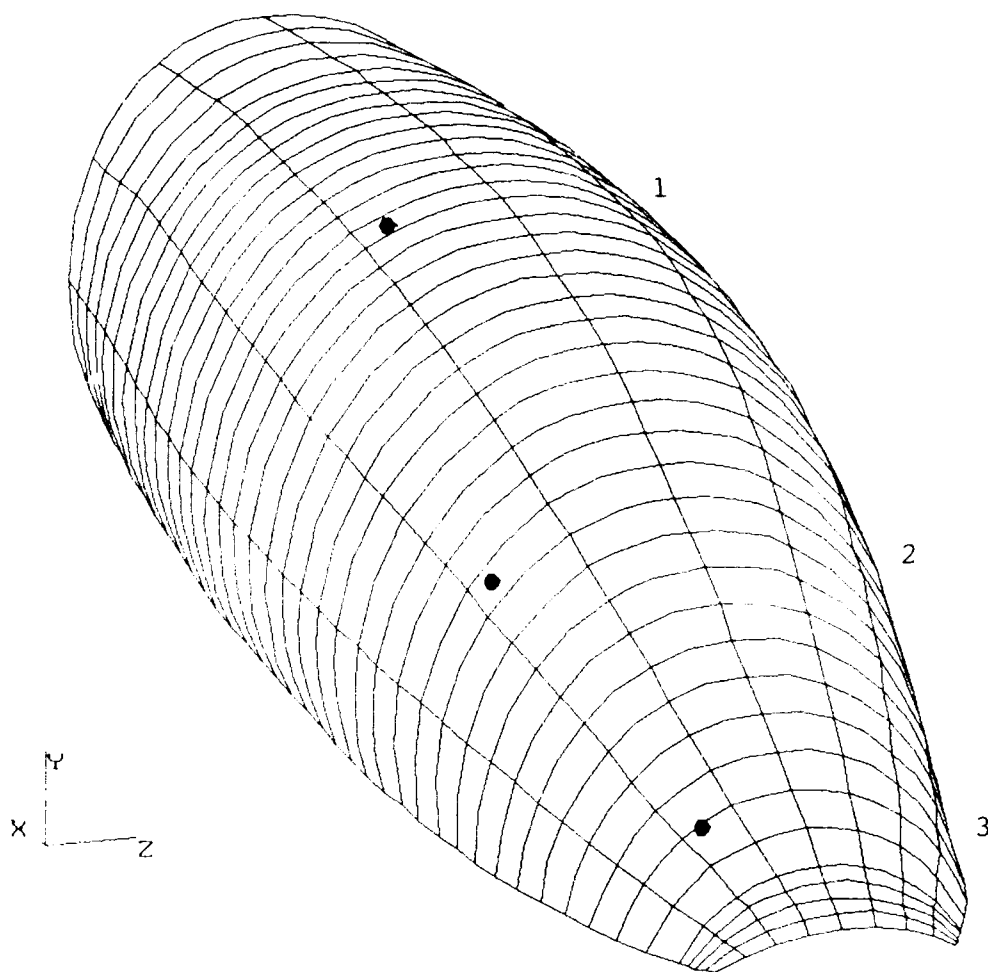


Figure C11. Rosette Locations for Canopy #11 (S/N 133).

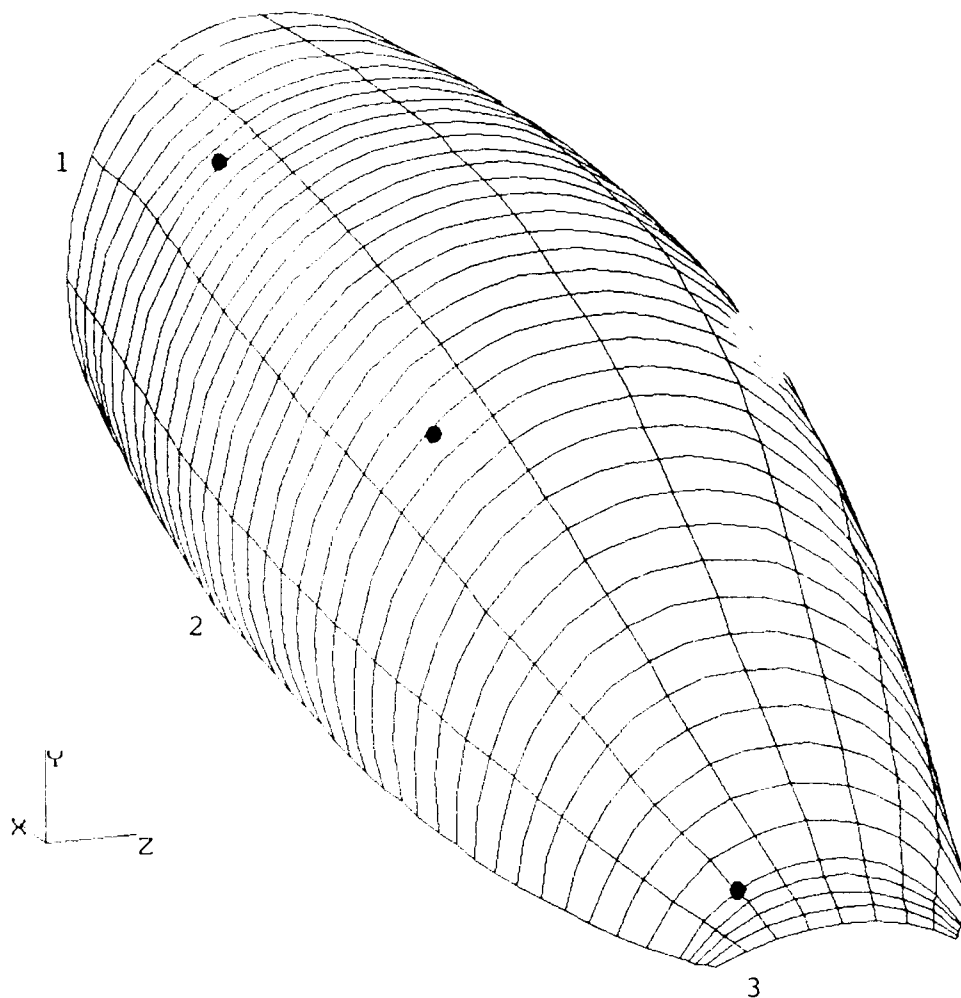


Figure C12. Rosette Locations for Canopy #12 (S/N 1358).

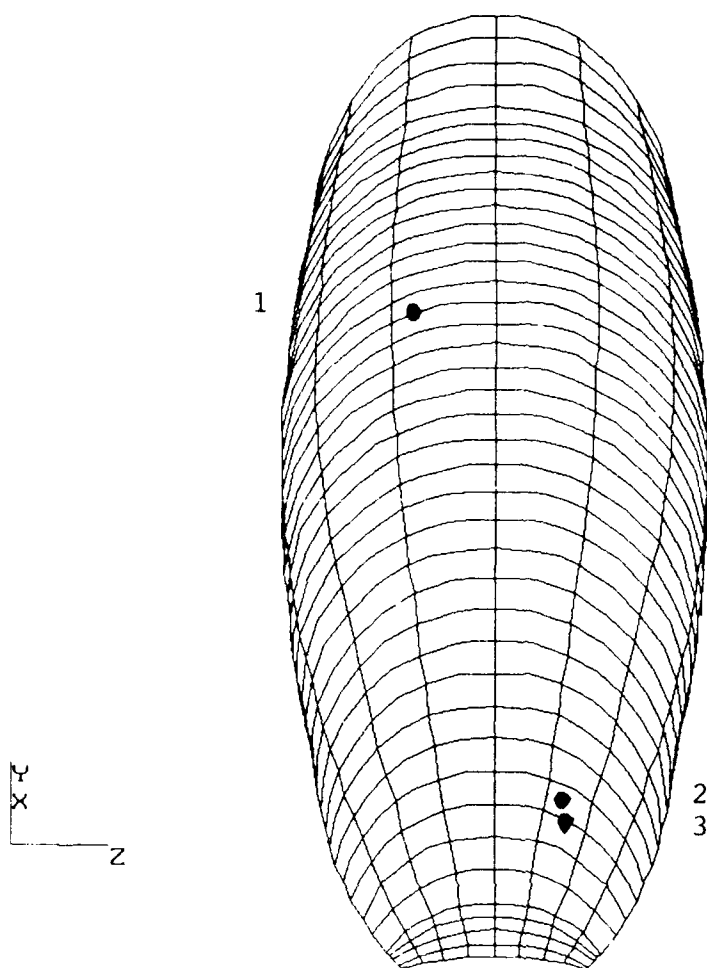


Figure C13. Rosette Locations for Canopy #13 (S/N 835).

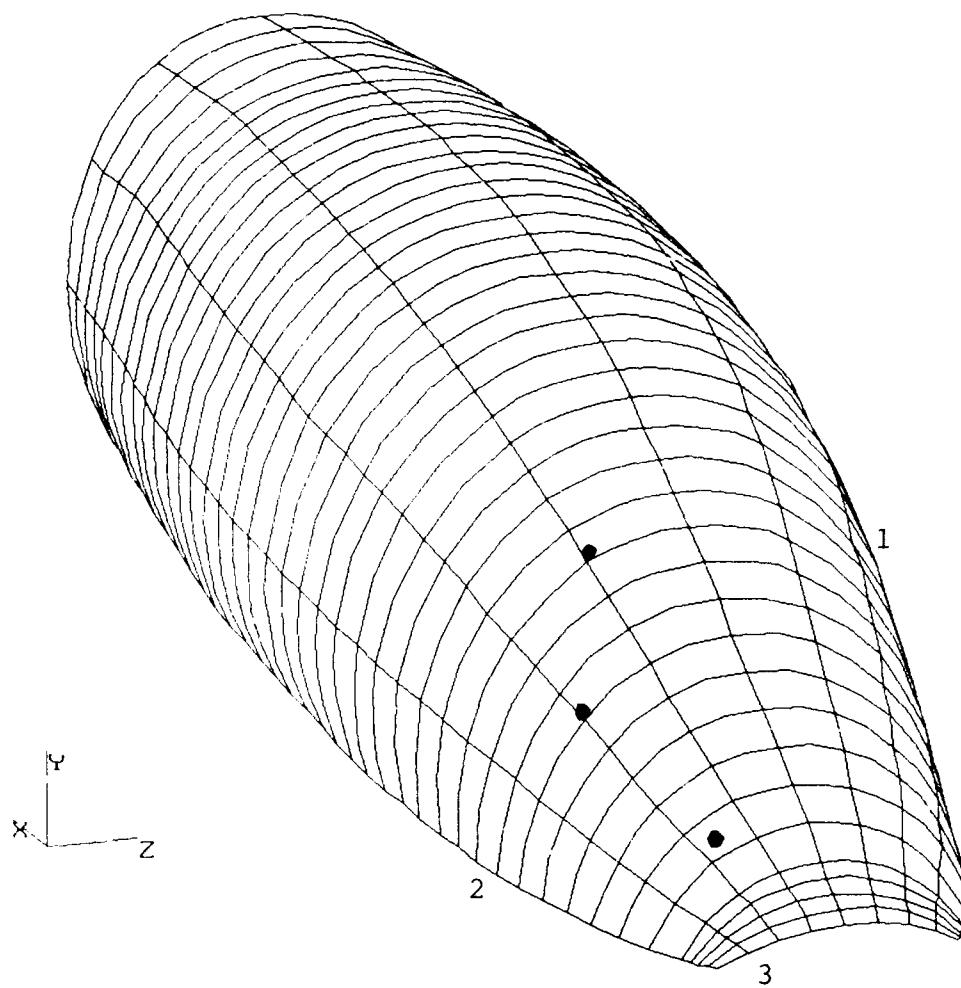


Figure C14. Rosette Locations for Canopy #14 (S/N 869).

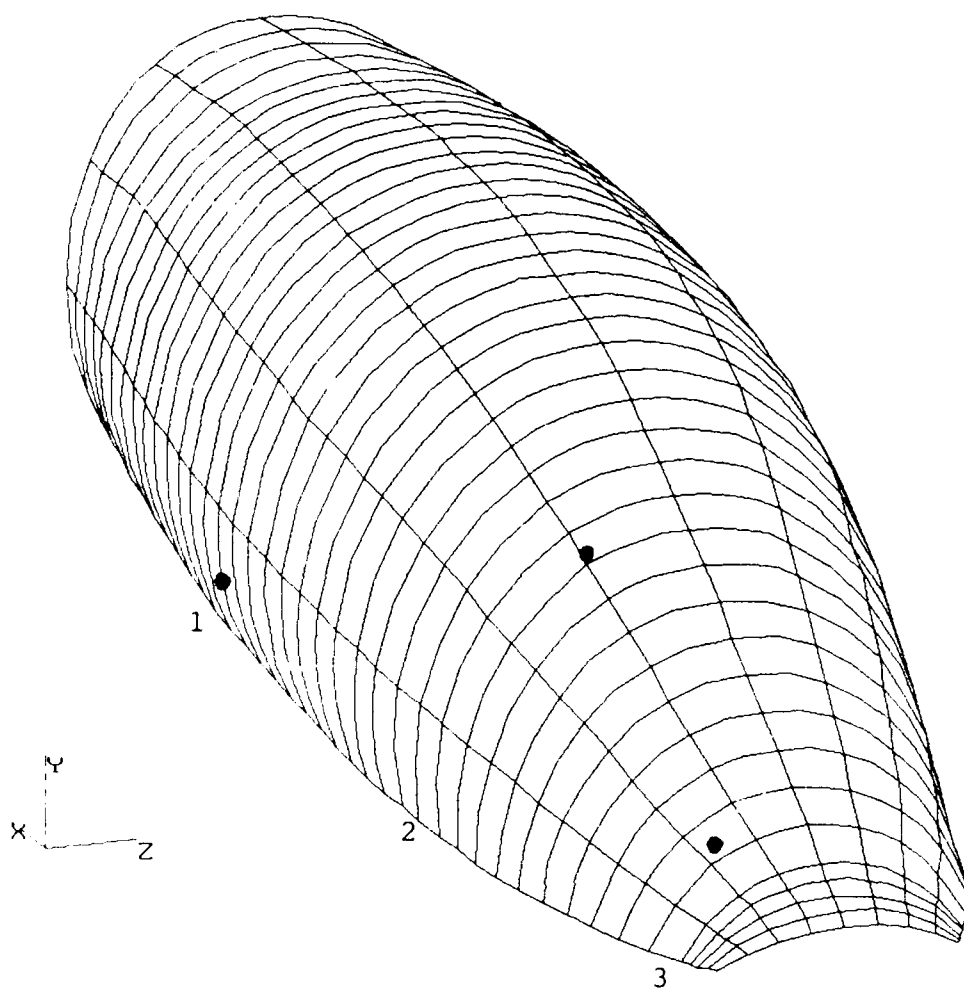


Figure C15. Rosette Locations for Canopy #15 (S/N 499).



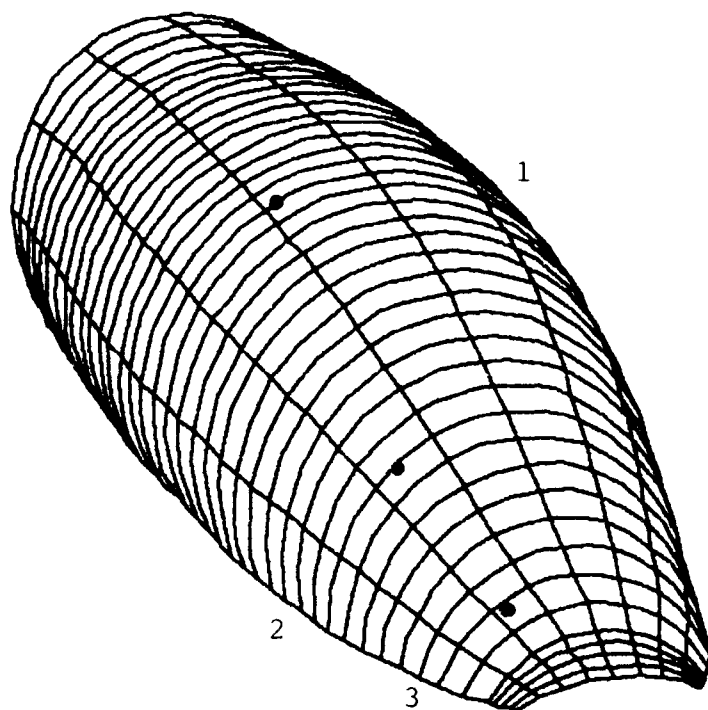


Figure C16. Rosette Locations for Canopy #16 (S/N 109).

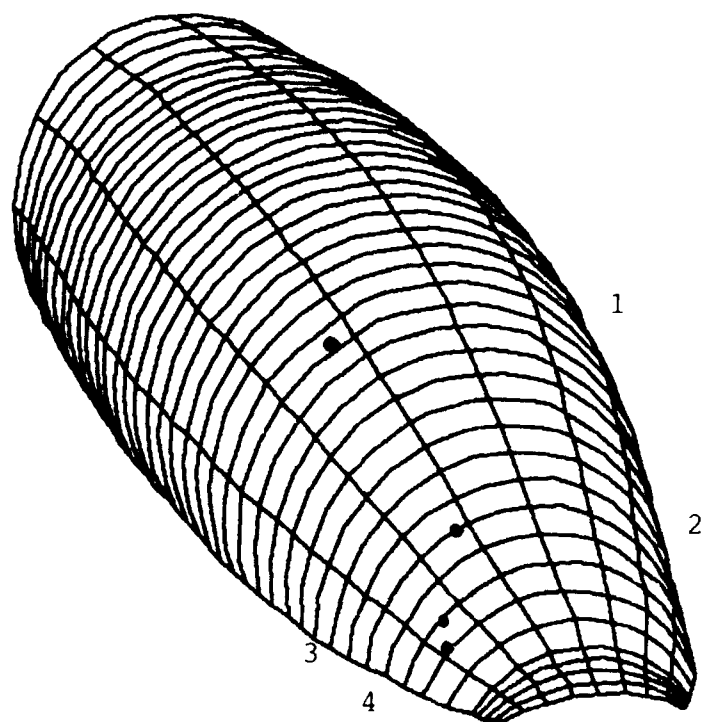


Figure C17. Rosette Locations for Canopy #17 (S/N 283).

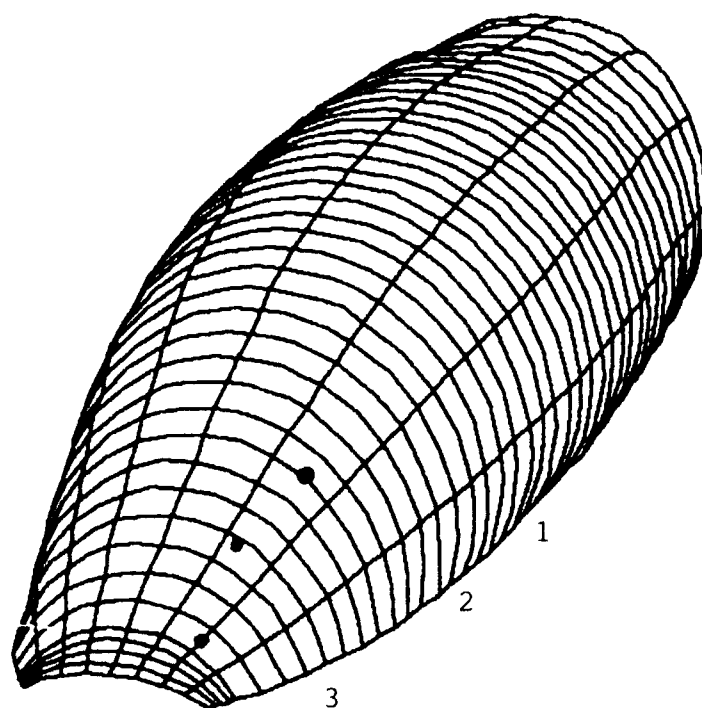


Figure C18. Rosette Locations for Canopy #18 (S/N 504).

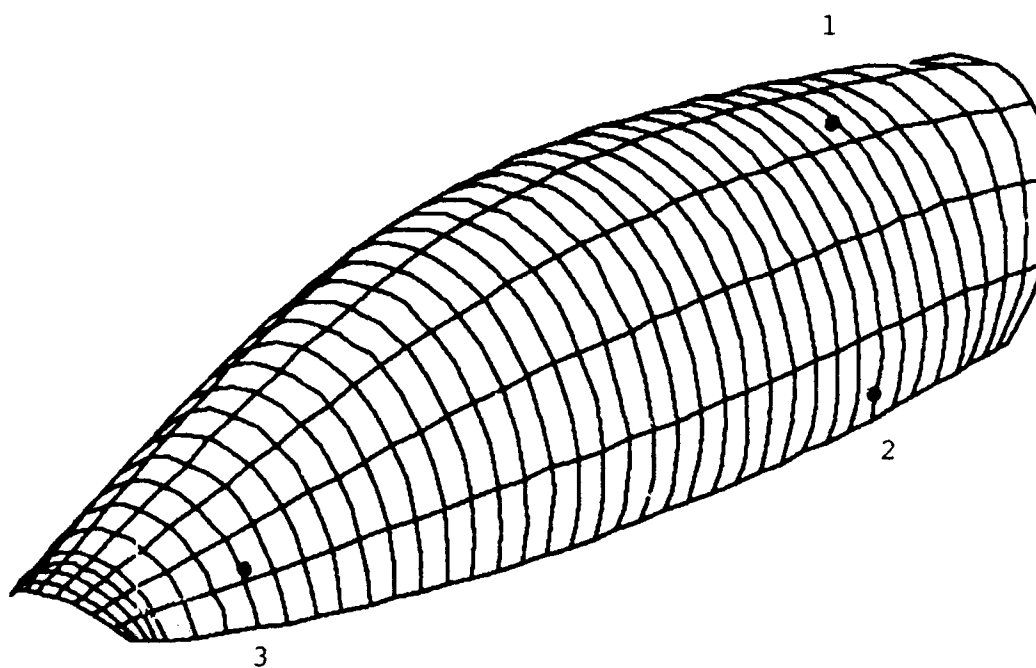


Figure C19. Rosette Locations for Canopy #19 (S/N 401).

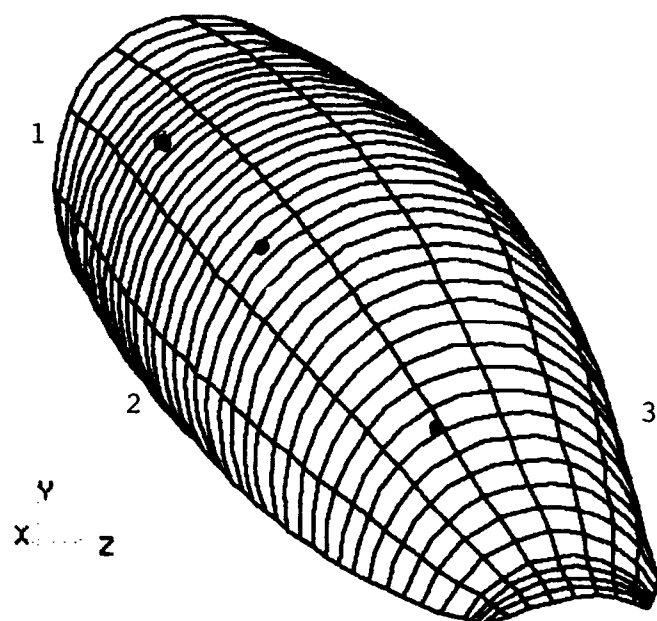


Figure C20. Rosette Locations for Canopy #20 (S/N 279).